



University
of Glasgow

<https://theses.gla.ac.uk/>

Theses Digitisation:

<https://www.gla.ac.uk/myglasgow/research/enlighten/theses/digitisation/>

This is a digitised version of the original print thesis.

Copyright and moral rights for this work are retained by the author

A copy can be downloaded for personal non-commercial research or study, without prior permission or charge

This work cannot be reproduced or quoted extensively from without first obtaining permission in writing from the author

The content must not be changed in any way or sold commercially in any format or medium without the formal permission of the author

When referring to this work, full bibliographic details including the author, title, awarding institution and date of the thesis must be given

Enlighten: Theses

<https://theses.gla.ac.uk/>
research-enlighten@glasgow.ac.uk

TORSIONAL VIBRATIONS OF CRANKSHAFTS

A STUDY OF FORCES, DISPLACEMENTS AND DAMPING
RELATED TO MULTI-CYLINDER ENGINES.

BY

FINN ØRBECK, B.Sc., A.R.T.C.

Thesis submitted to the University of Glasgow
in part fulfilment of the conditions
governing the award of the degree of
Doctor of Philosophy in the Faculty of Science

October, 1956.

ProQuest Number: 10646833

All rights reserved

INFORMATION TO ALL USERS

The quality of this reproduction is dependent upon the quality of the copy submitted.

In the unlikely event that the author did not send a complete manuscript and there are missing pages, these will be noted. Also, if material had to be removed, a note will indicate the deletion.



ProQuest 10646833

Published by ProQuest LLC (2017). Copyright of the Dissertation is held by the Author.

All rights reserved.

This work is protected against unauthorized copying under Title 17, United States Code
Microform Edition © ProQuest LLC.

ProQuest LLC.
789 East Eisenhower Parkway
P.O. Box 1346
Ann Arbor, MI 48106 – 1346

GLASGOW
UNIVERSITY
LIBRARY

C O N T E N T SPageSYNOPSIS

| | |
|---------------------------------------|-----|
| <u>FOREWORD</u> | 1. |
| <u>GENERAL INTRODUCTION</u> | 3. |
| <u>NOMENCLATURE</u> | 11. |

PART I.

THE ELASTIC BEHAVIOUR OF THE CRANK-
SHAFT IN A MULTI-CYLINDER ENGINE.

I. SINGLE CRANK.

| | |
|---|-----|
| <u>Introduction</u> | 26. |
| <u>Initial Reduction</u> | 27. |
| <u>Single Crank</u> | 29. |
| <u>Bending in the Plane of the Throw</u> | 31. |
| <u>Bending in the Plane Perpendicular to the Plane of the Throw</u> | 36. |
| <u>Twist of Simply Supported Throw</u> | 40. |

II. MULTI-THROW CRANKSHAFT.

| | |
|--|-----|
| <u>General Case</u> | 45. |
| <u>General Discussion</u> | 52. |
| <u>Numerical Computation</u> | 54. |

CENTRIFUGAL FORCES AND FORCES DUE
TO TORSIONAL VIBRATIONS ACTING ON
A MULTITHROW CRANKSHAFT.

| | |
|-------------------------------------|-----|
| <u>INTRODUCTION</u> | 56. |
| <u>CENTRIFUGAL FORCES</u> | 59. |

| | |
|--|------|
| | Page |
| VIBRATIONAL FORCES | 61. |
| <u>Radial Vibrational Forces</u> | 62. |
| <u>Tangential Vibrational Forces</u> | 63. |
| <u>and Vibrational Torques.</u> | |
| DISCUSSION | 67. |
| | |
| RESPONSE OF JOURNAL BEARINGS TO SMALL VARIATIONS IN A CONSTANT LOAD OR A CONSTANT CENTRIFUGAL FORCE. | |
| DISCUSSION | 70. |
| BEARING STIFFNESSES | 73. |
| <u>Introduction</u> | 73. |
| <u>Definitions</u> | 75. |
| <u>Conditions</u> | 75. |
| <u>Analysis</u> | 75. |
| VELOCITY-RESISTANCE COEFFICIENTS | 79. |
| DIFFERENTIAL EQUATIONS AND SOLUTION | 81. |
| NUMERICAL CALCULATIONS | 82. |
| <u>Eccentricity and Attitude Angle</u> | 83. |
| <u>Stiffnesses</u> | 83. |
| <u>Velocity-Resistance Coefficients</u> | 84. |
| <u>Applied Forces</u> | 85. |
| <u>Journal Displacements</u> | 85. |
| MEASURED DISPLACEMENTS | 86. |
| INERTIA FORCES | 87. |
| | |
| MEASUREMENT OF CRANKSHAFT TORSIONAL VIBRATIONS AND JOURNAL LATERAL DISPLACEMENTS. | |
| INTRODUCTION | 89. |

| | <u>Page</u> |
|--|-------------|
| CRANKSHAFT TORSIONAL VIBRATIONS | 91. |
| <u>Introduction</u> | 91. |
| <u>Calibration</u> | 91. |
| <u>Engine Tests</u> | 93. |
| <u>Discussion</u> | 94. |
| <u>CRANKSHAFT LATERAL JOURNAL DISPLACEMENT.</u> | |
| MEASUREMENT PROBLEM | 96. |
| <u>Location of Measurement Points</u> | 96. |
| <u>Specification of Measurement Problem</u> | 98. |
| MEASUREMENT GEAR | 99. |
| TESTING AND CALIBRATION OF MEASUREMENT GEAR. | |
| <u>Calibration Apparatus</u> | 101. |
| <u>Calibration Tests</u> | 102. |
| <u>Discussion</u> | 104. |
| MEASUREMENT OF LATERAL DISPLACEMENTS OF A CRANKSHAFT JOURNAL. | |
| <u>Arrangement of Apparatus</u> | 107. |
| <u>Test Programme</u> | 108. |
| <u>Test Procedure</u> | 109. |
| PRESENTATION AND DISCUSSION OF JOURNAL DISPLACEMENT TEST RESULTS | 112. |
| <u>Re-Plotting of Results from Test 1.</u> | 112. |
| <u>Records of Complete Journal Displacements</u> | 113. |
| <u>Presentation</u> | 116. |
| <u>Eccentricity Ratio - Load Number Graphs</u> | 117. |
| <u>Amplitude of 5th. and 7th. Harmonics</u> | 122. |
| CONCLUSION | 126. |

\$\$\$\$\$\$\$\$\$\$

PART II.

THEORETICAL ANALYSIS OF SHRINK-FITTED
ASSEMBLIES LOADED IN TORSION.

GENERAL DISCUSSION.

| | | | |
|--|-----|-----|------|
| Inherent Stresses, Working Stresses and Superposition | ... | ... | 127. |
| Shrink-fitted Assemblies, Plastic and Elastic Behaviour | ... | ... | 128. |
| The Shrink-fitted Assembly as an Intermittent Stage and a Solid Shaft with a Collar | | | 130. |
| SUMMARY | ... | ... | 133. |
| ANALYSIS | ... | ... | 134. |
| Differential Equation and Boundary Conditions | | | 134. |
| Numerical Solution | ... | ... | 135. |
| DERIVED RESULTS | ... | ... | 138. |
| Introduction | ... | ... | 138. |
| Torsional Stiffness | ... | ... | 138. |
| Differential Slip and Damping Capacity | ... | ... | 141. |
| Stress Concentrations | ... | ... | 145. |
| FINAL DISCUSSION | ... | ... | 147 |

MEASUREMENT OF DAMPING CAPACITY AND ENDURANCE
TESTING RELATED TO SHRINK-FITTED ASSEMBLIES.

| | | | |
|---------------------------------------|-----|-----|------|
| Introduction | ... | ... | 150. |
| Historical Development | ... | ... | 151. |
| Factors Affecting Design of Apparatus | ... | ... | 155. |
| APPARATUS | ... | ... | 158. |
| Test Specimen | ... | ... | 158. |
| Excitation | ... | ... | 159. |

| | <u>Page.</u> |
|--|--------------|
| <u>Recording System</u> | 161. |
| <u>Operation</u> | 161. |
| TEST PROGRAMME | 164. |
| DISCUSSION OF EXPERIMENTAL GRAPHS | 167. |
| <u>Scatter of Experimental Points</u> | 167. |
| <u>Differential Slip</u> | 168. |
| <u>Effect of Air Friction and Internal Damping</u> | 169. |
| <u>Coefficient of Friction</u> | 171. |
| PRACTICAL IMPORTANCE OF SHRINK-FIT DAMPING | 175. |
| CONCLUSION | 176. |
| APPENDIX I | 177. |
| APPENDIX II | 187. |
| APPENDIX III | 188. |
| APPENDIX IV | 189. |
| APPENDIX V | 190. |
| APPENDIX VI | 194. |
| APPENDIX VII | 195. |
| LIST OF REFERENCES | 196. |

\$

SYNOPSIS

The work of this Thesis is presented in two parts.

Part I gives a force analysis for the crankshaft of a six-cylinder diesel engine with seven main bearings, later used as a test engine.

The action of centrifugal forces, and all forces due to the torsional vibrations of the crankshaft, were considered.

The crankshaft was considered as a continuous elastic body simply supported in the bearings and, thus, the loads on the bearings due to the above force actions, were obtained.

The behaviour of the fourth main journal bearing subjected to a load, as described above, was then studied.

Firstly, analytical work was carried out to find the journal lateral displacements.

Secondly, the corresponding displacements were investigated experimentally.

Electronic measurement gear was designed for the purpose and found to function satisfactorily.

Finally, experimental and analytical results were compared, and the conditions for which the theoretical force-displacement analysis was valid, were thus established.

Part II contains a study of shrink-fitted assemblies loaded in torsion.

Firstly, an analytical examination was carried out for a ring fitted over a plain shaft. Stiffnesses, stress concentrations and energy dissipation for such assemblies were computed.

It was found that appreciable dissipation of vibrational energy occurs as a result of differential slip between the ring and the shaft.

Secondly, this energy dissipation was investigated experimentally in terms of percentage damping for test specimens incorporating shrink-fitted assemblies.

Experimental gear was developed for the purpose, introducing some improvements of arrangements used by investigators of internal damping.

The experimental results obtained confirmed the theoretical work and, thus, it was established that shrink-fit damping may be an important source of damping for built-up crankshafts.

Finally, some interesting information related to the coefficient of friction between the hub and the shaft of the shrink-fitted assemblies, was obtained.

FOREWORD

Before introducing the general work of this Thesis, it is the author's wish to say some words about people who directly or indirectly have made their contributions.

First of all, the author would like to convey his thanks to Professor A.S.T.Thomson, D.Sc., Ph.D., A.R.T.C., M.I.Mech.E., Professor J.C.Orkney, B.Sc., M.I.Mech.E., M.I.E.E., and Professor A.W.Scott, B.Sc., Ph.D., A.R.T.C., M.I.Mech.E., for advice and encouragement, as well as for the use of laboratories and the provision of materials and services.

Thanks are also due to Mr.W.B.McHutchison, B.Sc., A.R.T.C., Wh.Sch., A.M.I.E.E., A.M.I.Mech.E., for many valuable ideas and suggestions.

The author would also like to convey his thanks to the technicians in the vibration laboratory, the machine shops and the heat engines laboratory for their help, and would in particular like to mention Mr.J.Sey for his construction of electronic gear.

Many thanks are due to Rolls-Royce Ltd., Oil Engine Division, Derby, for the provision of the test engine R.R. C.60 Nr.51.

Many parts of the theoretical analysis which are presented in this Thesis can be found in available literature.

It was often necessary, however, to carry out modifications and sometimes extensions, to bring the analysis into complete units.

The crankshaft analysis is, but for minor differences, taken from Timoshenko.

The journal bearing analysis originates from Stodola and has been developed later, but it was necessary for the author to carry out modifications where previous work showed contradictions between analysis and definition.

The analysis of shrink-fitted assemblies is, but for technique, entirely due to the author.

The experimental work has been carried out at the Royal College of Science and Technology, Glasgow.

Besides the general laboratory assistance, the author has been fortunate to be able to direct the work of various students towards a common aim.

Naturally, this organisation of the experimental work paid dividends in the form of a larger volume of results.

GENERAL INTRODUCTION.

This Thesis is another work presented in a field which has already been studied for nearly fifty years. When it was first realised that vibration could be a serious danger to crankshafts, publications on the subject followed as a natural consequence. Through time the volume of publications has steadily increased, but it can by no means be said that the subject is yet exhausted.

A brief survey of the history of the subject will now be given, but it should be kept in mind that history in itself is not the object - the idea being to establish a background for present-day knowledge.

Vibrations are generally associated with dangerous resonance frequencies - conditions which the designer prefers to avoid. Naturally, the study of vibration was therefore in the beginning confined to determining these conditions or, in other words, resonance frequencies. For this purpose, a crankshaft system is most conveniently reduced to an equivalent system consisting of balanced inertias fixed to a plain shaft, and it is sufficient to consider inertia forces and stiffness forces only. Much work has been done on this side of the subject and today resonance frequencies for crankshafts can be predicted with

reasonable certainty.

However, with improved knowledge, the scope of the subject also increased and torsional vibrations were gradually considered in a different light.

As the requirements went up, resonance conditions could not always be avoided and interest had to be focussed on amplitudes of vibration as well as critical speeds. Consequently, it became necessary to extend the analyses to include velocity-resistant forces and energy dissipation. Thus, the study of damping arose as a side-line to that of crankshaft torsional vibrations.

Generally, damping has also been treated quite extensively in the available literature and, in particular, much attention has been paid to internal damping. However, the knowledge about damping in relation to torsional vibrations of crankshafts still remains somewhat obscure, although some publications make valuable contributions to the subject.

It will be convenient to give a short survey of some of the works.--

Dorey made a particular study of the importance of internal damping⁽¹⁾.

Shannon discovered that a main part of the energy

(1) Dorey, S.F. - Elastic Hysteresis in Crankshaft Steels.
(Proc.Inst.Mech.Eng.- Dec. 1932).

dissipation of the crankshaft system occurred in the bearings and Dramlinsky later carried out a closer study of the same phenomenon^(1,2).

The importance of cylinder friction damping has been discussed by various authors and found to be small and other sources of damping, such as fundament damping, are also small as well as difficult to approach by analyses.

The general picture emerging from the above is that, although various sources of damping have been studied in some detail, it is not yet possible to predict the damping of an engine crankshaft system quantitatively at the design stage. This is partly due to lack of detailed information about the various sources of damping but, in the author's opinion, the main obstacle lies in the lack of an overall force analysis for the crankshaft system.

A proper force analysis would also carry a second advantage. Since energy dissipation is a direct result of force action, principal sources of damping can be expected where the vibrational forces are largest. As well as helping to clarify the picture of already known sources of damping, a force analysis may therefore give a lead to other

-
- (1) Shannon, J.F.- Damping Influence in Torsional Oscillation.--(Inst.Mech.Eng.--Dec. 1935)
 - (2) Dramlinsky, P.- Daempningen Ved Torsionssvingninger I Krumtapaksler.-- Copenhagen, 1947.

sources which are, as yet, undiscovered.

With the above considerations as a background, it was decided by the author to make his first approach to the study of torsional vibrations in the form of an attempt on a force analysis.

By making some assumptions which seemed reasonable, it was found that a force analysis for the crankshaft system was possible, though somewhat lengthy.

The analysis developed, as it appears in its final form, is given in the first main section of this Thesis. It contains four chapters, the first of which is devoted to the elastic behaviour of single cranks. The second chapter is an extension which deals with the behaviour of multi-bearing crankshafts. The third chapter then gives an analysis of some general applied forces and, finally, the fourth deals with the effect of certain crankshaft loads on the bearings.

A numerical example related to the crankshaft of a six-cylinder diesel engine (R.R. C. 60.), on which tests were later carried out, has been taken right through the entire analysis as an illustration to the symbolical work.

Throughout the progress of a theoretical analysis, it is invariably found that certain points vital to the

analysis as a whole, cannot be investigated as thoroughly as would be desired. The necessity for experimental investigation will be obvious, but difficulties may be incurred. Under such circumstances, it is justifiable to make assumptions in the hope that progress with the theoretical analysis will later reveal features of the overall problem which suggest simpler experimental studies.

The above described state of affairs is characteristic of the author's work on crankshafts and, consequently, the need for experimental support is evident. Further, since actual crankshaft loads can only be measured with great difficulty, it was decided to seek other possibilities.

The solution finally was to make use of the variations in oil-film thickness for one of the journal bearings as a measure of the load carried by this bearing.

Experimental measurements of the variations in oil-film thickness for journal bearings have been carried out by various people, of whom, in particular, Kollmann and Hockel should be mentioned. They carried out measurements on a medium speed diesel engine, using capacity pick-up units in conjunction with electronic measurement gear operating on the principle of frequency modulation⁽¹⁾.

(1) Kollmann, K. and Hockel, H.L. - Ermittlung der Dicke des Schmierfilms in den Grundlagern einer Stationären Dieselmotors.- M.T.Z. Jahrgang 14. Nr.5. May, 1953.

Principally, the author has made use of the same system as Kollmann and Hockel, but some modifications were incorporated to suit particular requirements. It was found that reliable experimental readings could be obtained and soon a position was reached where crankshaft forces and bearing displacements for a multi-cylinder diesel engine could be discussed in the light of experimental, as well as theoretical information.

Finally, the following conclusion was reached. For an engine with normal bearing clearances and heavy crankshaft loads, the theoretical force analysis gives reasonably reliable values for the bearing loads and, consequently, the crankshaft forces. Although somewhat complicated, the analysis may therefore prove useful for design purpose.

The work on a general force analysis was thus concluded.

In the course of his work on a general force analysis for the crankshaft of a multi-cylinder engine, the author came across information which revealed notable differences between built-up and solidly forged crankshafts.

Russell had found by experiment that built-up cranks were much more flexible in torsion than solid⁽¹⁾. Draminsky

(1) Russell, R. - Experimental Studies on Crankshaft Stiffness - Journal of Royal Technical College, Volume IV, 1937-40.

gave results which show that engines with built-up crankshafts generally possess higher damping for the torsional vibrations⁽¹⁾.

It occurred to the author that the above information pointed towards a difference in principle between two varieties of design and, since the subject was of direct interest to the study of torsional vibrations, it was decided to devote time to further investigation.

Thus, a study of shrink-fitted assemblies loaded in torsion, was initiated and, in due course, it developed so well that it will now be presented as a second major section of this Thesis.

The author has applied principally the same technique in his study of this latter problem as was used for the general force analysis. A theoretical analysis based on certain assumptions was first developed. Experimental tests were then carried out, such that the problem was eventually displayed in the light of information obtained from both sides.

It was found that differential slip between the mating surfaces of shrink-fitted assemblies may provide a major contribution to the damping of a crankshaft and, further, that this contribution can be greatly increased by

(1) Draminsky, P. - Dæmpningen Ved Torsionssvingninger I Krumtapaksler. - Copenhagen, 1947.

improvement in design.

The discoveries were therefore of practical importance but we will return to this in the course of the detailed study presented later.

NOMENCLATURE

As a result of the large volume of theoretical analyses presented in this Thesis, the Nomenclature has become rather bulky.

A sub-division was therefore desirable and it has been found most convenient to present the Nomenclature under headings corresponding to the chapters to which it applies.

Nomenclature which does not apply to any of the main analyses has been collected under "Miscellaneous".

Generally, the author has made use of the same nomenclature in his Analysis, as was used by one of the previous writers in the same field.

The nomenclature for crankshafts is thus mainly taken from Timoshenko, and for the shrink-fitted assemblies from Love.

THE ELASTIC BEHAVIOUR OF THE CRANKSHAFT
IN A MULTICYLINDER ENGINE

(a) "SINGLE CRANK".-

| | | |
|----------------------|--|------------------------|
| <u>r</u> | = crank radius. | (in.) |
| <u>l</u> | = length of crank. | " |
| <u>e</u> | = length of left-hand side half-journal. | " |
| <u>f</u> | = length of crankpin. | " |
| <u>q</u> | = length of right-hand side half-journal. | " |
| <u>C₁</u> | = torsional rigidity of journals. | (lb.in ² .) |
| <u>C₂</u> | = torsional rigidity of web (twist around q-s). | " |
| <u>C₃</u> | = torsional rigidity of crankpin. | " |
| <u>B₁</u> | = flexural rigidity of journals. | " |
| <u>B₂</u> | = flexural rigidity of web (in plane perp. to paper). | " |
| <u>B₃</u> | = flexural rigidity of web (in plane of paper). | " |
| <u>B₄</u> | = flexural rigidity of crankpin. | " |
| <u>x</u> | = co-ordinate. | (in.) |
| <u>y</u> | = " | " |
| <u>z</u> | = " | " |
| <u>P</u> | = force applied at centre of crankpin. | (lb.) |
| <u>S</u> | = force applied at centre of crankpin. | (lb.) |
| <u>m</u> | = bending moment in the plane of the throw. | (lb. in.) |

M = bending moment in the plane perpendicular (lb. in.)
to the plane of the throw.

T = twisting moment. (" ")

The suffix l refers to the left-hand side of the crank.

Similarly, the suffix r refers to the right-hand side of the crank.

φ_l = angle of rotation in the plane of the (Rad.)
throw of the left end of a crank.

φ_r = angle of rotation in the plane of the (Rad.)
throw of the right end of a crank.

A = support reaction. (lb.)

B = support reaction (lb.)

φ_l' = angle φ_l due to load P. (Rad.)

t_l = deflection coefficient = φ_l'/P . (Rad./lb.)

φ_r' = angle φ_r due to load P. (Rad.)

t_r = deflection coefficient = $-\varphi_r'/P$. (Rad./lb.)

(φ_l'') = angle φ_l due to moment m_l . (Rad.)

(φ_r'') = angle φ_r due to moment m_r . (")

(φ_l''') = angle φ_l due to moment m_r . (")

(φ_r''') = angle φ_r due to moment m_r . (")

α_l^1 = slope at A caused by unit bending (Rad./lb.in.)
moment applied at A. = $(\varphi_l'')/m_l$.

α_l^r = slope at B caused by unit bending (Rad./lb.in.)
moment applied at B. = $(\varphi_r'')/m_r$.

α_r = slope at B caused by unit bending (Rad./lb.in.)
moment applied at A. or slope at A.
caused by unit bending moment applied
at B. = $(\varphi_l''')/m_r$ = $(\varphi_r'')/m_l$.

- $\underline{\psi}_1$ = angle of rotation in the plane perpendicular to the plane of the throw of the left end of a crank. (Rad.)
- $\underline{\psi}_2$ = angle of rotation in the plane perpendicular to the plane of the throw of the right end of a crank. (Rad.)
- $\underline{\psi}'_1$ = angle $\underline{\psi}_1$ due to load \underline{S} . (")
- $\underline{\psi}'_2$ = angle $\underline{\psi}_2$ due to load \underline{S} . (")
- \underline{u}_1 = deflection coefficient = $\underline{\psi}'_1/\underline{S}$. (Rad./lb.)
- \underline{u}_2 = deflection coefficient = $\underline{\psi}'_2/\underline{S}$. (" ")
- $(\underline{\psi}''_1)_l$ = angle $\underline{\psi}_1$ due to moment \underline{M}_l . (Rad.)
- $(\underline{\psi}''_2)_l$ = angle $\underline{\psi}_2$ due to moment \underline{M}_l . (")
- $(\underline{\psi}''_1)_r$ = angle $\underline{\psi}_1$ due to moment \underline{M}_r . (")
- $(\underline{\psi}''_2)_r$ = angle $\underline{\psi}_2$ due to moment \underline{M}_r . (")
- $\underline{\beta}_1^1$ = slope at A caused by unit bending moment applied at A. = $(\underline{\psi}''_1)_l/\underline{M}_l$. (Rad./lb.in.)
- $\underline{\beta}_2^r$ = slope at B caused by unit bending moment applied at B. = $(\underline{\psi}''_2)_r/\underline{M}_r$. (" " ")
- $\underline{\beta}_2$ = slope at B caused by unit bending moment applied at A, or vice versa. = $(\underline{\psi}''_1)_r/\underline{M}_r = (\underline{\psi}''_2)_l/\underline{M}_l$. (" " ")
- $\underline{\psi}_1'''$ = angle $\underline{\psi}_1$ due to deflection of webs and twist of crankpin under the action of a moment \underline{M} . (Rad.)
- $\underline{\psi}_2'''$ = angle $\underline{\psi}_2$ due to deflection of webs and twist of crankpin under the action of a moment \underline{M} . (")
- $\underline{\theta}$ = angle of twist of crank. (")
- $\underline{\theta}_1$ = angle of twist of right-hand journal. (")
- $\underline{\theta}_2$ = angle of twist of left-hand journal. (")

- θ_2 = angle of twist of crankpin. (Rad.)
- θ_4 = change of slope of webs. (")
- w = deflection coefficient = $\frac{\theta}{I}$. (Rad./lb.in.)
- ψ = angle of rotation about the Y-axis of the ends of a crank due to a twisting moment I . (Rad.)
- δ = deflection corresponding to the angle ψ . (in.)
- χ = deflection due to the flexure of the web. (")
- χ_1 = deflection due to the twist of the crankpin. (")
- s = deflection coefficient = $\frac{\psi}{I}$. (Rad./lb.in.)
- θ_0 = twist of crank produced by moment M . (Rad.)
- ψ_1^{III} = angle ψ_1 due to twisting moment I and force S . (")
- ψ_2^{III} = angle ψ_2 due to twisting moment I and force S . (")
- η = deflection coefficient = $\frac{-sr/2 + u_1}{I}$. (Rad./lb.)
- η_2 = deflection coefficient = $\frac{sr/2 + u_2}{I}$. (" ")

(b) "MULTI-THROW CRANKSHAFT".--

The suffix i applied to a symbol indicates the crank number or support number for which the symbol is valid.

See introduction to "Multi-throw Crankshafts".

- χ = angle between two consecutive throws. (Rad.)
(looking on the front end of the crankshaft, the angle χ is measured positive in the clock-wise direction).

n = integral number.

a_{mn} = coefficient in a system of simultaneous equations.

The subscript m denotes the number of the equation and the subscript n the number of the unknown to which the coefficient applies.

C_m = constant in the above equations.

A = matrix notation of coefficients in the above equation.

M = matrix notation of the unknown moments.

C = matrix notation of the constants.

G = modulus of rigidity (lb./in²)

CENTRIFUGAL FORCES AND FORCES DUE TO TORSIONAL VIBRATIONS ACTING ON A MULTI-THROW CRANKSHAFT

This section also covers the nomenclature which applies in Appendix I.

| | | |
|-----------------|--|--------------------------|
| θ | = angular co-ordinate of crank. | (Rad.) |
| A_n | = amplitude of nth. harmonic of torsional vibration of a crank. | (Rad.) |
| ξ_n | = phase angle of nth. harmonic of torsional vibration of a crank. | (Degrees) |
| ω | = constant angular velocity of crank. | (1/sec.) |
| $\dot{\theta}$ | = angular velocity of crank. | (" ") |
| $\ddot{\theta}$ | = angular acceleration of crank. | (1/sec. ²) |
| α_r | = tangential acceleration of crankpin. | (in./sec. ²) |
| α_e | = radial acceleration of crankpin. | (" ") |
| R | = crank radius | (in.) |
| N | = one particular harmonic number. | |
| u | = displacement of the reciprocating mass from its position at T.D.C. | (" ") |
| \dot{u} | = velocity of reciprocating mass. | (in./sec.) |
| \ddot{u} | = acceleration of reciprocating mass. | (in./sec. ²) |
| l | = length of connecting-rod | (in.) |
| k_0 | = coefficient. | |
| k_2 | = coefficient. | |
| k_4 | = coefficient. | |
| k_n | = coefficient. | |

| | | |
|------------------------------------|---|----------------------------|
| <u>t</u> | = time | (sec.) |
| <u>θ</u> | = angle between any crank and crank number 1. | (Rad.) |
| <u>m'</u> | = rotating mass. | (lb.sec ² /in.) |
| <u>r</u> | = distance between centre of gravity and axis of rotation. | (in.) |
| <u>m'r</u> | = rotating out-of-balance. = <u>mR</u> | (lb.sec ²) |
| <u>m</u> | = equivalent mass at crankpin. | (lb.sec ² /in.) |
| <u>M</u> | = reciprocating mass. | (" " ") |
| <u>T</u> | = thrust between piston and cylinder wall. | (lb.) |
| <u>ψ</u> | = angle between connecting rod and cylinder centre line. | (Rad.) |
| <u>F_T</u> | = tangential force on crankpin. | (lb.) |
| <u>F_R</u> | = radial force on crankpin. | (") |
| <u>(F_T)_N</u> | = above tangential force due to Nth. harmonic of crankshaft torsional vibrations. | (") |
| <u>(F_R)_N</u> | = above radial force due to Nth. harmonic of crankshaft torsional vibrations. | (") |
| <u>C.F.</u> | = mean value of the centrifugal force. | (") |

RESPONSE OF JOURNAL BEARINGS TO SMALL VARIATIONS IN
A CONSTANT LOAD OR A CONSTANT CENTRIFUGAL FORCE.

| | | |
|------------------------------|---|------------------------------|
| <u>α</u> | = attitude angle. | (Degrees) |
| <u>e</u> | = mean eccentricity. | (in.) |
| <u>C_e</u> | = radial clearance. | (") |
| <u>C_d</u> | = diametral clearance. | (") |
| <u>ϵ</u> | = eccentricity ratio = <u>e/c_e</u> | |
| <u>D</u> | = diameter of journal. | (") |
| <u>R</u> | = radius of journal. | (") |
| <u>L</u> | = length of shell. | (") |
| <u>N_s</u> | = shaft speed. | (R.P.M.) |
| <u>ω</u> | = shaft speed. | (1/sec.) |
| <u>P</u> | = constant load. | (lbs.) |
| <u>$C.F.$</u> | = mean centrifugal force. | (") |
| <u>ω_n</u> | = frequency of Nth. harmonic variation of centrifugal force. | (1/sec.) |
| <u>μ</u> | = viscosity. | (lb.sec./in. ² .) |
| <u>p</u> | = nominal pressure = <u>$C.F./DL$</u> . | (lbs./in. ² .) |
| <u>C_n</u> | = capacity number. | |
| <u>$1/C_n$</u> | = load number = <u>$\frac{p}{\mu\omega} \left(\frac{C_d}{D}\right)^2 \left(\frac{D}{L}\right)^2$</u> . | |
| <u>X</u> | = co-ordinate. | |
| <u>Z</u> | = co-ordinate. | |
| <u>S_{xx}</u> | = Displacement in x-direction due to force in x-direction. | (in.) |
| <u>C_{xx}</u> | = stiffness = <u>$\delta P_x/S_{xx}$</u> . | (lb./in.) |

- δP_x = small change of load P in x-direction (lb.)
 S_{zx} = displacement in x-direction due to force in z-direction. (in.)
 C_{zx} = stiffness = $\delta P_z / S_{zx}$. (lb./in.)
 δP_z = small change of load P in z-direction. (lb.)
 S_{xz} = displacement in z-direction due to force in x-direction. (in.)
 C_{xz} = stiffness = $\delta P_x / S_{xz}$. (lb./in.)
 S_{zz} = displacement in z-direction due to force in z-direction. (in.)
 C_{zz} = stiffness = $\delta P_z / S_{zz}$. (lb./in.)
 B_{xx} = velocity resistance coefficient in x-direction. (lb.sec./in.)
 B_{zz} = velocity resistance coefficient in z-direction. (")
 F_z = small cyclic force in z-direction. (lb.)
 F_x = small cyclic force in x-direction. (")
 β = phase angle of F_x . (Degrees)
 γ = phase angle of F_z . (")
 F = force. (lb.)
 F_z = " (")
 F_x = " (")
 N = harmonic number.
 θ = angular position of any pick-up unit with respect to the cylinder centre lines. (Degrees)
 IF = inertia force. (lb.)

THEORETICAL ANALYSIS OF SHRINK-FITTED ASSEMBLIES

LOADED IN TORSION

r = radial co-ordinate (See Fig. 52.)

z = axial co-ordinate (" ")

θ = angular co-ordinate (" ")

θ_z = axial shear stress (" ")

θ_r = radial shear stress (" ")

ψ = stress function.

ψ_0 = constant value of ψ over boundary A.B.C.D.

k_1 , k_2 etc. constants.

μ = coefficient of friction.

p = normal pressure.

T = applied torque.

v = circumferential displacement at any point.

ϕ = angular displacement at any point. = v/r .

C = torsional stiffness = T/ϕ .

R_0 = radius of shaft.

e = nominal shear strain, i.e. shear strain in the shaft far away from the corner.

q = ratio of any shear strain in the assembly to the nominal shear strain.

e_{ax} = axial shear strain.

e_{cr} = circumferential shear strain.

q_{ax} = axial strain ratio.

q_{cr} = circumferential strain ratio.

$\underline{q_r}$ = resultant strain ratio. = stress concentration factor.

$\underline{\sigma}$ = ratio of interface grip to nominal shear stress

$$= \frac{\mu_p}{G_e}.$$

\underline{s} = tangential motion between two corresponding points on the mating surfaces in the shrink-fitted assembly.

The suffix \underline{s} to a symbol indicates that the symbol applies to the shaft.

The suffix \underline{h} to a symbol indicates that the symbol applies to the hub.

\underline{A} indicates -- area.

\underline{F} " -- force.

\underline{W} " -- work.

$\underline{\%D}$ " -- percentage damping.

\underline{E} " -- energy.

\underline{J} " -- polar moment of inertia.

\underline{l} " -- length.

\underline{G} = modulus of rigidity.

$\underline{\tau}$ = resultant shear stress.

$$\underline{I} = \frac{\int_{z_1}^{z_2} \int_{z_1}^{z_2} (q_{zs} - q_{zh}) dz dz}{}$$

MISCELLANEOUS

The following nomenclature was used in the design of experimental gear for tests on shrink-fitted assemblies:-

| | | |
|----------------------------|------------------------------------|----------------------------|
| <u>W</u> | = energy dissipation. | (lb.in./cycle) |
| <u>T</u> | = applied vibrational torque. | (lb.in.) |
| <u>ω</u> | = frequency. | (1/sec.) |
| <u>C</u> | = stiffness coefficient. | (lb.in.) |
| <u>S</u> | = velocity resistance coefficient. | (lb. in. sec.) |
| <u>I</u> | = angular inertia. | (lb.in.sec. ²) |

The following nomenclature applies to an optical system used for measuring small angular deflections.

| | | |
|----------------------------|---|--------|
| <u>h</u> | = movement of virtual point object. | (in.) |
| <u>δ</u> | = movement of point image on screen. | (") |
| <u>a</u> | = distance of light source from lens. | (") |
| <u>b</u> | = distance of screen from lens. | (") |
| <u>s</u> | = distance of light source from mirror. | (") |
| <u>θ</u> | = angular deflection of mirror. | (Rad.) |

PART I

AN ANALYSIS

OF

CRANKSHAFT FORCES AND JOURNAL DISPLACEMENTS

RELATED TO

A SIX CYLINDER DIESEL ENGINE.

COMPUTATION OF FORCES AND DISPLACEMENTS.

THE ELASTIC BEHAVIOUR OF THE CRANKSHAFT IN A MULTICYLINDER ENGINE.

I. SINGLE CRANK.

Introduction.

The crankshaft in a multi-cylinder engine has been the subject of study for many authors, and suitable treatments for most practical purposes can be found in the available literature. The object of the following two chapters is therefore not so much to provide any original work, as to give a survey of work which is necessary for other parts of this Thesis.

The main bulk of work on crankshafts is primarily concerned with how to find the stiffness of this body in torsion as this characteristic is required for the important analyses of the torsional vibrations⁽¹⁾. Quite a few papers, however, also treat the aspects of bending rather thoroughly⁽²⁾, and a few later ones consider the longitudinal stiffness⁽³⁾.

(1) Die Reduktion der Kurbelkröpfung, by Seelmann, Z. V.D.I. s. 601, 1925.

(2) Applied Elasticity, by Timoshenko and Lessels, ch.VIII.

(3) Strength of Marine Engine Shafting, by S.F.Dorey, North-East Institution of Engineers and Shipbuilders, Trans. vol.IV, 1938-39, p.203.

The following two chapters have been arranged with the aim of giving a clear preparatory treatment of the problem such that the final solutions can be found by means of the "relaxation method". In approach the treatment is very similar to that given by Timoshenko and Lessells (ref. 2 on the previous page), but slight modifications have been necessary to make the expressions derived directly applicable to the practical problem of interest.

For convenience the same notation as Timoshenko and Lessells used, has also been used here, only a few new symbols have been introduced as will be indicated later.

The numerical calculations of the chapter relate to the crankshaft of a six cylinder high speed diesel engine (Rolls Royce C.60, No.51.), and the figures may therefore be taken as representative for a working design.

Initial Reduction.

For the subsequent treatment of the crankshaft in this chapter it is essential that the actual physical cranks can be considered as built up of beams and torsion bars of negligible cross-sectional area. In other words, the actual crank must be reduced to a more convenient representation, which will be termed the "reduced crank", and the process of carrying this out will be referred to as the

"initial reduction".

Owing to the complex shape of an actual crank, it is readily understood that the initial reduction to a great extent must be based on empirical information and judgement. Certain rules of course should be adhered to, as for instance:

The reduced crank should be made to coincide with the centre-lines of the actual crank.

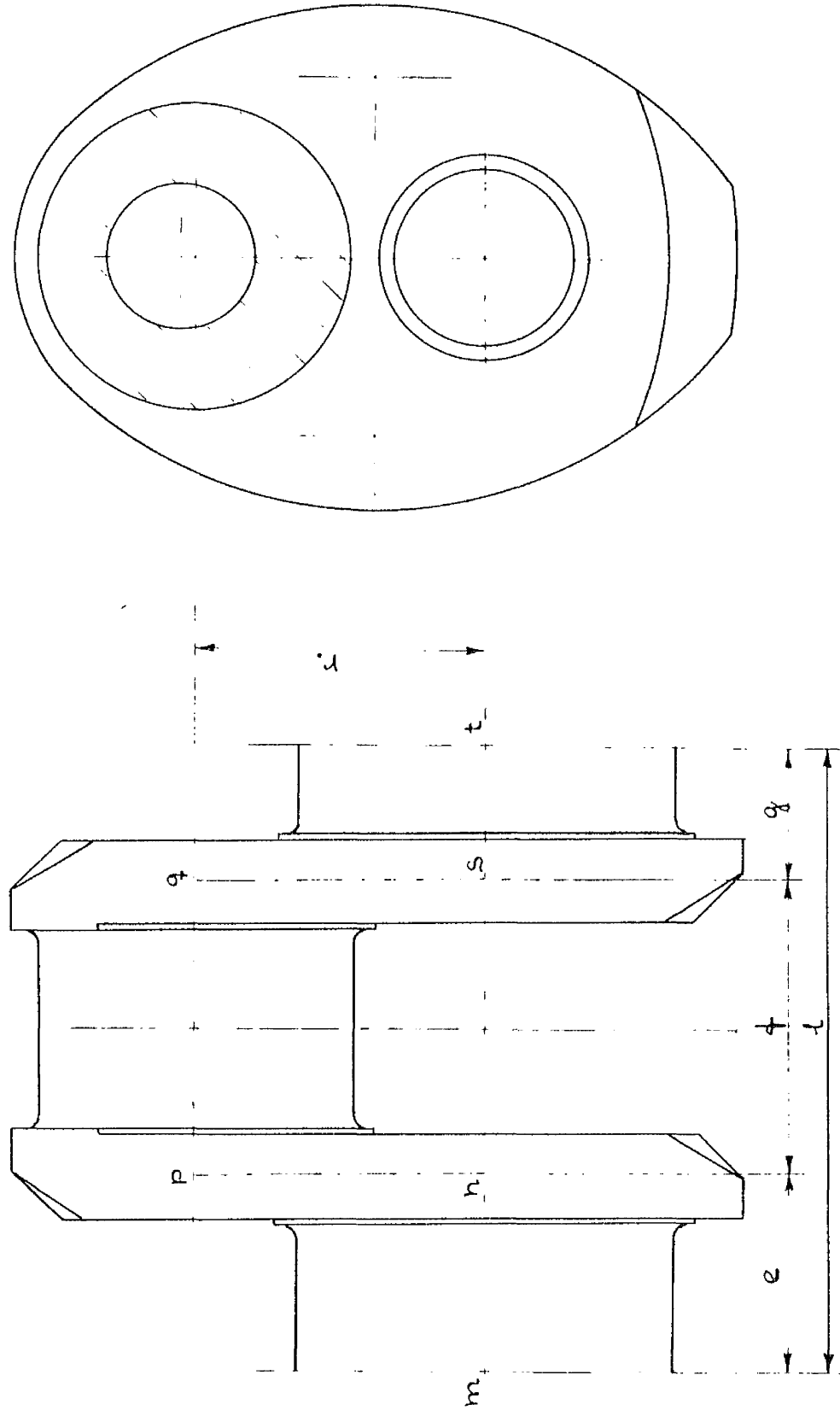
As a consequence of the above statement all lengths should remain unaltered through the initial reduction.

The size effects of the pin-web or journal-web junctions, the effect of fillet radii or other features which would affect the stiffness of the actual crank, must therefore be taken into account by proper adjustments of the rigidities of the reduced crank.

The main uncertainty in the initial reduction definitely arises from the behaviour of the junctions between the journals and the webs and the pins and the webs. However, a profound consideration of this topic has been given in the chapter: "Theoretical Analyses of Shrink-fitted Assemblies Loaded in Torsion.", which may be referred to for further consultations.

A further consideration which also may be of some importance rests on the fact that the torsional stiffness of

FIG. 1.



R.R.C. 60, NR. 51, CRANK NR. 1.

FIG. 2.

| CRANK NR. | 1 | 2 | 3 | 4 | 5 | 6 |
|-----------------------------------|-------------------------|-------|-------|-------|-------|-------|
| r in | 3 | 3 | 3 | 3 | 3 | 3 |
| e " | 2.119 | 1.482 | 1.482 | 2.170 | 1.482 | 1.482 |
| f " | 3.288 | 3.288 | 3.288 | 3.288 | 3.288 | 3.288 |
| g " | 1.482 | 1.482 | 2.170 | 1.482 | 1.482 | 2.119 |
| l " ^{1.)} | 6.889 | 6.252 | 6.94 | 6.94 | 6.252 | 6.889 |
| C ₁ lb in ² | 273.6 × 10 ⁶ | | | | | |
| C ₂ " | 25.1 " | | | | | |
| C ₃ " | 132.5 " | | | | | |
| B ₁ " | 318 " | | | | | |
| B ₂ " | 406.5 " | | | | | |
| B ₃ " | 18.7 " | | | | | |
| B ₄ " | 154 " | | | | | |

$$1. \quad l = e + f + g$$

DIMENSIONS OF REDUCED CRANK.

a crank is the most important of its characteristics. One should therefore aim at accurate representation, preferably as far as twist of crank-pin and journals and bending of the webs are concerned, at the expense of accuracy of the other characteristics, rather than vice versa.

Fig.1 shows a sketch of the actual crank, for which the numerical calculations are carried out. The lettering m-n-p-q-s-t indicates the reduced crank.

It is thought unnecessary to present the actual calculations, and therefore the results only are given in Fig.2. Since the cranks in the actual crankshaft vary slightly along the engine, this table presents complete figures for all the different cranks, and in that way gives all the required information for the next step in the calculations. (See Nomenclature for meaning of symbols.)

Single Crank.

This section will give a study of the behaviour of a single crank under the various types of loads which may be imposed on it. Bearing in mind that the single cranks which are treated will ultimately be linked together to form a multithrow crankshaft, it has been found most convenient to represent their elastic behaviour by means of deflection coefficients and the object of this section is really to

derive these.

Let us consider a crank loaded as shown in Fig.3. The axes of co-ordinates are chosen, such that the XY-plane coincides with that of the throw, and the Z-axis is so directed that rotation of a right-hand screw from Y to Z would produce motion in the positive direction of the X-axis.

The external forces acting on the throw are:-

1. The thrust of the connecting rod, centrifugal forces and vibrational forces.

It will be assumed that these forces can all be represented by two components, P and S, parallel to the Y- and Z- axis respectively.

2. The couple at the left-hand side of the crank.

This couple is resolved into three components, viz.-

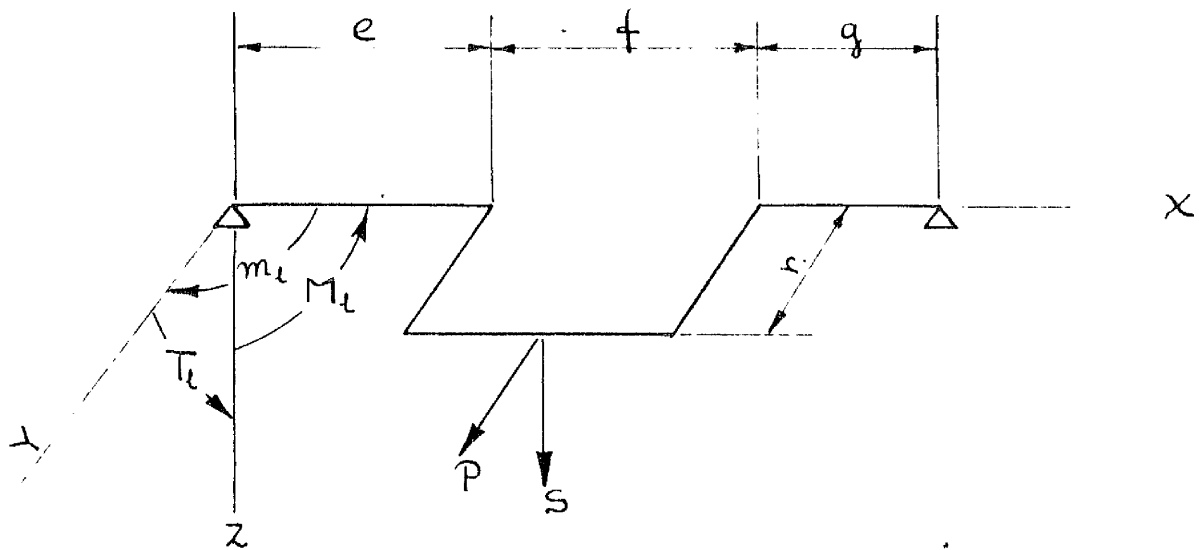
\underline{m}_1 = the bending moment in the plane of the throw,

\underline{M}_1 = the bending moment in the plane perpendicular to the plane of the throw and

\underline{I}_1 = the twisting moment.

It will also be necessary at a later stage to consider a couple at the right-hand side of the crank, the components of which will be given by:- \underline{m}_r , \underline{M}_r and \underline{I}_r .

FIG. 3.



LOAD SYSTEM ON SINGLE CRANK

The positive direction of the above moments is shown in Fig.3 by arrows.

The effects due to the above different groups of forces will now be analysed separately and the combined effect will be obtained by the method of superposition. In this manner, formulae necessary for the study of multi-throw crankshafts will be obtained.

Bending in the Plane of the Throw - Figure 4(a)

Let us consider the bending of the throw produced by the force P and a couple m_1 acting in the XY-plane at the left support. In order to make further development clear, the following rule of signs for couples and rotation of ends is adopted. The relation between the positive sense of the moment m_1 and the positive direction of the Z-axis is the same as that between rotation and translation of a right hand screw. The same rule is used in determining the sign of the angle of rotation of any cross-section of the journal. In accordance with this, the angle φ_1 (Fig.4(a)), representing the rotation of the left end is positive, and the angle φ_2 is negative.

The reactions A and B at the supports are as follows:

$$A = \frac{P(l + \frac{1}{2}l) - m_1}{l}$$

. . . 1.

$$B = \frac{P(e + \frac{t}{2}) + m_1}{l} \quad . . 2$$

The diagrams of bending moment for journals and crank-pin obtained as for a simply supported beam are given separately for different groups of forces in Fig.4(b) and (c). Since the effect of direct tension in the webs is small compared to that of twist and bending, it will be ignored. In discussing deformation the Grapho-Analytical method will be used⁽¹⁾.

The angles φ_1 and φ_2 of rotation of the supports of the throw will be calculated in terms of their component parts (φ'_1 , φ'_2) due to the force P , ($(\varphi'')_1$, $(\varphi'')_2$) due to the moment m_1 and ($(\varphi'')_r$, $(\varphi'')_r$) due to the moment m_r .

In the case of bending by the force P , the distributed imaginary load is represented in Fig.4(b) by the enclosed area. All the magnitudes required for further calculations are given on the diagram.

It is convenient at this stage to introduce the two deflection coefficients t_1 and t_2 , which are defined by the following equations:

$$\varphi'_1 = P t_1 \quad . . 3$$

(1) Applied Elasticity by Timoshenko and Lessels, first edition, 1925. Par.23, page 84.

$$\varphi_2' = -P t_2 \quad . . . 4.$$

Taking moments of the imaginary loading due to the force P on the crank about the support at B , the slope at A is readily found. Making use of equation (3) t_1 may then be expressed in terms of the crank dimensions as follows:

$$t_1 = \frac{1}{l^2} \left[\begin{array}{l} \frac{1}{B_4} \left\{ \frac{1}{3} (e + \frac{r}{2}) (g + \frac{r}{2})^3 \right. \\ \quad \left. + \frac{1}{2} (e + \frac{r}{2})^2 (g + \frac{r}{2}) (e/3 + 2\frac{r}{3} + g) \right. \\ \quad \left. - (\frac{1}{B_4} - \frac{1}{B_1}) \left\{ \frac{1}{3} (e + \frac{r}{2}) g^3 + \frac{1}{2} e^2 (g + \frac{r}{2}) (e/3 + r + g) \right\} \right. \\ \quad \left. \left. + \frac{1}{B_2} \{ e r (g + \frac{r}{2}) (r + g) + g^2 r (e + \frac{r}{2}) \} \right\} \right] \quad . . . 5.$$

Similarly an expression may be obtained for t_2 :

$$t_2 = \frac{1}{l^2} \left[\begin{array}{l} \frac{1}{B_4} \left\{ \frac{1}{3} (g + \frac{r}{2}) (e + \frac{r}{2})^3 \right. \\ \quad \left. + \frac{1}{2} (g + \frac{r}{2})^2 (e + \frac{r}{2}) (g/3 + 2\frac{r}{3} + e) \right\} \\ \quad \left. - (\frac{1}{B_4} - \frac{1}{B_1}) \left\{ \frac{1}{3} (g + \frac{r}{2}) e^3 + \frac{1}{2} g^2 (e + \frac{r}{2}) (g/3 + r + e) \right\} \right. \\ \quad \left. \left. + \frac{1}{B_2} \{ g r (e + \frac{r}{2}) (r + e) + e^2 r (g + \frac{r}{2}) \} \right\} \right] \quad . . . 6.$$

It should be noticed that the expressions for t_1 and t_2 are symmetrical, i.e. interchanging e and g in one of them gives the other.

Fig.4(c) shows the second type of loading applied to the single cranks when they are bent in the plane of the crank. To represent the behaviour of the crank in this case, it will be necessary to introduce the following three deflection coefficients α_1^l , α_1^r and α_2 , which are defined to be:

α_1^l = slope at A caused by unit bending moment applied at A .

α_1^r = slope at B caused by unit bending moment applied at B .

α_2 = slope at B caused by unit bending moment applied at A , or the slope at A caused by unit bending moment applied at B⁽¹⁾.

Making use of the information given in Fig.4(c), the three above deflection coefficients are readily obtained in terms of the crank dimensions as shown by the following equations:

$$\alpha_1^l = \frac{1}{l^2} \left[\frac{l^3}{3B_1} + \left(\frac{1}{B_2} - \frac{1}{B_1} \right) \frac{1}{3} \{ (l+g)^3 - g^3 \} + \frac{1}{B_2} \{ (l+g)^2 r + g^2 r \} \right] \dots 7.$$

- (1) It follows from "Rayleigh's Reciprocal Theorem" that the slope at A caused by unit bending moment applied at B is equal to the slope at B caused by unit bending moment applied at A .

See: The Escalator Method in Engineering Vibration Problems, by Joseph Morris; Chapter 7, p.73.

$$\alpha_1^r = \frac{1}{l^2} \left[\begin{array}{c} \frac{l^3}{3B_1} \\ + (\frac{1}{B_4} - \frac{1}{B_1}) \frac{1}{3} \{ (\frac{1}{2} + e)^3 - e^3 \} \\ + \frac{1}{B_2} \{ (\frac{1}{2} + e)^2 r + e^2 r \} \end{array} \right] \dots 8.$$

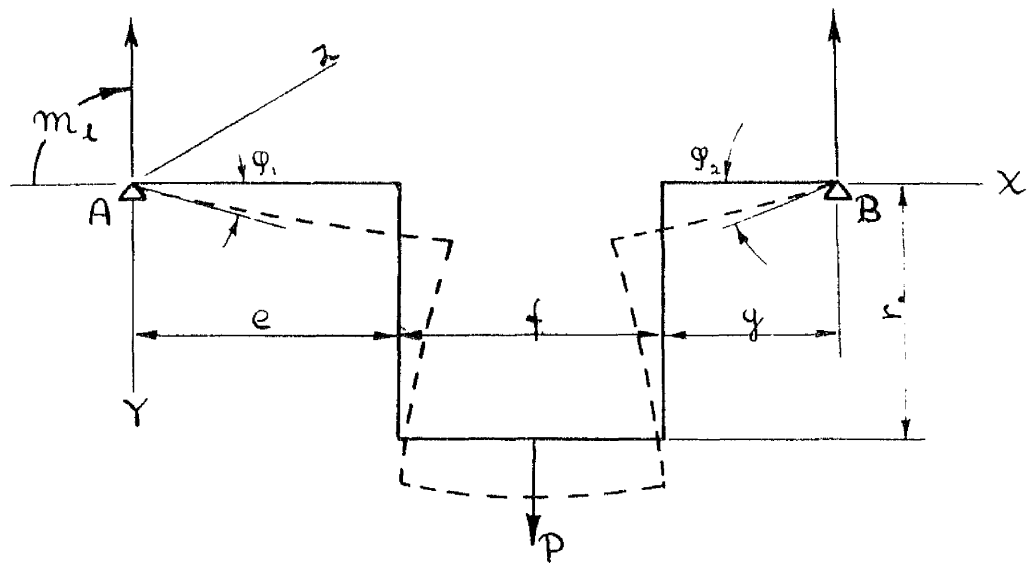
$$\alpha_2 = \frac{1}{l^2} \left[\begin{array}{c} \frac{l^3}{6B_1} \\ + (\frac{1}{B_4} - \frac{1}{B_1}) \frac{1}{2} \{ (\frac{1}{2} + g)^2 (e + \frac{1}{3}g) - g^2 (e + \frac{1}{2} + \frac{1}{3}g) \} \\ + \frac{1}{B_2} \{ (\frac{1}{2} + g)er + (\frac{1}{2} + e)gr \} \end{array} \right] \dots 9.$$

Expressions for all the required deflection coefficients for a representation of the behaviour of a single crank when subjected to the most common loads of bending in the plane of the crank, have now been derived. Through the formulae given any of these deflection coefficients which may be required, can easily be calculated, and hence the effect of the corresponding load may be obtained.

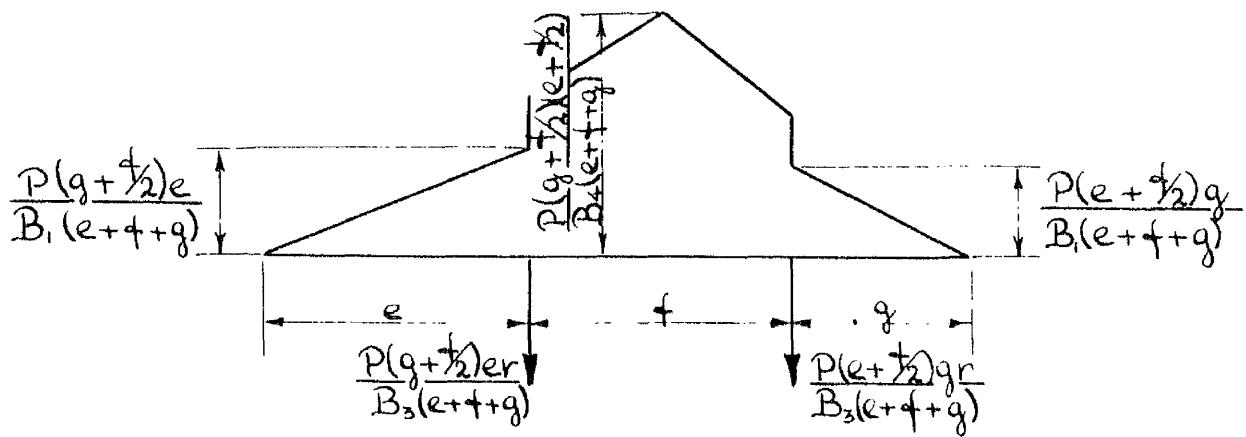
The total values for the end slopes are thereafter simply obtained through an algebraic summation of the slopes caused by the various load components.

For the angles φ_1 and φ_2 , which are the total angles of rotation of the cross-sections of the crank at

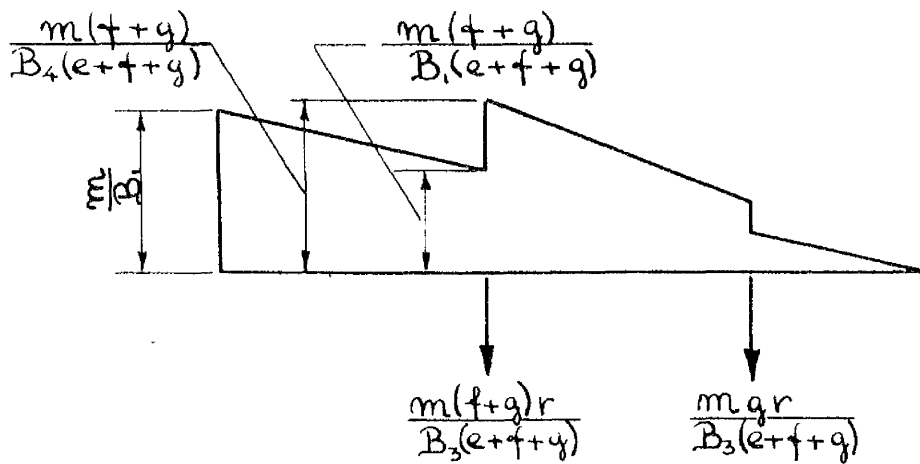
FIG. 4.



(a)



(b)



(c)

BENDING IN THE X-Y-PLANE.

the supports A and B respectively, the following equations therefore hold:

$$\underline{\varphi_1 = m_1 \alpha_1^l - m_r \alpha_2 + P_{t_1}} \quad . . . 10$$

$$\underline{\varphi_2 = -(m_1 \alpha_2 - m_r \alpha_1^r + P_{t_2})} \quad . . . 11$$

Bending in the Plane Perpendicular to the Plane of the
Throw. (Fig.5 (a)).

The bending of the throw by the force S , parallel to the Z-axis, and, further, a couple M acting in the XZ-plane, is now to be considered.

The reactions at the supports A and B are given by equations (12) and (13) respectively:

$$\underline{A = \frac{M + S(g + \frac{1}{2})}{l}} \quad . . . 12$$

$$\underline{B = \frac{-M + S(e + \frac{1}{2})}{l}} \quad . . . 13$$

In addition to the above reactions, a moment $Sr/2$, about the X-axis is applied at each support to prevent rotation under the action of the force S .

For the angles of rotation produced by the force S the imaginary loading is shown by Fig.5(b). Two deflection coefficients μ_1 and μ_2 as defined by the

following equations, will be introduced:

$$\underline{\psi_1'} = \underline{\mu_1 S} \quad . . . 14$$

and

$$\underline{\psi_2'} = - \underline{\mu_2 S} \quad . . . 15$$

$\underline{\psi_1'}$ and $\underline{\psi_1''}$ represent the components of the angle of rotation of the cross-section of the crank at the support A, caused by S and M respectively.

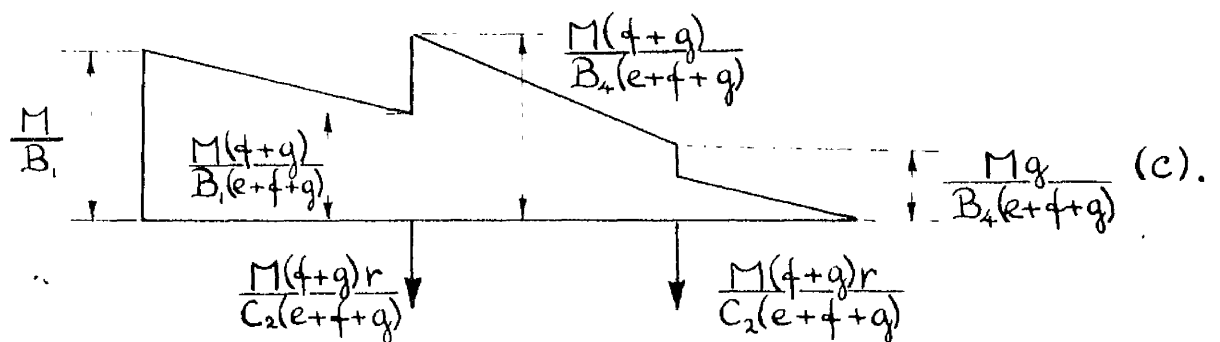
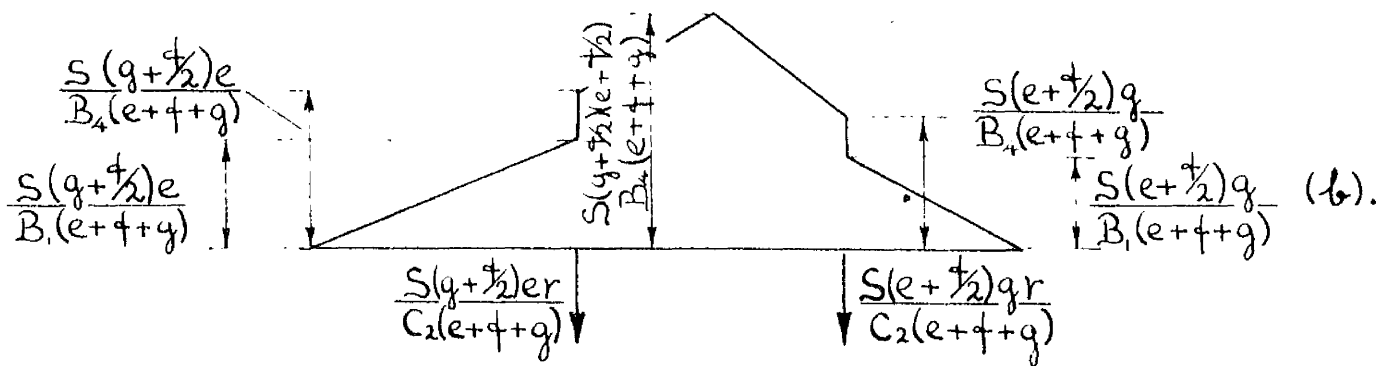
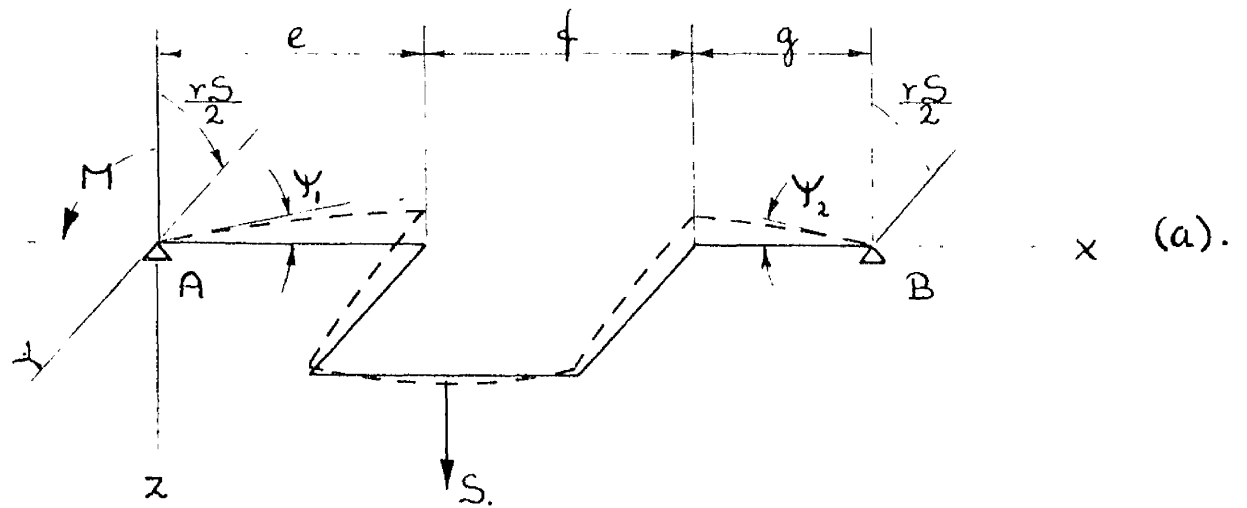
$\underline{\psi_2'}$ and $\underline{\psi_2''}$ represent the components of the angle of rotation of the cross-section of the crank at the support B, caused by S and M respectively.

$\underline{\psi_1}$ and $\underline{\psi_2}$ give the total angles of rotation of the cross-sections at A and B respectively.

Expressions for the deflection coefficients required to represent the crank when loaded in bending in the plane perpendicular to the plane of the throw, are most easily obtained by a comparison with the case of bending in the plane of the throw. Comparing Fig.4(b) and (c) with Fig.5(b) and (c) it is readily seen that the diagrams of the imaginary loading are exactly similar, if $\underline{B_2}$ in Fig.4 is replaced by $\underline{C_2}$ or vice versa.

For the deflection coefficients $\underline{\mu_1}$ and $\underline{\mu_2}$ we may therefore write directly from equations (5) and (6)

FIG. 5.



BENDING IN THE XZ-PLANE.

the following expressions:

$$u_1 = \frac{1}{l^2} \left[\begin{array}{l} \frac{1}{B_4} \left\{ \frac{1}{3} (e + \frac{1}{2}l) (g + \frac{1}{2}l)^3 \right. \\ \frac{+ \frac{1}{2} (e + \frac{1}{2}l)^2 (g + \frac{1}{2}l) (e/3 + 2\frac{1}{3}l + g) \left. \right\}}{-(\frac{1}{B_4} - \frac{1}{B_1}) \left\{ \frac{1}{3} (e + \frac{1}{2}l) g^3 + \frac{1}{2} e^2 (g + \frac{1}{2}l) (e/3 + g + \frac{1}{2}l) \right\}} \\ \frac{+ \frac{1}{C_2} \{ cr (g + \frac{1}{2}l) (l + g) + g^2 r (e + \frac{1}{2}l) \}} \end{array} \right] \dots 16$$

and

$$u_2 = \frac{1}{l^2} \left[\begin{array}{l} \frac{1}{B_4} \left\{ \frac{1}{3} (g + \frac{1}{2}l) (e + \frac{1}{2}l)^3 \right. \\ \frac{+ \frac{1}{2} (g + \frac{1}{2}l)^2 (e + \frac{1}{2}l) (e + 2\frac{1}{3}l + g/3) \left. \right\}}{-(\frac{1}{B_4} - \frac{1}{B_1}) \left\{ \frac{1}{3} (g + \frac{1}{2}l) e^3 + \frac{1}{2} g^2 (e + \frac{1}{2}l) (e + l + g/3) \right\}} \\ \frac{+ \frac{1}{C_2} \{ gr (e + \frac{1}{2}l) (e + l) + e^2 r (g + \frac{1}{2}l) \}} \end{array} \right] \dots 17$$

The case of the bending moment M is more complicated than the previous two. The angles of rotation of the ends are now not only affected by the angular deformation of different parts of the throw in the plane of M , but also by the deflection of the webs and the twist of the crankpin.

As for the case of bending in the plane of the crank by a moment m , three deflection coefficients denoted by β_1^l , β_1^r and β_2 , and defined as follows, will be required.

$\underline{\beta}_1^1$ = slope at A caused by unit bending moment applied at A .

$\underline{\beta}_1^r$ = slope at B caused by unit bending moment applied at B .

$\underline{\beta}_2$ = slope at B caused by unit bending moment applied at A , or vice versa.

The angles of rotation of the ends due to angular deformations of the various parts of the crank are obtained for unit moment by replacing \underline{B}_2 by \underline{C}_2 in the equations (7), (8) and (9).

The effect of the deflection of the webs, and the twist of the crankpin is most readily obtained from Fig.6, which shows these latter crank-deformations largely exaggerated. From the figure it is seen that:

$$\underline{y}_1''' = \underline{y}_2''' = \delta/l \quad . . . 18$$

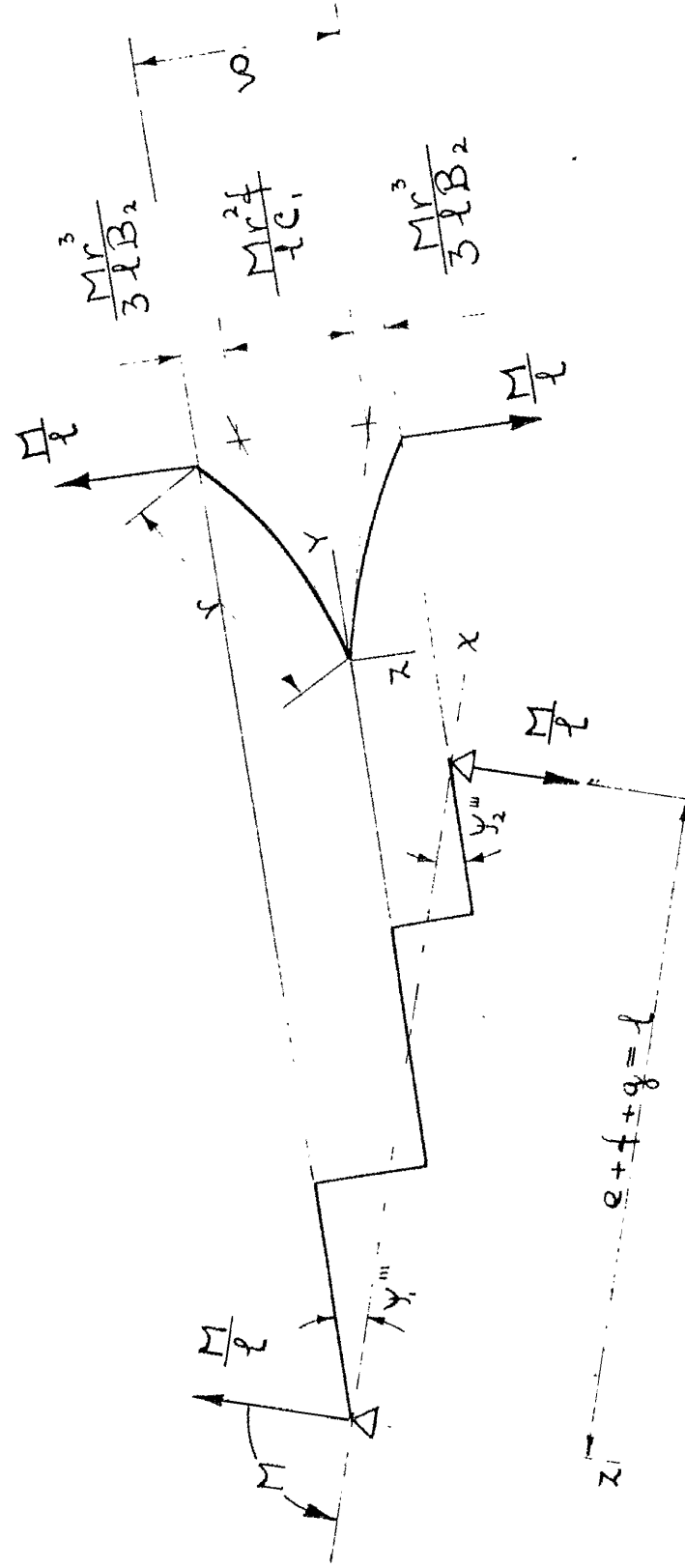
and hence

$$\underline{y}_1''' = \underline{y}_2''' = \frac{1}{l^2} \left\{ \frac{2r^3}{3B_2} + \frac{r^3}{C_3} \right\} M \quad . . . 19$$

Making use of the above equations, the three required deflection coefficients can therefore be written in terms of the crank dimensions as follows:

$$\beta_1^1 = \frac{1}{l^2} \left[\begin{array}{c} \frac{l^3}{3B_1} + \frac{2r^3}{3B_2} \\ + (\frac{1}{B_2} - \frac{1}{B_1}) \frac{1}{3} \{ (q+r)^3 - q^3 \} \\ + \frac{1}{C_3} \{ (q+r)^2 r + q^2 r \} + \frac{r^3}{C_3} \end{array} \right] \quad . . . 20$$

FIG. 6.



BENDING IN THE XZ-PLANE.

$$\beta_1^r = \frac{1}{l^2} \left[\begin{array}{c} \frac{l^3}{3B_1} + \frac{2r^3}{3B_2} \\ \hline + (\frac{1}{B_2} - \frac{1}{B_1}) \frac{1}{3} \{ (l+e)^3 - e^3 \} \\ \hline + \frac{1}{C_2} \{ (l+e)^2 r + e^2 r \} + \frac{r^3}{C_2} \end{array} \right] \dots 21$$

$$\beta_2 = \frac{1}{l^2} \left[\begin{array}{c} \frac{l^3}{6B_1} - \frac{2r^3}{3B_2} \\ \hline + (\frac{1}{B_2} - \frac{1}{B_1}) \frac{1}{2} \{ (l+g)^2 (e + \frac{l+g}{3}) - g^2 (e + l + \frac{g}{3}) \} \\ \hline \frac{1}{C_2} \{ (l+g)er + (l+e)gr - \frac{r^3}{C_2} \} \end{array} \right] \dots 22$$

The total value of the end slopes for a crank subjected to bending in the plane perpendicular to the plane of the throw can now be obtained through an algebraic summation of all the component effects. Remembering the definitions of the deflection coefficients, and the sign-convention, the following two equations may be written:-

$$\underline{Y_1 = \beta_1^l M_l - \beta_2 M_r - u_1 S} \dots 23$$

$$\underline{Y_2 = -\beta_2 M_l + u_2 S + \beta_1^r M_r} \dots 24$$

Twist of Simply Supported Throw.

Fig.7 is a diagrammatic representation of a throw twisted by the moment \underline{T} applied at the middle cross-section of the journals. As before, the dotted lines

represent the deformed crankshaft. The total twist consists of the sum of the deformations of the portions e. and g. of the journals, of the crankpin, and of the two webs. Now, if θ_1 and θ_2 are angles of twist of the journals, and θ_3 of the crankpin, respectively,

$$\theta_1 = \frac{T_e}{C_1}, \quad \theta_2 = \frac{T_g}{C_1} \quad \text{and} \quad \theta_3 = \frac{T_f}{C_2}$$

Further, the bending of each web produces the angular displacement θ_4 equal to the angles between the tangents to the curve of flexure at its ends. The bending moment is equal to the twisting moment T . Since the moment at each cross-section is constant, the curve of flexure of the web is a circle. Considering it as a beam of length r ,

$$\theta_4 = \frac{Tr}{B_2}$$

The total relative angular displacement θ , measured between the middle sections of the journals, will be the sum of the above components.

A deflection coefficient w will now be introduced such that:-

$$\theta = Tw \quad . . . 25$$

Using the above relations, w can be expressed in terms of the crank dimensions as follows:

$$w = \frac{e+g}{C_1} + \frac{f}{C_2} + \frac{2r}{B_2} \quad . . . 26$$

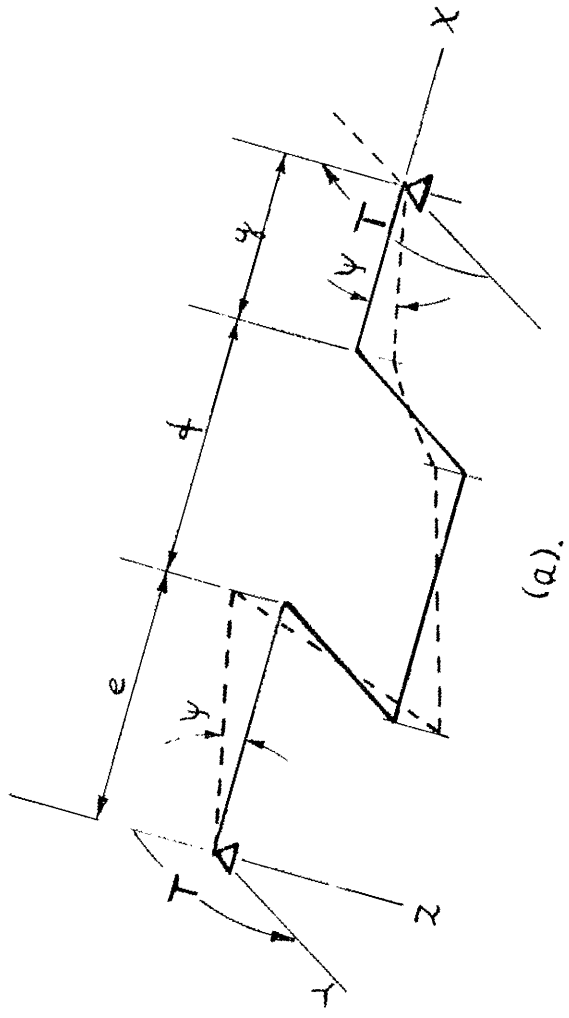
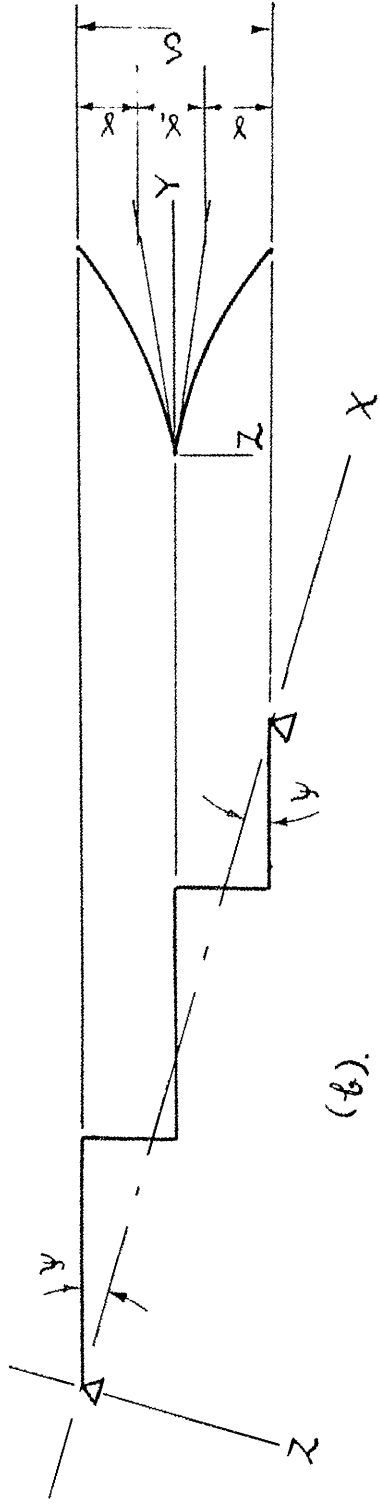


FIG. 7.



TWISTING OF CRANK.

The couple T produces not only the twist θ , but also a rotation ψ of the terminal cross-sections about the Y - and the Y' axis. This rotation, due to the bending of the webs and the twist of the crankpin (Fig.7 (b)), is given by the following equation:-

$$\psi = \frac{\delta}{l}$$

δ is a deflection as indicated in Fig.7(b).

The flexure of the web produces a deflection,

$$\gamma = \frac{Tr^2}{2B_2}$$

and the deflection due to the twist of the crankpin is,

$$\gamma_1 = \frac{Tr}{C_2}$$

The deflection coefficient s as defined by the following equation will be introduced:-

$$\psi = Ts \quad \dots 27$$

From the above equations it is readily shown that this deflection coefficient can be expressed in terms of the crank dimensions as follows:-

$$s = \frac{1}{l} \left\{ \frac{r^2}{B_2} + \frac{r}{C_2} \right\} \quad \dots 28$$

Now, the twist of the throw produced by the moment M of Fig.5(a) can easily be found. Denoting this twist by θ_0 , and applying the "Reciprocal Theorem" to the cases of Figs.5(a) and 7(a), it is found that:-

$$M\psi = T\theta_0$$

and, employing (27) and (28)

$$\theta_o = M_s \quad . . . 29$$

~~This twist is in the direction of the twisting couple~~
 This twist is in the direction of the twisting couple \underline{T} of Fig.7(a). When there are two bending moments, \underline{M}_l and \underline{M}_r , one at each support, the corresponding twist is obtained in the same manner and will be equal to:-

$$\theta_o = (M_l + M_r)s \quad . . . 29a$$

If, in the case of Fig.5(a), M be made equal to zero and in Fig.7(a) the moment $(T + Sr/2)$ be substituted for T , the combination of these two cases gives the case shown in Fig.8.

In the further development of the subject the values of the angles $\underline{\psi}_1'''$ and $\underline{\psi}_2'''$, Fig.8, are necessary. Using equations (23), (24) and (27) we get:-

$$\underline{\psi}_1''' = (T + \frac{Sr}{2})s - \mu_s S$$

$$\underline{\psi}_2''' = (T + \frac{Sr}{2})s + \mu_s S$$

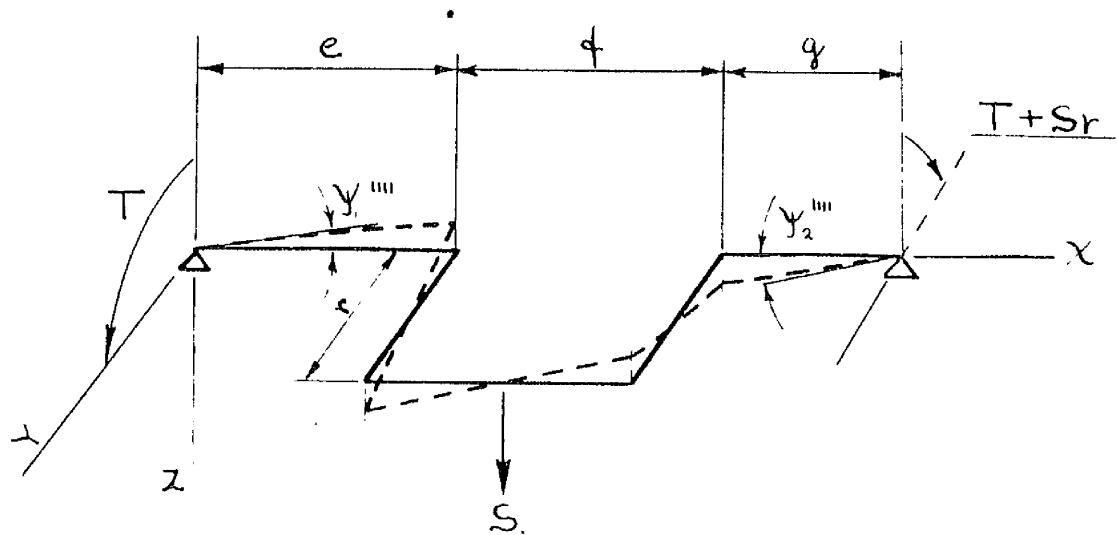
The above two equations may be written as follows:-

$$\underline{\psi}_1''' = T_s - \eta_s S \quad . . . 30$$

$$\underline{\psi}_2''' = T_s + \eta_s S \quad . . . 31$$

The two new deflection coefficients $\underline{\eta}_1$ and $\underline{\eta}_2$, are expressed in terms of the crank dimensions by means of

FIG. 8.



TWISTING AND BENDING OF CRANK.

the following equations:-

$$\eta_1 = -\frac{sr}{2} + u_1 \quad . . . 32$$

$$\eta_2 = \frac{sr}{2} + u_2 \quad . . . 33$$

The deflection coefficients u_1 and u_2 , are obtained from equations (16) and (17). s is obtained from equation (28).

This completes the treatment of a single crank as formulae have been derived for all the deflection coefficients which are required for the subsequent treatment of a multi-throw crankshaft.

Fig.9 gives the numerical values of these deflection coefficients as obtained for the various cranks in the crankshaft of the six cylinder diesel engine (RR. C. 60.).

FIG. 9.

| CRANK NR. | 1 | 2 | 3 | 4 | 5 | 6 |
|---|-------|--------|-------|-------|--------|-------|
| $t_1 \frac{1}{lb} \times 10^6$ | .146 | .133 | .169 | .151 | .133 | .166 |
| t_2 " | .166 | .133 | .151 | .169 | .133 | .146 |
| $\alpha_1^l \frac{1}{lb.in.} \times 10^6$ | .0937 | .112 | .126 | .0928 | .112 | .1242 |
| α_1^p " | .1242 | .112 | .0928 | .126 | .112 | .0937 |
| α_2 " | .0674 | .0638 | .0675 | .0675 | .0638 | .0674 |
| $\mu_1 \frac{1}{lb.} \times 10^6$ | .113 | .103 | .131 | .117 | .103 | .128 |
| μ_2 " | .128 | .103 | .117 | .131 | .103 | .113 |
| $\beta_1^l \frac{1}{lb.in} \times 10^6$ | .0775 | .0929 | .102 | .0772 | .0929 | .101 |
| β_1^p " | .101 | .0929 | .0772 | .102 | .0929 | .0775 |
| β_2 " | .0461 | .0422 | .0463 | .0463 | .0422 | .0461 |
| w " | .0528 | .0504 | .0529 | .0529 | .0504 | .0528 |
| s " | .0140 | .0155 | .0139 | .0139 | .0155 | .0140 |
| $\eta_1 \frac{1}{lb.} \times 10^6$ | +.092 | +.0792 | +.110 | +.096 | +.0792 | +.107 |
| η_2 " | .149 | .126 | .138 | .152 | .126 | .134 |

DEFLECTION COEFFICIENTS FOR

CRANKSHAFT OF R.R.C.60, NR.51.

II. MULTI-THROW CRANKSHAFT

General Case.

Let us now consider a crankshaft with many throws, a portion of which is shown in Fig. 10.

The bearing constraints are assumed to be equivalent to simple supports at the middle cross-sections of the journals, i.e. the crankshaft is free to move directionally whereas no lateral movement is permitted.

The supports will be numbered 1, 2, 3, i, etc., and the throws similarly, such that the throw lying between the supports $i-1$ and i will be the $(i-1)$ th throw. All external forces acting on a throw, and all deflection coefficients applying to a throw will carry the same subscript as that throw. The bending moments which act between the throws where they are joined together at the supports are loads, internal to the crankshaft considered as a whole. These moments will be given suffices which are the same as the number of the support at which they act. If the above moments act on the throw to the left of the support, they will also be given a subscript 1 and, similarly, if they act on the throw to the right of the

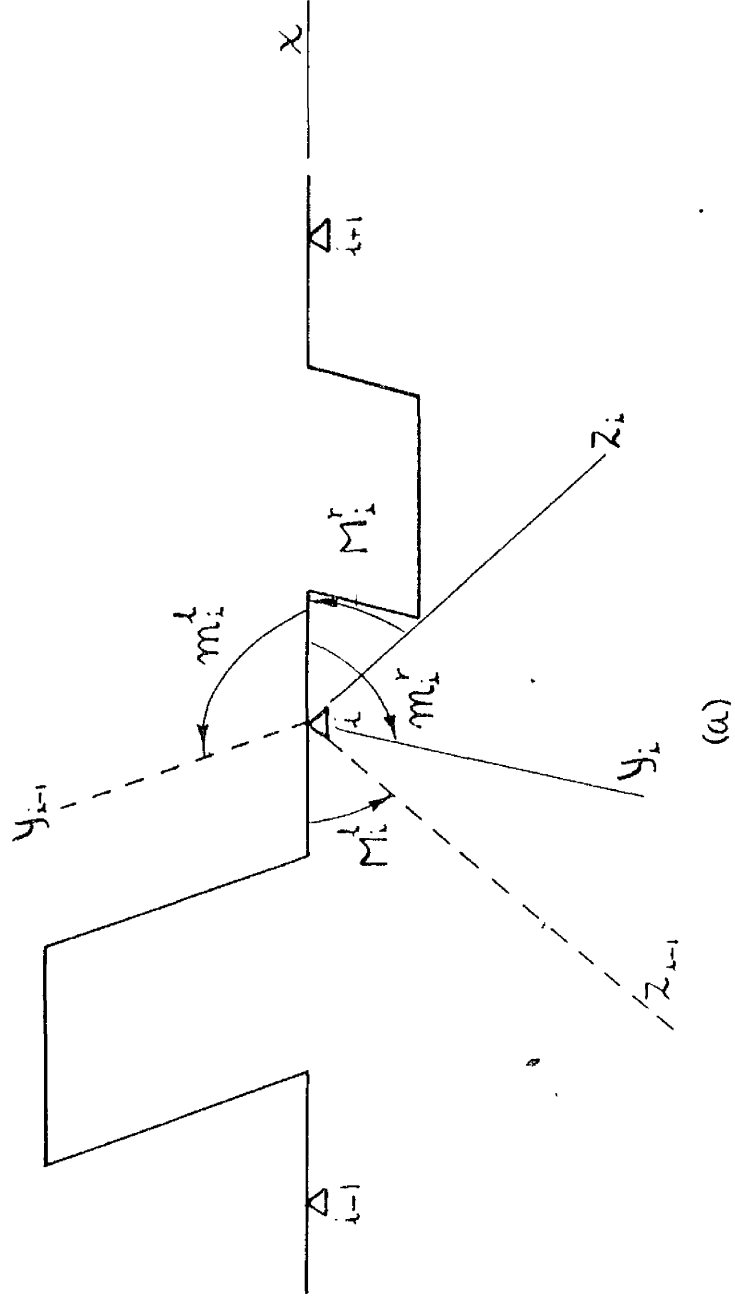
support the subscript r will be used⁽¹⁾.

When the twisting and bending moments at every support are known, it is easy to calculate the deformations of any throw from equations given in the foregoing chapter. The twisting moment at any support can be calculated without difficulty from the equations of statics. For calculating the bending moments, the condition of continuity of the elastic curve at the supports must be taken into consideration. In Fig.10, two consecutive throws cut out of a multi-throw crankshaft and having supports $i-1$, i , and $i+1$, are represented. The bending moment at the support i is resolved twice into two components, namely the components \underline{m}_i^l and \underline{M}_i^l , when the throw on the left of the support i is considered, and the components \underline{m}_i^r and \underline{M}_i^r for the throw on the right of the support i .

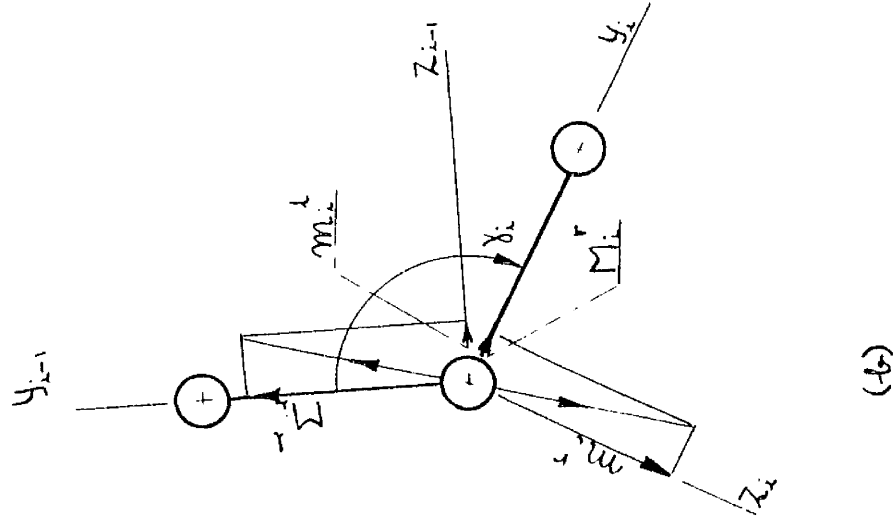
As before, \underline{m} denotes bending moments in the plane of the throw considered, and \underline{M} bending moments in the plane perpendicular to the plane of the throw. The positive directions of these moments are shown in Fig.10(a). The

(1) This notation deviates somewhat from the one used in the previous chapter as, for instance, the bending moment which is applied at the right hand end to the $(i-1)$ th throw in the plane of the throw would previously be denoted by \underline{m}_{i-1}^r as against \underline{m}_i^l in the new notation. The new notation has been introduced, since, in the following work, the main attention is directed towards the throw-junctions rather than the actual throws.

FIG. 10.



(a)



(b)

ADJACENT THROWS.

representation of the same moments by vectors is given in Fig.10(b). As there are no other moments acting, the resultant of $\underline{m_i^l}$ and $\underline{M_i^l}$ must be equal and opposite to the resultant of $\underline{m_i^r}$ and $\underline{M_i^r}$. Therefore, denoting by $\underline{\gamma_i}$ the angle between the consecutive throws at i , and resolving the couples in the directions $\underline{Y_{i-1}}$ and $\underline{Z_{i-1}}$, the following two equations are obtained (1);--

$$\underline{M_i^l + M_i^r \cos \gamma_i - m_i^l \sin \gamma_i = 0} \quad . . . \quad 34$$

$$\underline{m_i^l + M_i^r \sin \gamma_i + m_i^r \cos \gamma_i = 0} \quad . . . \quad 35$$

Two more equations are obtained from the conditions of continuity. Consider the throw on the left of the support i . The positive directions of all the forces and couples acting on this throw are shown in Fig.11. Denote by $\underline{\varphi_i^l}$ and $\underline{\gamma_i^l}$ the angles of rotation of the cross-section at the support i about the $\underline{Z_{i-1}}$ and $\underline{Y_{i-1}}$ axis, respectively (2). The same rule holds for the signs of the angles as before.

The above angles can be expressed in terms of the loads on the $(i-1)$ th throw and its deflection coefficients. Using equation (11) we obtain:--

$$\underline{\varphi_i^l = m_{i-1}^l \alpha_{i-1} - m_{i-1}^r \alpha_{i-1} - P_{i-1} \alpha_{i-1}} \quad . . . \quad 36$$

- (1) Looking on the front end of the crankshaft the angle $\underline{\gamma_i}$ is measured positive in the clock-wise direction.
- (2) The same rule as applied to the suffices of the moments also applies to the suffices of the angular deflections.

where \underline{t}_2 , $\underline{\alpha}_1^r$ and $\underline{\alpha}_2$ are given by the equations (6), (8) and (9) respectively.

In the same manner, by using equations (24) and (31), i.e. by putting S equal to zero in equation (24) and adding the two equations, we obtain:-

$$\underline{Y}_i^t = M_i^t \beta_{i(i-1)}^r - M_{i(i-1)}^r \beta_{2i(i-1)} + \overline{T}_{i(i-1)} S_{i(i-1)} + S_{i(i-1)} \eta_{2i(i-1)} \dots 37$$

where $\underline{\beta}_1^r$, $\underline{\beta}_2$, \underline{S} and $\underline{\eta}_2$, are given by the equations (21), (22), (28) and (33) respectively.

Considering now the throw on the right of the support i and denoting by $\underline{\varphi}_i^r$ and \underline{Y}_i^r the angles of rotation of the cross-section at i about the \underline{Z}_i - and \underline{Y}_i - axis of this throw, the following equations are obtained in the same manner as above:-

$$\underline{\varphi}_i^r = m_i^r \alpha_i^t - m_{i(i+1)}^t \alpha_{2i} + P_i t_{i,i} \dots 38$$

$$\underline{Y}_i^r = M_i^r \beta_{2i}^t - M_{i(i+1)}^t \beta_{2i} + \overline{T}_{i(i+1)} S_i - S_i \eta_{2i} \dots 39$$

Here, \underline{T}_i which is equal to $\overline{T}_{i(i+1)} + S_{i(i+1)} r$, represents the twisting moment at the support i , and the coefficients \underline{t}_1 , $\underline{\alpha}_1^t$, $\underline{\beta}_1^t$ and $\underline{\eta}_1$ are given by the equations (5), (7), (20) and (32) respectively.

The small angles of rotation calculated from (36), (37), (38) and (39) can be represented by vectors whose directions coincide with the directions of the corresponding

FIG. 11.

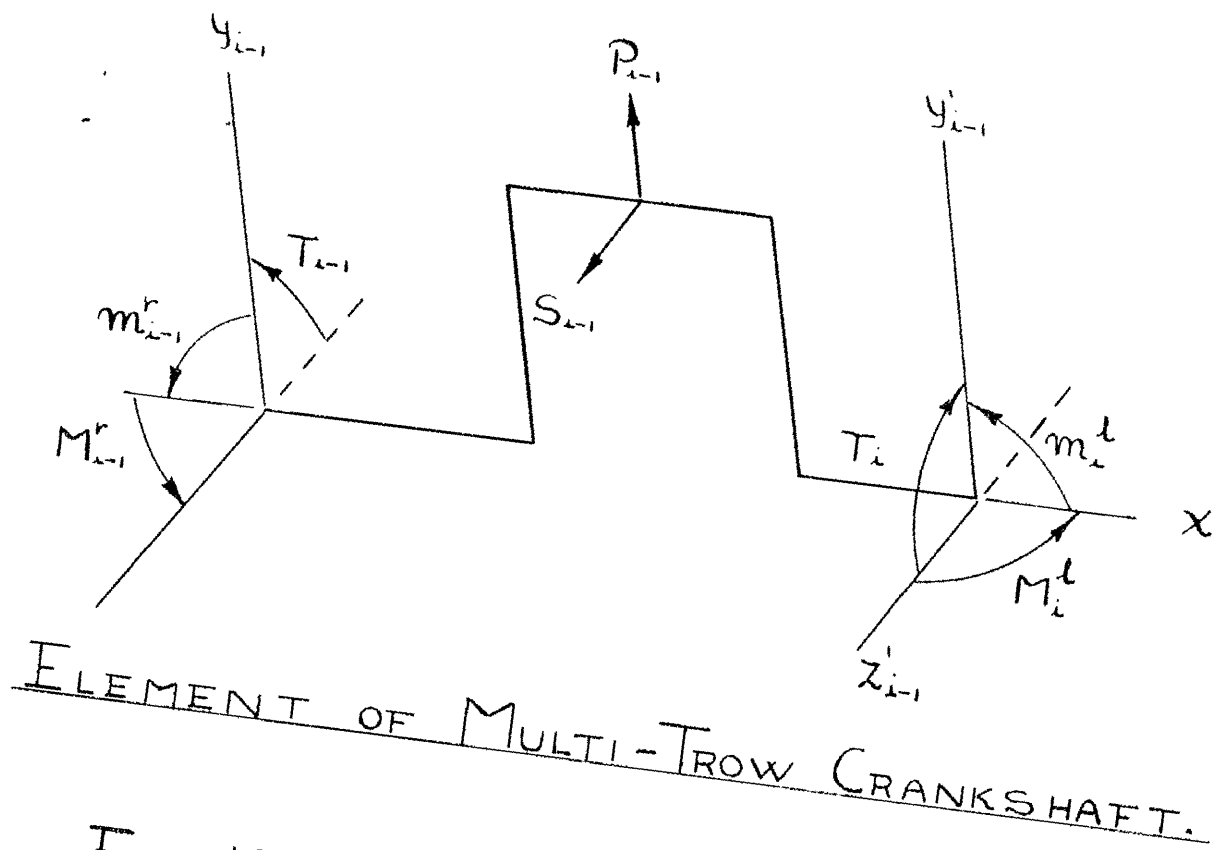
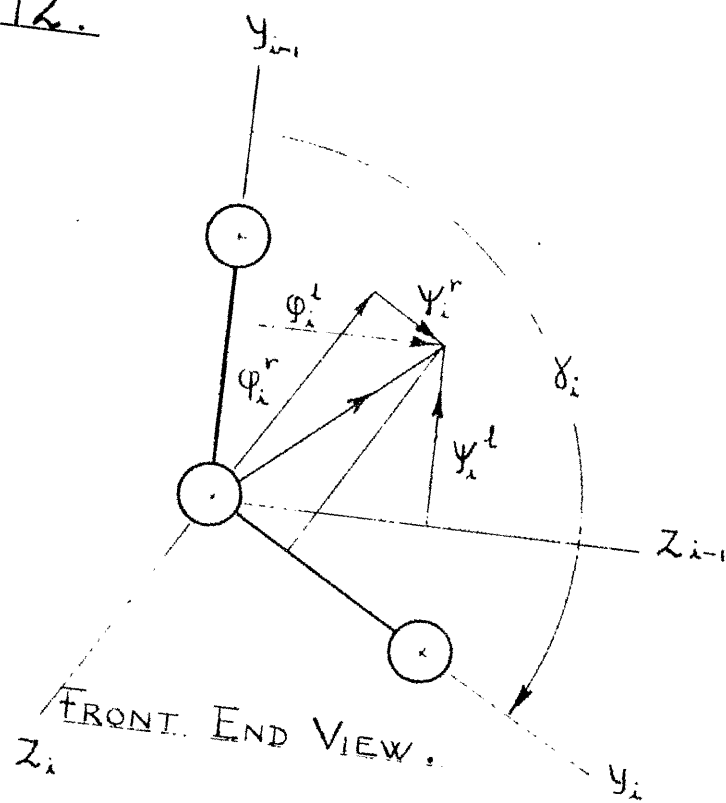


FIG. 12.



CONDITION OF CONTINUITY AT SUPPORT.

axis of rotation⁽¹⁾, and whose magnitudes are proportional to the corresponding angles of rotation, (Fig.12). Now, as φ_i^l and ψ_i^l on one side and φ_i^r and ψ_i^r on the other represent the rotations of the same cross-section of the journal at the support i , the resultant rotation of φ_i^l and ψ_i^l must be equal to that of the rotations φ_i^r and ψ_i^r as shown in Fig.12.

From Fig.12 the following two equations are obtained:--

$$\varphi_i^l = \varphi_i^r \cos \chi_i + \psi_i^r \sin \chi_i \quad \dots 40$$

$$\psi_i^l = -\varphi_i^r \sin \chi_i + \psi_i^r \cos \chi_i \quad \dots 41$$

Substituting from equations (36), (38) and (39) in (40) an equation which relates the various bending moments at the support i is obtained. After some rearrangement this equation may be written:--

$$\begin{aligned} & m_i^l \alpha_{i(i-1)}^r - m_{i(i-1)}^r \alpha_{2i(i-1)} + m_{i(i-1)}^l \alpha_{2i} \cos \chi_i - m_i^r \alpha_{i2}^l \cos \chi_i \\ & + m_{i(i-1)}^l \beta_{2i} \sin \chi_i - m_i^r \beta_{2i}^l \sin \chi_i = P_{i(i-1)} t_{2i(i-1)} \\ & + P_i t_{2i} \cos \chi_i + (\bar{T}_i S_i - S_i \bar{T}_i) \sin \chi_i \end{aligned} \quad \dots 42$$

Similarly, by making use of equations (37), (38) and (39) in (41) and rearranging we obtain:--

- (1) There exists between the positive direction of the axis of rotation and the direction of rotation the same relation as between rotation and translation in a right-hand screw.

$$\begin{aligned}
& \underline{m_i^l \alpha_i^l \sin \gamma_i - m_{(i-1)}^l \alpha_i \sin \gamma_i + M_i^l \beta_{(i-1)}^r - M_{(i-1)}^r \beta_{2(i-1)}} \\
& + M_{(i-1)}^l \beta_{2i} \cos \gamma_i - M_i^r \beta_{2i}^l \cos \gamma_i = -T_{(i-1)} S_{(i-1)} - S_{(i-1)} \eta_{(i-1)} \quad \dots 43 \\
& - P_{2i} \sin \gamma_i + (T_i S_i - S_i \eta_i) \cos \gamma_i
\end{aligned}$$

These two above equations together with equations (34) and (35) form a system of four equations for the support i . Analogous equations can be written for all the supports of the multi-throw crankshaft. In this way a number of equations equal to the number of unknown quantities $\underline{m_i^l}$, $\underline{m_i^r}$, $\underline{M_i^l}$ and $\underline{M_i^r}$, are obtained, as $i = 1, 2, 3, \dots, n$, and n is the number of supports.

When $\underline{\gamma_{(i-1)}}$, $\underline{\gamma_i}$ and $\underline{\gamma_{(i+1)}}$ are all different from zero, equations (34) and (35) will enable us to express $\underline{m_i^l}$ and $\underline{m_i^r}$ in terms of $\underline{M_i^l}$ and $\underline{M_i^r}$. The following four equations may therefore be written down:-

$$\underline{m_i^l = -\frac{M_i^r + M_i^l \cos \gamma_i}{\sin \gamma_i}} \quad \dots 44$$

$$\underline{m_i^r = \frac{M_i^l + M_i^r \cos \gamma_i}{\sin \gamma_i}} \quad \dots 45$$

$$\underline{m_{(i-1)}^r = \frac{M_{(i-1)}^l + M_{(i-1)}^r \cos \gamma_{(i-1)}}{\sin \gamma_{(i-1)}}} \quad \dots 46$$

$$\underline{m_{(i+1)}^l = -\frac{M_{(i+1)}^r + M_{(i+1)}^l \cos \gamma_{(i+1)}}{\sin \gamma_{(i+1)}}} \quad \dots 47$$

Making use of equations (44), (45), (46) and (47) equation (42) may be written as follows:-

$$\begin{aligned}
& - \frac{\alpha_{2(i-1)}^l}{\sin \gamma_{(i-1)}} M_{(i-1)}^l - \frac{\alpha_{2(i-1)}^r \cos \gamma_{(i-1)}}{\sin \gamma_{(i-1)}} M_{(i-1)}^r - \left(\frac{\alpha_{1(i-1)}^r \cos \gamma_i + \alpha_{1i}^l \cos \gamma_i}{\sin \gamma_i} \right) M_i^l \\
& - \left(\frac{\alpha_{1(i-1)}^r}{\sin \gamma_i} + \frac{\alpha_{1i}^l \cos^2 \gamma_i}{\sin \gamma_i} + \beta_{1i}^l \sin \gamma_i \right) M_i^r \\
& - \left(\frac{\alpha_{2i} \cos \gamma_i \cos \gamma_{(i+1)}}{\sin \gamma_{(i+1)}} - \beta_{2i} \sin \gamma_i \right) M_{(i+1)}^l - \frac{\alpha_{2i} \cos \gamma_i}{\sin \gamma_{(i+1)}} M_{(i+1)}^r \quad \dots 48 \\
& = P_{i-1} t_{2(i-1)} + P_i t_{1i} \cos \gamma_i \\
& + (T_i s_i - S_i \eta_i) \sin \gamma_i
\end{aligned}$$

Similarly equation (43) may be written as:-

$$\begin{aligned}
& - \beta_{2(i-1)} M_{(i-1)}^r + (\alpha_{1i}^l + \beta_{1(i-1)}^r) M_i^l + (\alpha_{1i}^l \cos \gamma_i - \beta_{1i}^l \cos \gamma_i) M_i^r \\
& + \left(\frac{\alpha_{2i} \sin \gamma_i \cos \gamma_{(i+1)}}{\sin \gamma_{(i+1)}} + \beta_{2i} \cos \gamma_i \right) M_{(i+1)}^l + \frac{\alpha_{2i} \sin \gamma_i}{\sin \gamma_{(i+1)}} M_{(i+1)}^r \\
& = - (T_{(i+1)} s_{(i+1)} + S_{(i+1)} \eta_{2(i+1)}) \quad \dots 49 \\
& - P_i t_{1i} \sin \gamma_i + (T_i s_i - S_i \eta_i) \cos \gamma_i
\end{aligned}$$

The above two equations play the same role in calculating multi-throw crankshafts as the well known equations of three moments of Clapeyron for the calculation of continuous beams.

When either $\gamma_{(i-1)}$, γ_i or $\gamma_{(i+1)}$ is equal to zero, the corresponding expression for the bending moment in the plane of the throw breaks down. In that case it will be

most convenient to work from equations (34), (35), (42) and (43), which will provide sufficient relations for a solution of the problem.

General Discussion.

To illustrate a few general properties which are common to all elastic systems subjected to load, the subscript i in the equations of the previous section will now be replaced by its actual values (i.e. 1, 2, 3, etc.), and the coefficients and constants in the equations thus obtained are calculated.

Let us denote the coefficients to the unknown quantities (i.e. M_2^l , M_2^r , M_2^{loer} ) in the above mentioned equations by a_{mn} , where the subscript m denotes the number of the equation, and the subscript n the number of the unknown to which the coefficient applies.

The constants of the same equations will be denoted by C_m .

The complete system of equations for a crankshaft may then be written as:-

$$a_{11}M_2^l + a_{12}M_2^r + \dots + a_{1n}M_{(\frac{n}{2}+1)}^{loer} = C_1$$

$$a_{21}M_2^l + a_{22}M_2^r + \dots + a_{2n}M_{(\frac{n}{2}+1)}^{loer} = C_2$$

etc.

$$a_{m1}M_2^l + a_{m2}M_2^r + \dots + a_{mn}M_{(\frac{n}{2}+1)}^{loer} = C_m$$

Introducing matrix notation, the above equations may be written as⁽¹⁾:-

$$\begin{vmatrix} a_{11} & a_{12} & \dots & a_{1n} \\ a_{21} & a_{22} & \dots & a_{2n} \\ \vdots & \vdots & \ddots & \vdots \\ a_{m1} & a_{m2} & \dots & a_{mn} \end{vmatrix} \begin{vmatrix} M_2^L \\ M_2^r \\ \vdots \\ M_{(\frac{n}{2}+1)}^{lower} \end{vmatrix} = \begin{vmatrix} C_1 \\ C_2 \\ \vdots \\ C_m \end{vmatrix}$$

..... 50(a)

or:

$$AM = C$$

..... 50(b)

In equation (50(b)) the matrix A represents the elastic properties of the crankshaft. This matrix will be called the "characteristic matrix" of the crankshaft.

All the elements of the characteristic matrix are derived from the material or the dimensions of the crankshaft, and the matrix is independent of the external loads.

The matrix C in the same equation represents the external loads, and it will therefore be referred to as the "load matrix". All the elements of the load matrix are linearly dependent on one external load or another, and the

(1) Determinants and Matrices - A.C.Aitken, M.A., D.Sc., F.R.S. Seventh Edition, 1951, page 3.

load matrix will therefore vanish if all the external loads are equal to zero.

Numerical Computation.

The classification carried out in the above paragraph suggests the following procedure for the numerical computation related to the effect of any combination of loads applied to a crankshaft.

Let us assume that it is desired to find the effects of each load separately.

First of all, since the characteristic matrix of our system of equations is purely dependent on the crankshaft dimensions, this matrix, which is valid for any load system, can be calculated once and for all.

The characteristic matrix for the six-cylinder diesel engine (R.R. C 60., Nr. 51) is shown in Fig.14.

Secondly, the load matrices must be considered and it will be necessary to derive the load matrix for each load system under study. Resultant effects can be obtained, either by obtaining the load matrix due to the resultants of the loads, or by a final addition of the effects due to the separate load systems.

A consideration of various systems of forces applied

to a crankshaft is given in the following chapter which may therefore be considered as a part of the numerical example carried out in previous work.

Before this chapter is concluded, however, it will be convenient to give a short survey of methods for practical solutions of large sets of linear simultaneous equations.

It is immediately evident that the orthodox method of successive elimination would involve large practical difficulties. Fortunately, recent developments have given more efficient methods, of which the "Difference Iteration Method"⁽¹⁾ and the "Relaxation Method"⁽²⁾ should be mentioned.

The success of the method applied depends largely on the skill of the operator, and the "Relaxation Method", with which the author is best acquainted, has therefore been chosen for the solution of our particular problems.

-
- (1) Morris, J.:— The Escalator Method in Engineering Vibration Problems, Chapman and Hall, 1947, page 63.
- (2) Allen, D.M.de G.:— Relaxation Methods, 1954.

FIG. 13.

| | | | | | | | |
|---------------------|-----------|-----|-----|---|-----|-----|-----------|
| 1.) BEARING NR. | 1 | 2 | 3 | 4 | 5 | 6 | 7 |
| 2.) X (DEGREES). | / | 120 | 120 | 0 | 240 | 240 | / |
| END - | $M^l = 0$ | / | | | | | |
| CONDITIONS. | $M^r = 0$ | | | | | | |
| | | | | | | | $M^l = 0$ |
| | | | | | | | $M^r = 0$ |

CRANK ANGLES.

1. BEARINGS AND CRANKS ARE NUMBERED FROM THE FRONT
END OF THE ENGINE.
2. SEE FIG. 12.

FIG. 14.

| UNKNOWN | BEARING NR. | | | | | | | | | | | |
|---------|-------------|---------|---------|---------|---------|---------|---------|---------|---------|---------|---------|---------|
| | M_2^i | M_2^r | M_3^i | M_3^r | M_4^i | m_4^i | m_4^r | M_4^r | M_5^i | M_5^r | M_6^i | M_6^r |
| 2 | .1365 | -.2565 | .0181 | .0369 | | | | | | | | |
| | .2130 | -.0096 | -.0530 | .0638 | | | | | | | | |
| 3 | -.0738 | .0369 | .1375 | -.2532 | .0401 | -.0338 | | | | | | |
| | | -.0422 | .2189 | -.0120 | -.0232 | -.0584 | | | | | | |
| 4 | | | | | | | | | | | | |
| | | | | | | | | | | | | |
| 5 | | | -.0780 | .0390 | | .0928 | -.0928 | | -.0390 | .0780 | | |
| | | | | -.0463 | .0772 | | | -.0772 | .0463 | | | |
| 6 | | | | | | | | | -.1375 | .2581 | -.0181 | -.0369 |
| | | | | | | | | -.0463 | .2140 | -.0096 | -.0530 | .0638 |
| 6 | | | | | | | | | .0738 | -.0369 | -.1365 | .2527 |
| | | | | | | | | | | -.0422 | .2171 | -.0116 |

CHARACTERISTIC MATRIX.

CENTRIFUGAL FORCES AND FORCES DUE TO TORSIONAL
VIBRATIONS ACTING ON A MULTI-THROW CRANKSHAFT.

INTRODUCTION:

In this chapter, use will be made of the method developed in the two previous chapters to carry out analyses of the effects of various systems of applied loads on the crankshaft of a multi-cylinder engine.

It is possible, by treating the crankshaft in a succession of angular positions covering a complete revolution, to obtain the effects of the complete force actions which occur in a reciprocating engine. To obtain accurate results, however, this procedure requires laborious numerical work and would be very lengthy without the aid of a computing machine.

For practical reasons, it has therefore been necessary to confine our attention to the forces which are of main interest in conjunction with the rest of the work in this Thesis. These forces may be listed as the mean centrifugal forces and all the forces and torques due to the torsional vibrations of the crankshaft.

As we shall now see, the above listed forces will, under special circumstances, possess a common feature which will simplify their analyses.

It will be remembered that for general crankshaft loads treatments were required for a succession of angular positions of the crankshaft. This procedure is necessitated by the variation of the loads as the crankshaft is rotating. However, loads which are independent of the angular position of the crankshaft can be analysed once and for all in one treatment.

The mean values of the centrifugal forces are independent of the angular position of the crankshaft and, consequently, their effects can readily be examined.

The various force actions due to the torsional vibrations of the crankshaft are also independent of the angular position of the crankshaft as these forces rotate with it.

Forces due to the torsional vibrations of the crankshaft do, however, have difficult phase relations, if the torsional vibrations are off resonance.

In order to simplify the treatment of these forces, we will assume resonance conditions.

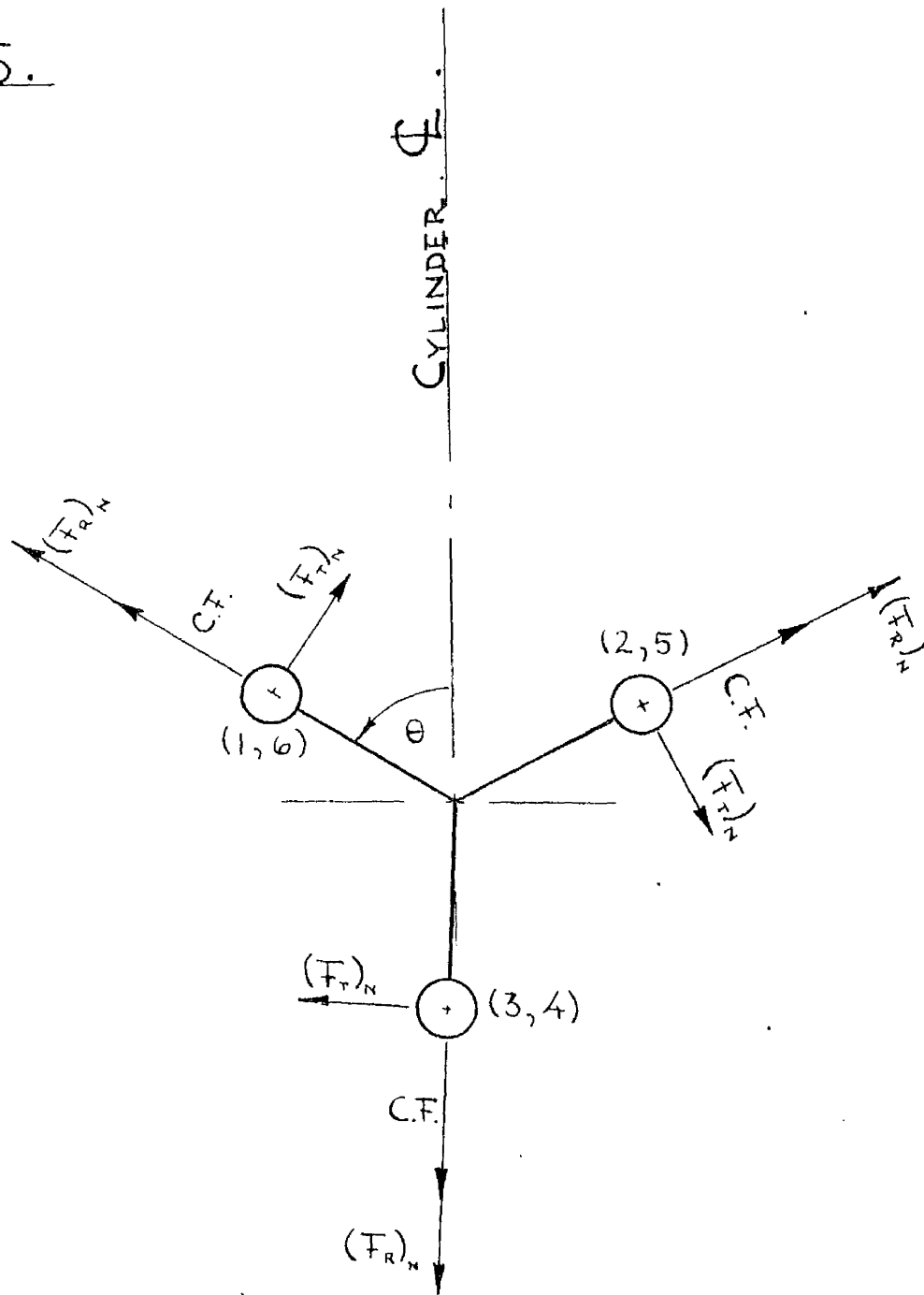
The mean value of the centrifugal forces, as well as the forces due to the torsional vibrations of the crankshaft, have been examined for single cranks in Appendix I. When applied to a multi-throw crankshaft, their action will be as shown in Fig. 15, which gives a front-end view of the crankshaft.

It should be remembered that the forces due to the torsional vibrations of the crankshaft vary sinusoidally with the same frequency as the torsional vibrations.

In the work which follows each of the above-discussed force actions will be treated in turn.

.

FIG. 15.



FRONT END VIEW ON CRANKSHAFT SHOWING APPLICATION
OF CENTRIFUGAL FORCES AND N^{TH} HARMONIC VIBRATIONAL FORCES.

CENTRIFUGAL FORCES:

Let us first of all consider the effects of the centrifugal forces due to the motion of the out-of-balance masses which follows a steady rotation of the crankshaft.

Generally, there are both reciprocating and rotating out-of-balance masses present in a crankshaft system, and these are distributed between the bearings in ways which vary from design to design. Rotating out-of-balance masses are easily treated, but the effect of the reciprocating masses is more complex, being dependent on the angular position of the crankshaft. The resultant value of the centrifugal force will therefore also vary with the crank angle.

In this work, however, we will only confine our attention to the average value of this varying centrifugal force as this generally is larger than the variations.

It will be assumed that the point of application of the centrifugal force is at the centre of the crankpin, and the inaccuracies introduced by this assumption are probably of minor importance.

Using the following notation:-

mR = rotating out-of-balance.

M = reciprocating mass.

R = crank radius.

l = length of connecting rod.

ω = angular velocity of the crankshaft.

the average value of the centrifugal force per crank will be given by ⁽¹⁾:-

$$C.F. = R\omega^2 \left(m + \frac{M}{2} \left(1 + \frac{1}{2} \left(\frac{R}{l} \right)^2 \right) \right) . \quad . . 51$$

For further progress in the analysis it will now be necessary to resort to numerical values rather than symbolic expressions. The numerical example chosen for our purpose refers to a six-cylinder diesel engine, and we will confine our attention to the resonance speed for the sixth harmonic of the torsional vibrations of the crankshaft.

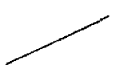
The centrifugal forces as calculated out are now entered into the Table shown in Fig.16., which also gives the necessary deflection coefficients for calculations of the load matrix. Making use of equations (42) and (43), the load matrix, as also seen in the same Table, has been obtained.

The set of linear equations formed by the load matrix, the characteristic matrix (Fig.14) and the unknown bending moments are solved by applying the relaxation method, and each crank is henceforth treated separately.

The results of these calculations are presented in Fig.17

(1) Appendix I, equation 29.A.

FIG. 16.

| BEARING | 1.) $P_i = P_{i-1}$ | 2.) $t_{2(i-1)}$ | 2.) t_{1i} | γ_i | LOAD MATRIX. |
|---------|------------------------|---------------------|-----------------|------------|---|
| NR. | lb | $\frac{1}{lb}$ | $\frac{1}{lb}$ | DEGREES. |  |
| 2 | 7290 | .166 | .133 | 120 | 729 |
| | | | | | -839 |
| 3 | 7290 | .133 | .169 | 120 | 350 |
| | | | | | -1066 |
| 4 | 7290 | .151 | .151 | 0 | 0 |
| | | | | | 0 |
| | | | | | 2200 |
| | | | | | 0 |
| 5 | 7290 | .169 | .133 | 240 | 751 |
| | | | | | 838 |
| 6 | 7290 | .133 | .166 | 240 | 365 |
| | | | | | 1046 |

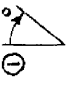
1. CENTRIFUGAL FORCES.

2 FROM FIG 9

LOAD MATRIX FOR THE CENTRIFUGAL FORCES.

FIG. 17.

C.F./CRANK = 7290 lb.

| BEARING NR | 1 | 2 | 3 | 4 | 5 | 6 | 7 |
|---|-------|-------|-------|--------|-------|-------|-------|
| $M^t \text{ lb in} \times 10^{-2}$ | 0 | -36 | -37 | -30 | 50.5 | 57.5 | 0 |
| M^r " | 0 | -57.5 | -51 | 30 | 37 | 36 | 0 |
| m^t " | 0 | 45.7 | 37.5 | 108.5 | 13.5 | 8.3 | 0 |
| m^r " | 0 | -8.3 | -13.3 | -108.5 | -37 | -45.7 | 0 |
| BEARING - lb REACTION | 2700 | 5930 | 5810 | 9580 | 5770 | 5930 | 2700 |
| ANGLE  | 168.9 | 222.7 | 349 | 74.1 | 349.1 | 222.8 | 168.9 |

BEARING REACTIONS DUE TO THE CENTRIFUGAL FORCES.

which, first of all, gives the bending moments occurring at the main journals of the crankshaft and, secondly, the bearing reactions for the journal bearings in amplitude and direction.

VIBRATIONAL FORCES:

Treatments for the various force actions which occur on the crankshaft as a result of its vibrational motion will be very similar to that given for the centrifugal forces. There is, however, one difference between the two force systems - namely, that the latter depends on the amplitudes of the torsional vibrations, whereas the former depends purely on the speed of rotation.

For an analysis of the vibrational forces, it will be necessary, according to the above paragraph, to establish the vibrational amplitudes along the crankshaft.

If we confine our attention to resonance conditions, the relative vibrational amplitudes can be obtained from the Holzer Table, which is calculated through to find the natural frequency of the crankshaft system. Fig.18 gives the Holzer Table for the lowest natural frequency of the crankshaft of the diesel engine under consideration.

Having obtained the relative values for the vibrational

FIG. 18.

$$\omega^2 = 1490,000 \text{ } 1/\text{sec}^2$$

| PART | I lb.in.sec ² | $I\omega^2$ lb.in. $\times 10^{-6}$ | θ RAD. | $I\omega^2\theta$ lb.in. $\times 10^{-6}$ | $\Sigma I\omega^2\theta$ lb.in. $\times 10^{-6}$ | τ RAD/lb.in. $\times 10^6$ | $\Delta\theta$ RAD |
|---------------|-----------------------------|--|------------------|--|---|------------------------------------|-----------------------|
| DAMPER FLANGE | .35 | .521 | 1 | .521 | .521 | .109 | .0567 |
| GEARS | .3 | .447 | .9433 | .422 | .943 | .038 | .0359 |
| CYLINDER 1 | .75 | 1.117 | .9074 | 1.012 | 1.955 | .048 | .0938 |
| " 2 | .74 | 1.101 | .8136 | .895 | 2.850 | .048 | .1370 |
| " 3 | .75 | 1.117 | .6766 | .756 | 3.606 | .053 | .1912 |
| " 4 | .75 | 1.117 | .4854 | .542 | 4.148 | .048 | .1990 |
| " 5 | .74 | 1.101 | .2864 | .315 | 4.463 | .048 | .2145 |
| " 6 | .81 | 1.207 | .0719 | .087 | 4.550 | .039 | .1775 |
| FLYWHEEL | 28.84 | 43 | -.1056 | -4.540 | .010 | | |

HOLZER TABLE

amplitudes along the crankshaft, it now remains to find the absolute value for one of them.

The most accurate way of doing this is to take measurements at the most convenient place on the actual engine.

However, since crankshaft forces and bearing reactions are strictly proportional to the amplitude of the torsional vibrations at any point in the crankshaft system, our calculations will be carried out for a deflection of one radian at the front end of the engine. This is rather convenient as it makes our analysis at this stage independent of experimental work.

For convenience, the force actions due to the torsional vibrations of the crankshaft will be divided into three separate effects which will each be treated in turn.

Applying this procedure, the relative importance of each of the effects is displayed clearly and, finally, the resultant action may be found by superposition.

Radial Vibrational Forces:

The radial vibrational forces may be described as cyclic variations in the centrifugal forces. These variations are due to changes in the angular velocity of the crankshaft as a result of its torsional vibrations.

The radial vibrational forces will therefore vary with the same frequency as the corresponding torsional vibrations.

Denoting the amplitude of the N th. harmonic of the torsional vibrations of the crankshaft at one particular crank by A_N , the amplitude of the radial vibrational force will be given by⁽¹⁾,--

$$(F_R)_N = 2NR\omega^2 A_N \left(m + \frac{M}{2} \left(1 + \frac{1}{2} \left(\frac{R}{l} \right)^2 \right) \right) \cos N(\omega t + \epsilon_N) \quad . . . 52$$

where all other symbols have the same meaning as given in the previous section.

From now on, the procedure is the same as for the centrifugal forces. Fig.19 gives the radial vibrational forces acting on each crank, the required deflection coefficients and, finally, the load matrix. The solutions for the moment equations of the crankshaft are given in Fig.20, which also presents the bearing reactions in magnitude and direction.

Tangential Vibrational Forces and Vibrational Torques:

As well as radial vibrational forces, the vibrational motion of the out-of-balance masses of a crankshaft will also cause tangential vibrational forces and vibrational torques.

Tangential vibrational forces are simply obtained by

(1) Appendix I, equation 28 A.


Fig. 19.

| BEARING | $(A_N)_{i-1}$ (RAD) | P_{i-1} (lb) | $t_{2(i-1)}$ | $t_{1,i}$ | γ_i | LOAD-MATRIX. |
|---------|---------------------|----------------|---------------|---------------|------------|--------------|
| NR | $(A_N)_i$ " | P_i " | γ_{lb} | γ_{lb} | DEGREES. | |
| 2 | .9074 | 79400 | | | | 8480 |
| | .8136 | 71100 | .166 | .133 | 120 | -8180 |
| 3 | .8136 | 71100 | | | | 4450 |
| | .6766 | 59200 | .133 | .169 | 120 | -8660 |
| 4 | | | | | | 0 |
| | | | | | | 0 |
| | .6766 | 59200 | | | | 15350 |
| | .4854 | 42500 | .151 | .151 | 0 | 0 |
| 5 | .4854 | 42500 | | | | 5510 |
| | .2864 | 25100 | .169 | .133 | 240 | 2890 |
| 6 | .2864 | 25100 | | | | 2820 |
| | .0719 | 6300 | .133 | .166 | 240 | 910 |

1. FROM HOLZER TABLE.

LOAD MATRIX FOR THE RADIAL VIB. FORCES.

FIG. 20.

| BEARING NR. | 1 | 2 | 3 | 4 | 5 | 6 | 7 |
|--|------|------|-------|------|-------|-------|-------|
| $M^1 \text{ lb in} \times 10^{-3}$ | 0 | -35 | -35 | -19 | 16 | 7 | 0 |
| M^r " | 0 | -61 | -49 | 19 | 12 | 11.5 | 0 |
| m^1 " | 0 | 50.2 | 36.4 | 77 | 4.6 | 9.2 | 0 |
| m^r " | 0 | -5.2 | -12.1 | -77 | -11.5 | -1.4 | 0 |
| BEARING REACTION $\text{lb} \times 10^{-3}$ | 29.3 | 62.5 | 55.1 | 67.2 | 19.9 | 13.8 | 3.2 |
| ANGLE $^\circ$  | 170 | 219 | 347.1 | 72.7 | 357.2 | 269.5 | 147.8 |

BEARING REACTIONS DUE TO THE RADIAL VIBRATIONAL FORCES.

considering the tangential acceleration of the centres of gravity of the masses under consideration. Vibrational torques are found by considering the angular accelerations of the inertias of the same masses about their axes of rotation.

It follows from the above, that the total vibrational torques are formed by an addition of the torque effects produced by the tangential vibrational forces which act on an arm equal to the distance from the centre of gravity to the axis of rotation, and the pure torques which are due to the angular acceleration of the balanced inertias.

Because of the close connection between the tangential vibrational forces and the vibrational torques, these two effects will both be treated in the same section. Separate treatments are, however, given as it is of interest to find the effect of out-of-balance on the bearing reactions which follow from the vibrational motion of the crankshaft.

The resultant effects of both force and torque actions are finally obtained by superposition.

Let us now consider the effect of the tangential vibrational forces which are due to any out-of-balance in the crankshaft system.

It will be assumed for convenience that these forces

act at the centres of the crankpins. Making use of the same notation as in the previous section, the tangential vibrational force for any crank will be given by the following equation (1):-

$$(F_T)_n = -R\omega^2 N^2 A_n \left(m + \frac{M}{2} \left(1 + \frac{1}{4} \left(\frac{R}{l} \right)^2 \right) \right) \sin N(\omega t + \epsilon_n) \quad . . . 53$$

Making use of the appropriate deflection coefficients, the load matrix is now worked out in the same way as in the previous section. (See Fig.21).

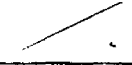
The moment equations are then solved and finally the bearing reactions are found by treating each crank separately. The results of these calculations are given in Fig.22.

For a study of the vibrational torques, it is again convenient to return to the Holzer Table. Column 6 of this Table gives a summation of all the inertia torques acting on one side of any cross-section of the crankshaft system. From torque equilibrium considerations this summation of torques must be carried by the cross-section of the crankshaft and the torques acting over the crankshaft cross-sections at the bearing centres are therefore obtained.

These latter torques are entered into Fig.23 with their appropriate deflection coefficients and the load matrix is calculated by making use of equations (48) and (49) of the

(1) Appendix I, equation 27 A..

FIG. 21.

| BEARING | $\frac{1}{J}$ $(A_N)_{i-1} \text{ (RAD)}$ | $S_{i-1} \text{ lb} \times 10^{-6}$ | $\eta_2 (i-1)$ | $\eta_{1,i}$ | δ_i | LOAD MATRIX |
|---------|--|-------------------------------------|-----------------|-----------------|------------|---|
| NR | $(A_N)_i$ " | S_i " | $\frac{1}{J_b}$ | $\frac{1}{J_b}$ | DEGREES. |  |
| 2 | .9074 | .237 | .149 | .0792 | 120 | -14550 |
| | .8136 | .2124 | | | | -26880 |
| 3 | .8136 | .2124 | .126 | .110 | 120 | -16800 |
| | .6766 | .1767 | | | | -17100 |
| 4 | | | .138 | .096 | 0 | 0 |
| | | | | | | 0 |
| | .6766 | .1767 | | | | 0 |
| | .4854 | .1267 | | | | -36500 |
| 5 | .4854 | .1267 | .158 | .0792 | 240 | 5130 |
| | .2864 | .0748 | | | | -16300 |
| 6 | .2864 | .0748 | .126 | .107 | 240 | 1740 |
| | .0719 | .0188 | | | | -8420 |

1. FROM HOLZER TABLE.

LOAD MATRIX FOR THE TANGENTIAL VIB. FORCES.

FIG. 22.

| BEARING NR. | 1 | 2 | 3 | 4 | 5 | 6 | 7 |
|---|------|--------|-------|-------|------|------|-------|
| $M^1 \text{ lb in} \times 10^{-3}$ | 0 | -163 | -129 | -222 | -36 | -36 | 0 |
| M^r " | 0 | -38 | 10 | 222 | 17 | 0 | 0 |
| m^1 " | 0 | -50.2 | -86.2 | -72 | 40.4 | 20.8 | 0 |
| m^r " | 0 | -166.3 | -155 | 72 | 51.4 | 41.6 | 0 |
| BEARING REACTION $\text{lb} \times 10^{-3}$ | 84.2 | 177 | 171.5 | 200 | 62.8 | 46.8 | 10.3 |
| ANGLE $^\circ$ | 265 | 303 | 71.9 | 164.2 | 94.4 | 0 | 234.2 |

BEARING REACTIONS DUE TO THE TANGENTIAL VIB. FORCES.

previous chapter.

The moment equations are now solved as before and the crankshaft moments and bearing reactions are entered into the table given in Fig.24.

Finally, to complete this section, the resultant bearing reactions due to both the tangential vibrational forces and the vibrational torques are found by adding the component reactions vectorially. These resultant bearing reactions are shown in Fig.25 .

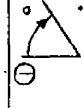
FIG. 23.

| BEARING | 1.) $M_{ti(i-1)}$ | 1.) M_{ti} | $S_{ti(i-1)}$ | S_{ti} | γ_{ti} | LOAD MATRIX. |
|---------|-------------------------------|-------------------------------|---------------------------|---------------------------|---------------|-----------------|
| NR | $\text{lb in} \times 10^{-6}$ | $\text{lb in} \times 10^{-6}$ | $\frac{1}{\text{lb in.}}$ | $\frac{1}{\text{lb in.}}$ | DEGREES. | |
| 2 | | | | | | 26240 |
| | .943 | 1.955 | .0140 | .0155 | 120 | -28350 |
| 3 | | | | | | 34280 |
| | 1.955 | 2.850 | .0155 | .0139 | 120 | -50100 |
| 4 | | | | | | 0 |
| | | | | | | 0 |
| | | | | | | 0 |
| | 2.850 | 3.606 | .0139 | .0139 | 0 | 10500 |
| 5 | | | | | | -55700 |
| | 3.606 | 4.148 | .0139 | .0155 | 240 | -82250 |
| 6 | | | | | | -54100 |
| | 4.148 | 4.463 | .0155 | .0140 | 240 | -95500 |

1. FROM HOLZER TABLE.

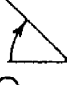
LOAD MATRIX FOR THE VIBRATIONAL TORQUES.

Fig. 24.

| BEARING NR. | 1 | 2 | 3 | 4 | 5 | 6 | 7 |
|--|------|-------|------|------|-------|------|-------|
| $\gamma^t \text{ lb} \times 10^{-3}$ | 0 | -127 | -245 | 122 | -456 | -580 | 0 |
| M^r | 0 | -225 | -259 | -122 | -586 | -485 | 0 |
| m^t | 0 | 187 | 158 | 106 | -415 | -225 | 0 |
| m^r | 0 | -17 | -134 | -106 | 165 | 390 | 0 |
| BEARING REACTION $\text{lb} \times 10^{-3}$ | 32.7 | 109.6 | 92.2 | 93.4 | 292 | 274 | 90.2 |
| ANGLE θ°  | 34.2 | 199.4 | 7.5 | 19.5 | 205.5 | 38.9 | 231.2 |

BEARING REACTIONS DUE TO THE VIBRATIONAL TORQUES

FIG. 25.

| BEARING NR | 1 | 2 | 3 | 4 | 5 | 6 | 7 |
|--|-------|-------|------|-------|-------|------|-------|
| BEARING REACTION $\text{lb} \times 10^{-3}$ | 68.5 | 185 | 230 | 136.6 | 275.5 | 312 | 100.3 |
| ANGLE $^\circ$  | 286.8 | 267.8 | 49.8 | 140 | 193.2 | 33.5 | 231.5 |

RESULTANTS OF THE BEARING REACTIONS FROM FIG. 22 AND 24.

DISCUSSION:

At this stage, it may be of some interest to review and discuss some of the results derived by calculations in this Chapter.

Let us first consider some technical aspects of the arithmetic, such as the amount of work involved and the accuracy obtained.

All calculations presented have been carried out on an eleven inch slide rule. In order to eliminate arithmetical mistakes, it was generally found necessary to check every step by recalculation. This procedure tends to be tedious. Sometimes, however, simpler checks can be carried out on the final results. For instance, since both the crankshaft and the mean centrifugal forces are symmetrical about the centre bearing, so should also all crankshaft moments and bearing reactions be.

Generally, final checks are obtained by finding the resultant of the bearing reactions which should be equal and opposite to the resultant of the applied loads from force balance. Where the applied loads are pure torques, it then follows that all the bearing reactions should add up to zero.

The checks carried out on the final results will also give some idea about the accuracy of the arithmetical work.

From Fig.17 it is seen that the work of this Chapter gives crankshaft moments and bearing reactions which are symmetrical to within an error of one-half percent. This one-half percent includes all inaccuracies introduced throughout the entire arithmetic, and indicates that work on an eleven inch slide rule gives quite sufficient accuracy.

The actual values of the bearing reactions for a multi-throw crankshaft obtained in this Chapter give rise to certain interesting observations.

It is seen from Fig.17 that the centrifugal forces at high speeds give rise to rather large bearing reactions. For our particular crankshaft, the largest bearing reaction which occurs on the centre bearing is considerably larger than the value of the centrifugal force for one crank. Consequently, it would be wrong to assume that the centrifugal forces of each separate crank balance each other out through the connections between the cranks in the multi-throw crankshaft.

Related to the effects of the vibrational motions of the crankshaft, it is seen from Fig.22 and 24 that the vibrational torques create considerably larger bearing reactions than the vibrational forces due to out-of-balance masses. Balance weights fixed to the individual cranks

will therefore not reduce the bearing reactions greatly.

It should be noticed that the bearing reactions due to the tangential vibrational forces and the vibrational torques can be added vectorially in space - see Fig.25 - as they have the same phase angle. The phase angle of the radial vibrational forces, however, differs by 90 degrees and this latter force action must therefore be treated separately.

This Chapter is intended to complete the pure force analysis on the multi-throw crankshaft. Further attention, however, will be given to the effects of the derived forces on the bearings and it is hoped that in time this will help to throw more light on the assumptions concerning bearing constraints which were necessary for the force analysis of the crankshaft.

RESPONSE OF JOURNAL BEARINGS TO SMALL VARIATIONS IN
A CONSTANT LOAD OR A CONSTANT CENTRIFUGAL FORCE.

DISCUSSION:

Fundamentally, the characteristics of journal bearings are derived from considerations of the relative velocities between the journal and the shell. By making use of the conditions for viscous and incompressible flow, these considerations lead to the pressure throughout the oil-film in the bearing and, therefore, its load carrying capacity.

Only relative velocities matter and it is therefore immaterial whether the load systems applied to the oil-film are stationery with respect to the shaft or the shell.

Centrifugal forces can therefore be treated in an exactly analogous manner to forces which are directionally fixed with respect to the shell, and treatments given for one are equally valid for the other.

The original purpose of this Chapter was to study the effects of small variations in the centrifugal load. However, since the purpose can be achieved equally easily by studying similar forces which are directionally fixed with respect to the shell, this latter alternative will be preferred, being simpler to visualise.

Analytical treatments of journal bearings tend to be

complicated and approximations are often essential to obtain any solution at all. Nevertheless, both narrow and long journal bearings subjected to constant loads have been studied comprehensively - analytically as well as by experiment⁽¹⁾.

The effects of variations in the applied load, however, are more uncertain, although known in the main principle, and, as the analyses available reveal certain contradictory features, it was found necessary to investigate the problem as a part of the programme of this Thesis⁽²⁾.

It is assumed for the treatment given by the author that the response to increasing constant loads of the bearing under consideration - i.e. the graphs of attitude angle as well as eccentricity ratio versus load number - is known. However, the actual shape of these curves is immaterial.

The treatment put forward is similar in its main features to that originated by Stodola and developed by Hummel and Hagg. It consists of representing the resistance offered by the oil-film to journal motions by

-
- (1) Analytical studies are due to:- Sommerfeld, Harrison, Swift, Mitchell, Ocvirk and many others.
Experimental studies are due to:- Nücker, Pattie, DuBois and Ocvirk, Kreisler, etc.
 - (2) References are given and contradictions pointed out in the introduction to "Bearing Stiffnesses".

stiffness- and velocity-resistance coefficients followed by a representation of the journal motion by two simultaneous differential equations.

The coefficients in these equations can be taken as constants when the journal motion under consideration is small. For small variations in the applied load it is therefore possible to find the corresponding journal displacements.

BEARING STIFFNESSES:Introduction.

It was first discovered by Newkirk⁽¹⁾ and Stodola⁽²⁾ in 1925 that bearings possess quasi-elastic qualities and that resonance conditions may occur for the lateral motion of the journal.

These quasi-elastic qualities are best explained considering the effects of a static load applied to a rotating journal. See Figure 26. Under the action of the load P , the journal will take up a position indicated by the eccentricity e and the attitude angle α , where these latter two quantities are given as functions of the magnitude of the load and the bearing dimensions. See Figure 27.

Infinitely slow variations in the magnitude of the applied static load will alter the position of the journal strictly in accordance with the equilibrium curves given for the eccentricity and the attitude angle.

In other words, the oil-film deflects and, since this deflection is a recoverable response to a change in the magnitude of a static load, the bearing appears to possess

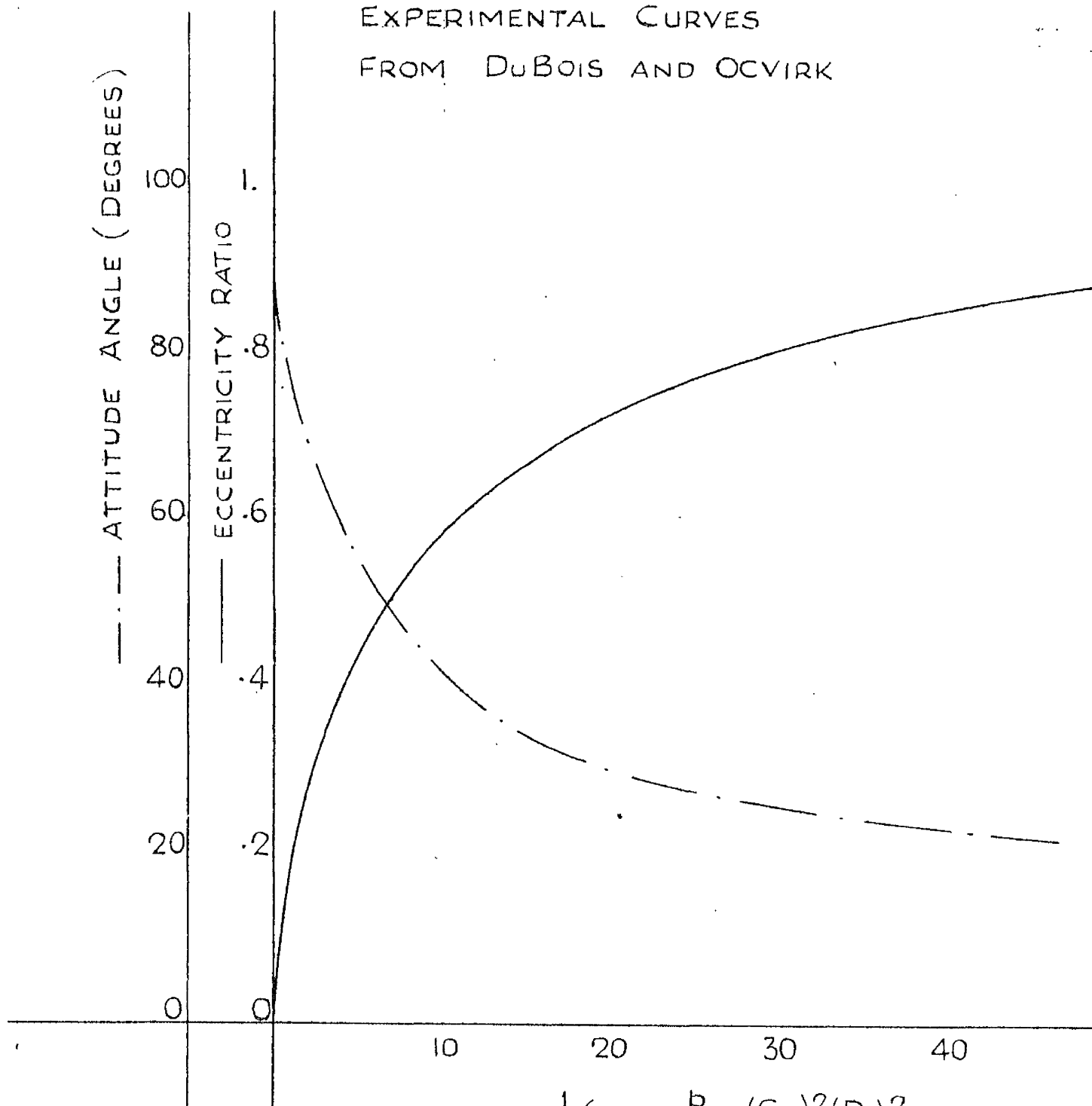
(1) B.L.Newkirk and H.D.Taylor - "General Electric Review" 28 (1925) Page 559.

(2) A.Stodola - "Schweiz Bauztg". 85 (1925) Page 265.

5451

FIG. 27.

EXPERIMENTAL CURVES
FROM DuBOIS AND OCVIRK



$$\text{LOAD } N^{\circ} = \frac{1}{C_h} = \frac{p}{\mu \omega} \left(\frac{C_D}{D} \right)^2 \left(\frac{D}{L} \right)^2$$

elastic properties⁽¹⁾

Before completing this Introduction, it should be remarked that the load-carrying capacity of a bearing subjected to static loads is due entirely to the angular velocity of the journal.

The bearing stiffnesses will therefore in later work be taken as a representation of the effect of this angular velocity.

-
- (1) Stodola's treatment for bearing stiffnesses, which is developed and used by Hummel (2), Hagg (3), Pestel (4) and Cameron (5), is built on the assumption that the journal is offset from its equilibrium semi-circle due to a disturbance. This equilibrium semi-circle represents the variation of attitude angle with eccentricity ratio and it follows from the above that the journal cannot leave this path purely under the action of a variable static load. The bearing stiffnesses derived by Stodola are therefore obtained on a basis which is contradictory to the definition of stiffnesses.
- (2) C. Hummel - "V.D.I. Forschungsheft" No. 287, 1926.
- (3) A. C. Hagg - Trans. A. S. M. E. 1946 A 211-220.
- (4) E. Pestel - "Beitrag zur Ermittlung der hydrodynamischen Dämpfungs und Federeigenschaften von Gleitlagern."
 - "Ingenieur-Archiv" XXII Band, Drittes Heft, 1954, Page 147 to page 155.
- (5) A. Cameron - "Oil Whirl in Bearings" - "Engineering"-February, 1955, Page 237.

Definitions.

$\underline{S_{xx}}$ = Displacement in x-direction due to (in)
force in x-direction.

$\underline{C_{xx}}$ = Stiffness = $\underline{\delta P_x / S_{xx}}$ (lb/in)

$\underline{S_{zx}}$ = Displacement in x-direction due to (in)
force in z-direction.

$\underline{C_{zx}}$ = Stiffness = $\underline{\delta P_z / S_{zx}}$ (lb/in)

$\underline{S_{xz}}$ = Displacement in z-direction due to (in)
force in x-direction.

$\underline{C_{xz}}$ = Stiffness = $\underline{\delta P_x / S_{xz}}$ (lb/in)

$\underline{S_{zz}}$ = Displacement in z-direction due to (in)
force in z-direction.

$\underline{C_{zz}}$ = Stiffness = $\underline{\delta P_z / S_{zz}}$ (lb/in)

Conditions.

$$\underline{\delta P_x} \text{ and } \underline{\delta P_z} \ll \underline{P}$$

and hence

$$\underline{S_{xx} + S_{zx}} \text{ and } \underline{S_{xz} + S_{zz}} \ll \underline{e}$$

Analysis.

Let us decompose $\underline{\delta P_x}$ into components in line with
and perpendicular to \underline{P} .

$$\underline{\delta P_x \sin \alpha}$$

$$\underline{\delta P_x \cos \alpha}$$

$\delta P_x \sin \alpha$ causes a radial displacement:-

$$\underline{(\partial e / \partial p) \delta P_x \sin \alpha}$$

and a tangential displacement:-

$$\underline{e (\partial \alpha / \partial p) \delta P_x \sin \alpha}$$

$\delta P_x \cos \alpha$ causes a tangential displacement only:-

$$\underline{\frac{e \delta P_x \cos \alpha}{P}}$$

Hence:-

$$\underline{S_{xx} = e \delta P_x \left(\frac{\cos \alpha}{P} + (\partial \alpha / \partial p) \sin \alpha \right)}$$

and

$$\underline{C_{xx} = e \left(\frac{\cos \alpha}{P} + (\partial \alpha / \partial p) \sin \alpha \right)}$$

. . . 54

Further:-

$$\underline{S_{xz} = (\partial e / \partial p) \delta P_x \sin \alpha}$$

and

$$\underline{C_{xz} = (\partial e / \partial p) \sin \alpha}$$

. . . 55

Let us decompose δP_x into components in line with and perpendicular to P .

$$\underline{\delta P_2 \cos \alpha}$$

$$\underline{-\delta P_2 \sin \alpha}$$

$\delta P_2 \cos \alpha$ causes a radial displacement:-

$$\underline{(\partial e / \partial p) \delta P_2 \cos \alpha}$$

and a tangential displacement:-

$$\underline{e (\partial \alpha / \partial p) \delta P_2 \cos \alpha}$$

$-\delta P_2 \sin \alpha$ causes a tangential displacement

only:-

$$\underline{\frac{-e \delta P_2 \sin \alpha}{p}}$$

Hence:-

$$\underline{S_{22} = (\partial e / \partial p) \delta P_2 \cos \alpha}$$

and

$$\underline{C_{22} = \frac{1}{(\partial e / \partial p) \cos \alpha}} \quad \dots 56$$

Further:-

$$\underline{S_{2x} = e \delta P_2 ((\partial \alpha / \partial p) \cos \alpha - \frac{\sin \alpha}{p})}$$

and

$$\underline{C_{2x} = \frac{1}{e ((\partial \alpha / \partial p) \cos \alpha - \frac{\sin \alpha}{p})}} \quad \dots 57$$

Making use of equations (54), (55), (56) and (57), it is now possible to derive the variations of the stiffness coefficients of a journal bearing with load number corresponding to any two curves of eccentricity ratio and attitude

angle versus the same variable.

A complete specimen calculation will be given at the end of this chapter.

VELOCITY-RESISTANCE COEFFICIENTS:

Let us now assume that the variations in the constant applied force which were treated as static in the previous section become variations of a frequency $\frac{1}{T_N} = \frac{\omega_N}{2\pi}$.

For most practical purposes, these variations in the constant applied force will be higher harmonics of the engine speed. Writing ω for the angular velocity of the engine, we therefore obtain $\omega_N = N\omega$, where N is an integral number.

Since the lateral motion of the journal in the shell is now performed with an appreciable velocity, the oil-film will provide an additional resistance of a viscous nature.

Conversely, since this resistance is entirely due to the lateral velocity of the journal, it may be studied by considering a non-rotating journal.

On this basis, and using the conditions for viscous incompressible fluid flow, the velocity resistance coefficients valid for small displacements and no side-leakage, can easily be derived.

As we shall see later, it is necessary to take side-leakage into consideration for bearings of length/diameter ratios which are common in practice.

Pestel derives an approximate correction for side-

leakage by considering the two-dimensional oil-flow between two approaching flat plates and finally obtains the following two formulae for the velocity-resistance coefficients in the z - and x -directions ⁽¹⁾:-

$$B_{zz} = \frac{12\mu\pi L R^3}{C_r^3(1-\varepsilon^2)^{3/2}} \left\{ 1 - \frac{192}{\pi^3} \frac{R}{L} \sum_{i=0}^{\infty} \frac{\tanh\left[(2i+1) \frac{\pi L}{2\sqrt{1-\varepsilon^2}} R\right]}{(2i+1)^3} \right\} \quad \dots 58$$

$$B_{xx} = (1-\varepsilon^2)^{3/2} B_{zz} \quad \dots 59$$

(1) E. Pestel - "Beitrag zur Ermittlung der hydrodynamischen Dämpfungs und Federeigenschaften von Gleitlagern."
 "Ingenieur-Archiv" XXII Band, Drittes Heft,
 1954, Page 152, equations (15).

DIFFERENTIAL EQUATIONS AND SOLUTION:

Since for our purpose inertia forces on the journal, due to its lateral motion, are negligible, sufficient information is now available for the differential equations related to the bearing⁽¹⁾.

Denoting the applied forces in the x- and z-directions by $\underline{F_x}$ and $\underline{F_z}$ respectively, and the corresponding displacements by \underline{X} and \underline{Z} , the conditions of force balance for the journal will give:-

$$\underline{F_x} = C_{xx}X + C_{xz}Z + B_{xx}\dot{X}$$

$$\underline{F_z} = C_{zz}Z + C_{zx}X + B_{zz}\dot{Z}$$

For steady state conditions solution of the above equations gives:-

$$\hat{X} = \frac{\hat{F_x} e^{i\beta} - \frac{C_{xz}}{C_{zz} + i\omega_N B_{zz}} \hat{F_z} e^{i\gamma}}{C_{xx} + i\omega_N B_{xx} - \frac{C_{zx} C_{xz}}{C_{zz} + i\omega_N B_{zz}}} \quad \dots 60$$

$$\hat{Z} = \frac{\hat{F_z} e^{i\gamma} - \frac{C_{zx}}{C_{xx} + i\omega_N B_{xx}} \hat{F_x} e^{i\beta}}{C_{zz} + i\omega_N B_{zz} - \frac{C_{xz} C_{zx}}{C_{xx} + i\omega_N B_{xx}}} \quad \dots 61$$

This concludes the symbolic work of this Chapter, but to complete the analysis, numerical calculations relating to the centre bearing of a six cylinder diesel engine are given in the following section.

(1) For actual figures see:- "Numerical Calculations."

NUMERICAL CALCULATIONS:

From previous calculations considering the properties of the crankshaft, the forces as shown by Fig. 28 were found to act on bearing number 4. of our six cylinder diesel engine.

To revise the findings in the previous chapter, \bar{F}_1 is the bearing force due to mean centrifugal forces acting on the crankshaft, \bar{F}_2 the bearing force due to the radial vibrational forces and \bar{F}_3 the bearing force due to the vibrational torques and the tangential vibrational forces.

It should also be kept in mind that the latter two force actions are due to resonance torsional vibrations of the crankshaft and refer to one radian maximum amplitude.

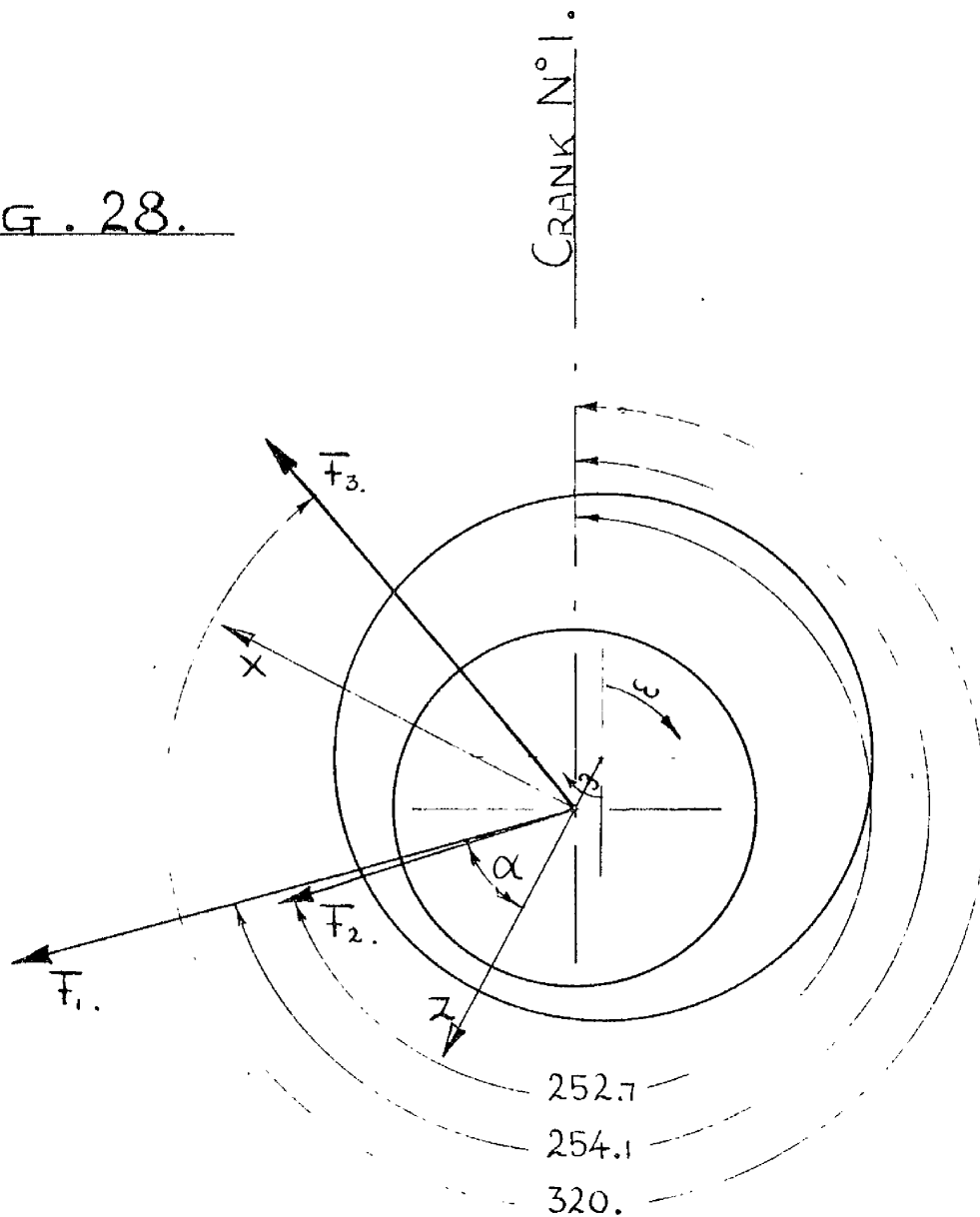
The scheme for the bearing calculations will now be as follows:-

The average eccentricity and the attitude angle for the journal are obtained by considering the effect of the mean centrifugal forces.

The stiffness and the velocity resistance coefficients of the journal bearing may then be found from the formulae derived in the previous sections.

Making use of these coefficients, the journal deflections corresponding to the bearing forces, which are due to

FIG. 28.



$$\bar{F}_1 = \text{MEAN C.F.} = 9580 e^{i(\omega t + 254.1)} \quad (1b)$$

$$\bar{F}_2 = \text{R.V.F./RAD.} = 67,200 \cos 6(\omega t + \epsilon_0) e^{i(\omega t + 252.7)} \quad (1b)$$

$$\bar{F}_3 = (\text{VIB. TORQUE} + \text{T.V.F.})/\text{RAD.} = -136,600 \sin 6(\omega t + \epsilon_0) e^{i(\omega t + 320)} \quad (1b)$$

$$\omega = 203 \text{ } \frac{1}{\text{sec.}}$$

FORCES ON BEARING NR. 4.

the torsional vibrations of the crankshaft, may then finally be calculated using equations (60) and (61).

Eccentricity and Attitude Angle.

The following dimensions and conditions will be used:-

$$L = 2.657'' , \quad D = 3.9''$$

$$C_p = 9.3 \times 10^{-34} , \quad \omega = 203 \text{ } \frac{1}{\text{sec}} ,$$

$$t = 60^\circ \text{C} , \quad \mu = 5.22 \times 10^{-6} \text{ lbsec/in}^2 .$$

$$\text{Nominal Pressure:- } p = \frac{9580}{2.657 \times 3.9} = 926 \text{ lb/in}^2 .$$

$$\text{Load Number:- } \frac{1}{C_h} = \frac{p}{\mu \omega} \left(\frac{C_p}{D} \right) \left(\frac{D}{L} \right)^2 = 10.7 .$$

The attitude angle and the eccentricity ratio can now be read against the above load number from the experimental graph obtained by DuBois and Ocvirk, as shown in Fig.27:-

$$\underline{\varepsilon} = .6 ; \quad \underline{\alpha'} = 41^\circ .$$

Hence the journal eccentricity will be:-

$$\underline{e} = \underline{t \varepsilon C_p} = 2.78 \times 10^{-3}''$$

Stiffnesses.

We will again make use of the graphs which are shown in Fig.26. For the same load number as referred to above,

and applying the proper scale correction factors, we obtain:-

$$\frac{\partial e}{\partial p} = 1 \times 10^{-7} \text{ in/lb}$$

$$\frac{\partial \alpha}{\partial p} = 3.77 \times 10^{-5} / \text{lb}$$

Sufficient information is now available to find all the required bearing stiffnesses from equations (54), (55) (56) and (57).

This leads to:-

$$C_{xx} = 3.98 \times 10^6 \text{ lb/in.}$$

$$C_{xz} = 15.25 \times 10^6 \text{ lb/in}$$

$$C_{zx} = 2.22 \times 10^6 \text{ lb/in}$$

$$C_{zz} = 13.25 \times 10^6 \text{ lb/in}$$

Velocity-Resistance Coefficients.

The velocity-resistance coefficients are calculated from equations (58) and (59):-

$$B_{xx} = 5210 \text{ lbsec/in.}$$

$$B_{zz} = 10160 \text{ lbsec/in.}$$

Applied Forces.

The applied forces are given by _____ and _____ of Fig. 28. For further calculations, however, it will be necessary to refer these forces to the x- and z-directions.

We thus obtain:-

$$\underline{F_x = 137,500 \cos \{6(\omega t + \epsilon_0) + 71.7\}}$$

$$\underline{F_z = 65,200 \cos \{6(\omega t + \epsilon_0) - 37.5\}}$$

Journal Displacements.

Sufficient information is now available to obtain the displacement of the journal in the x- and z-directions corresponding to the applied loads $\overline{F_x}$ and $\overline{F_z}$ by making use of equations (60) and (61).

$$\underline{x = 23.2 \times 10^{-3} \cos \{6(\omega t + \epsilon_0) + 8.5\}}$$

$$\underline{z = 2.6 \times 10^{-3} \cos \{6(\omega t + \epsilon_0) - 132.3\}}$$

MEASURED DISPLACEMENTS.

It will be remembered that the above two displacements are derived with respect to a co-ordinate system which rotates with the crankshaft. To make the values obtained comparable with experimental readings, it will be necessary to refer the displacements to a stationery co-ordinate. Further, this co-ordinate should coincide with the direction in which experimental readings of the journal displacements are to be taken.

Fig.29 shows the journal displacements derived above in relation to the position of four pick-up units which will be used for experimental readings.

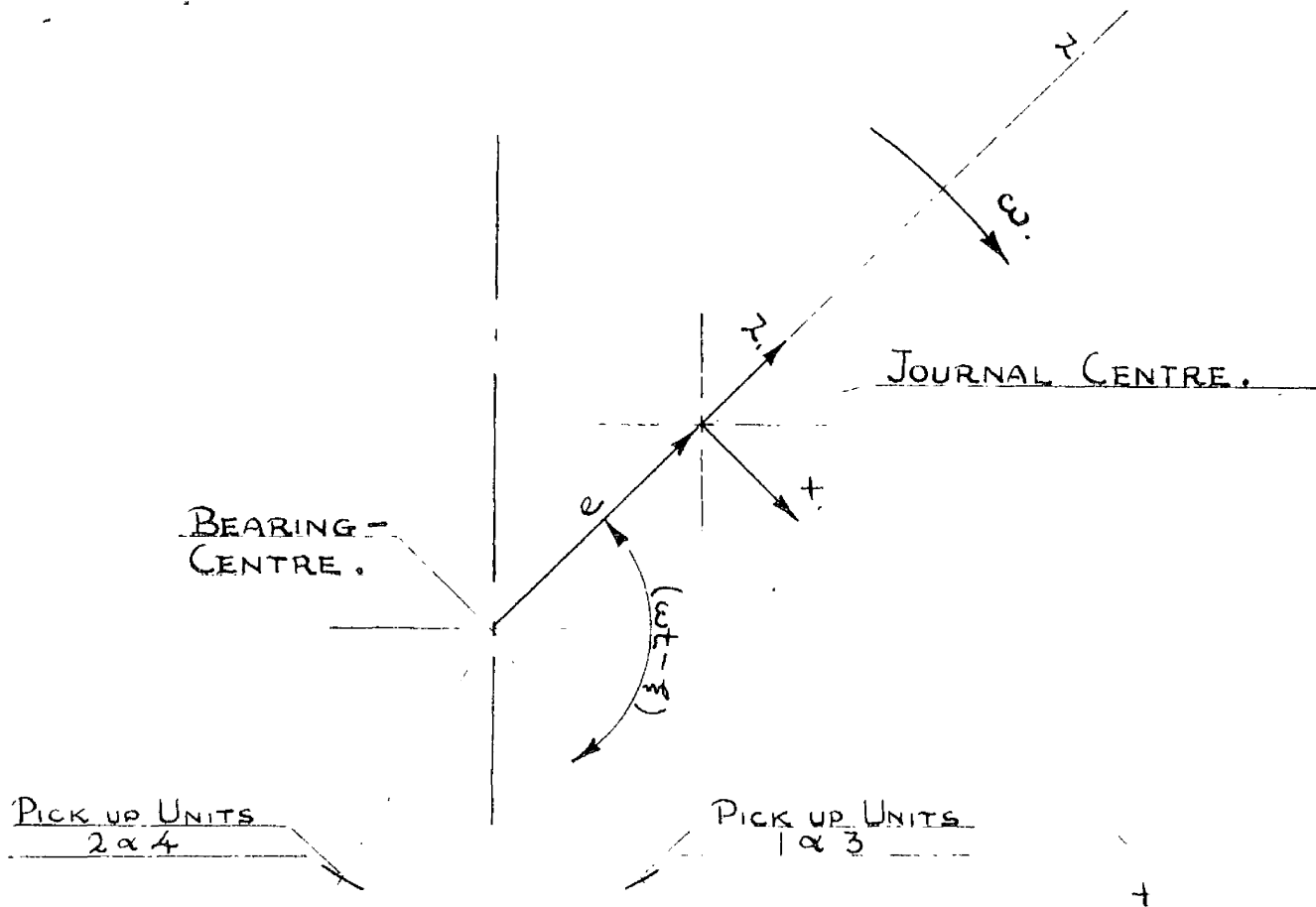
Denoting the angular position of any pick-up unit with respect to the cylinder centre lines by θ , the 6th. harmonic of journal displacement rotating with the crankshaft leads to the following 5th. and 7th. harmonics with respect to the stationery pick-up units.

$$\underline{A_5 = 10.81 \times 10^{-3} \cos(5\omega t + 6\theta_c - \theta + 103.9)} \quad . . . 62$$

$$\underline{A_7 = 12.45 \times 10^{-3} \cos(7\omega t + 6\theta_c - \theta - 86.2)} \quad . . . 63$$

It should be noticed that the angular position of the pick-up unit used affects only the phase angle of the harmonics measured and not the amplitude.

FIG. 29.



$$x_1 = 23.2 \times 10^{-3} \cos(6(\omega t + \epsilon_0) - 132.3)$$

$$z_1 = 2.6 \times 10^{-3} \cos(6(\omega t + \epsilon_0) + 8.5)$$

SIXTH HARMONIC OF JOURNAL DISPLACEMENTS.

INERTIA FORCES:

Finally, before this chapter is completed, a brief consideration should be given to the magnitude of the inertia forces acting on the journal due to its 6th. harmonic lateral motion.

For the six cylinder diesel engine under consideration, the total mass per crank will be less than 50 lbs.

Hence the inertia forces are determined by:-

$$\underline{I.F. < \frac{50}{386} \times 1220^2 \times 23.2 \times 10^{-3} = 4500 \text{ lb}}$$

which is less than 10% of any of the applied forces \overline{F}_x and \overline{F}_y . The inertia forces are in quadrature with the viscous forces which are the main resistance forces and, consequently, they may be neglected.

MEASUREMENT
OF
CRANKSHAFT TORSIONAL VIBRATIONS
AND
JOURNAL LATERAL DISPLACEMENTS.

INTRODUCTION.

This section will give a description of experimental work carried out on a six-cylinder diesel engine (R.R. C.60).

The experiments were conducted to correspond to the theoretical work carried out in the previous section and, consequently, they are arranged under the following two main headings:--

(a) Measurement of Crankshaft Torsional Vibrations.

and

(b) Measurement of Lateral Displacements
of a Crankshaft Main Journal.

The former of the above two experimental investigations is today developed into an almost standard test and only a short description of apparatus, followed by a presentation and discussion of results, has therefore been given.

The measurement of journal lateral displacements, however, implied various difficulties and a more complete description of experimental gear, as well as the procedure adopted, is therefore presented.

All tests were carried out for the engine idling, such that the effects of driving torques on the crankshaft are completely removed. Thus, the importance of the firing loads is also reduced to a minimum and, consequently, the

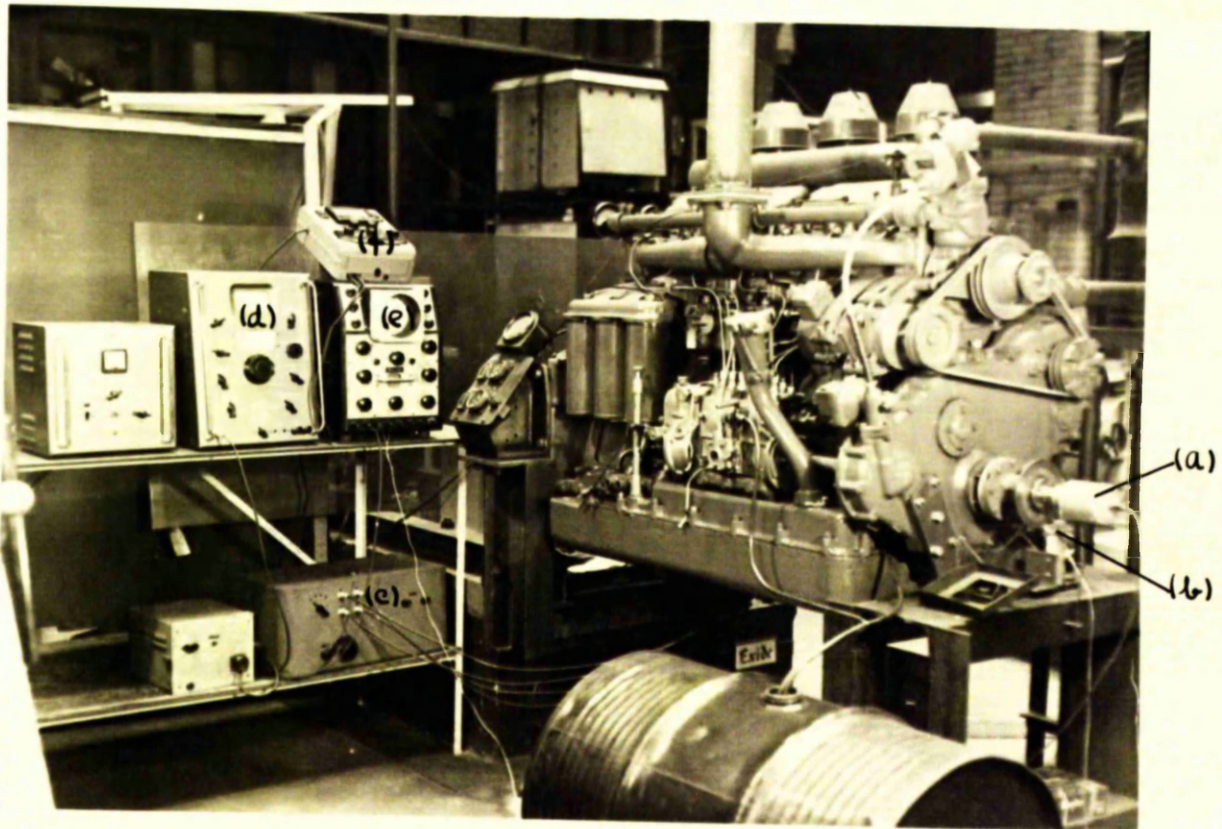
effects of the loads analysed in the previous section will emerge with the least possible obscurity.

Finally, it should be mentioned that a viscous damper originally mounted at the front end of the crankshaft was removed to make the resonance peaks for the torsional vibrations distinct and of reasonable magnitude. It was, however, checked by amplitude measurements that the stresses in the crankshaft were not excessive.

A photograph of the test arrangement is shown in Fig. 30.

PHOTOGRAPH OF THE TEST ARRANGEMENT

FIGURE 30.



- a). Sperry Electromagnetic Torsiograph.
- b). T.D.C. marker.
- c). Oscillator-Discriminator Unit.
- d). Wave Analyser.
- e). Oscilloscope.
- f). Testmeter.

ARRANGEMENT OF MEASUREMENT
APPARATUS FOR ENGINE TESTING.

CRANKSHAFT TORSIONAL VIBRATIONS.

Introduction.

Let us for a moment return to the Holzer Table calculated for the crankshaft of the six-cylinder diesel engine (R.R. C.60) in the previous section. (See Fig.18).

It is seen from this Table that for the first mode of torsional vibrations the largest amplitudes occur at the front end of the crankshaft. Consequently, this point will be the most desirable for taking measurements.

Because of the relatively high natural frequencies of the crankshaft, considerations had to be given to possible inertia effects in the measurement gear. Electronic gear was therefore preferred. Finally, a "Sperry Electromagnetic Torsiograph"⁽¹⁾ was used as a pick-up unit in conjunction with a "Muirhead Pametrada Wave Analyser" as the recording instrument.

Calibration:

Before the actual engine tests, it was necessary to

- (1) Stansfield, R. - "The Measurement of Torsional Vibrations" (Inst. of Mech. Eng. Feb. 1942).

Wilson, W. Ker, - "Practical Solution of Torsional Vibration Problems", (Chapman & Hall London, 1941, Vol.2., Page 265).

carry out calibrations of the measurement gear and, for this purpose, the apparatus shown in Fig.31 was used.

A short description will be necessary.-

The pick-up unit (a) is bolted to a dummy-shaft (b) which is supported in ball-bearings. The shaft is excited in torsional vibrations by a moving coil exciter (c), driven by a power-supply panel (d). The excitation can be controlled to give shaft vibrations of different frequencies and amplitudes.

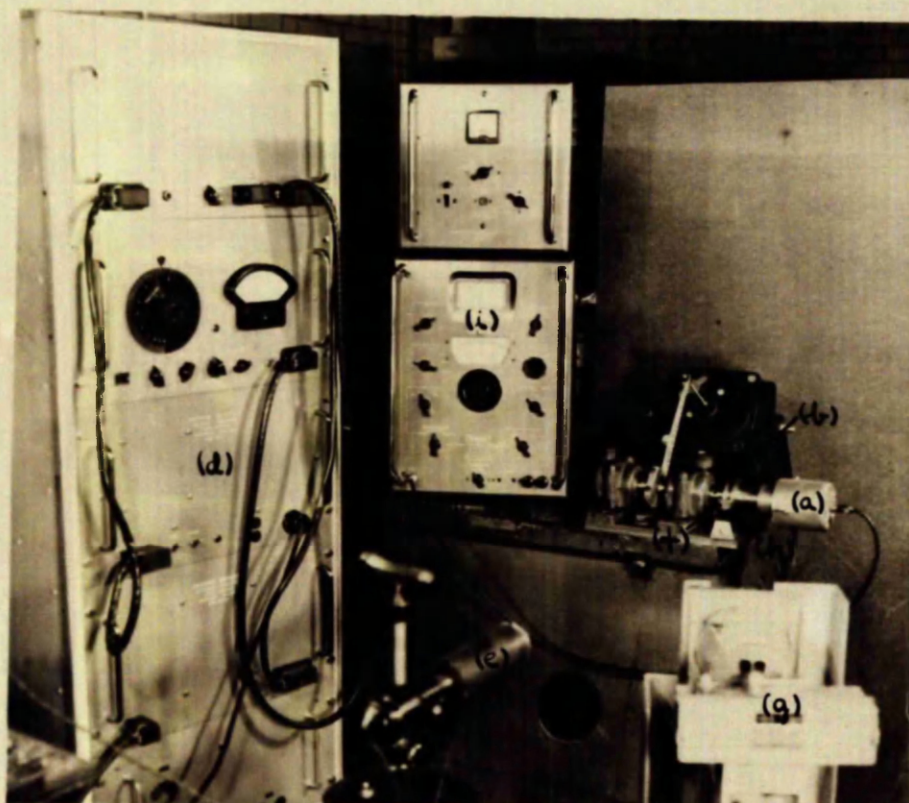
The vibrational amplitudes of the dummy-shaft are measured by means of an optical system. Light from a point source (e) is reflected by a plane mirror (f), attached to the shaft end, finally, focused on the screen of a moving film camera (g) by means of a long focal length lens (h).

A point image of the light source is thus formed on the camera screen and angular vibrations of the dummy-shaft are recorded as variations in the position of this image.

Calibration constants for the optical system are obtained from measurements of the distances between the light source and the mirror, the mirror and the lens, and the lens and the camera screen. (See Appendix II).

The torslograph was connected to the wave analyser (i) for measurements of the output voltage.

FIGURE 31.



- a). Sperry Electromagnetic Torsiograph.
- b). Dummy-shaft.
- c). Moving Coil Exciter.
- d). Power-Supply Panel.
- e). Point Source of Light.
- f). Plane Mirror.
- g). Moving Film Camera.
- h). Lens.
- i). Wave Analyser.

TORSIOGRAPH CALIBRATION APPARATUS.

A series of tests was carried out in order to study the behaviour of the Sperry Electromagnetic Torsiograph for a range of shaft vibrations of amplitudes from zero to .8 degrees and frequencies from 100 cycles per second to 300 cycles per second; this range being sufficient to cover the application of the instrument. Particular attention was paid to the natural frequency of the crankshaft which will later be studied by means of the torsiograph - i.e. 194 cycles per second.

It was found that a velocity calibration factor of .688 Mv.Sec./Degree could be used for the instrument within the above range. The accuracy of this constant was given to within an error of $\pm 8\%$; this being the maximum deviation from the average observed in the experimental results.

The above-quoted error was primarily due to instability of the instrument and difficulties were encountered in improving upon this condition.

Engine Tests:

The Sperry Electromagnetic Torsiograph was bolted to the front end of the crankshaft of the diesel engine (R.R. C. 60).

The engine was run at constant speeds differing by 50 R.P.M. throughout the entire speed range. For each speed

measurements were taken of the 6th., $7\frac{1}{2}$ th., 9th. and 12th. harmonic of the angular motion of the front end of the crankshaft by means of the Muirhead Pametrada Wave Analyser.

Other harmonics were of no interest, being of negligible magnitude within the speed range.

The engine speeds were measured by means of a tachometer, the readings of which checked against the Wave Analyser.

The results obtained are presented as graphs in Fig.32, which give torsional amplitudes in degrees plotted versus the engine speed.

Discussion.

The graphs of Fig.32 show the usual features of frequency response curves for vibrational systems. Each harmonic increases to a maximum value at the engine speed which corresponds to the natural frequency of the crankshaft and, thereafter, decreases rapidly.

The largest resonance amplitude occurs for the 6th. harmonic and we will therefore, in following work, pay particular attention to this resonance peak.

This peak value of the amplitudes is used in conjunction with the theoretical analysis of the previous section to predict lateral displacements of one of the crankshaft main

6TH. HARMONIC

FIG. 32.

CRANKSHAFT TORSIONAL VIBRATIONS.
FREQUENCY RESPONSE CURVES.

AMPLITUDE OF VIBRATION DEGREES.

0.5

0.4

0.3

0.2

0.1

0

500

750

1000

1250

1500

1750

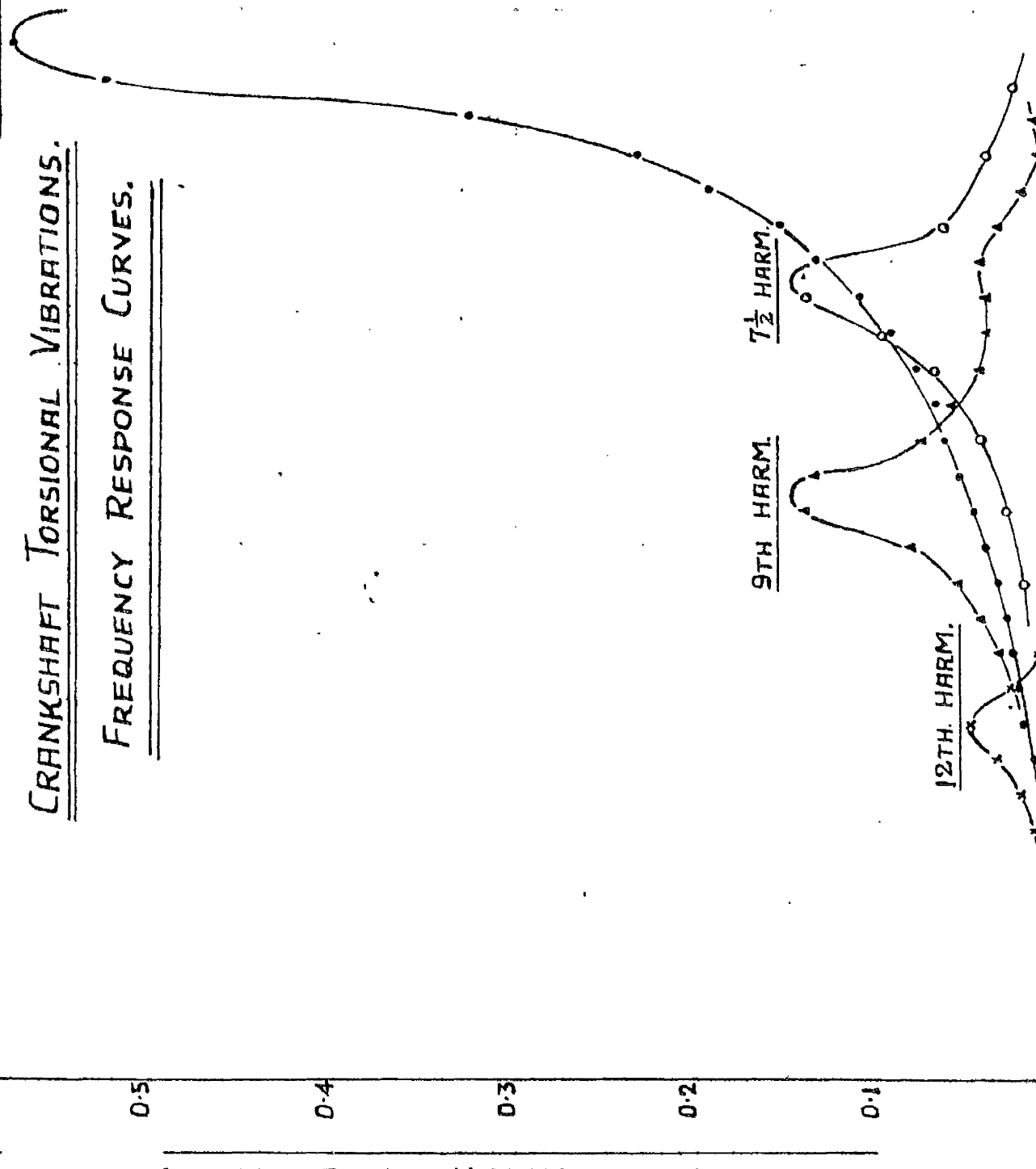
2000

7½ HARM.

9TH HARM.

12TH. HARM.

ENGINE SPEED R.P.M



journals. Later, the same displacements will be measured.

In this connection, it should be mentioned that, since the accuracy of the results obtained with the torsigraph lies in the region of $\pm 8\%$, it can be assumed that the same degree of accuracy applies to the amplitude values obtained for the torsional vibrations of the crankshaft.

Finally, some words should be said about the calculation of the crankshaft natural frequency, as presented in the Holzer Table. (See Fig.18).

From observation of the engine speeds at which the resonance peaks occur, it was possible to obtain a measure of the crankshaft natural frequency of vibration which could be compared to the calculated natural frequency of 194 cycles per second.

Such a comparison shows a deviation in the measured natural frequency, from the calculated value, of approximately $\pm 2\%$.

CRANKSHAFT LATERAL JOURNAL DISPLACEMENTS.

MEASUREMENT PROBLEM.

Location of Measurement Points.

As we proceed to discuss the experimental measurements of the lateral displacements of a crankshaft journal, it should be emphasised again that the object of these measurements is to throw light on the theoretical analysis of the crankshaft forces. It is, therefore, of importance that the measurement gear should be designed and applied according to information already available about these forces.

Let us first of all consider the bearing reactions due to the mean centrifugal forces - (See Fig.17). These are rotating forces of constant magnitude and will, consequently, cause the journal centres to move round the bearing centres with a constant eccentricity.

Unfortunately, the above-described effect is obscured by the firing loads. However, by selecting the bearing for which the bearing reaction due to the mean centrifugal forces is largest, the relative importance of the firing loads will be minimised. This suggests the selection of bearing number 4. for our measurements⁽¹⁾.

Secondly, the forces due to the torsional vibrations

(1) The bearings are numbered from the front end of the engine.

of the crankshaft should be considered - (See Fig.25).

These forces cause the largest bearing reactions to be set up on bearings 5. and 6., but the reaction on bearing 4. is of reasonable magnitude.

From practical considerations, bearing 4. again revealed some advantages. It was longer than the bearings 5. and 6. and, consequently, gave more room for pick-up units. In addition to this, it was found to be reasonably accessible.

As a result of the considerations given above, it was decided to measure the lateral displacements of the crankshaft journal in bearing 4.

With regard to the position of the measurement points within the actual bearing, it is clear that the best angular position is where the firing loads have the least effect - i.e. in a line approximately perpendicular to the cylinder centre line.

Unfortunately, such positions were not readily accessible in practice. To simplify the machining, the pick-up units were fitted in the bottom bearing cap at 30 degrees off the cylinder centre line. - (See Fig.33).

The pick-up units were also spaced axially such as to register any journal slope.

Specification of Measurement Problem.

Concerning the magnitudes of the displacements to be measured, it is seen from Page (83) that the constant rotating eccentricity for bearing 4. is estimated to be equal to .00278 in. This journal displacement must lie fully within the range covered by the measurement gear.

Related to the vibrations of the crankshaft, we are interested in a 5th.- and a 7th.-harmonic of the journal lateral displacements. - (See Page (86) Equations 62 and 63). These harmonics have amplitudes of the order of 0.0001", and, for a reasonably accurate measure of these quantities, the measurement gear should give readings down to 0.00001".

It will be realised that the above requirements are severe; the main obstacle being high required accuracy in conjunction with a relatively wide range.

Finally, some features related to the practical operation of the measurement gear should also be reviewed.

It is essential that a calibration can be carried out for the measurement system such that output readings can be interpreted in terms of displacements of the journal from its centre position. This implies the necessity for a location of the shaft centre position in relation to the output from the measurement gear.

MEASUREMENT GEAR.

The features of our measurement problem drafted in the previous section suggest the use of electronic gear and, it was decided to take advantage of experience gained by Kollmann and Hockel⁽¹⁾, who were successful in tackling a similar problem.

They used a variable capacity type of pick-up unit in conjunction with an oscillator-discriminator unit as the signal generating pre-circuit.

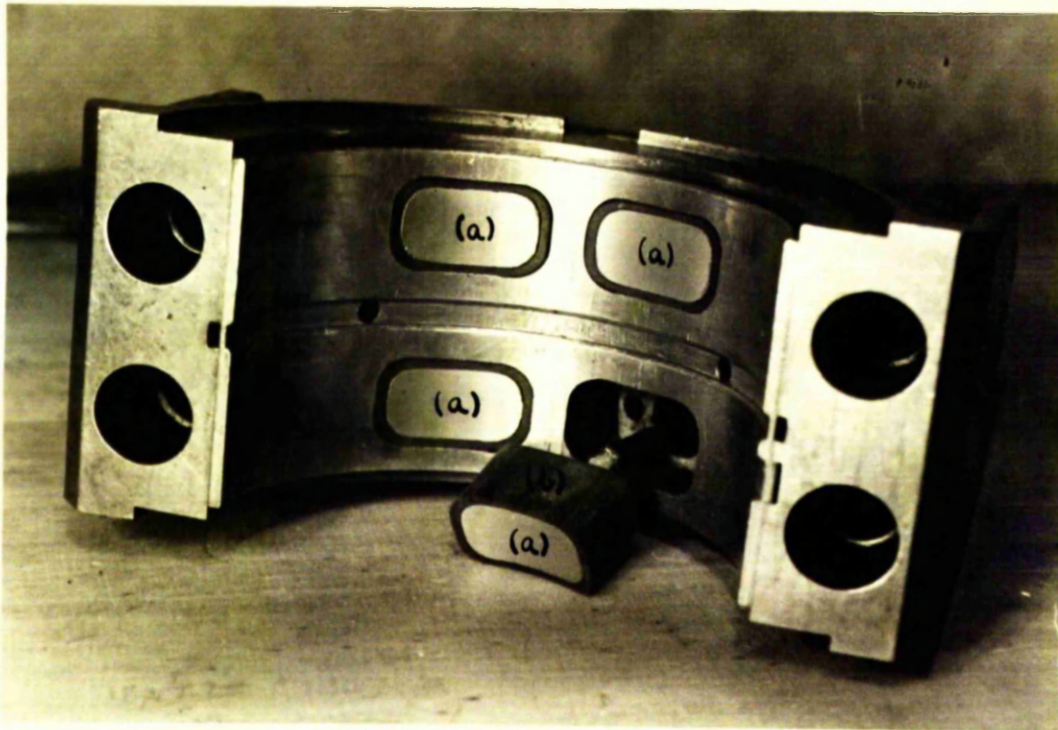
A similar system was designed and built for our measurement problem. Four pick-up units, each consisting of a brass disc (a), forming the live plate of a condenser, fitted to an insulating support made of fibre-base bakelite (b), were positioned in the lower cap of bearing 4. - (See Fig. 33).

The crankshaft journal formed the earthed side of the pick-up units, such that variations in the oil-film thickness appeared as variations in capacity.

The pick-up units were connected through co-axial cables to the pre-circuit input where a switch was incorporated, such that each pick-up unit could be used in turn.

(1) Kollmann, K. and Hockel, H.L. - Ermittlung der Dicke des Schmierfilms in den Grundlagern einer Stationären Dieselmotors. - M.T.Z. Jahrgang 14. Nr. 5. May, 1953.

FIGURE 33.



- a). Live Condenser Plates.
- b). Insulating Support.

JOURNAL BEARING CAP SHOWING
METHOD OF MOUNTING PICK-UP UNITS.

The pre-circuit was designed to convert the variations in capacity between the live plates of the pick-up units and the shaft into voltage variations of sufficient amplitude to be measured by the Muirhead Pametrada Wave Analyser, or drive the Cossor Double Beam d.c. Oscilloscope⁽¹⁾.

The above-described measurement system promised sufficient sensitivity and range for our purpose, and, further, it possessed the advantage that a direct calibration could be carried out.

(1) For constructional details and circuit diagram of the Oscillator-Discriminator Unit see Appendix III.

TESTING AND CALIBRATION OF MEASUREMENT GEAR.

Calibration Apparatus.

The first consideration in designing the calibration apparatus was to simulate engine conditions as closely as possible. However, it was also necessary to take simplicity in design as well as operation into account.

After some development, the Apparatus shown in Fig.34 came into shape.

A short steel shaft (a) ground to the same diameter as the crankshaft journal, was used as a substitute for the actual journal.

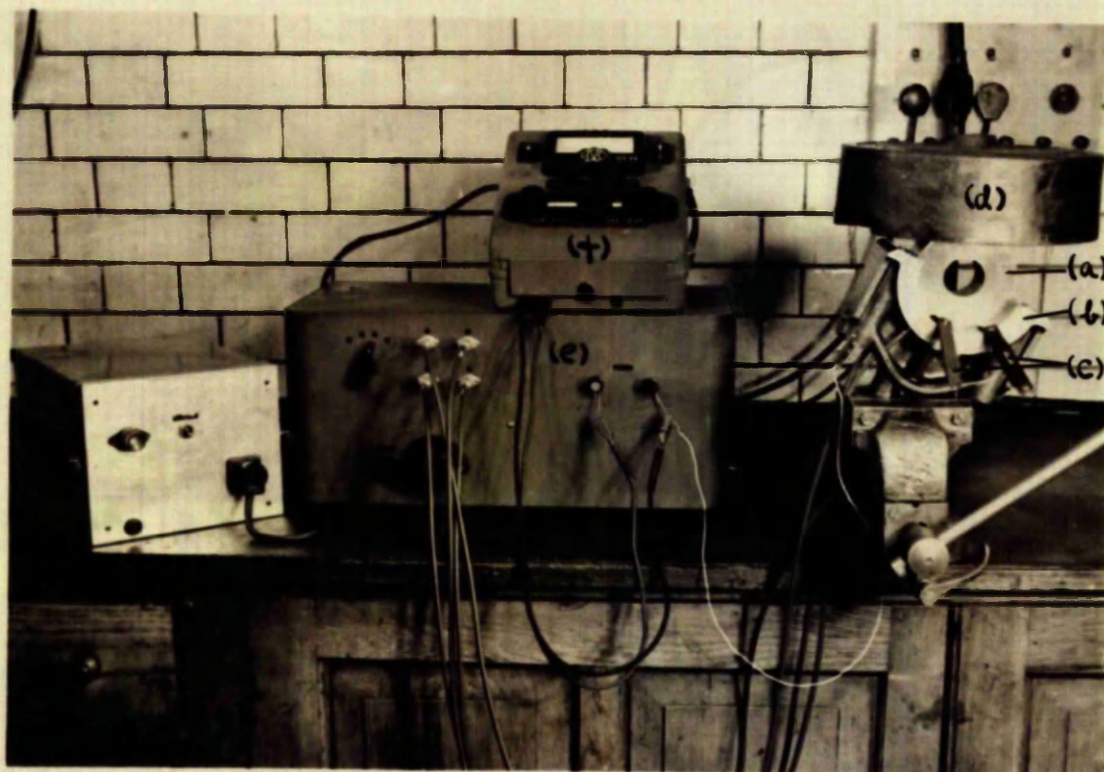
The bearing cap (b) was fixed in a vice and the bottom of the shell filled with the same lubricating oil as was used in the engine.

Two feeler gauges (c), one on each side of the pick-up unit under test, were used to maintain the correct oil-film thickness between the substitute journal and the shell.

When positioned in the shell, the substitute journal was kept down by a heavy weight (d), which was required to give sufficient pressure on the feeler gauges for consistent readings.

Both the bearing shell and the substitute journal were

FIGURE 34.



- a). Steel Shaft.
- b). Bearing Cap.
- c). Feeler Gauges.
- d). Weight.
- e). Oscillator-Discriminator Unit.
- f). Electronic Test Meter.

CALIBRATION APPARATUS.

earthed to the chassis of the oscillator-discriminator unit (e).

Since the calibration tests were static tests taken at various fixed values of oil-film thickness, an electronic test meter (f), operating on the volts d.c. range, was used to measure the output potential of the oscillator-discriminator unit.

Before completing the description of the calibration apparatus, it should be mentioned that for practical reasons the variations of dielectric constant for the lubricating oil with temperature, was ignored.

It is, however, shown by Mücke⁽¹⁾ that such variations for a similar lubricating oil are small and, consequently, the error introduced is not expected to be of great importance.

Calibration Tests.

As well as carrying out straight-forward calibrations for the measurement gear, it was necessary to study its behaviour with the aim of establishing a test procedure.

First of all, however, a description will be given of the calibration tests.

It will be noticed from Appendix III, that two condensers

(1) Mücke - "Über den Schmiervorgang im Gleitlager"
(Forschungsheft. 352).

are available for adjustment on the oscillator-discriminator unit. A condenser C₂ in series with the pick-up unit provides sensitivity adjustment, and, a condenser C₁ in parallel with the pick-up unit is incorporated for tuning purposes.

The series condenser setting which gave the most convenient sensitivity for the instrument, was obtained from preliminary trials and later maintained constant throughout all tests.

To display the effect of varying the capacity of the parallel condenser, tests were carried out using five settings of this condenser for each pick-up unit⁽¹⁾.

In short, the procedure of each test may be outlined as follows:-

To reach stable conditions all instruments were switched on two hours before use.

Feeler gauges were selected to give approximately the maximum value of oil-film thickness, and placed in position⁽²⁾.

The series condenser was set to give the selected

-
- (1) Using different settings for the parallel condenser means the same as working on different parts of the discriminator characteristic.
 - (2) The maximum oil-film thickness for the bearing is equal to the diametral clearance. This was measured for bearing 4. by taking a lead wire impression, and found to be .0093".

sensitivity and the parallel condenser adjusted to give the required starting voltage for the discriminator output voltage.

A series of readings for a range in oil-film thickness, from maximum to zero, was now taken for each setting of the parallel condenser.

A complete calibration test was carried out for each pick-up unit in turn.

Discussion.

The graphs shown in Fig.35 and 36 are presented to illustrate the characteristics of our measurement system.

These are first of all a complete set of calibration curves related to pick-up unit 1., and obtained for different settings of the parallel condenser. - (Fig.35).

Secondly, curves are given for all four pick-up units of calibration factors valid for small displacements of the shaft about its central position. - (Fig.36). In other words, the latter curves are simply the slopes of the former at .00465" oil-film thickness.

As seen from the graphs of Fig.35., the characteristics of the measurement gear are unfortunately non-linear. This non-linearity is related fundamentally to the design of the

pick-up units and could not be improved without loss of sensitivity and possibly the introduction of other complications.

Further, from Fig.36, it is seen that the calibration factors vary a great deal with the setting of the parallel condenser.

Being uncertain whether improvements could be incorporated into the measurement gear without a time consuming development, it was decided to accept its characteristics if answers could be found to the following two problems.

First of all, as a result of the non-linearity of the calibration curves, it will be required to know the shaft central position (or some other position) in relation to the output from the measurement gear during test. This difficulty was overcome by making use of records taken during actual engine tests, as we shall see later.

Secondly, since the calibration factor of the measurement gear varies with the parallel condenser, it will be necessary to ensure that the measurement gear can be reset to calibration conditions for later tests.

For a discussion of this problem, let us again confine our attention to the curves of Fig.36.

It is seen from these curves that the calibration factor in volts per thou. displacement for all pick-up units

CALIBRATION CURVES

PICK-UP UNIT N° 1

FIG. 35

BANDSPREAD SETTING 7

CURVES FOR FIVE DIFFERENT
SETTINGS OF TRIMMER CONDENSER

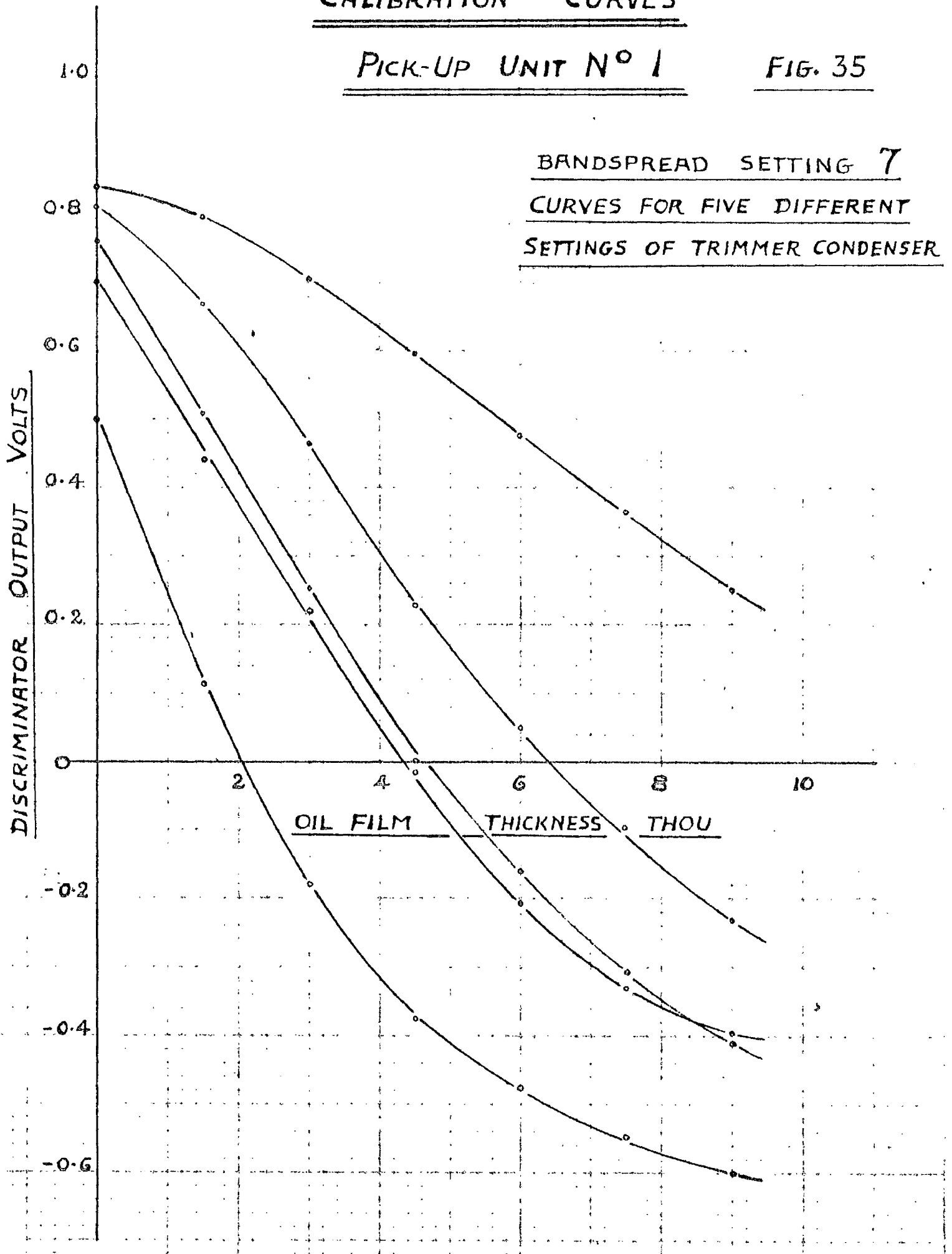
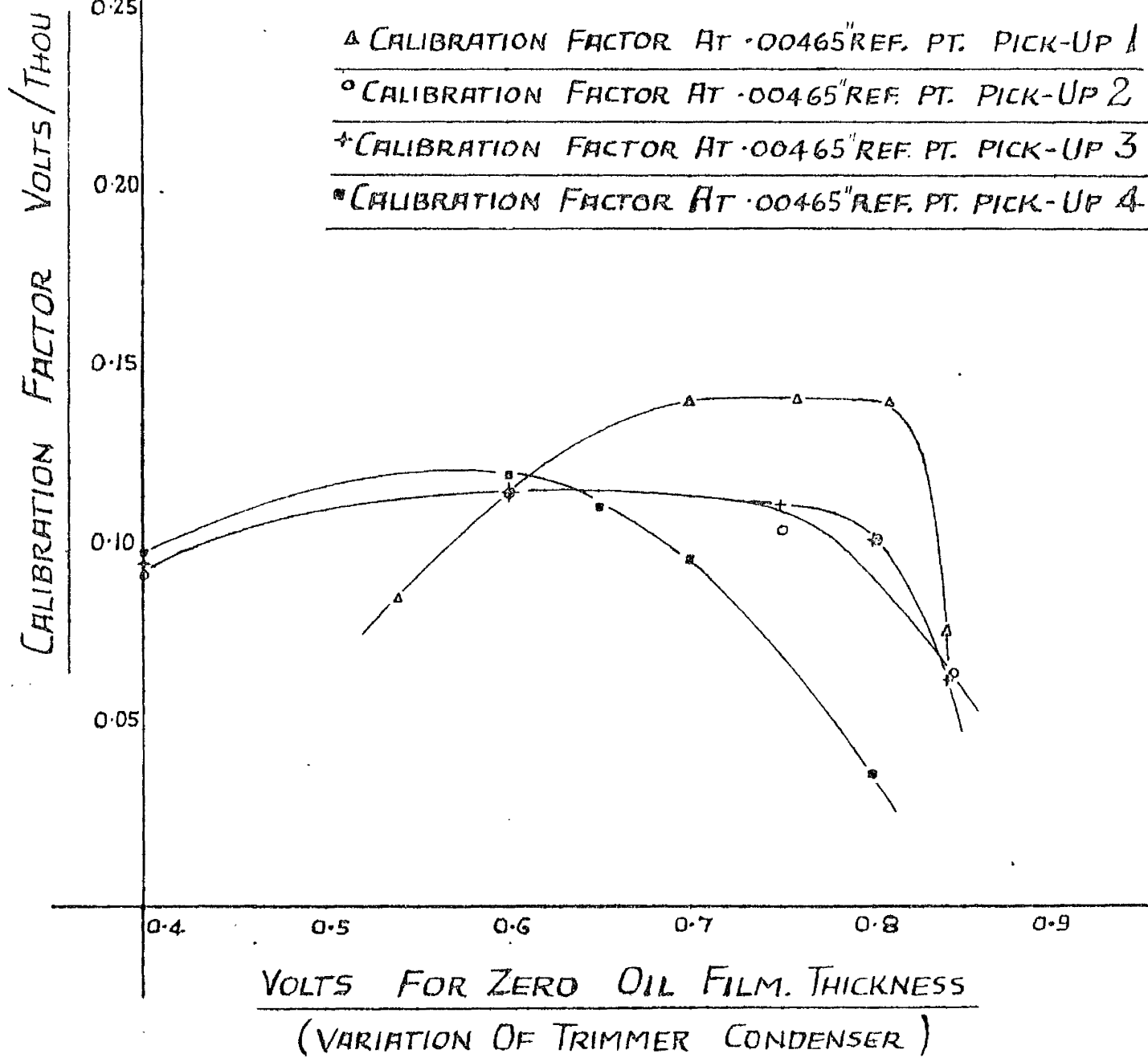


FIG. 36

VARIATION OF CALIBRATION FACTOR
WITH TRIMMER CONDENSER SETTING



increases from lower values to a relatively flat maximum, after which it drops off sharply. This variation corresponds to an increase in the "Volts for zero Oil-Film Thickness" which represents the settings of the parallel condenser.

For a constant input signal to the measurement gear, there will consequently be one maximum output signal according to the setting of the parallel condenser, and, for this setting, the correct calibration curve can easily be selected from Fig.35.

When the measurement gear is employed for engine testing, the procedure will be as follows -

The parallel condenser is adjusted until maximum signal appears on the oscilloscope screen and the calibration curve of maximum slope, corresponding to this setting, can then be used.

MEASUREMENTS OF LATERAL DISPLACEMENTS OF A CRANKSHAFT JOURNAL.

Arrangement of Apparatus.

After the calibration tests were completed, the bearing cap with the four pick-up units was refitted in the engine and the measurement gear arranged for test, as shown in Fig.30.

Both a Muirhead Pametrada Wave Analyser and a Cossor Double Beam d.c. Oscilloscope, complete with high speed moving-film camera, were available for recording the output from the Oscillator-Discriminator Unit⁽¹⁾.

An electronic test meter was used for the purpose of oscilloscope calibrations, in the manner explained under "Test Procedure".

For recordings of the complete journal displacements, both beams were used on the oscilloscope. The discriminator output was fed through the channel of highest amplification to one set of deflector plates. The other set was utilised for the purpose of obtaining a mark on the records corresponding to top dead centre of Crank 1. of the engine.

The reference marking was accomplished by a contact breaker circuit designed to deliver a short voltage pulse to

(1) Unfortunately, the camera was not available when the photograph of Fig.30 was taken.

the oscilloscope on the arrival of Crank 1. at top dead centre position.

The Wave Analyser was used to measure the amplitudes of various harmonics in the output from the Oscillator-Discriminator Unit.

During these tests, the contact breaker was disconnected and the oscilloscope used purely to provide a visual check.

For all tests, the temperature of the lubricating oil was measured in the sump⁽¹⁾.

The engine speed was measured with a tachometer.

Test Programme.

The following Test Programme was arranged in accordance with theoretical work carried out earlier for the test engine.

TEST 1. - The oscilloscope and high speed camera were used to compile records of the complete journal displacements, as registered by pick-up unit 1., for a range of speed from 600 R.P.M. to 2,000 R.P.M.

TEST 2. - Measurements were taken on the Wave Analyser of the fundamental of the output from the Oscillator-Discriminator Unit, and, neglecting the non-linearity of the relations

(1) This temperature is used as a measure of the oil temperature in the bearing for purposes of calculation. Since the oil temperature in the sump is lower than that in the bearing, an error is thereby introduced.

between this output and the actual journal displacements, these measurements will be taken as indicative of the fundamental of the journal displacements.

This test was carried out for engine speeds from 1,200 R.P.M. to 2,000 R.P.M.⁽¹⁾, and all four pick-up units were used.

TEST 3. - Measurements were taken on the Wave Analyser of the 5th. and 7th. harmonics of the journal lateral displacements with the aim of obtaining the effect of the 6th. harmonic of torsional vibrations of the crankshaft.

A speed range from 900 R.P.M. to 2,000 R.P.M. for the engine was covered, but most measurements were taken round the resonance speed for the crankshaft - (See Fig.32). Here also, the effect of the non-linearity of the calibration curves for the Oscillator-Discriminator Unit has been neglected. All four pick-up units were used.

Test Procedure.

It was noticed during preliminary trials on the engine that continuous prolonged running had the effect of reducing the apparent amplitudes of the journal displacements.

Since no reason could be found for a decrease in the

- (1) Since the lower limit of the Wave Analyser frequency range is 19 cycles per second, fundamentals for lower speeds than 1,200 R.P.M. cannot be measured.

actual amplitudes, this effect was explained by a reduction in the dielectric constant of the oil-film due to froth formation in the lubricating oil and, as such, the phenomenon was a direct cause of errors in the experimental results.

To reduce the importance of the above-described effect, the engine was never run continuously during test for more than ten minutes. Thereafter, the engine was stopped for thirty minutes to allow the lubricating oil to recover before another test was carried out.


No errors were noticeable after this procedure had been adopted.

When the oscilloscope with the recording camera was used, it was found necessary to carry out static calibrations for these instruments of input voltage versus output deflection.

With the engine stationery, convenient d.c. voltages for this calibration were obtained from the output of the Oscillator-Discriminator Unit, by adjusting the parallel condenser. These voltages were measured with the electronic test meter.

The output deflections were measured on a scale on the oscilloscope screen, and the camera amplification found by taking a photograph of this scale.

The Muirhead Pametrada Wave Analyser gives readings in volts. These readings were interpreted by neglecting the non-linear effect of the pick-up units and using the maximum values of the calibration factors given in Fig.36.



PRESENTATION AND DISCUSSION OF JOURNAL DISPLACEMENT TEST RESULTS.

Before any particular results are presented, some general remarks related to all tests should be made.

Since the viscosity curve for the lubricating oil of the test bearing, as well as the effect of viscosity on journal displacement, are known, it has been possible to recalculate all experimental readings to a common reference temperature. 60 Degrees Centigrade was selected as the most convenient reference temperature.

Only variations in the force actions on the bearing should thus affect the results for journal displacements presented.

Re-Plotting of Results from Test 1.

Samples of the records obtained with the oscilloscope camera for Test 1. are shown in Fig.37(a-h).

These records are re-plotted making use of the calibration curves of Fig.35 to give graphs of journal lateral displacements versus crankangle.

The method of fixing the crankshaft central position on the trace records can now be outlined as follows:-

It will be observed that at low values of engine speeds

such as 600 R.P.M. - (Fig.37 (a)) -. the predominant factor responsible for displacements of the journal from its central position is the firing load which causes a sharp displacement peak of approximately 70 crankangle degrees duration.

The remaining 290 degrees show only slight irregularities, the main value of which should give the journal central position to a fair degree of accuracy. To mark the journal central position, the best straight line was drawn through this latter part of the test records.

For other engine speeds, the shaft central position was obtained from a corresponding record obtained at 600 R.P.M.

The re-plotted curves showing journal lateral displacements versus crankangle for speeds ranging from 600 R.P.M. to 2,000 R.P.M. are presented in Appendix IV.

Records of Complete Journal Displacements.

The behaviour of the crankshaft journal bearing over the speed range 600 R.P.M. - 2,000 R.P.M. is illustrated in the graphs given in Appendix IV.

These graphs reveal that the crankshaft journal displacements are determined by two main crankshaft loads of completely different character:-

FIGURE 37.



^{7 A} (a). 600 R.P.M., 60 C.



^{13 A} ¹⁴ ^{14 A} ¹⁵ ^{15 A}
(b). 800 R.P.M., 60 C.



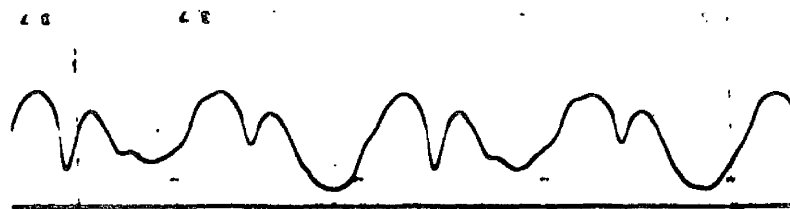
^{21 A} ²²
(c). 1,000 R.P.M., 60 C.



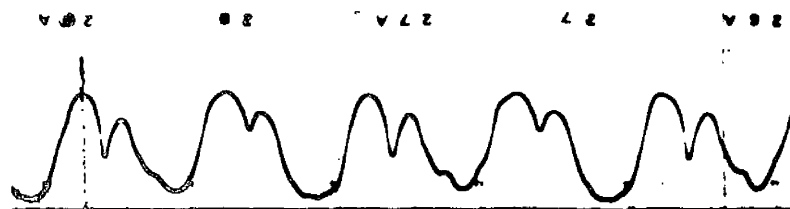
²⁷ ²⁷
(d). 1,200 R.P.M., 60 C.

OSCILLOSCOPE RECORDS OF
JOURNAL DISPLACEMENTS.

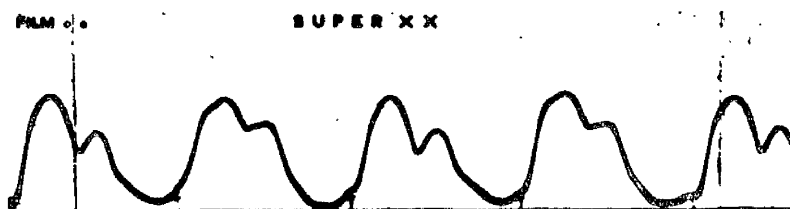
FIGURE 37.



(e). 1,400 R.P.M., 60 C.



(f). 1,600 R.P.M., 60 C.



(g). 1,800 R.P.M., 60 C.



(h). 2,000 R.P.M., 43 C.

OSCILLOSCOPE RECORDS OF
JOURNAL DISPLACEMENTS.

(a) Firing Loads - As has already been mentioned, the firing load appears on the displacement records as a sharp peak of relatively short duration.

Since the complete pattern of journal displacement is exactly repeated once only in every two revolutions, two adjacent cycles are shown on each trace record, the magnitude of the firing peak being slightly different in each of these cycles.

This effect is produced by the alternate firing of the two cylinders on either side of the pick-up unit and the fact that the pick-up unit is not exactly the same distance from each.

The firing load from the cylinder nearest the pick-up unit will therefore have the greatest effect on the measured displacement.

It is also apparent that the effect of the firing loads on journal displacement diminishes progressively with engine speed. From general bearing theory, it is known that the bearing resistance to load increases with engine speed. Firing loads, although also increasing with engine speed, will probably not do so to the same extent.

The overall diminishing effect of firing load with increasing engine speed can therefore be expected.

(b) Centrifugal Forces - A study of the displacement records reveals a clear tendency for the wave-trace to become more sinusoidal in shape with increase in engine speed. A sinusoidal variation of journal displacement, recorded by a stationery pick-up unit, such as the one in operation, would provide an indication that the crankshaft journal was rotating with a constant eccentricity within its bearing shell. (See Fig.38).

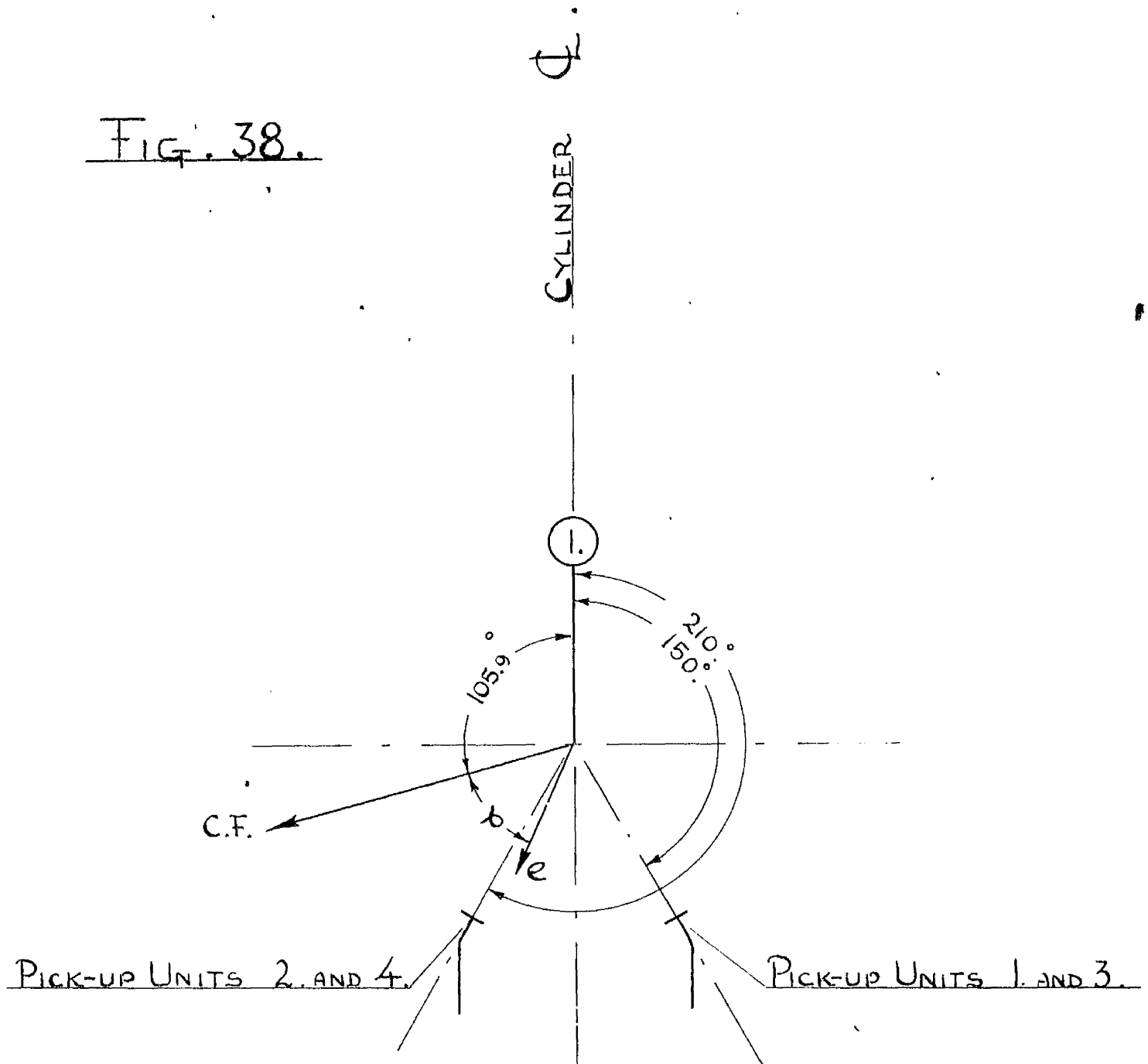
This would suggest a rotating force of reasonably constant magnitude acting on the bearing, such as a centrifugal force, and, accordingly, may be the effect of the force F_c shown in Fig.28.

The fact that the magnitude of this sinusoidal motion increases rapidly with engine speeds would also point to the presence of centrifugal forces which increase in relation to the square of the crankshaft speed.

The record taken at 2,000 R.P.M. indicates clearly the importance of the centrifugal forces at high engine speed, compared to the relatively small effect of the firing loads.

Reviewed in conjunction with the force analysis which was carried out for the crankshaft in earlier parts of this Thesis, the above observations confirm that, for high engine speeds, the bearing load due to the mean centrifugal forces is the predominant load on bearing 4.

FIG. 38.



FRONT END VIEW OF ENGINE SHOWING
CENTRIFUGAL FORCE ON BEARING 4.

Presentation.

The above findings are rather fortunate for further development of the subject, because they mean that we possess numerical values for the most important load acting on our test bearing⁽¹⁾.

Consequently, the load numbers for the bearing can be calculated, and it will be possible to present the results obtained for journal displacements in a way generally used in bearing research. (See Fig.27).

To adopt the standard presentation completely, the measured journal displacements will also be converted into eccentricity ratios.

Naturally, since the values used for the constant rotating force acting on our test bearing are obtained through a complicated analysis, certain doubts may be attached to their validity.

Along with our own graphs for eccentricity ratios versus load numbers, we will therefore present a similar graph obtained experimentally for a bearing subjected to loads, the magnitudes of which are known accurately⁽²⁾.

- (1) F₁ of Fig.28 gives the value of this load for ω = 203 1/sec. For other engine speeds, it is easily obtained, being proportional to the engine speed.
- (2) A graph obtained by Dubois and Oovirk for narrow journal bearings was chosen for the purpose. See Fig.27.

Thus a direct comparison can be carried out to give information about the values of the load acting on our test bearing, as obtained through the force analysis of the crankshaft.

Eccentricity Ratio - Load Number Graphs. - (Tests 1. and 2.)

Having decided to present the results in the manner suggested in the previous section, attempts were directed toward obtaining the best measure of the crankshaft journal eccentricity due to the centrifugal load.

It was apparent that some difficulty would be encountered in this respect because of the obscuring effect of firing loads.

An examination of the journal displacement graphs - (Appendix IV) - suggested that it would be possible to obtain a measure of the eccentricity due to the centrifugal load by two different methods, one which would give a slightly higher value than the actual value, and the other which would give a slightly lower value than the actual value.

The two methods used are as follows:-

Method (a) - The 2,000 R.P.M. record is a good illustration of the fact that the firing load opposes the centrifugal load over the first half cycle of journal displacement with reference to Crank 1. top dead centre. Consequently, the

journal eccentricity due to the centrifugal load will be somewhat reduced over this half cycle. Conversely, in the second half cycle of journal displacement, any small residual effect of firing load will add to the centrifugal load in producing crankshaft eccentricity.

It can therefore be expected that eccentricity ratios taken for the second half cycle, as indicated on the journal displacement graphs, will furnish a reasonable but slightly excessive measure of the centrifugal load effect.

Method (b) - In this case, the fundamental of journal displacement, as recorded by a Wave Analyser, was taken as the measure of the journal eccentricity due to the centrifugal load⁽¹⁾.

Since it has been demonstrated that the main peak displacement due to firing opposes the effect of centrifugal load over the first half cycle, it is evident that the fundamental of journal displacement will indicate values for the centrifugal load eccentricity which are smaller than the actual value.

The effect of firing loads on the fundamental of journal displacement is displayed by measurements taken with all four pick-up units, as shown in Fig.39 and 40.

(1) See description of Test 2. on Page 108.

A short discussion of these graphs will be necessary:-

From the symmetrical characteristics of the firing load, the centrifugal load and the geometry of the crankshaft, it will be expected that pick-up units in the same angular position, with reference to the cylinder centre line, will give similar readings for the fundamental of the journal displacement⁽¹⁾.

That this is the case, is illustrated by Fig.39 where readings from pick-up units 1. and 3. are superimposed, and by Fig.40 where readings from pick-up units 2. and 4. are also superimposed.

It will also be noticed that readings taken with pick-up units 2. and 4. are lower than the readings for pick-up units 1. and 3.

This is due to the fact that measurements of firing load eccentricities, which generally oppose the centrifugal load eccentricities, are dependent on the angular position of the pick-up unit.

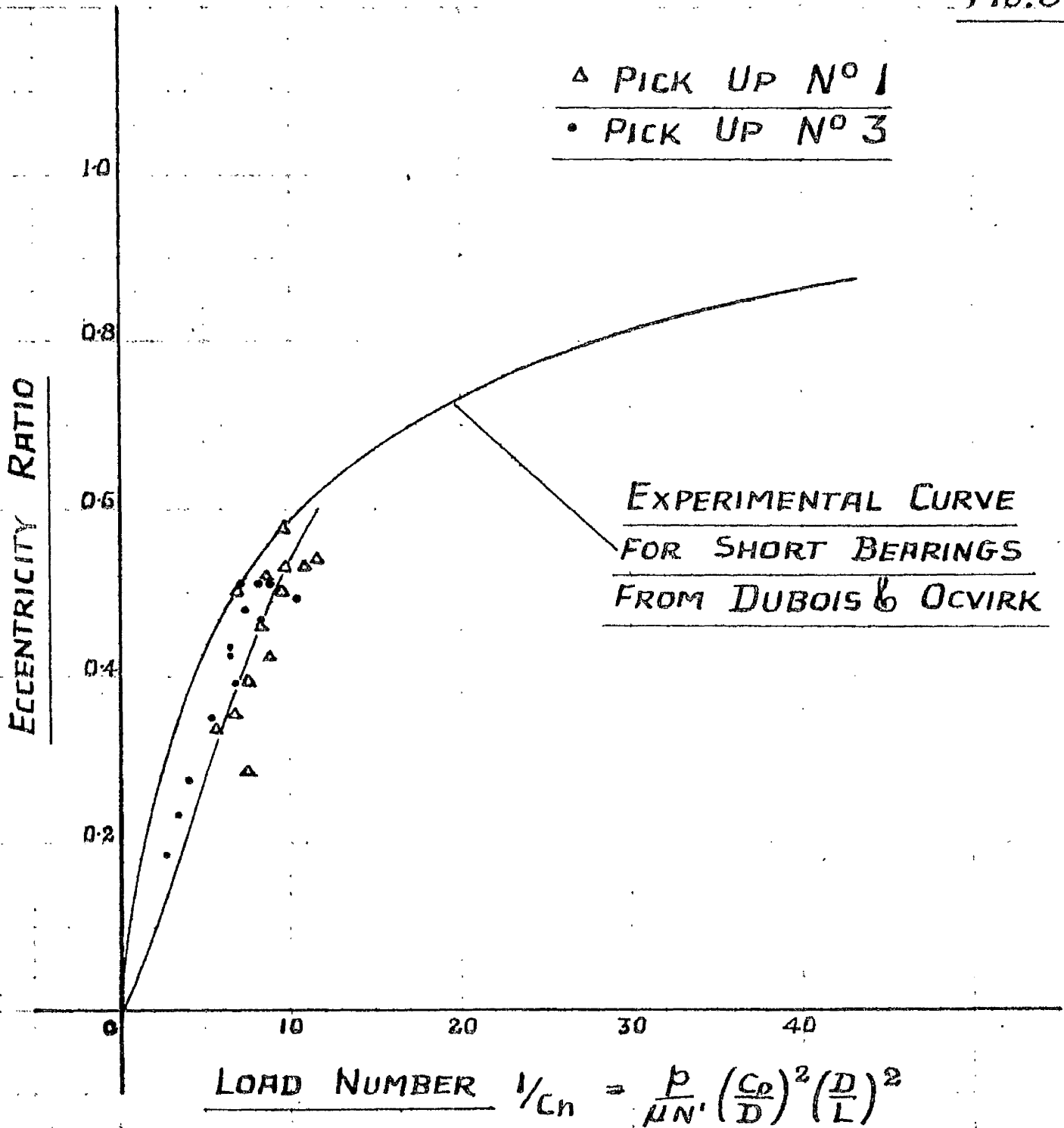
Since pick-up units 1. and 3. show the largest value for the fundamental of the journal displacement, readings from these pick-up units are least affected by the firing loads and, consequently, the best representation of the journal eccentricity due to the centrifugal load.

(1) For the angular positions of the pick-up units, see Fig.38.

FUNDAMENTAL OF BEARING DISPLACEMENT

AS RECORDED BY PICK-UP N^os 1 & 3

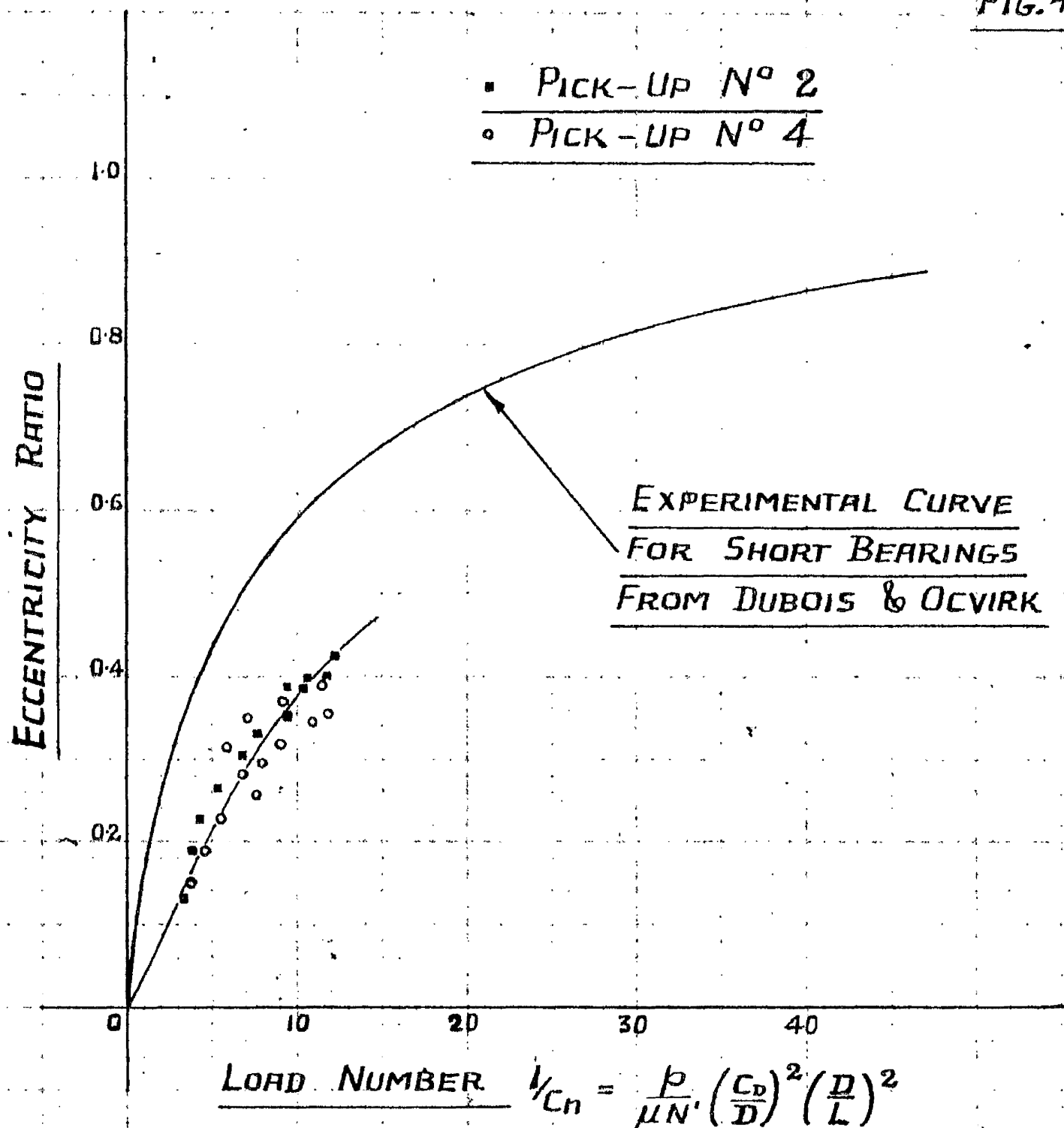
FIG. 39.



FUNDAMENTAL OF BEARING DISPLACEMENT

AS RECORDED BY PICK-UP N^o 2 & 4

FIG. 40.



It follows from the description of the measurements taken by methods (a) and (b), that the actual values of the eccentricity ratio due to the centrifugal load, must lie somewhere in the region between the graphs obtained by these two methods.

We can now therefore draw a comparison between these actual eccentricity values, obtained for the test engine centre journal bearing, and the graph from Dubois and Ocvirk.

It is seen from Fig.41, which refers to results obtained with pick-up unit 1., that below a certain load number the actual values of the eccentricity ratio, due to the centrifugal load acting on the test engine centre journal bearing, are lower than corresponding values obtained by Dubois and Ocvirk.

Above this load number, however, the values obtained for the test engine increase rapidly, thus approaching the curve given by Dubois and Ocvirk.

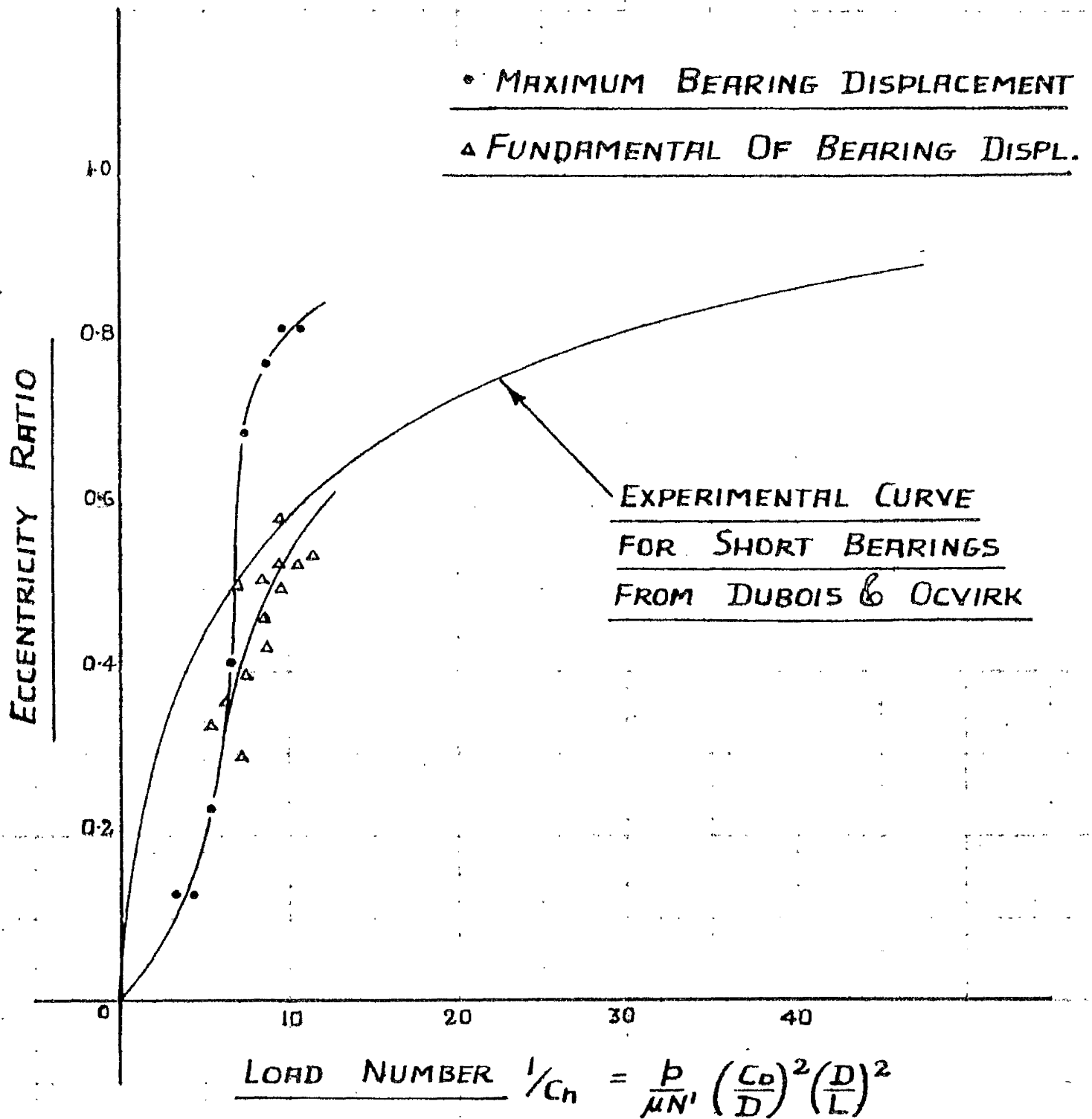
For an explanation of the features described above, it will be necessary to return to the basis of calculation for the centrifugal forces on the test engine journal bearings.

To simplify the crankshaft force analysis, it was then assumed that the engine bearings offered simple point supports to the crankshaft - i.e. the effect of the journal

ECCENTRICITY RATIO AS RECORDED

BY PICK-UP N° 1

FIG. 41.



displacements were neglected⁽¹⁾.

Since bearing displacements of appreciable magnitude do occur, the bearing in actual fact offers less support or constraint to the crankshaft and, consequently, the force action actually present between the bearing and the crankshaft will be less than the calculated value.

In plotting the test engine experimental readings of eccentricity ratios, the calculated values of bearing centrifugal loads were used to derive the load numbers.

Values of load number in excess of the actual values occurring in the test engine were therefore used as a basis for the eccentricity ratios.

The major deviation between the experimental curves obtained for the test engine and the graph of Dubois and Ocavirk can therefore be attributed to the effect of journal displacements in introducing variations from the calculated bearing loads.

(1) See Page 45.

Amplitude of 5th. and 7th. Harmonics. - (Test 3.)

The results obtained for the amplitudes of the 5th. and 7th. harmonics of the journal lateral displacements, making use of all four pick-up units, are presented in Fig.42-50.

It will be noted that results obtained by using pick-up units 1. and 3. are presented on the same sheet and, similarly, for pick-up units 2. and 4. Thus, the results from pick-up units of the same angular position, but different axial positions, can be easily compared.

For an explanation of the graphs, it will again be necessary to consider two different load actions - the firing loads and the bearing loads, due to torsional vibrations of the crankshaft, - and, by special considerations of each of them, it will be possible to distinguish between their effects on the measured amplitudes.

(a) Firing Loads.- As mentioned in the discussion of results from Tests 1. and 2., symmetry considerations show that the firing loads should have the same effect on two pick-up units which are positioned symmetrically about the centre line of bearing 4. - i.e. the effect of these loads on pick-up unit 3. should be the same as on pick-up unit 1., and similarly for pick-up units 2. and 4.

With reference to Fig.42-49, it is seen that using pairs

of symmetrically positioned pick-up units, the same readings are obtained to within a reasonable margin of error for speeds ranging from 900 R.P.M. to 1,700 R.P.M.

For this part of the graphs, the amplitudes are therefore primarily due to the firing loads.

Naturally, the firing loads will also have some bearing on the amplitudes in the remaining speed range - (1,700 R.P.M. to 2,000 R.P.M.) - and, considering the effect at lower speeds, a rough estimate was made of this.

(b) Bearing Loads due to the Torsional Vibrations of the Crankshaft.

It is seen from Fig.42,44,46 and 48, that the amplitudes of the 5th. and 7th. harmonics of the lateral displacement of the crankshaft journal, particularly as measured with pick-up units 1. and 2., show distinct peaks near the top of the engine speed range.

A corresponding peak is found for the 6th. harmonic of the torsional vibrations of the crankshaft, (see Fig.32), and, consequently, it may be concluded that the former effects are due to the latter⁽¹⁾.

The same peaks for the journal displacement are smaller

- (1) It is seen from Page 86, that a 6th. harmonic of the torsional vibrations of the crankshaft, as a result of the crankshaft rotation, will give rise to 5th. and 7th. harmonics of the journal displacement.

and less distinct in the graphs obtained from measurements taken with pick-up units 3. and 4. (See Fig. 43, 45, 47 and 49). This, however, is to be expected since the torsional amplitudes along the crankshaft increase towards the front end - (see Fig. 18) - and, consequently, the crankshaft journal will vibrate obliquely.

Under the discussion of firing loads, it was seen that these loads also have some effect on the amplitudes measured between 1,700 R.P.M. and 2,000 R.P.M.

This latter effect, however, could be estimated from the lower speed end of the graphs and, as a result, the effect of the torsional vibrations of the crankshaft can be isolated. Dimensions which correspond roughly to the effect of the torsional vibrations are shown on the graphs.

It will now be assumed that the amplitudes of the 5th. and 7th. harmonics of the journal displacements at the centre of the test bearing are averages of the amplitudes measured on pick-up units spaced symmetrically about the bearing centre. This is true if the journal remains straight between the pick-up units.

Thus, the 5th. and 7th. harmonics of the journal displacement at the centre of the test bearing can be obtained from pick-up units 1. and 3., and from pick-up units 2. and 4. These values are entered into the Table of Fig. 50.

FIG. 42. 5TH HARMONIC PICK UP UNIT 1.

TEST 1 (24-7-56) +

TEST 2 (5-9-56) •

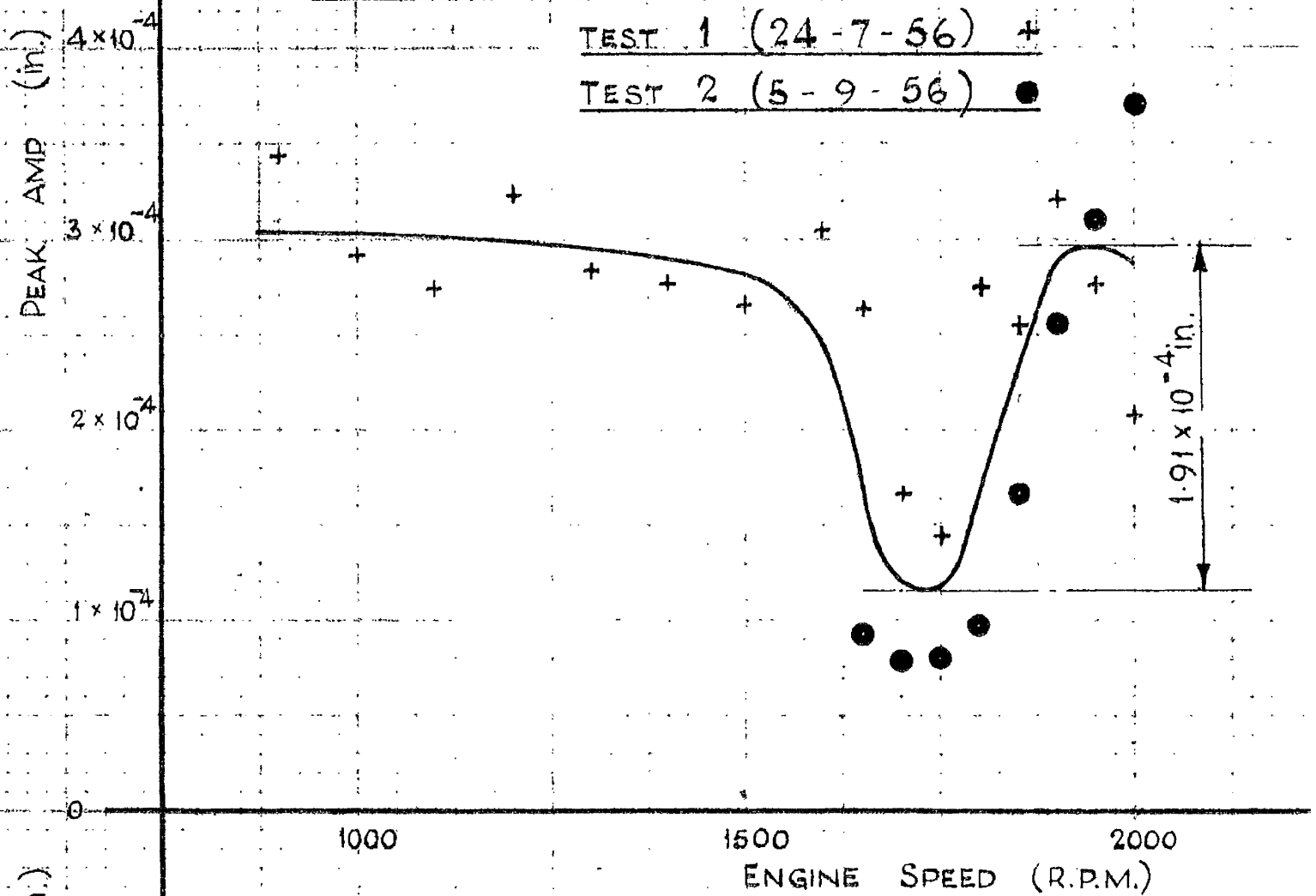


FIG. 43. 5TH HARMONIC PICK UP UNIT 3.

TEST 1 (30-7-56) +

TEST 2 (30-7-56) •

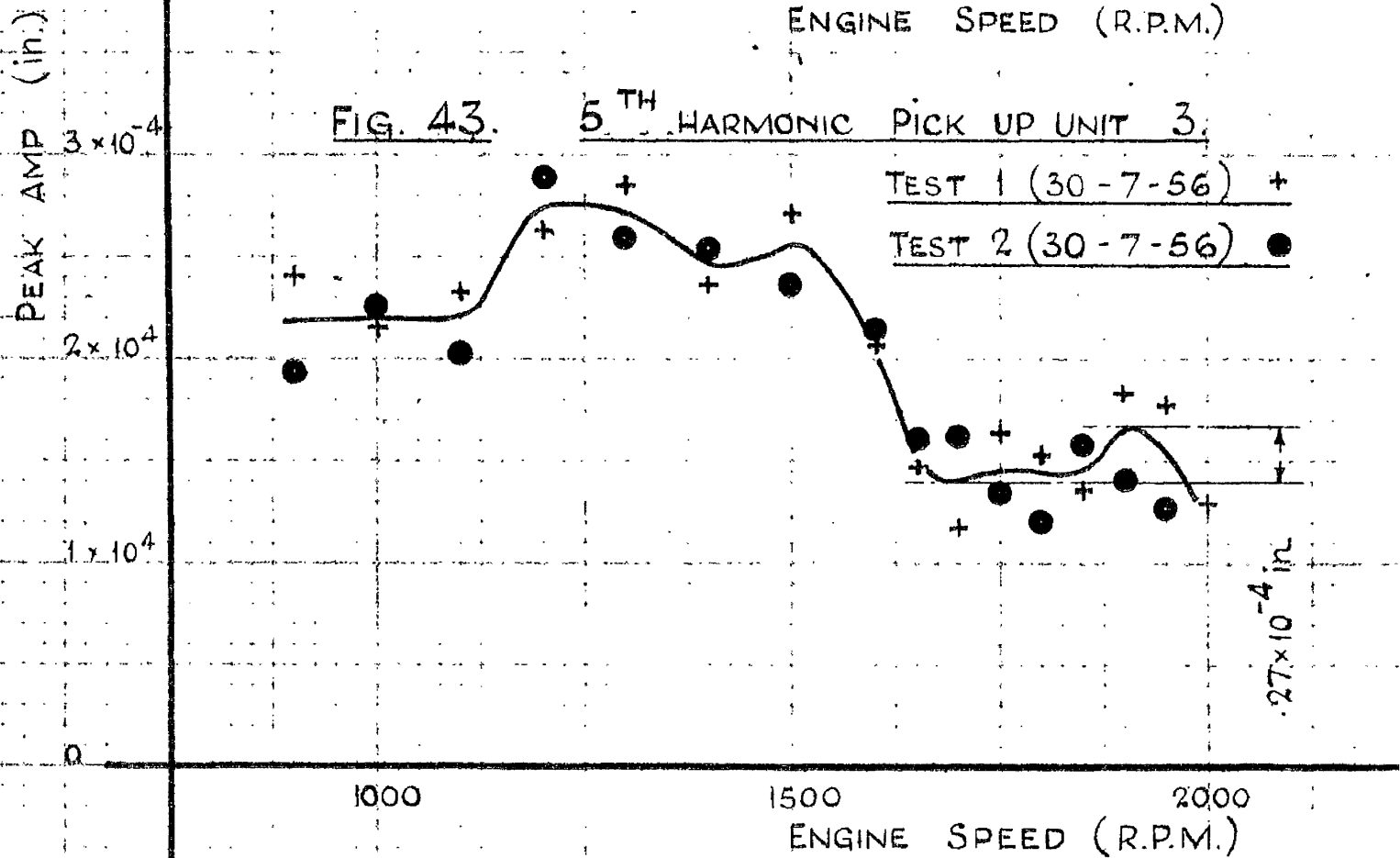


FIG. 44.

5TH. HARMONIC
PICK UP UNIT. 2.

+ TEST No. 1, (27-7-56)

• TEST No. 2, (6-9-56)

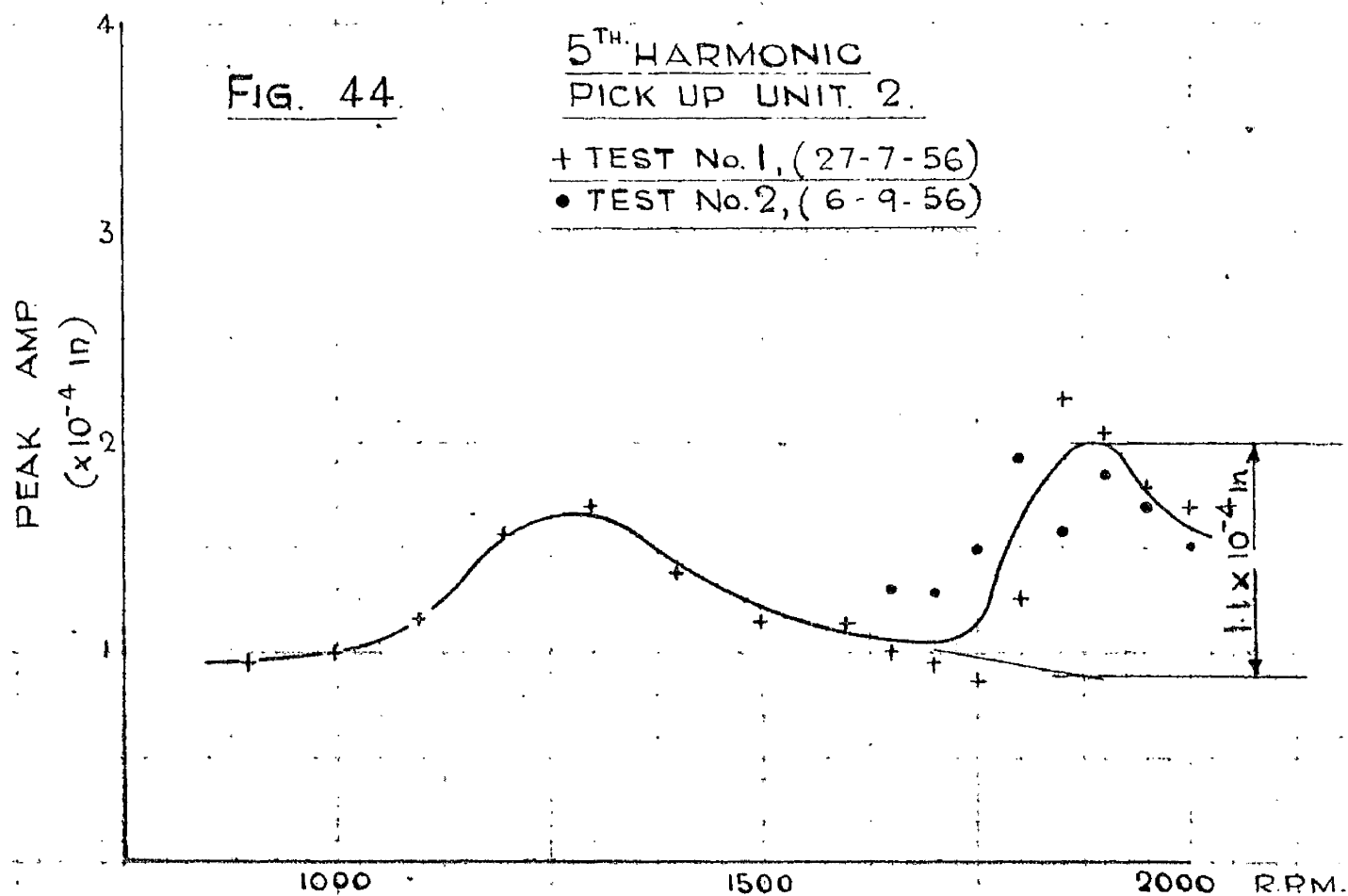


FIG. 45.

5TH. HARMONIC
PICK UP UNIT 4

+ TEST No. 1, (31-7-56)

• TEST No. 2, (6-9-56)

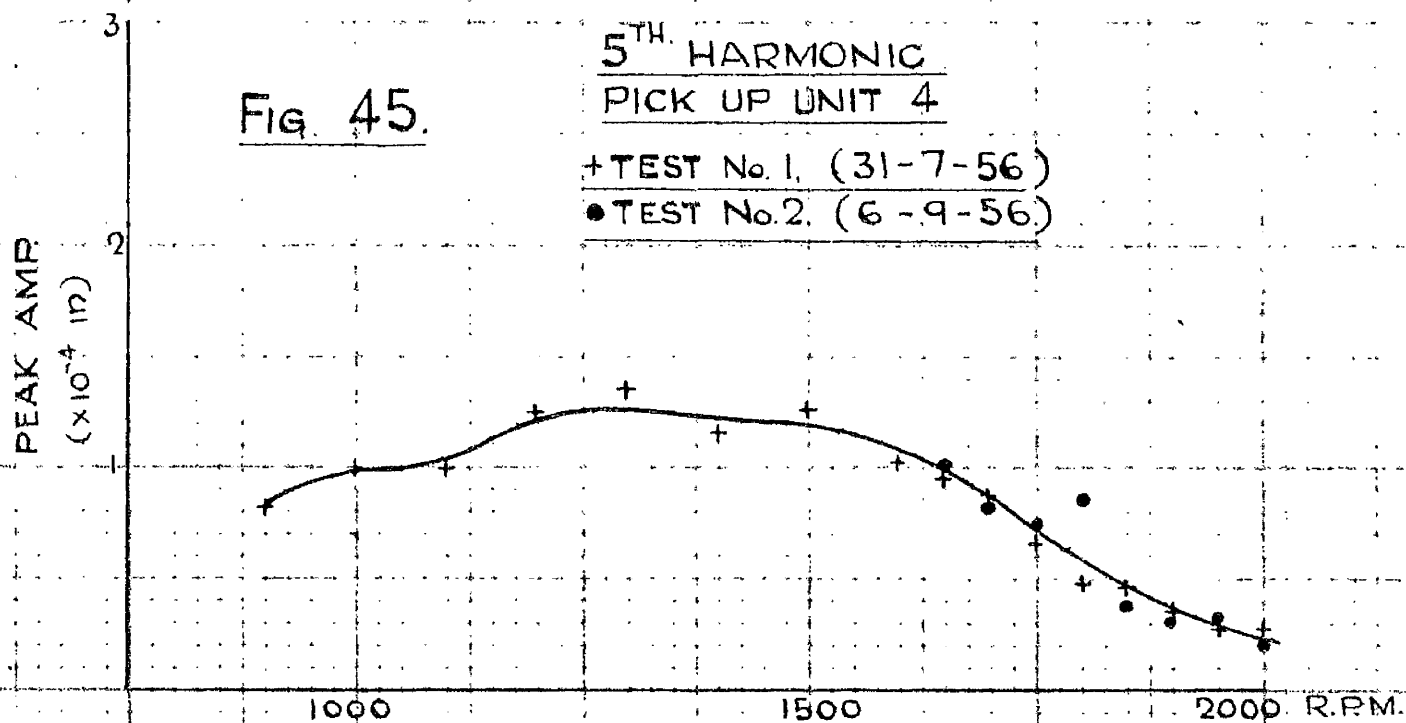


FIG. 46.

7TH HARMONIC PICK UP UNIT 1

+ TEST No.1. (24-7-56)

• TEST No.2. (5-9-56)

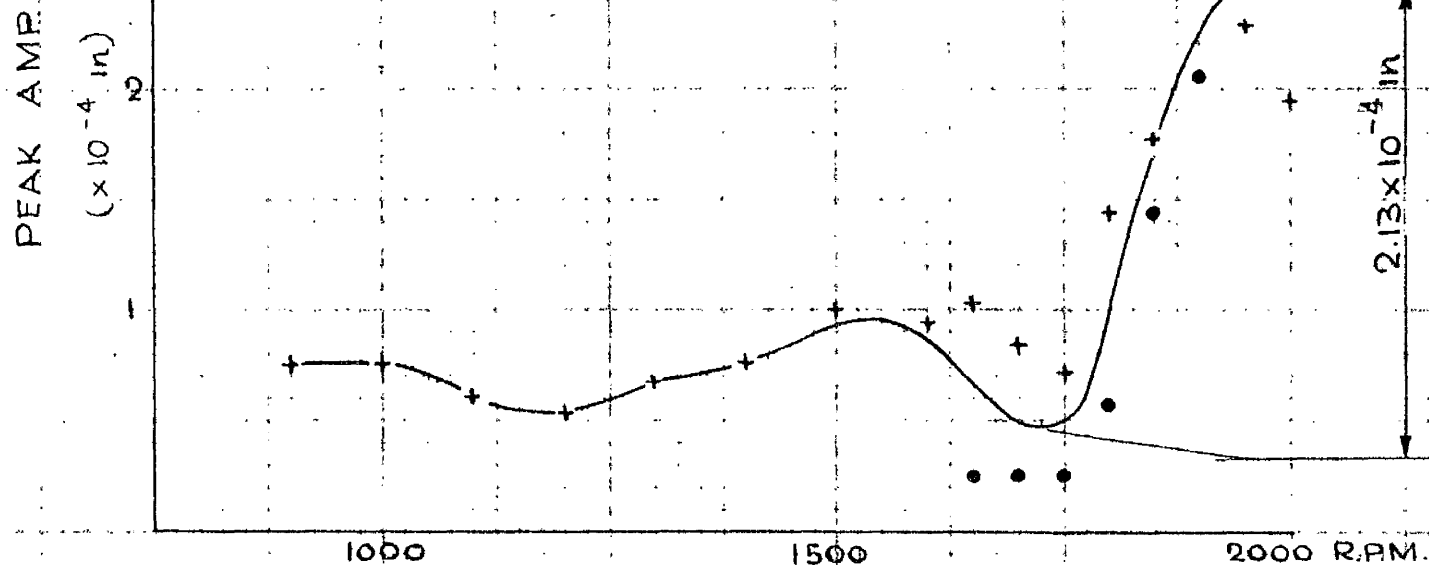


FIG. 47.

7TH HARMONIC PICK UP UNIT 3

+ TEST No.1

• TEST No.2

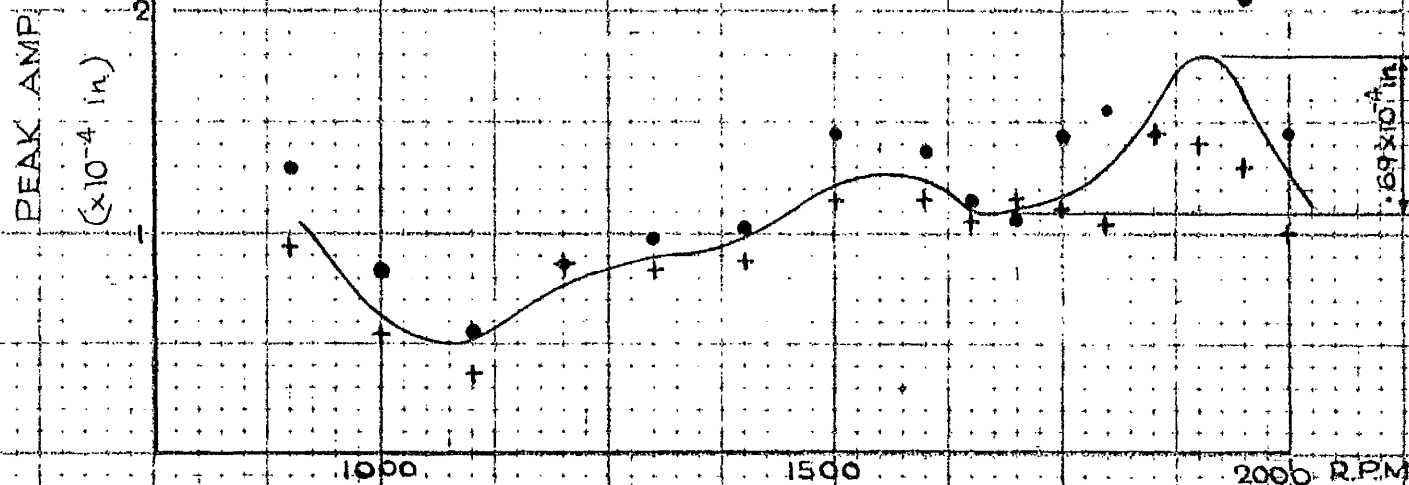


FIG. 48 7TH HARMONIC PICK UP. 2

TEST 1. (26-7-56) +

TEST 2. (6-9-56) ●

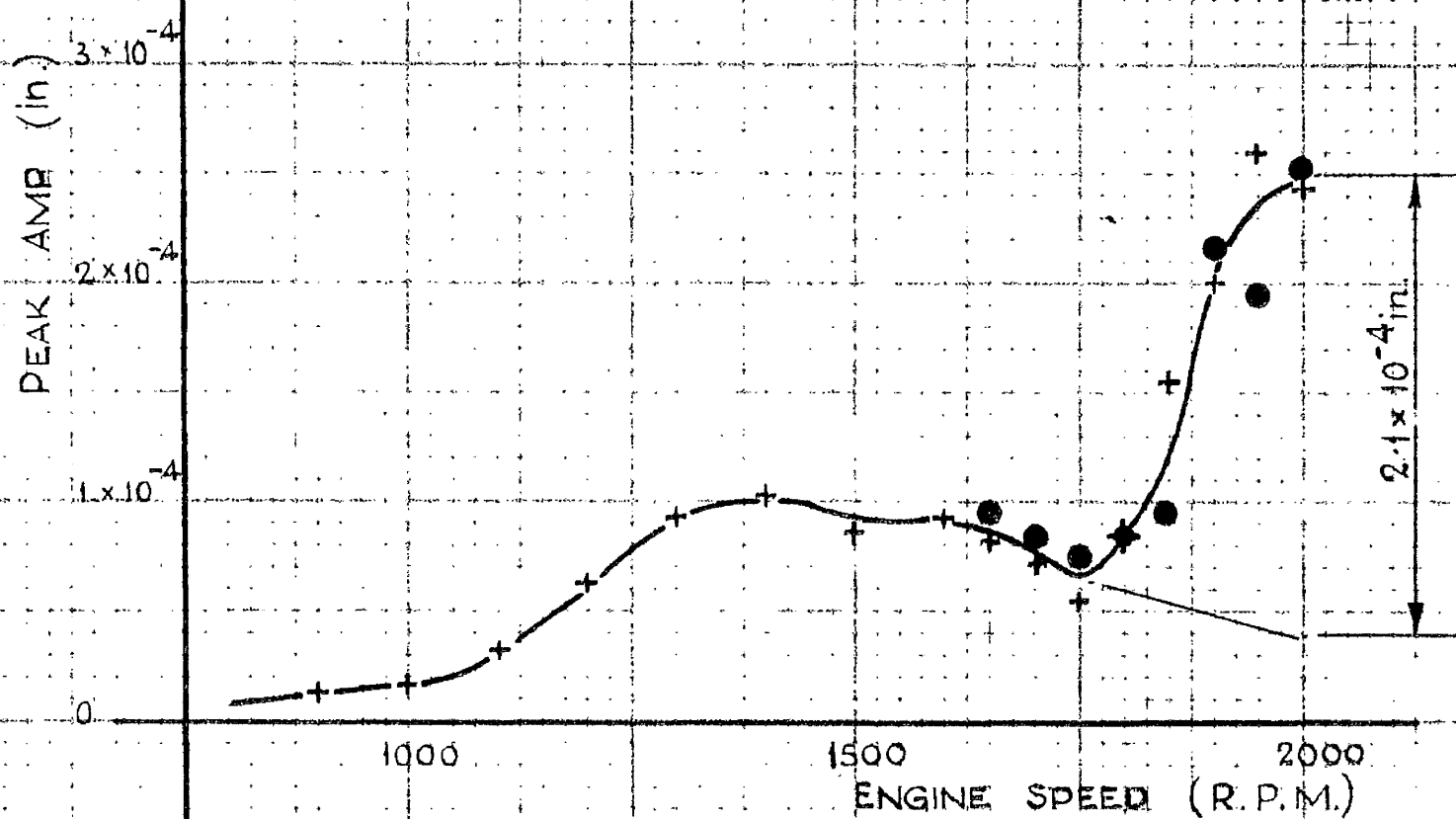
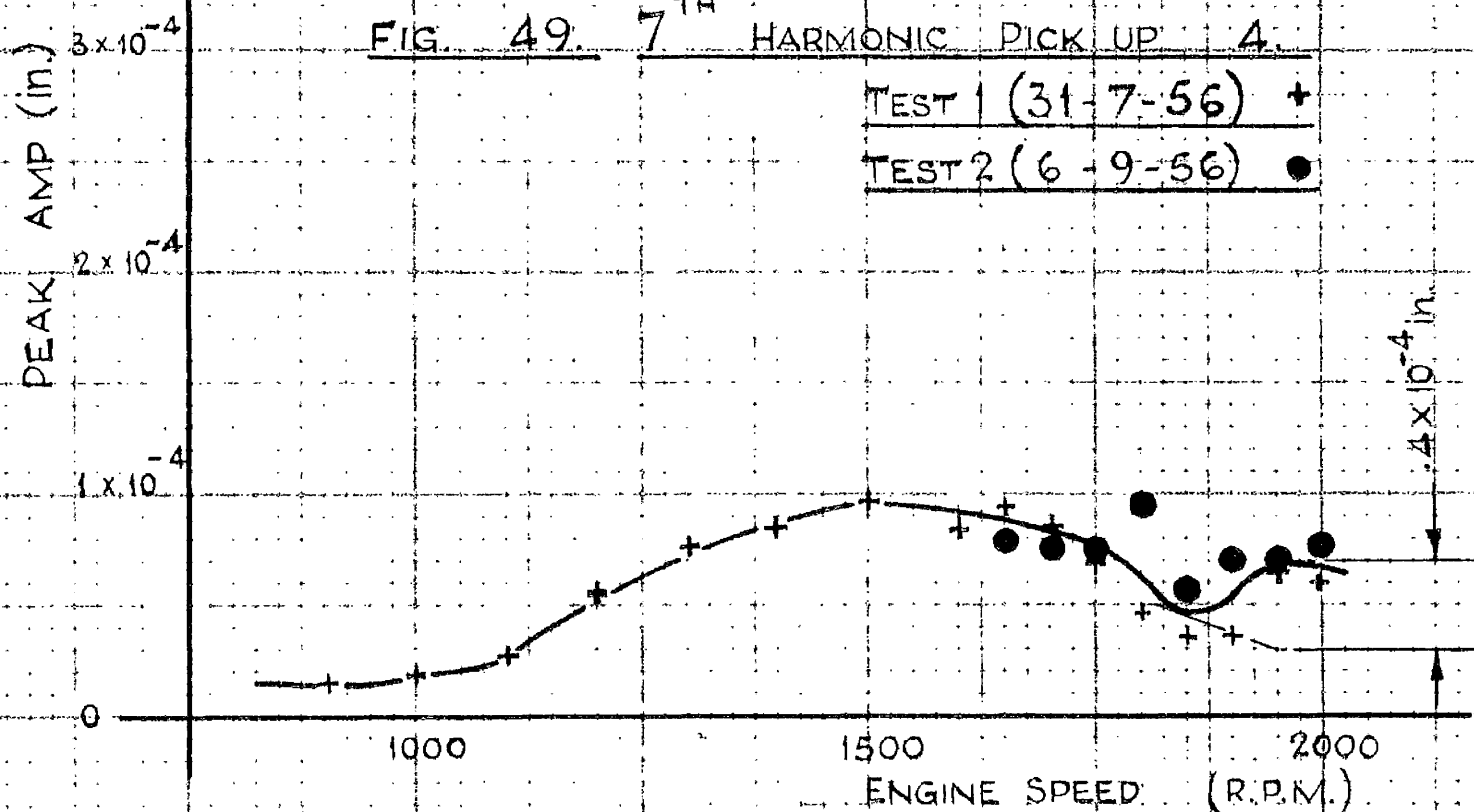


FIG. 49 7TH HARMONIC PICK UP. 4

TEST 1 (31-7-56) +

TEST 2 (6-9-56) ●



It should be noticed that, since bearing loads due to the torsional vibrations of the crankshaft are independent of the angular position of the crankshaft, so should also be the corresponding displacements ⁽¹⁾.

Results obtained on both sets of pick-up units should therefore be the same and, consequently, they can be averaged.

Fig.50 also gives values for the 5th. and 7th. harmonics of the journal displacement, as obtained from measurements of the torsional vibrations of the crankshaft through the theoretical analysis carried out in the first main section of this Thesis.

Considering the complexity of the analysis, as well as difficulties encountered in experimental work, the results of Fig.50 compare favourably.

(1) See Page 57.

FIG. 50.

| METHOD OF DERIVATION | AMPLITUDE OF 5 TH HARM (in.) | AMPLITUDE OF 7 TH HARM(in.) |
|--|---|--|
| MEASURED ON PICK-UP UNITS 1 & 3 | 1.09×10^{-4} | 1.41×10^{-4} |
| MEASURED ON PICK-UP UNITS 2 & 4 | $.55 \times 10^{-4}$ | 1.25×10^{-4} |
| AVERAGE | $.82 \times 10^{-4}$ | 1.33×10^{-4} |
| CALCULATED FROM MEASUREMENTS OF TORSIONAL VIBRATIONS | 1.08×10^{-4} | 1.25×10^{-4} |

1. FROM FIG. 32. AND EQUATIONS 62 & 63
AMPLITUDES OF 5TH AND 7TH HARMONICS.

CONCLUSION:

Experimental measurements of journal displacements show that a force analysis for a multi-throw crankshaft, treating the crankshaft as a continuous elastic body simply supported in the bearings, will be valid for engines of normal bearing clearances, provided that the loads applied to the crankshaft are large, or vary with a frequency which is much higher than the frequency of rotation of the crankshaft.

For smaller loads, or very large bearing clearances, the deflections of the crankshaft journals in the bearings will be of importance, thus destroying the basis for the force analysis.

Since heavy crankshaft loads are of the greatest practical importance, the discussed force analysis may be useful for design purposes.

PART II

SHRINK-FITTED ASSEMBLIES LOADED IN TORSION.

THEORETICAL ANALYSIS
OF
SHRINK-FITTED ASSEMBLIES LOADED IN TORSION.

GENERAL DISCUSSION.

Inherent Stresses, Working Stresses and Superposition.

As a rule, some stresses will always be present in the components of an engineering design although no actual working loads are applied to the system. These are stresses which may be caused by the process of manufacture or method of assembly and they form a characteristic feature of the finished arrangement. As such they will be referred to in later parts of this work as "inherent stresses", and they are defined as the stresses present in an assembly when all external loads are equal to zero.

In contrast to the inherent stresses of a system, stresses actually caused by externally applied loads will be called "working stresses".

The above classification is convenient as it leads up to separate treatments for the analysis of each of the component stress systems, bearing in mind that the resultant effect of all stresses can be found afterwards by means of superposition. If an engineering arrangement follows Hooke's Law of Elasticity, the superposition of one stress system on to

another may be carried out by simple addition, and the resultant effect is accordingly easy to find. When a design is worked beyond its elastic limits, however, the problem of superimposing stress systems immediately becomes much more complex and proper analysis is often beyond the reach of practical possibilities.

Shrink-fitted Assemblies, Plastic and Elastic Behaviour:

The above general considerations will now be applied to a particular case - the analysis of a shrink-fitted assembly loaded in torsion.

Where shrink-fitting is used in practice, as, for instance, in built up crankshafts, interferences high enough to cause plastic flow are quite common. Yield must therefore take place during assembly and further yield is to be expected when the components are loaded by working stresses additional to the inherent stresses.

Analyses are available which will give the inherent stresses taking plastic flow into account⁽¹⁾, but to find the resultant stress when a working stress is superimposed on the inherent stress under these conditions is a problem, the solution of which is hardly obtainable at present in

(1) On the Overstraining of Thick-walled Cylinders under Internal Fluid Pressure and under Interference Fit Pressure, by M.C.Steele. (Thesis for Ph.D. at Glasgow University). 1950.

practice.

This paper is concerned mainly with the effects of torsional loads on shrink-fitted assemblies. It appears that even for loads below the elastic limit of the material, a complete analysis of this problem has not yet been carried out. It has therefore been decided to seek a solution for the elastic case first before any additional complications, due to plastic flow in the material, are brought in.

To obtain a foundation for the theoretical analysis of the proceeding work, the following assumption has therefore been made:— The resultant stress of the shrink-fitted assembly under load does not at any point exceed the elastic limit of the material.

Resting on the above assumption, use can now be made of the simplification that the resultant stress due to any number of superimposed stress systems can be obtained by simple addition. There are no effects carried from one stress system to any other and it is therefore fully justified to treat each stress system separately. The following work can therefore be concentrated directly on the effects of torsional loads on a shrink-fitted assembly, and the only reference made to the system of inherent stresses is for obtaining the strength of the grip between the two shrink-fitted components.

The Shrink-fitted Assembly as an Intermittent Stage between
a Plain Shaft and a Solid Shaft with a Collar.

Some general observations on twists of shrink-fitted assemblies may be quite useful before the analytical work on the same problem is started.

Let us consider a hub fitted to a plain shaft as shown in Fig. 51, and assume in the beginning that the interface grip between the hub and the shaft is very light. The assembly, when loaded in torsion, will then behave very nearly as if the hub were not there. The shaft will twist like an unrestricted plain shaft and the hub will remain nearly undeflected. This is only possible if slip takes place at the interface between the hub and the shaft. Reversing the argument, it may be stated that slip takes place because the components behave as described above.

It should also be observed that, since the shaft behaves approximately as a plain unrestricted shaft, there will be no stress concentrations along its length.

Let us now consider a series of shrink-fitted assemblies of successively stronger interface grip. The hubs will then more and more tend to follow the shafts as they twist but also to restrict them and thereby make the assemblies stiffer. The slip will become smaller and smaller as the grip between the mating surfaces increases, and, at the same time, it is

likely that the restricting effects of the hubs on the shafts will set up stress concentrations in the shafts at the corner where they enter the hubs⁽¹⁾.

Theoretically, this process may be continued until the grip between the shaft and the hub has become perfectly solid. In other words, this means that there will be no slip over the mating surfaces of the shrink-fitted assembly when loaded in torsion and, consequently, it behaves like a solid shaft.

Again, it will be observed that the above argument can only be applied when the assembly is stressed within its elastic limits.

Based on the above argument, a natural analytical approach to the problem of a shrink-fitted assembly loaded in torsion can now be outlined as follows.

The shrink-fitted assembly is initially considered as a solid shaft with a collar and the stress distribution resulting from a pure torque is found⁽²⁾. This treatment gives certain values for a shear stress which would occur over the mating surfaces of the shrink-fitted assembly if no slip took place. This shear stress is compared with the friction

- (1) No papers have been found dealing with stress concentrations in shrink-fitted assemblies loaded in torsion, but for the same effect in bending see:- Fatigue of Shafts at Fitted Members with a Related Photo-elastic Analysis, by R.E. Peterson and A.M. Wahl. Trans. A.S.M.E. 1935, Vol. 57, p. 559.
- (2) The solution of the torsion problem for circular shafts of varying diameter, by A. Thom and J. Orr. Proc. Royal Society of London, ser. A. vol. 131, 1931, p. 30.

force per unit area which actually exists in the shrink-fitted assembly and, where the shear stress exceeds the friction force, it is assumed that slip takes place. Slip limits the maximum value of the shear stress which occurs over the mating surfaces to a value given by the friction grip. The coefficient of friction⁽¹⁾, the normal pressure⁽²⁾ and therefore the friction grip are assumed to be known for this particular problem. The friction grip may therefore be introduced as a boundary condition over the mating surfaces where slip takes place and the corresponding stress distribution, which is the actual stress distribution in the shrink-fitted assembly, may be found⁽³⁾.

This concludes the general discussion of torsional loads on shrink-fitted assemblies. The aim of this section of the chapter is to survey the physical features of the problem and it is hoped that a sufficiently clear picture has been established to form a reliable background for the analytical work.

-
- (1) Erhoeung des Haftbeiwertes bei Schrumpfpassungen, by F. Wenck. English Abs. in Engineers Digest, vol. 13, nr. 1, 1952, p. 13-15.
 - (2) (Theory based on Lamé's Eq. covers the elastic case.)
 - (3) Transmission of torques by means of press and shrink-fits, by J. W. Baugher, Trans. A.S.M.E. 1931, vol. 53, M.S.P. 53-10, p. 85.

In the discussion of this paper John Mansa suggests a similar procedure.

SUMMARY:

The theoretical analysis of a shrink-fitted assembly given in this chapter will follow a procedure common to most problems of this nature.

First of all the problem is defined mathematically as a differential equation with sufficient boundary conditions. This work has already been carried out for a solid shaft of varying diameter⁽¹⁾ and only slight modifications are required for shrink-fitted assemblies.

The second stage is to obtain a mathematical solution to the problem. Again, the method employed is very similar to that applied to a solid shaft and, since no general solution is available, a series of numerical solutions were carried out. The characteristics of shrink-fitted assemblies of varying fits are thus obtained in terms of numerical values for the most convenient mathematical function.

The final stage consists of bringing the results of the above-mentioned numerical calculations into a form which reveals the physical characteristics of the problem. For this purpose, the desired characteristics have been expressed by formulae which are based on the numerical work.

(1) The Mathematical Theory of Elasticity, by A.E.H. Love. Fourth Edition, Page 325.

ANALYSIS:

Differential Equation and Boundary Conditions.

The differential equation with boundary conditions for a shrink-fitted assembly loaded in torsion may be summarised as follows.

Let us consider the shrink-fitted assembly shown in Fig. 51. From general theory of elasticity, the differential equation with its boundary conditions for a solid assembly may be stated as follows⁽¹⁾

Differential equation:

$$\frac{\partial^2 \psi}{\partial r^2} - \frac{3}{r} \frac{\partial \psi}{\partial r} + \frac{\partial^2 \psi}{\partial z^2} = 0 \quad \dots 64$$

Boundary conditions:

On A-B-C-D $\psi = \text{constant} = \psi_0$

On D-E $\psi = Kr^4$, where K_1 is a constant.

On E-F $\psi = 0$.

On F-A $\psi = K_2 r^4$, where K_2 is a constant.

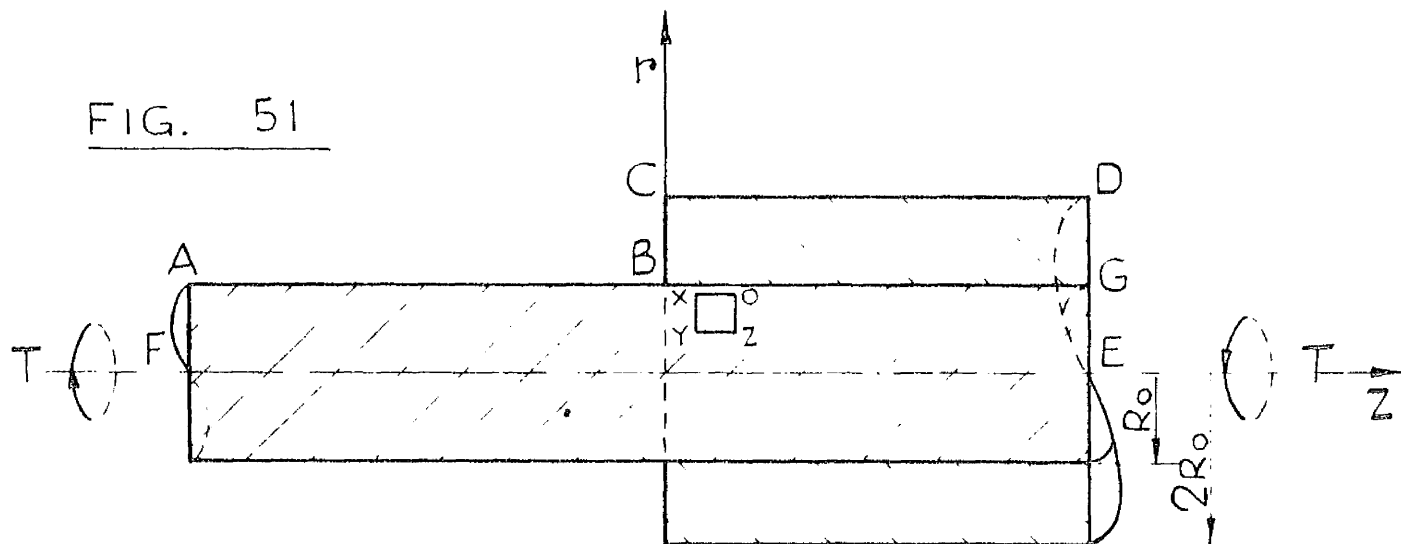
The stresses occurring in the assembly are as shown in Fig. 52. They are related to the function ψ of the differential equation by the following two equations:--

$$\hat{\theta}_z = \frac{G}{r^2} \frac{\partial \psi}{\partial r} \quad \dots 65$$

$$\hat{\theta}_r = -\frac{G}{r^2} \frac{\partial \psi}{\partial z} \quad \dots 66$$

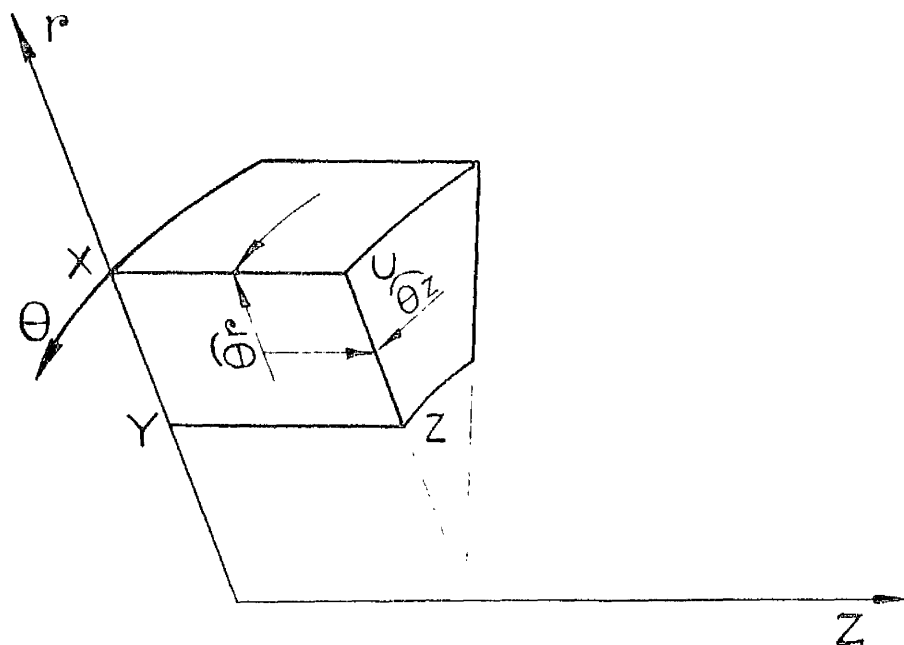
(1) See Footnote (1), Page 133.

FIG. 51



SHRINK FIT ASSEMBLY

FIG. 52



STRESSED ELEMENT.

For the shrink-fitted assembly an additional condition not required for the solid case must be fulfilled. It may be stated as follows: The shear stress over the mating surfaces cannot exceed the product of the coefficient of friction and the normal pressure.

Writing μ for the coefficient of friction, and p for the normal pressure, the additional condition over the mating surfaces will be:-

$$\sigma_r \leq \mu p = \text{CONSTANT} \quad \dots 67$$

It should be remembered that the differential equation stated above is only valid for solids of revolution. An essential condition for the shrink-fitted assembly is therefore that the product of the coefficient of friction and the normal pressure is independent of angular position round the mating surfaces.

Numerical Solution:

Again, it will be a convenient starting point to survey methods available for the study of solid shafts. These may be listed as follows:-

1. Approximate symbolic solutions (1)(2).

1. Method developed by F.A. Willers, Zeitschr. f. Mathem. u. Phys. Vol. 55, p. 225, 1907; See also:- Applied Elasticity by Timoshenko and Wessells, p. 35.
2. Zum Torsionsproblem der abgesetzten Welle und anderer Wellenformen des Maschinenbaues, von Rudolf Sonntag. Z.A.M.M. Band 34, Jan./Feb. 1954, p. 19.

2. Numerical solutions based on the "relaxation method"⁽¹⁾.
3. Solutions based on physical measurements taken on analogous systems, usually electrical systems⁽²⁾.
4. Photo-elastic analysis.

Each of the above methods has its own particular advantages such as generality, accuracy and speed. The important question, however, for our particular case is what is the best method for tackling the special feature of a shrink-fitted assembly, the differential slip over the mating surfaces?

The relaxation method is well known for its strength in tackling a variety of boundary conditions and, as it will be seen later, it can easily deal with slip. This feature favoured method 2. and it was decided to take the heavy burden of numerical computation which is involved.

The use of relaxation methods for the solution of partial differential equations is so common today that it is hardly necessary to elaborate upon the principle of the method.

Fig. 53 gives an arbitrary point in the relaxation net used and Fig. 54 the relaxation pattern derived for our

(1) See Footnote 2. on Page 131.

(2) Handbook of Experimental Stress Analysis by M. Hetenyi.

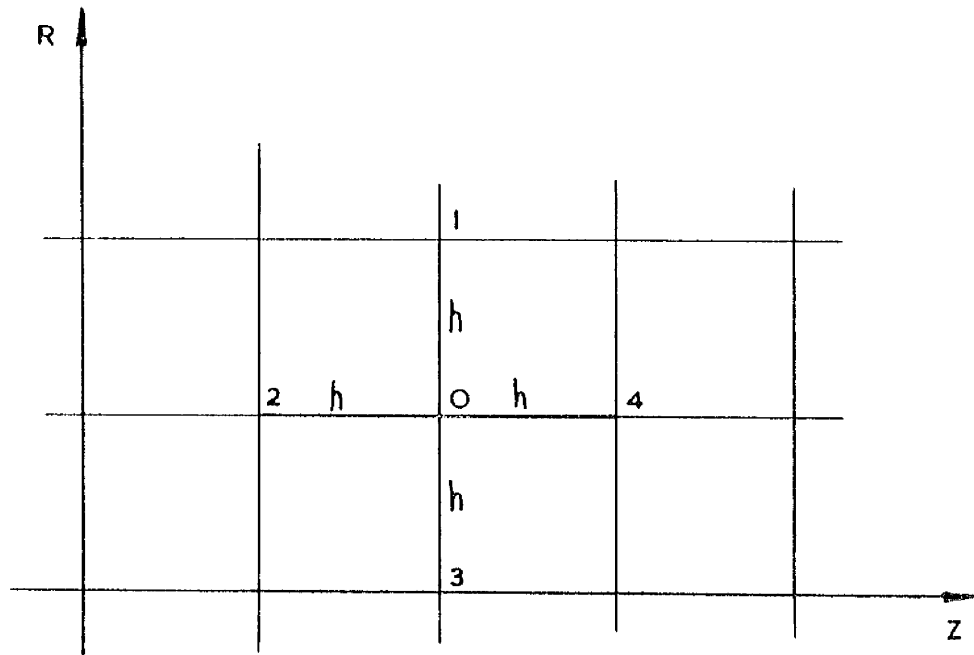


FIGURE 53

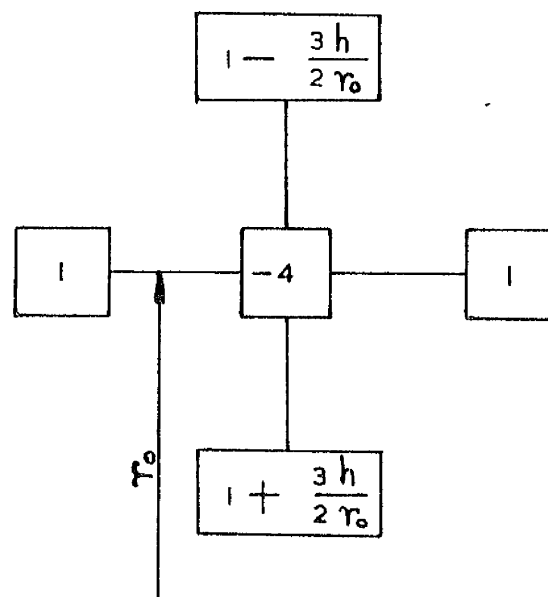


FIGURE 54

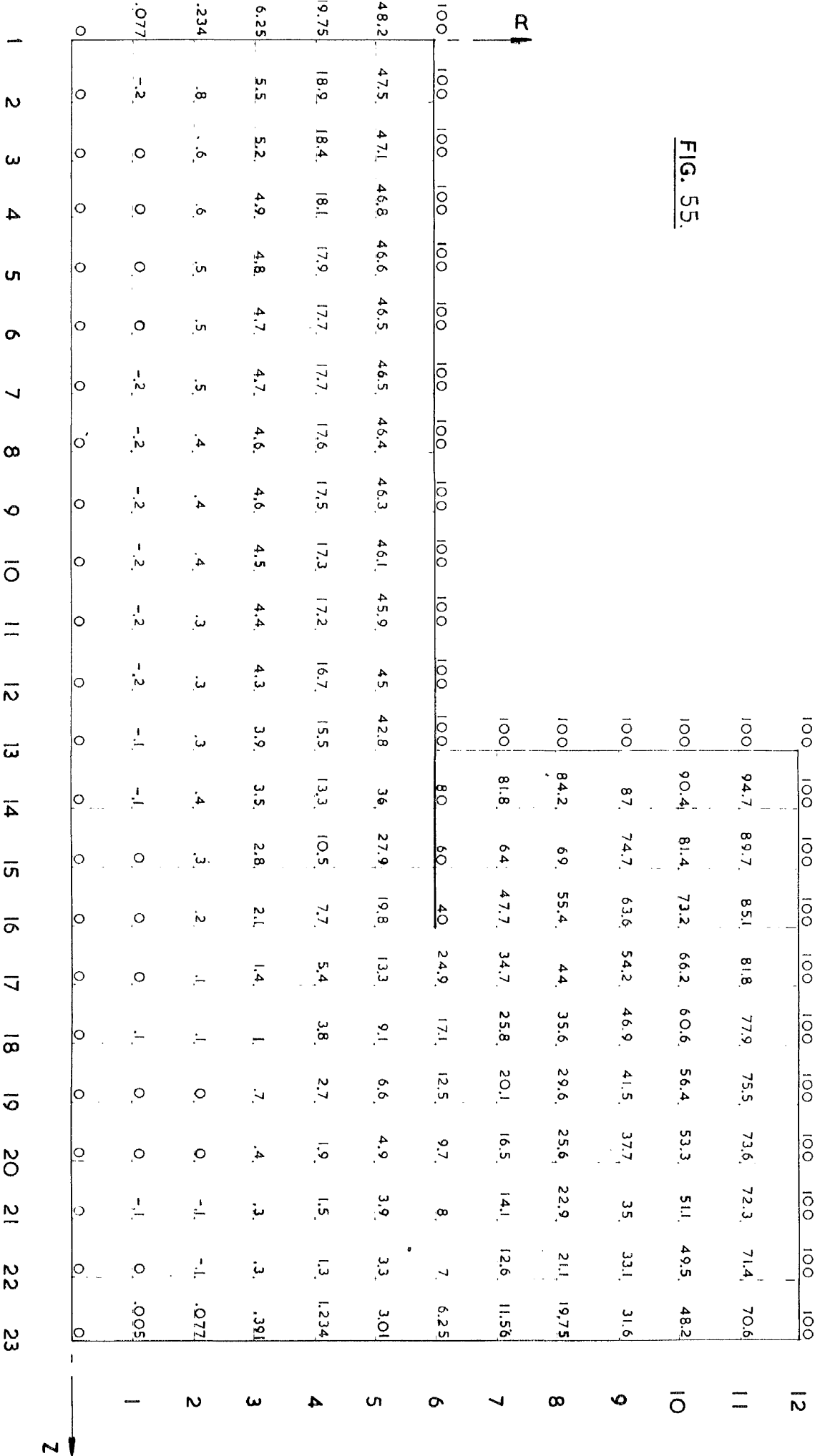
differential equation (1).

The numerical work has been carried out for an arrangement similar to that shown in Fig.51. The upper half of the assembly was divided into a mesh as shown in Fig.55. In deciding the size of the squares, it was necessary to compromise between the labour involved and the accuracy obtained.

Six different cases of varying values for the ratio of friction grip to nominal shaft stress were worked out and the finished relaxation nets from these calculations are given in Appendix V.

The effects of varying fits on the characteristics of a shrink-fitted assembly are thus displayed.

FIG. 55.



RELAXATION NET 4.

SCALE: 4X FULL SIZE.

DERIVED RESULTS:

Introduction:

From a mathematical point of view, complete numerical solutions for various shrink-fitted assemblies loaded in torsion were obtained through the work of the previous section and presented in Appendix V. The results, however, as they appear on the relaxation nets are rather unintelligible and further development is therefore required to reveal the important physical features of the problem.

Returning to the general discussion, it will be remembered that the three characteristics of a shrink-fitted assembly with which we are primarily concerned are the torsional stiffness, the damping capacity and the stress concentrations.

Each of the three above aspects will now be treated in turn in order to derive results of greater practical significance.

Torsional Stiffness:

Torsional stiffnesses are mainly of interest in connection with calculations of natural frequencies and critical speeds of crankshaft systems and available literature contains a number of publications which deal with this

problem generally⁽¹⁾⁽²⁾.

The author, however, is not aware of any treatments which are given particularly for shrink-fitted designs. It is therefore thought that, although the analysis presented applies strictly to a simplified case, the results may prove to be of some interest to crankshaft designers.

Definition:- The torsional stiffness between sections of a body is defined as the torque required to twist one section one radian relative to the other, i.e.

$$\underline{C = \frac{T}{\phi}} \quad \dots \dots \dots 68$$

It also follows from definition that:-

$$\underline{\phi = \frac{\nu}{r}} \quad \dots \dots \dots 69$$

where

$$\underline{\nu = \int e_{\phi z} dz} \quad (3)$$

If $\underline{z_1}$ and $\underline{z_2}$ are the z-coordinates of the two sections between which it is desired to find the twist, the integral must be taken between these two limits and, consequently, equation 69 becomes:-

$$\underline{\phi = \frac{1}{r} \int_{z_1}^{z_2} e_{\phi z} dz} \quad \dots \dots \dots 70$$

(1) Die Reduktion der Kurbelkropfung. Z. VDI, s.601, 1925 by Seelmann.

(2) Torsional Vibration. London 1934, by W.A.Tuplin.

(3) See Footnote 1. Page 133.

For the assemblies under consideration, it is preferable to work along the radius $\underline{r} = \underline{R_0}$, which is the radius of the mating surfaces.

Also for numerical computation, it is convenient to work in terms of strain ratios rather than the stress function as given by the relaxation nets. A conversion will therefore be necessary.

From the boundary conditions we obtain:-

$$\underline{K_2 = \psi_0 / R_0^4}$$

and hence at the boundary point A.:-

$$\underline{\partial \psi / \partial r = 4 \psi_0 / R_0} \quad 71$$

Making use of equation (65), the axial shear strain at a radius $\underline{R_0}$ can be expressed as:-

$$\underline{e_{\theta z} = e q_2 = \frac{1}{R_0^3} \frac{\partial \psi}{\partial r}} \quad 72$$

where $\underline{q_2}$ is the strain ratio for the axial shear strains at a radius $\underline{R_0}$.

Also from equations (65) and (71) we obtain:-

$$\underline{e = 4 \psi_0 / R_0^3} \quad 73$$

and $\underline{q_2}$ may therefore be expressed as:-

$$\underline{q_2 = \frac{R_0}{4 \psi_0} \frac{\partial \psi}{\partial r}} \quad 74$$

Making use of equations (72) and (73) and putting

$\underline{r} = \underline{R_0}$, equation (70) may now finally be written as:-

$$\phi = \frac{4\psi_0}{R_0^2} \int_{z_1}^{z_2} q_z dz \quad 75$$

The torque applied to the assembly may be expressed in terms of the nominal shear strain:-

$$T = \frac{\pi}{2} R_0^3 G \epsilon$$

and, making use of equation (73), the above equation may be rewritten as:-

$$T = 2\pi G \psi_0 \quad 76$$

Finally, the torsional stiffness of the shrink-fitted assembly can be found by making use of equations (75) and (76) in equation (69):-

$$C = \frac{\pi G R_0^4}{2 \int_{z_1}^{z_2} q_z dz} \quad 77$$

Numerical calculations are given in Appendix V.

Differential Slip and Damping Capacity:

The author is unaware of any previous investigations of the damping capacity of a shrink-fitted assembly.

It has been noticed that built-up crankshafts generally provide more damping for the torsional vibrations than solid forged crankshafts and one Paper makes a distinction between the two types in its classification of damping measured on actual engines⁽¹⁾. No explanation, however, is given to

(1) Dæmpningen ved Torsionssvingninger i Krumtapaksler, af Per Draminsky. Nyt Nordisk Forlag. Arnold Busck. Kjøbenhavn 1947.

show where the extra damping in built-up crankshafts comes from.

If differential slip occurs between the mating surfaces of a shrink-fitted assembly loaded in torsion, as assumed for the purpose of the theoretical analysis presented in this chapter, energy dissipation will be a natural consequence.

Differential slip may therefore be responsible for the increased damping which is a general characteristic of built-up crankshafts.

Following this line of thought, an analysis will now be made of the possible energy dissipation over the rubbing surfaces and, finally, consideration is given to the damping capacity of a vibrational system containing shrink-fitted assemblies.

Statement:- At any radial cross-section, the differential slip between the mating surfaces of a shrink-fitted assembly is equal to the difference between the torsional deflections of the shaft and the hub, i.e.:-

$$s = v_s - v_h$$

or

$$s = \int_{z_1}^{z_2} (e_{\theta z})_s dz - \int_{z_1}^{z_2} (e_{\theta z})_h dz \quad \dots \dots \dots 78$$

The range of integration - from z_1 to z_2 - is now the entire range over which differential slip occurs.

Equation (78) may be rewritten in terms of strain ratios as:-

$$\underline{s = e \int_{z_1}^{z_2} (q_{zs} - q_{zn}) dz} \quad \dots \dots \dots 79$$

or

$$\underline{s = \frac{4\psi_0}{R_0^3} \int_{z_1}^{z_2} (q_{zs} - q_{zn}) dz} \quad \dots \dots \dots 80$$

At this stage, it will be convenient to introduce the symbol σ for the ratio of the friction grip to the nominal shaft stress, i.e.:-

$$\underline{\sigma = \frac{\mu p}{G e}} \quad \dots \dots \dots 81$$

To obtain the energy dissipation over the rubbing surfaces, let us consider an elemental ring of length δz taken from the shaft surface.

The area of this ring equals:-

$$\underline{\delta A = 2\pi R_0 \delta z}$$

Making use of equation (81), the friction force on the same ring may be written as:-

$$\underline{\delta F = 2\pi R_0 \sigma G e \delta z}$$

Making use of equation (79), the work done by the elemental friction force over the corresponding slip will be given by:-

$$\underline{\delta W = 2\pi R_0 \sigma G e^2 \int_{z_1}^{z_2} (q_{zs} - q_{zn}) dz} \quad \dots \dots \dots 82$$

Equation (82) also represents the energy dissipation per

quarter cycle of vibration for the elemental ring. Multiplying by four and integrating over the whole rubbing area, i.e. from z_1 to z_2 , we arrive at the total energy dissipation per cycle in the shrink-fitted assembly:-

$$W = 8\pi R_0 \sigma G e^2 \int_{z_1}^{z_2} \int_{z_1}^{z_2} (q_{zs} - q_{zh}) dz dz \dots \dots \dots 83$$

For practical test purposes, energy dissipation in vibrational systems is expressed most conveniently in terms of percentage damping.

Definition:- The percentage damping of a vibrational system is defined as the ratio of the loss of energy of the system in one half-cycle to the energy of the system at the commencement of that half-cycle, the system being subjected to transient vibrations.

Let it now be assumed that the shrink-fitted assembly forms a part of a vibrational system of maximum vibrational energy E where:-

$$E = GJl e^2 / 2R_0^2$$

In the above equation, J is the polar moment of inertia of a shaft and l the length of the same shaft.

Let $J = \frac{\pi}{2} R_0^4$ and E may accordingly be expressed as:-

$$E = \frac{\pi}{2} G l e^2 R_0^2 \dots \dots \dots 84$$

From equations (83) and (84), the percentage damping may now be found for this particular vibrational system:-

$$\%D = \frac{1600\sigma}{1R_0} \int_{z_1}^{z_2} \int_{z_1}^{z_2} (q_{zs} - q_{zn}) dz dz \quad \dots \quad 85$$

Numerical examples corresponding to the above section are given in Appendix V.

Stress Concentrations:

The author is not aware of any studies which have been made of stress concentrations occurring in shrink-fitted assemblies loaded in torsion. In this particular respect, however, shrink-fitted assemblies are very similar to solid shafts and, after the stress function has been found, the same methods apply in deriving the stress concentrations.

From general theory of elasticity, it can be shown that the resultant shear stress at any point in an assembly, which complies with our conditions, may be expressed as ⁽¹⁾:-

$$\tau = (\sigma_r^2 + \sigma_z^2)^{\frac{1}{2}} \quad \dots \quad 86$$

The above equation can be rewritten in terms of strain ratios as:-

$$q = (q_z^2 + q_r^2)^{\frac{1}{2}} \quad \dots \quad 87$$

where q_z is obtained from equation (74) and, using

(1) See Reference 2. Page 131.

equations (66) and (73), we obtain:-

$$\underline{q_r = - \frac{R_o}{4y_o} \frac{\partial y}{\partial r} \quad 88}$$

From inspection of the relaxation nets in Appendix V, it can be seen that the maximum stress concentration occurs in the corner where the shaft enters the hub. It is therefore only necessary to investigate this particular point.

FIG. 56

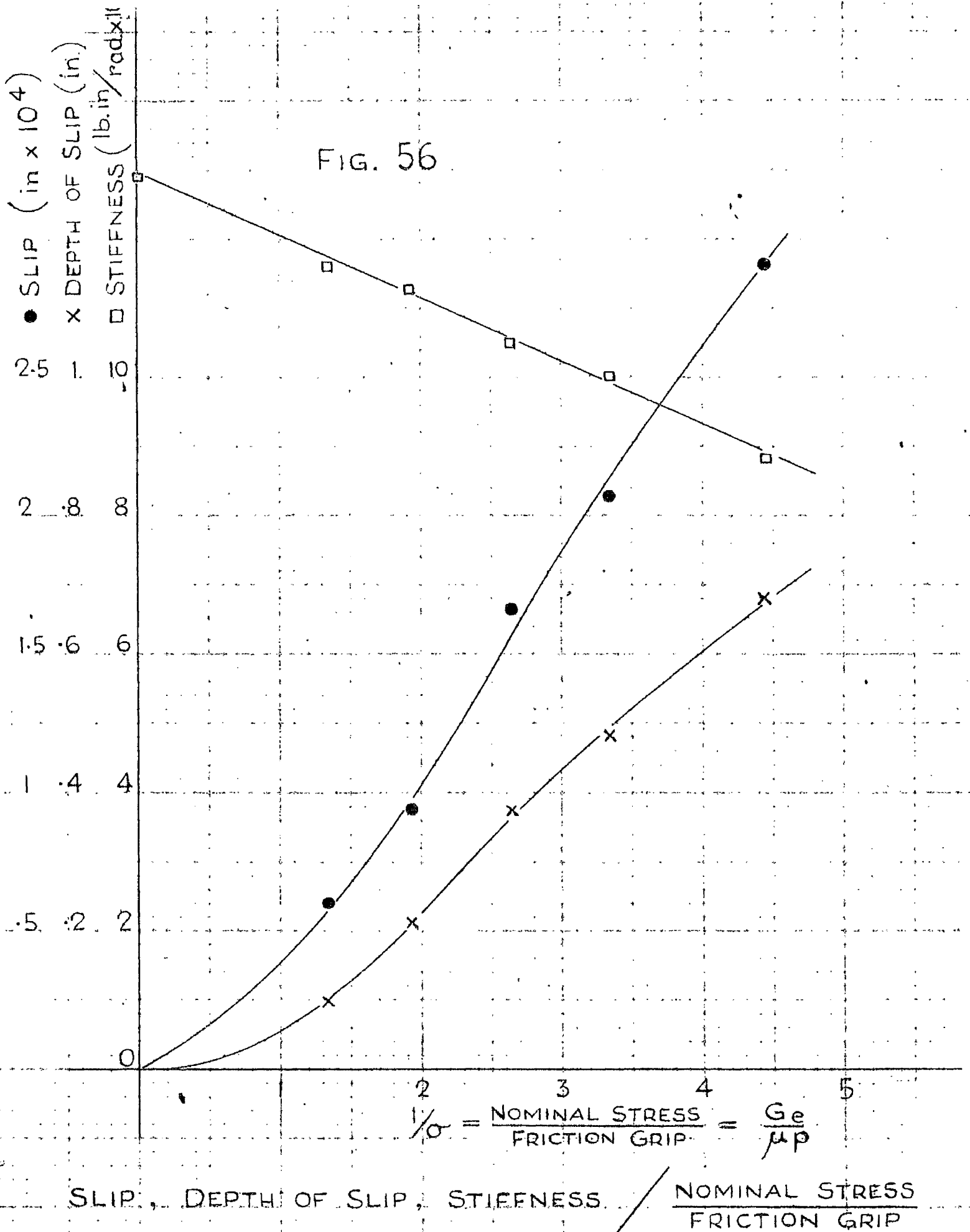
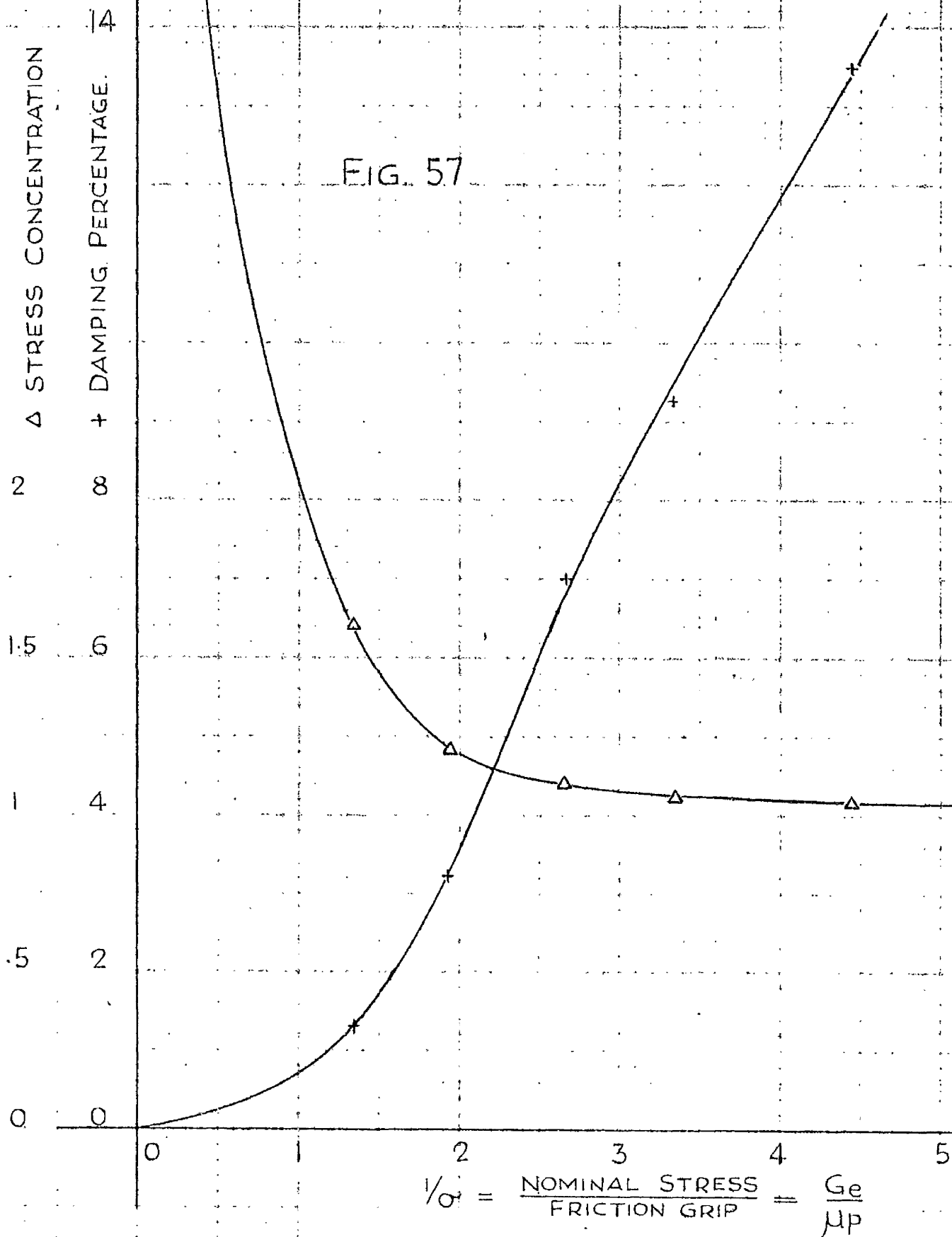


FIG. 57



PERCENTAGE DAMPING AND STRESS CONC. / $\frac{\text{NOMINAL STRESS}}{\text{FRICTION GRIP}}$

FINAL DISCUSSION.

It will be remembered from the general discussion how the assumption that all stresses had to be within the elastic limit of the material, was made to form a rigid foundation for the analytical work. The validity of this assumption can now be judged from an examination of the stress concentrations occurring in the shrink-fitted assembly.

Fig. 57 shows the variation of the stress concentration factor for the shaft at the corner where it enters the bush plotted versus the ratio of nominal stress to friction grip. When a shrink-fitted assembly is gradually loaded in torsion, this latter ratio increases linearly with the shaft stress. At the same time the stress concentration falls rapidly from infinity, bends off and finally tends asymptotically to one, as will be seen from the graph. The maximum stress in the assembly due to applied torque will therefore for low values be considerably greater than that for a plain shaft, but will, as they both increase, ultimately tend to the same value. If the inherent stresses of the shrink-fitted assembly are reasonably well below the yield point, it is therefore justifiable to assume that the elastic limits are not exceeded even for comparatively high loads in torsion.

We will now direct our attention to the second fundamental assumption made for the theoretical analysis, namely that

differential slip takes place between the mating surfaces of the hub and the shaft⁽¹⁾.

It will be seen from the graph of this slip plotted against the ratio of the nominal stress to the friction grip in Fig. 56, that its magnitude varies from zero and up to .0003 in.

Great practical difficulties would therefore be encountered in taking experimental measurements of this slip, and, consequently, for experimental support, it will be necessary to look for a more convenient approach.

Let us therefore consider the graph of stiffness versus the ratio of nominal stress to friction grip. This graph shows that theoretically the stiffness decreases with increase in nominal stress, or applied torque, for any particular shrink-fitted assembly.

Experimental results obtained by Russell⁽²⁾ and Davidson⁽³⁾ show a similar tendency.

Carrying out experimental work on cranks, Russell found that of geometrically identical test specimens, the shrink-

(1) See Page (130).

(2) Russell, R. - "Experimental Studies on Crankshaft Stiffness." - Journal of R.T.C., Glasgow, Vol.IV. 1937-40. Page 467.

(3) Davidson, W.R.S. - "Shrink-Fit Stress Systems in Built Crankshafts." - Ph.D. Thesis, Glasgow University, 1951. (See Fig. 44, 45, 46 and 47.)

fitted specimens were more flexible than the solid.

Also working with cranks, Davidson obtained torque deflection curves for shrink-fitted designs, and these curves show a clear decrease in stiffness with increased torque.

Further experimental studies of the stiffness of shrink-fitted assemblies might consequently give conclusive support.

However, an even better basis for experimental work is found in the study of percentage damping.

Fig. 57 shows that our theoretical work, which is related to a simple vibrational system containing a shrink-fitted assembly, predicts damping up to fifteen per cent.

Percentage damping of this order can easily be measured in practice and hence it was decided to direct our further attention towards this side of the problem.

MEASUREMENT OF DAMPING CAPACITY AND ENDURANCE TESTING RELATED TO SHRINK-FITTED ASSEMBLIES.

Introduction.

It will be remembered from the previous chapter that a basic assumption in the theoretical analysis implies the occurrence of differential slip between the hub and the shaft of a shrink-fitted assembly loaded in torsion.

Further, it was found that investigation into the dissipation of vibrational energy caused by this slip, would provide suitable experimental tests supporting the theoretical work.

To define our aim in this chapter, we will therefore make the object of the experimental work, which consists of the measurement of damping capacity, the proving of the existence of this differential slip.

The work, however, will also be extended for the purpose of studying the effect of differential slip on the conditions of the mating surfaces, and their mutual coefficient of friction.

Since energy dissipation between the mating surfaces of a shrink-fitted assembly is a newly discovered phenomenon, there is no available literature describing experimental gear

designed specifically for the study of this effect. However, experimental investigations have been carried out on a closely related problem. Many authors have described apparatus designed for the study of internal damping⁽¹⁾ and, in the design of our experimental gear, advantage was taken of their experience.

Historical Development.

A short historical summary will now be given of experimental works on internal damping.

Since our problem is confined to the effect of torques on shrink-fitted assemblies, this summary will be limited to test arrangements using specimens loaded in torsion. Thus, only a few of the total number of papers on internal damping will be mentioned.

Pertz⁽²⁾, in 1928, was among the first investigators to make substantial headway with the problem of damping capacity of metals. Later, in collaboration with Föppl⁽³⁾, he designed an apparatus which, for many years, became the standard machine for this type of testing.

(1) Also called "material hysteresis damping".

(2) Pertz, E. - "Die Bestimmung der Baustoffdämpfung" (Vieweg 1928).

(3) Föppl - "The Practical Importance of Damping Capacity in Metals, especially Steels." - Iron and Steel Institute (1936), Vol. 134, Page 393.

In its essentials the Föppl-Pertz machine consists of a two mass system. An inertia is clamped to one end of the test specimen which acts as the stiffness. The other end of the specimen is clamped to the frame of the machine which therefore acts as the second inertia.

The test specimen is stressed in torsion and its damping capacity obtained from records of transient vibrations.

There are many variations of the Föppl-Pertz type of machine, each differing in its methods of setting up initial stress, recording, damping and suspension and, as an example, the Cambridge Torsional Damping Recorder should be mentioned⁽¹⁾.

The results obtained on these machines, however, were somewhat inconsistent and, consequently, an element of error is implied.

The next significant step in the development was achieved by Hanstock and Murray⁽²⁾, closely followed by Cottel, Entwistle and Thomson⁽³⁾. Since, however, Cottel, Entwistle and Thomson's apparatus is more closely related to

-
- (1) Hatfield, W.H., Stanfield, G., and Rotherham, L., - "The Damping Capacity of Engineering Materials", North East Coast Institution of Engineers and Shipbuilders, Trans. LVIII, Part 7. June 1942.
 - (2) Hanstock, R.D. and Murray, A. - "Damping Capacity and the Fatigue of Metals." - The Journal of the Institute of Metals 1946, Vol. 72, Page 97.
 - (3) Cottel, Entwistle and Thomson - "Measurement of Damping Capacity of Metals in Torsional Vibration." - The Journal of the Institute of Metals 1948, Vol. 74, Page 373.

the original Föppl-Pertz machine than that of Hanstock and Murray, a short discussion of their arrangement will be given first.

Cottel, Entwistle and Thomson improved the conventional Föppl-Pertz machine by careful consideration of possible external sources of error. Re-design of the apparatus reduced the measured internal damping substantially and, thus, it was made obvious that the results obtained on the original machines were badly affected by errors.

The main improvements carried out on the original Föppl-Pertz machine were:--

The clamping of the specimen was improved to reduce energy dissipation due to possible slip or high stress concentrations.

The machine frame was made stiffer, changing from a bolted to a welded design.

Finally, air friction was removed by working in near vacuum.

The apparatus designed by Cottel, Entwistle and Thomson made use of mechanical means of setting up the initial stress, and recording was done optically.

The apparatus of Hanstock and Murray deviated somewhat in design from the test arrangements of earlier investigators.

A major improvement, that of using the test specimen as the entire vibrational system, was introduced by them. Thus, all energy dissipations due to vibrational torques or forces across clamping or in surrounding apparatus were eliminated; as a result, the chance of errors in the measured internal damping was greatly reduced.

Electrical excitation and recording were used.

The damping of the specimen was obtained by measuring the difference between the input power of the exciter and the output power of the recording unit.

Hanstock later made use of the same apparatus to establish relationships between damping capacity, strain hardening and fatigue, carrying out endurance tests on aluminium alloy specimens⁽¹⁾.

A similar apparatus to that developed by Hanstock and Murray seemed to be the best answer to our measurement problem, but, to see if any further improvements could be incorporated, a short analytical examination of the design conditions for apparatus measuring damping capacity has been carried out.

(1) Hanstock, R.F. - "Damping Capacity, Strain Hardening and Fatigue." - Proceedings of the Physical Society, 1947, Vol. 59, Page 275.

Factors Affecting Design of Apparatus.

For accurate measurements of the dissipation of vibrational energy in any test specimen, it is desirable that this energy dissipation should be as large as possible compared to that in the surrounding apparatus.

Let us make use of the following notation:-

\underline{W} = energy dissipation. (lb.in./cycle)

\underline{T} = applied vibrational torque. (lb.in.)

$\underline{\omega}$ = frequency. (1/sec.)

\underline{C} = stiffness coefficient. (lb.in.)

\underline{S} = velocity resistance coefficient. (lb.in.sec.)

\underline{I} = angular inertia. (lb.in.sec.².)

When a simple vibrational system of one degree of freedom is considered, the energy dissipation per cycle will be given by ⁽¹⁾:-

$$\underline{W} = \frac{\pi T^2 \omega S}{(C - \omega^2 I)^2 + \omega^2 S^2} \quad \dots 89$$

At resonance conditions this formula reduces to:-

$$\underline{W} = \frac{\pi T^2}{\omega S} \quad \dots 90$$

It is seen from equation (89) that for a simple system the dissipation of vibrational energy is directly proportional to the square of the applied torque, and it is also

(1) "Mechanics of Vibrations", Hansen and Chenea, Page 96.

dependent on a factor calculated from the physical constants of the system.

The same considerations may roughly be applied to a more complex vibrational system corresponding to our test apparatus.

Test Specimen.

Let us first of all consider the test specimen, the energy dissipation of which should be as large as possible.

For the purpose of damping measurement, both small and large torques have to be used and, hence, the only way to make the energy dissipated per cycle large, is to increase the factor governed by the physical constants. This is best achieved by working at the specimen's natural frequency.

Surrounding Apparatus.

Let us secondly examine the surrounding apparatus, the energy dissipation of which should be as small as possible. There are two distinct methods of achieving this purpose.

Firstly, the factor governed by the physical constants of the system can be made small by working at frequencies off resonance and using large stiffnesses⁽¹⁾.

The second method is to ensure that any torques or

(1) Used by Cottel, Entwistle and Thomson.

forces in the surrounding apparatus due to the vibration of the test specimen, are as small as possible. This is best achieved by balancing all vibrational torques within the specimen itself⁽¹⁾.

It was decided that the second alternative would give a better basis for the design of the apparatus and the following test specifications were laid down:-

- (a) The specimen is to be a balanced two mass system clamped at the node.
- (b) There is to be no mechanical connection between the pick-up and the specimen.
- (c) The forcing is to be at the specimen's natural frequency of torsional oscillation.
- (d) The drive is to be completely disconnected after the specimen has been forced to its maximum amplitude of oscillation.

It follows from condition (d) that the damping of the specimen must be obtained from records of the specimen's transient vibrations.

Special provisions for endurance testing should be incorporated in the apparatus.

(1) Used by Hanstock and Murray.

APPARATUS.

After considerable time an apparatus, as shown by Fig.58, was developed for the measurements of damping capacity and endurance testing of shrink-fitted assemblies.

It was found that this arrangement gave reliable, consistent results, and thus it served its purpose, although difficulties were encountered due to frequent breakdowns during endurance testing.

The principle of the arrangement is best understood from the block diagram of Fig.59.

A separate drawing of the test specimen is given in Fig.61, whereas all other detail drawings are given in Appendix VI.

A short description of the test arrangement will be necessary and let us begin by considering the test specimen.

Test Specimen.

The test specimen consists of two heavy fly-wheels shrink-fitted to the ends of a plain shaft, such as to form a two mass system.

The specimen was made of a robust size to diminish the effect of machining tolerances on its most important dimensions. An upper limit to its size, however, was imposed by

the power available for excitation.

The test specimen was clamped at the node, as shown in Fig. 59.

Excitation.

Excitation for the specimen under test was provided by two Goodmans moving coil exciters, connected in series through an ammeter to the output of a driving amplifier which supplied sufficient power to run the exciters at full capacity (4 amp.). Air-cooling of the exciters was then required, and air was supplied from a compressor, as shown in Fig. 58.

For taking records of the transient vibrations of the specimen, the driving amplifier was fed from a Beat Frequency Oscillator (B.F.O.) through a limiter circuit and a pre-amplifier⁽¹⁾. Thus, the exciter forces could be tuned to the natural frequency of the specimen by adjusting the B.F.O.

The same system could be used for endurance testing, but it was found that the frequency of the B.F.O. had a tendency to drift, making occasional re-tuning necessary to keep to resonance conditions.

A feed-back system which used the test specimen as the

(1) The limiter was unnecessary for this purpose but was kept in the circuit for convenience since it was necessary during endurance testing.

frequency controlling unit for the input to the driving amplifiers, was therefore devised. A small inductive pick-up unit converted the vibrations of the test specimen into a voltage signal. This signal was passed through a filter for the exclusion of other frequencies than that corresponding to the desired vibration of the test specimen. From the filter the signal was fed into the limiter- and phase change circuit to form an input signal for the amplifier.

A closed system with conditions for oscillation was consequently established and, when the amplifier power was turned up, this system would oscillate with the same frequency as the natural frequency of the specimen⁽¹⁾.

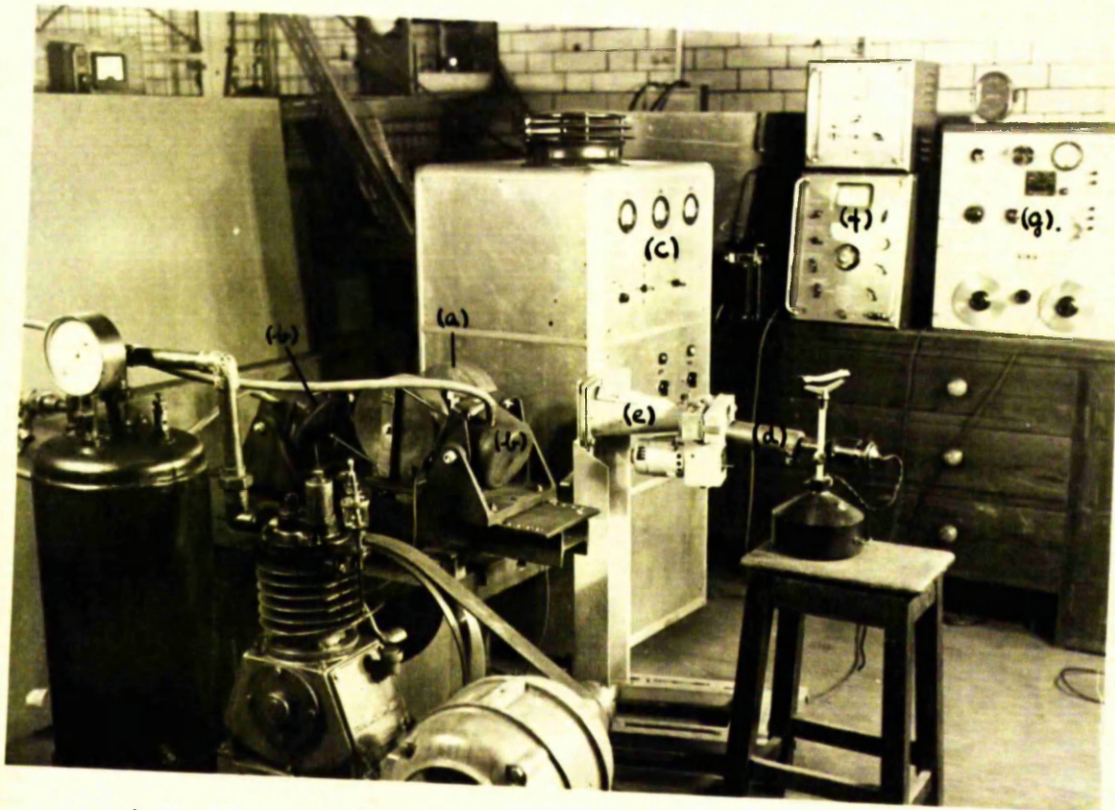
It should be noticed that the limiter circuit was now necessary to prevent instability.

Since the gear during endurance tests was switched on for considerable periods of time, it was found necessary for the prevention of accidents to incorporate an overload switch in the supply circuit. This switch would cut out all the electrical gear in the case of faults with either of the components.

A time switch was also incorporated, such that the gear could be made to stop by itself at any convenient pre-set time.

(1) The power output of the driving amplifier could be regulated by means of a variac.

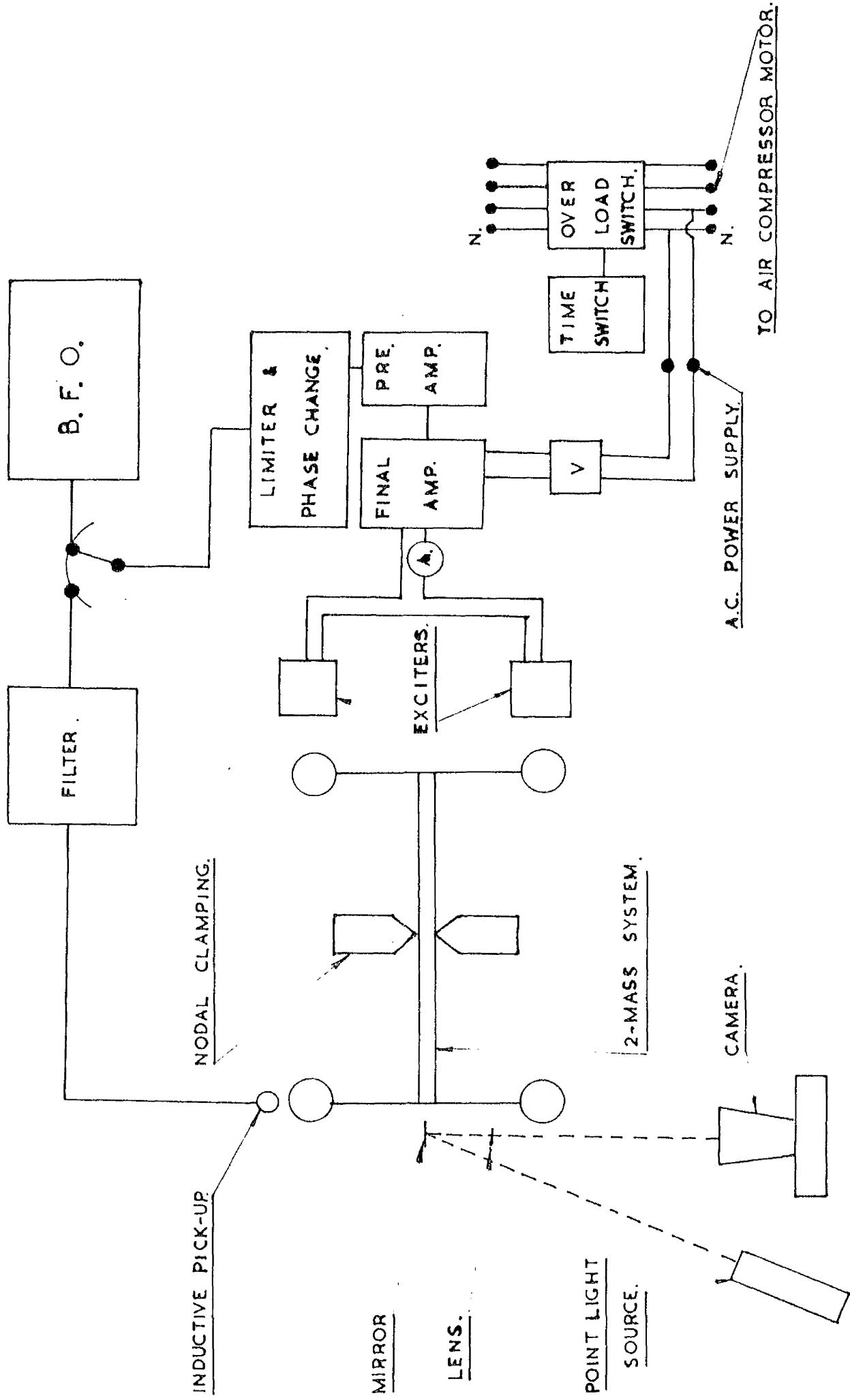
FIGURE 58.



- a). Test Specimen.
- b). Moving Coil Exciters.
- c). Driving Amplifier.
- d). Point Light Source.
- e). Moving Film Camera.
- f). Filter.
- g). Beat Frequency Oscillator.

ARRANGEMENT OF APPARATUS FOR
TESTS ON SHRINK-FITTED ASSEMBLIES.

FIG. 59.



ARRANGEMENT OF APPARATUS.

Recording System.

The amplitude of the torsional vibrations of the test specimen were recorded optically.

Light from a point source was reflected by a small plane mirror attached to the test specimen (See Fig.59). It was then focussed by means of a long focal length lens on the screen of a moving film camera. A standard Cossor Oscilloscope Camera designed for 35 mm. film, and with a film speed of 3.5 in./sec. was used. (See Fig.58).

The optical principle of the recording system is shown in Appendix II, which also gives a formula for its amplification factor.

For analysis, the film records were magnified fifteen times in a Hilger Universal Projector and measurements taken directly off the screen with a centimetre rule.

Percentage damping was calculated from these measurements, making use of the formula shown in Fig.60.

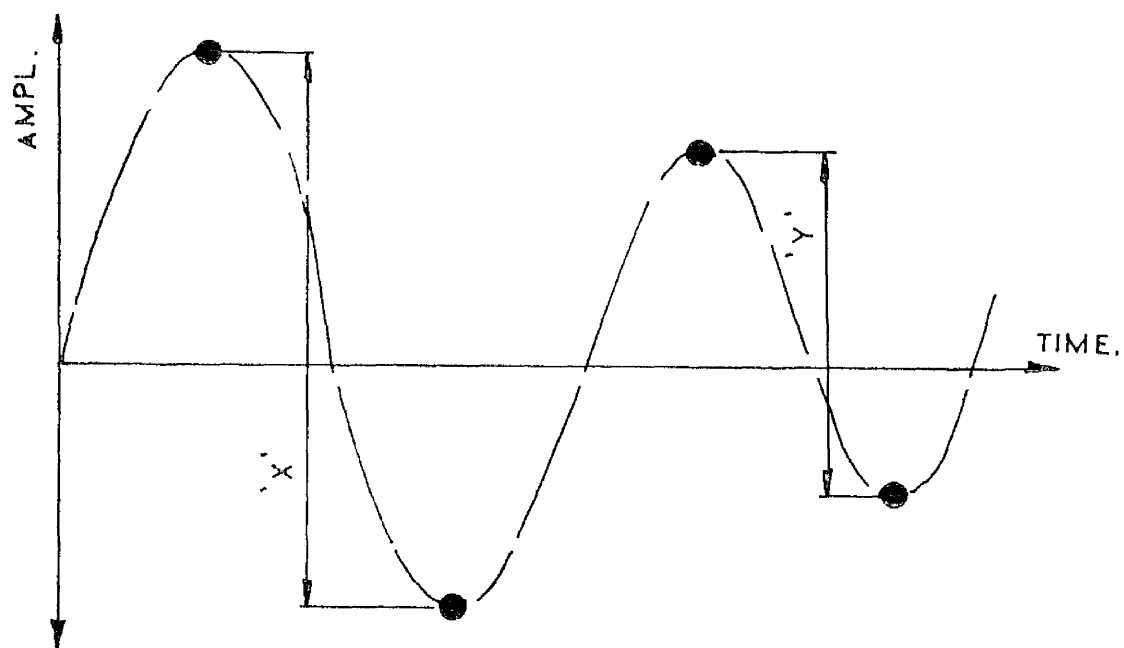
The shaft stress in the specimen was obtained from measured amplitudes, considering the corresponding twist.

Operation.

Finally, before this section on apparatus is concluded, a few words should be said about the operation of the

FROM DEFINITION :

$$\% \text{DAMPING} = \frac{\text{ENERGY DISSIPATION } 1/2 \text{ CYCLE}}{\text{TOTAL ENERGY AT BEGINNING OF } 1/2 \text{ CYCLE}} \times 100\%$$



AMPLITUDE DECAY TRACE.

$$\% \text{DAMPING} = 2 \cdot \left(\frac{X-Y}{X+Y} \right) 100\%$$

FIGURE 60.

experimental gear during test.

For taking a record of the transient vibrations of the test specimen, the following procedure was adopted:-

The B.T.O. was connected to the input of the amplifier.

The image of the point light source was set on the centre of the camera screen, and film thereafter loaded in the camera.

Appropriate driving rods for this test - (see Appendix VI) were fitted to the exciters, and the inductive pick-up unit, which was attached to the test specimen for endurance testing, was disconnected.

The driving amplifier was turned up to full power, while the exciter rods were engaged to the test specimen manually⁽¹⁾ and thus the test specimen was excited to maximum amplitude.

The camera motor was started and, shortly after, the exciter rods were pulled sharply away from the test specimen. The transient vibrations of the test specimen which then followed would be recorded by the camera.

For endurance testing, stiffer exciter rods were used. These were clamped to the test specimen by means of a spring clamp, which would take up any wear. (See Appendix VI).

(1) Two operators were required.

The inductive pick-up unit was connected to the test specimen and the B.F.O. replaced by the filter.

On turning up the variac of the driving amplifier, the system would now oscillate at the desired amplitude.

TEST PROGRAMME.

The following test programme was laid down to cover comprehensively the object of the experimental investigations of shrink-fitted assemblies, as drafted on page 150.

Two sets of specimens of varying interference were tested.

The first set, all the particulars of which are given in Fig.62, contained five specimens all lubricated with sperm oil before shrink-fitting. The set covered a range of surface pressures⁽¹⁾ from 1.3 T./in.² to 8.65 T./in.², which should be sufficient to cover most engineering applications of shrink-fitted assemblies.

All the specimens of the first set were tested immediately after shrink-fitting (initial tests) and the graphs of Percentage Damping versus shaft stress, as shown in Fig.65, were obtained.

Endurance tests were then carried out in the following way. After the initial curve of Percentage Damping versus shaft stress had been obtained, the specimen under test was vibrated at constant input current to the excitors a set number of cycles, before another record was taken of its transient vibrations.

(1) Calculated from the interference fit by making use of Lamé's equations for thick cylinders.

This procedure was repeated, taking records at intervals of 10 megacycles until the specimen had been vibrated 100 megacycles in all.

All five specimens were subjected to endurance tests during which the input current to the exciters was kept constant at 3.5 amp.

From the endurance tests, graphs of percentage damping versus number of cycles vibrated for constant shaft stress were obtained, as shown in Fig.66-70 for all specimens.

Finally, the graphs of Percentage Damping versus shaft stress, obtained after 100 megacycles for all specimens, are presented in Fig.71.

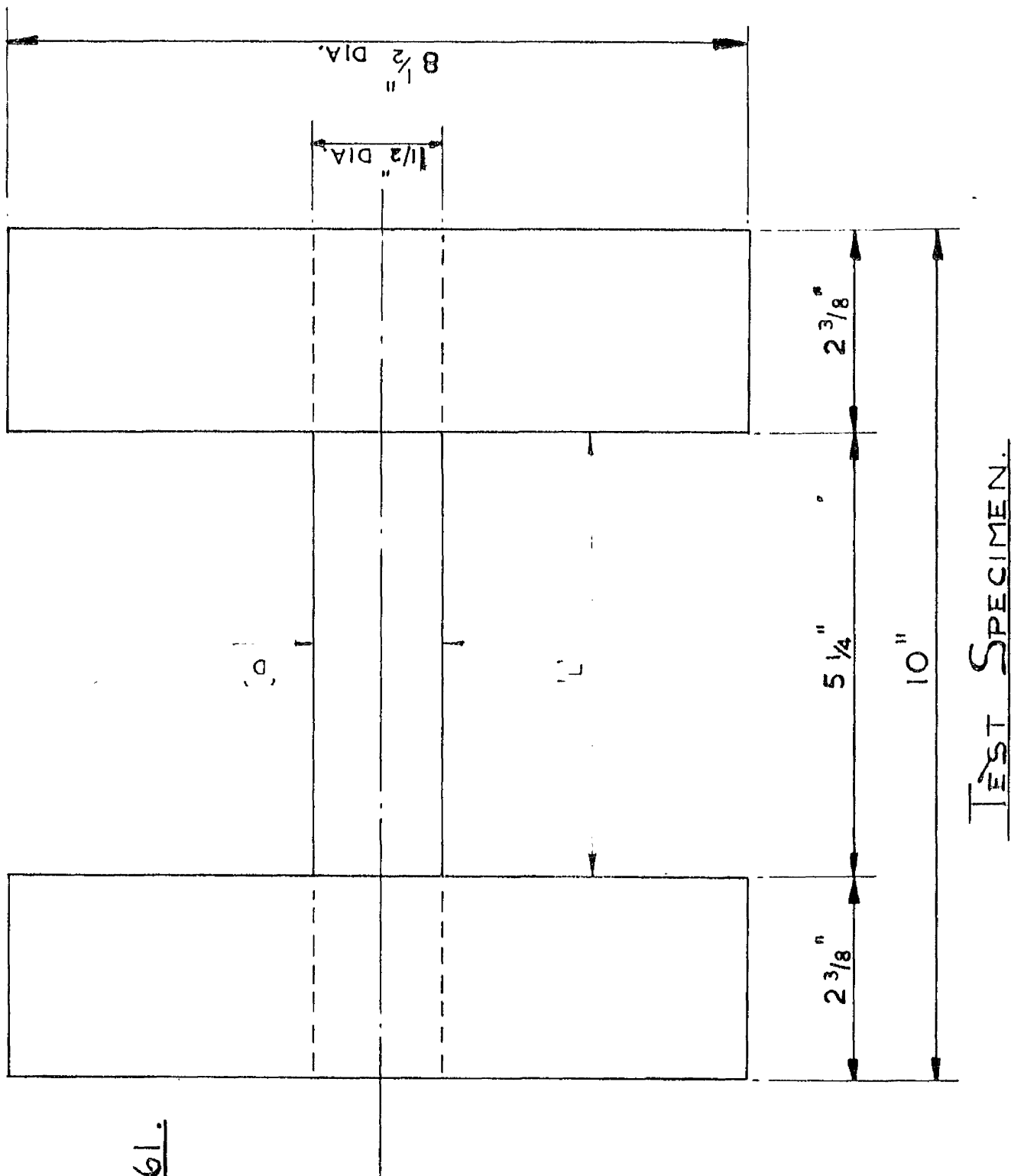
After all tests on the first set of specimens were completed, the shafts were tripped out of the fly-wheels for inspection.

Photographs of the shafts of specimens B and D are shown in Fig.72.

During the tests on the first set of specimens, discussion arose as to the importance of internal damping compared to the shrink-fit damping.

The second set of test specimens was therefore arranged as one solid specimen and four shrink-fitted specimens made from the same steel forging. All the particulars of this

FIGURE 61.



second set of specimens are given in Fig.63 -- properties of the material, as well as dimensions.

All the test specimens in the second set were cleaned with carbon tetrachloride before shrinking, to ensure that the mating surfaces were free from any grease.

Due to shortage of time, only initial tests were carried out for these specimens, and the results obtained are presented in the same way as before in Fig.73.

Thus the test programme for the purpose of this Thesis was finished, but it should be realised that a much greater variety of tests could be carried out with advantage, since this field of study is, as yet, relatively unexplored.

FIG. 62.

LUBRICATION: SPERM OIL

MATERIAL: MILD STEEL 28/32 T/in.² T.

| SPECIMEN | LENGTH (ins.) | DIAMETER 'D' (ins.) | DIAMETER D _s (ins.) | FLYWHEEL BORE (ins.) | INTER- FERENCE in./in.DIA. | PRESSURE p (LAMÉ) (T./in. ²) | SURFACE FINISH (C.L.A. 10 ⁻⁶ ins) |
|----------|------------------|---------------------------|--------------------------------------|----------------------------|----------------------------------|--|--|
| A | 5.248 | 1.495 | 1.5005 | 1.5002 | 0.0002 | 1.3 | 21 |
| | | | 1.5009 | 1.5006 | | | 24 |
| B | 5.245 | 1.499 | 1.5020 | 1.5015 | 0.00033 | 2.16 | 34 |
| | | | 1.5005 | 1.5000 | | | 23 |
| C | 5.201 | 1.498 | 1.5018 | 1.5008 | 0.00067 | 4.33 | 19 |
| | | | 1.5021 | 1.5011 | | | 22 |
| D | 5.232 | 1.497 | 1.5041 | 1.5026 | 0.001 | 6.5 | 25 |
| | | | 1.5032 | 1.5017 | | | 20 |
| E | 5.227 | 1.497 | 1.5026 | 1.5006 | 0.00133 | 8.65 | 20 |
| | | | 1.5031 | 1.5011 | | | 16 |

SPECIMEN SPECIFICATIONS.

SPECIMEN SPECIFICATIONS.

ALL SURFACE FINISHES UNDER 30×10^{-6} INS C.L.A.

SPECIMENS SHRUNK DRY.

CHEMICAL PROPERTIES :~

CARBON _ _ _ _ _ 0.215.

SILICON _ _ _ _ _ 0.05.

SULPHUR _ _ _ _ _ 0.045.

PHOSPHORUS _ _ _ _ 0.04.

MANGANESE _ _ _ _ 0.62.

MECHANICAL PROPERTIES :~

TENSILE _ _ _ _ _ 29.1 T/IN²

ELONGATION _ _ _ _ 31%

| SPECIMEN. | SHAFT DIA. INS. | FLYWHEEL BORE. INS. | INTER - FERENCE. IN/IN DIA. | PRESSURE p (LAMÉ) T/IN ² |
|-----------|-----------------------|---------------------------|-----------------------------------|---|
| 1 | SOLID SPECIMEN. | | | |
| 2 | 1.5007 | 1.5002 | .00033 | 2.16 |
| | | 1.5002 | | |
| 3 | 1.5024 | 1.5014 | .00067 | 4.33 |
| | | 1.5014 | | |
| 4 | 1.5032 | 1.5016 | .001 | 6.5 |
| | | 1.5017 | | |
| 5 | 1.5062 | 1.5042 | .00133 | 8.65 |
| | | 1.5041 | | |

FIG. 63.

DISCUSSION OF EXPERIMENTAL GRAPHS.

Scatter of Experimental Points.

Before a discussion on the general meaning of the experimental graphs is started, some words should be said about scatter of experimental points.

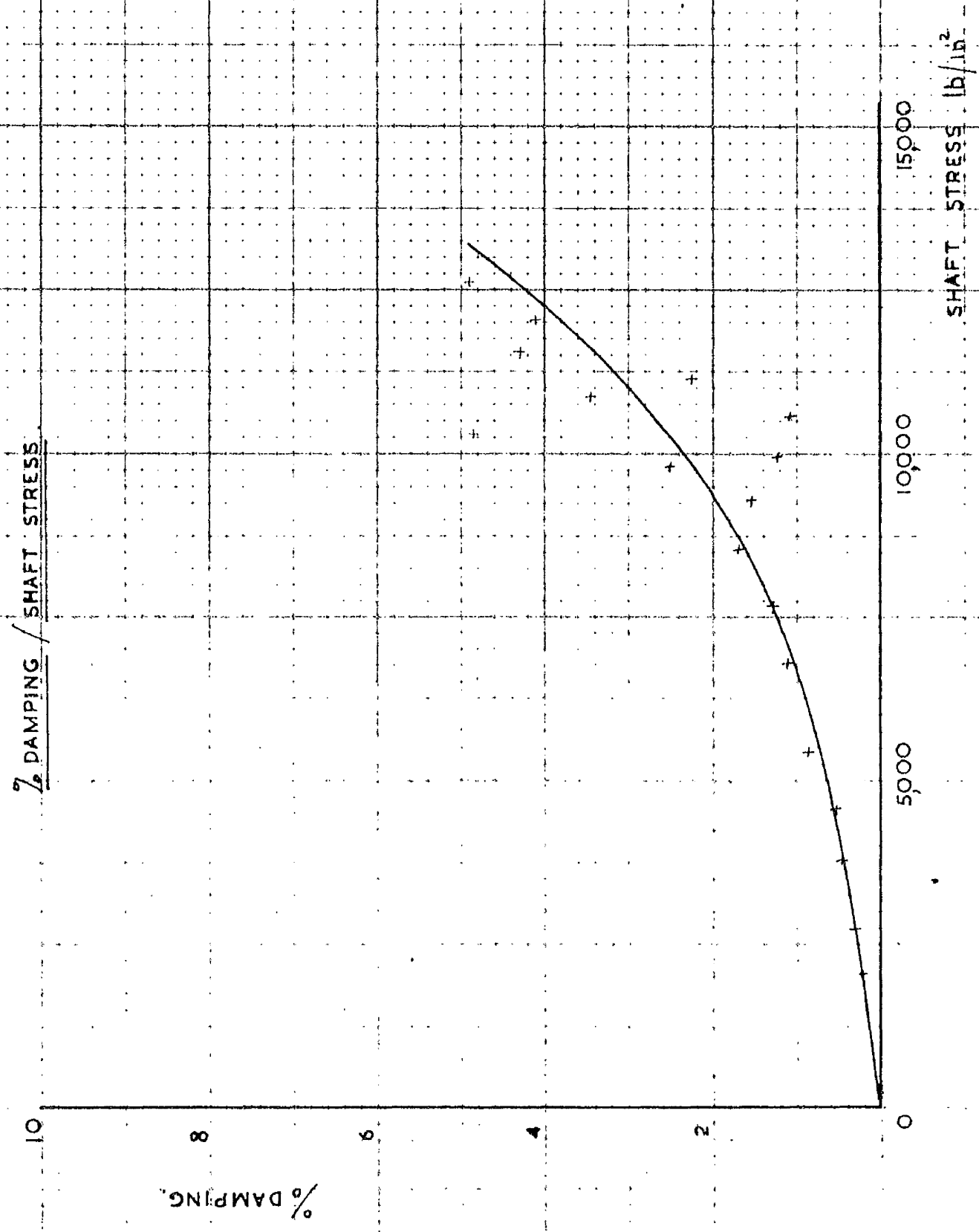
This question is best discussed with reference to Fig. 64, which has been presented as a fair example of the scatter normally present in the experimental results.

It is noticed that much scatter is present for the experimental points at the top end of the curve, whereas below a certain stress, the scatter is much reduced. This is due to the method of calculation of Percentage Damping.

For high stress values when the Percentage Damping is large, it is calculated as an average value over one cycle of vibration. As the damping decreases, however, the difference in amplitude between two consecutive cycles becomes so small that it will be necessary to calculate damping as an average over a number of cycles - first five, later ten and twenty are used.

The latter method of calculation reduces the effect of errors introduced in taking measurements off the records. However, any physical variations in Percentage Damping from cycle to cycle will also disappear.

FIGURE 64. SPECIMEN C, RECORD 12, 70×10^6 CYCLE.



It was noticed from points near the top end of the graphs, that the scatter of experimental points was much larger than could be expected from experimental errors, and this scatter was therefore believed to indicate significant variations in Percentage Damping.

In order not to obscure this effect, the former method of calculations was therefore used, wherever possible.

Differential Slip.

Some of the main features of the experimental graphs will now be disclosed and later viewed in relation to the theoretical analysis.

From an inspection of the graphs of Fig.65, it is seen that the Percentage Damping of any one of the sperm oil lubricated specimens tested immediately after shrink-fitting, increases rapidly with increase in shaft stress.

Further, it will be noticed that specimens with low interference fits generally show much higher damping than those with high.

The above features are repeated for the same set of specimens after 100 megacycles endurance test, as shown by Fig.71, and, from Fig.73, it is seen that also the second set of specimens, which were shrink-fitted dry, show the same characteristics.

Increased damping for increased shaft stress or decreased interface pressure can therefore be considered to be a general characteristic of shrink-fitted assemblies.

Let us now return to the graph of Percentage Damping versus the ratio of nominal stress to friction grip which was obtained as a result of the theoretical analysis. (See Fig. 57).

This graph expresses the same characteristics for shrink-fitted assemblies as were realised through the experimental tests.

Consequently, we may conclude that the basic assumption for the theoretical work - namely that differential slip takes place between the mating surfaces of the shaft and the hub of a shrink-fitted assembly when loaded in torsion - is valid.

Effect of Air Friction and Internal Damping.

Before proceeding any further in our discussion of shrink-fit damping, it will now be necessary to consider any other forms of damping which might appear in our experimental results.

Since all vibrational forces and torques are balanced within the test specimen, the only two additional effects possible are damping due to air friction and internal damping.

Let us now for a moment consider the graphs of Fig.73, which refer to the second set of test specimens and, in particular, we will pay attention to the graph for specimen 1. - the solid specimen.

This graph will indicate the effect of air friction and internal damping, since there is no shrink-fit damping present for this specimen.

As a result of geometrical identity, the same air friction damping will also apply to all the other specimens.

The internal damping, however, is expected to be highest for the solid specimen and to decrease for the shrink-fitted specimens with decreasing interference fits⁽¹⁾, but this decreasing effect must be small since, for our stress range, the graph for the solid specimen shows an approximately constant internal damping.

For the four remaining specimens in this set, a good measure of the pure shrink-fit damping can consequently

(1) This effect is due to the decrease in stress concentration factor as shown by Fig.57, as it is known that internal damping increases rapidly with stress⁽²⁾.

(2) Lazan, B.M. - "A Study with New Equipment of the Effects of Fatigue Stress on the Damping Capacity and Elasticity of Mild Steel." - Trans. Amer.Soc. For Metals, Vol.92, 1950, Pages 499-548.

be obtained by subtracting the damping measured for the solid specimen from the total damping.

Thus the graphs of Fig.74 are obtained, and for further work these graphs will be used, rather than those of Fig.73.

For the sperm oil lubricated specimens, it is clear from the graphs of Fig.65 and 71, that the effect of air friction and internal damping must be very small, and it will therefore be neglected in the following discussion.

For the final curve of specimen E. only, it is noticeable that the internal damping may be of slight importance.

Coefficient of Friction.

The discussion of our experimental graphs will now be carried a step further to explain variations in damping between dry shrunk and sperm oil lubricated specimens, and also the effect of endurance testing on the sperm oil lubricated specimens.

For this purpose, it will be necessary to consider a third parameter affecting the dissipation of vibrational energy in a shrink-fitted assembly - namely the coefficient of friction between the mating surfaces.

With reference to Fig.57, it is seen that an increase

in the coefficient of friction will cause a decrease in the percentage damping, and vice versa.

Let us consider the sperm oil lubricated specimens in the light of this information. It is seen by comparing the curves of Fig.65 with those of Fig.71 and 74, that, initially, these specimens provide a very high percentage damping and, consequently, a low coefficient of friction must exist. This would be expected for oil lubricated surfaces.

Endurance testing of the same specimens has the effect of reducing the high initial damping substantially over the first 10 to 40 megacycles, after which a constant level of damping is kept for the remaining part of the test (see Fig.66-70).

This effect is explained by a breakdown of the oil-film over the mating surfaces, followed by the formation of corrosive material of a much higher coefficient of friction (1)(2). Thus, the final curves for the sperm oil lubricated specimens of percentage damping versus shaft stress are determined by a higher coefficient of friction than the initial, and therefore show less damping.

The curves of Fig.74 show that dry shrunk specimens

- (1) Fretting corrosion is a well-known phenomenon resulting from rubbing motion between two metal surfaces.
- (2) Photographs of the corroded shaft surfaces are shown in Fig.72.

give less damping than lubricated specimens. This confirms the above observations, since the coefficient of friction should be higher for dry shrunk specimens than for lubricated specimens⁽¹⁾.

It will be understood from the above that the coefficient of friction between the mating surfaces of a shrink-fitted assembly has an important bearing on the damping.

With reference to the first section of this discussion, we may therefore, at this stage, explain the excessive scatter of experimental results by random variations in the coefficient of friction⁽²⁾.

For further development of the subject, it is now natural to try to obtain some numerical values for the coefficient of friction.

This can be achieved by considering the experimental graphs in relation to the theoretical graph of Fig.57.

Calculations of the coefficient of friction are carried out in Appendix VII, which also gives Tables of the results obtained.

-
- (1) Davidson, W.R.S. - "Shrink-Fit Stress Systems in Built Crankshafts." - Ph.D. Thesis, Glasgow University, 1951.
 - (2) Rabinowicz, Righmire, Tedholm and Williams, - "The Statistical Nature of Friction." - The Transactions of the American Society of Mechanical Engineers, 1955. Vol.77, Pages 981-984.

FIG. 65. % DAMPING / SHAFT STRESS SPECIMENS A, B, C, D, E

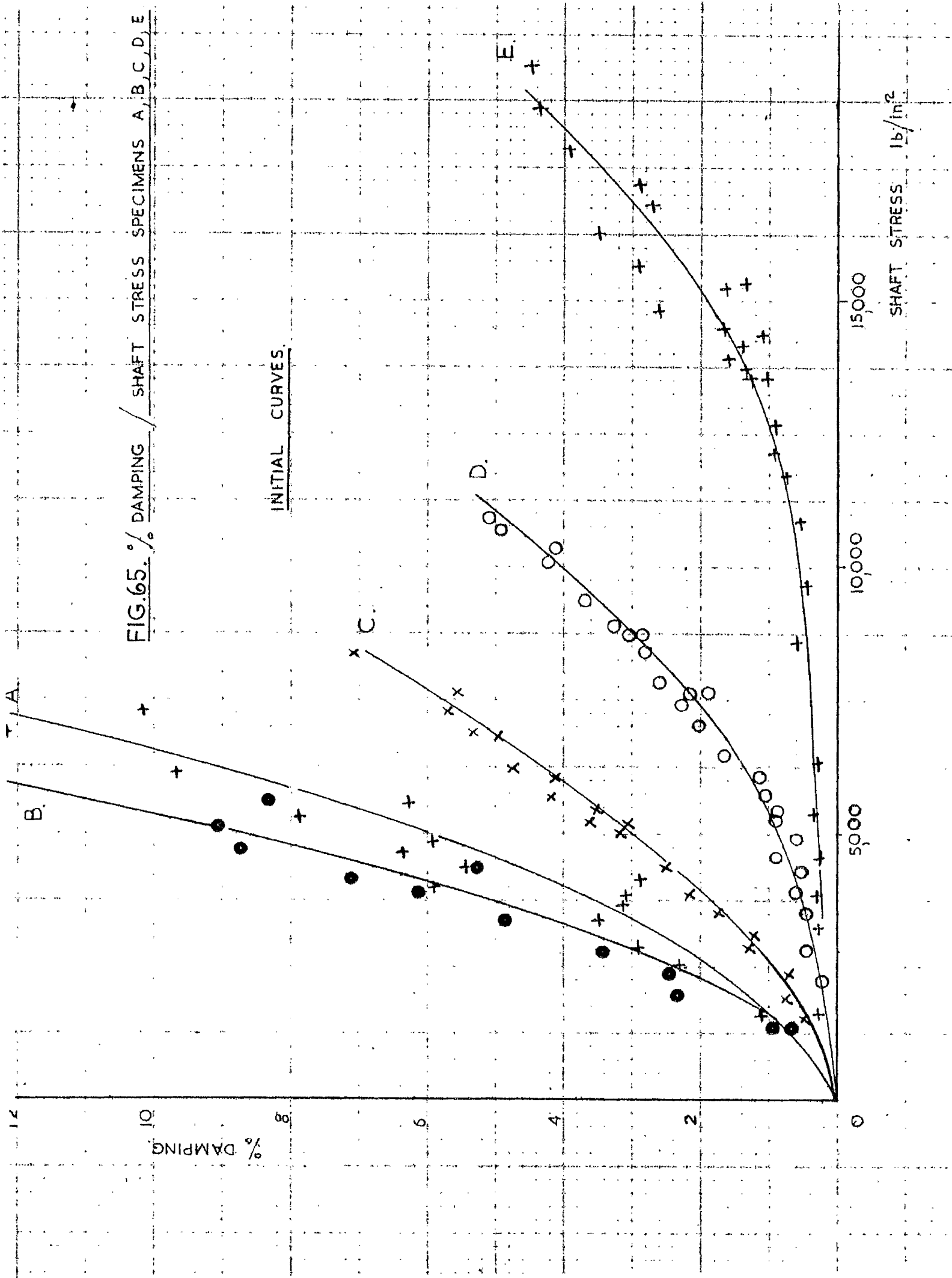


FIG. 66 SPECIMEN 'A' ENDURANCE CHARACTERISTICS

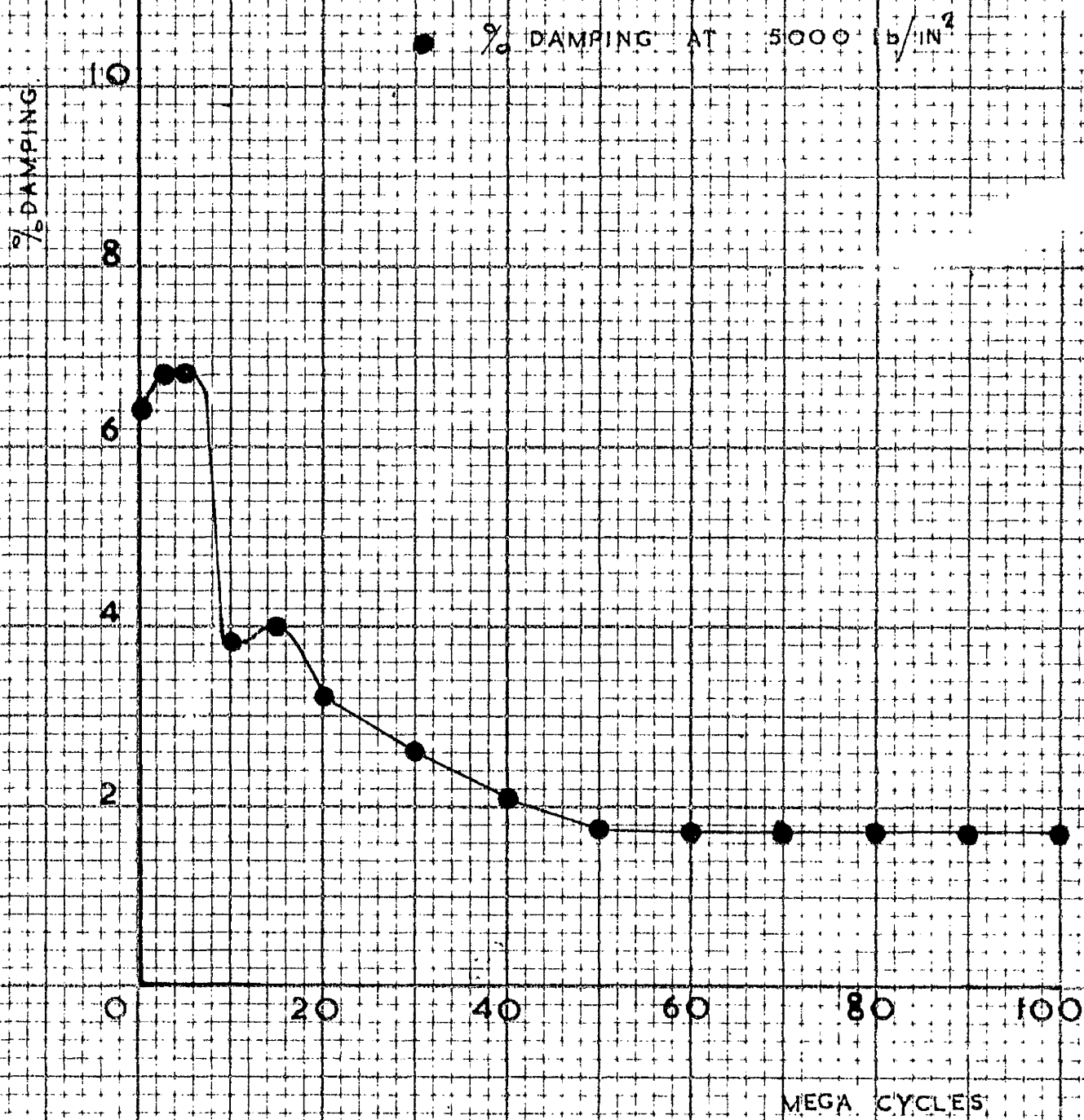


FIG. 67. SPECIMEN 'B' ENDURANCE CHARACTERISTICS.

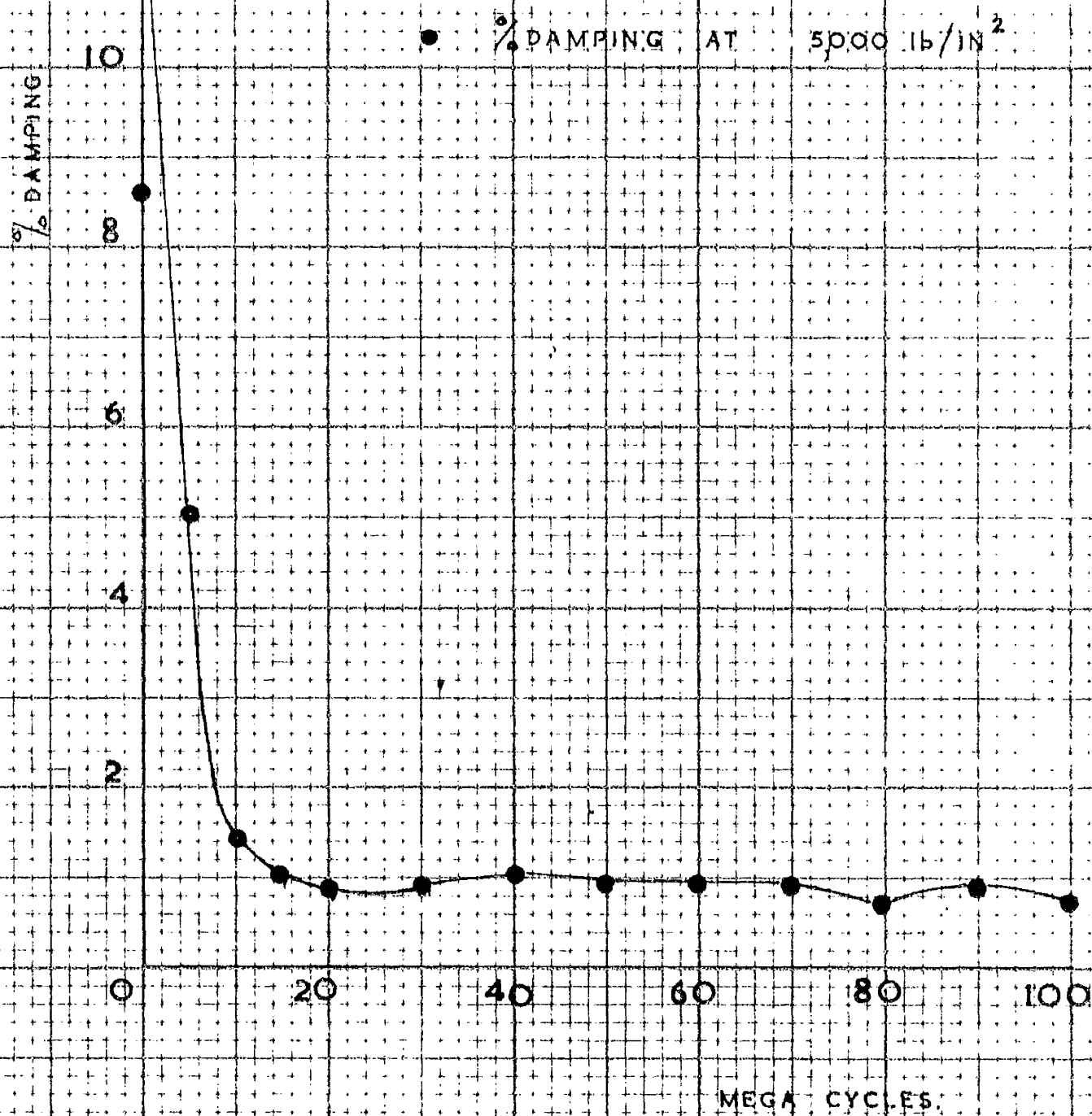


FIG. 68. SPECIMEN 'C' ENDURANCE CHARACTERISTICS

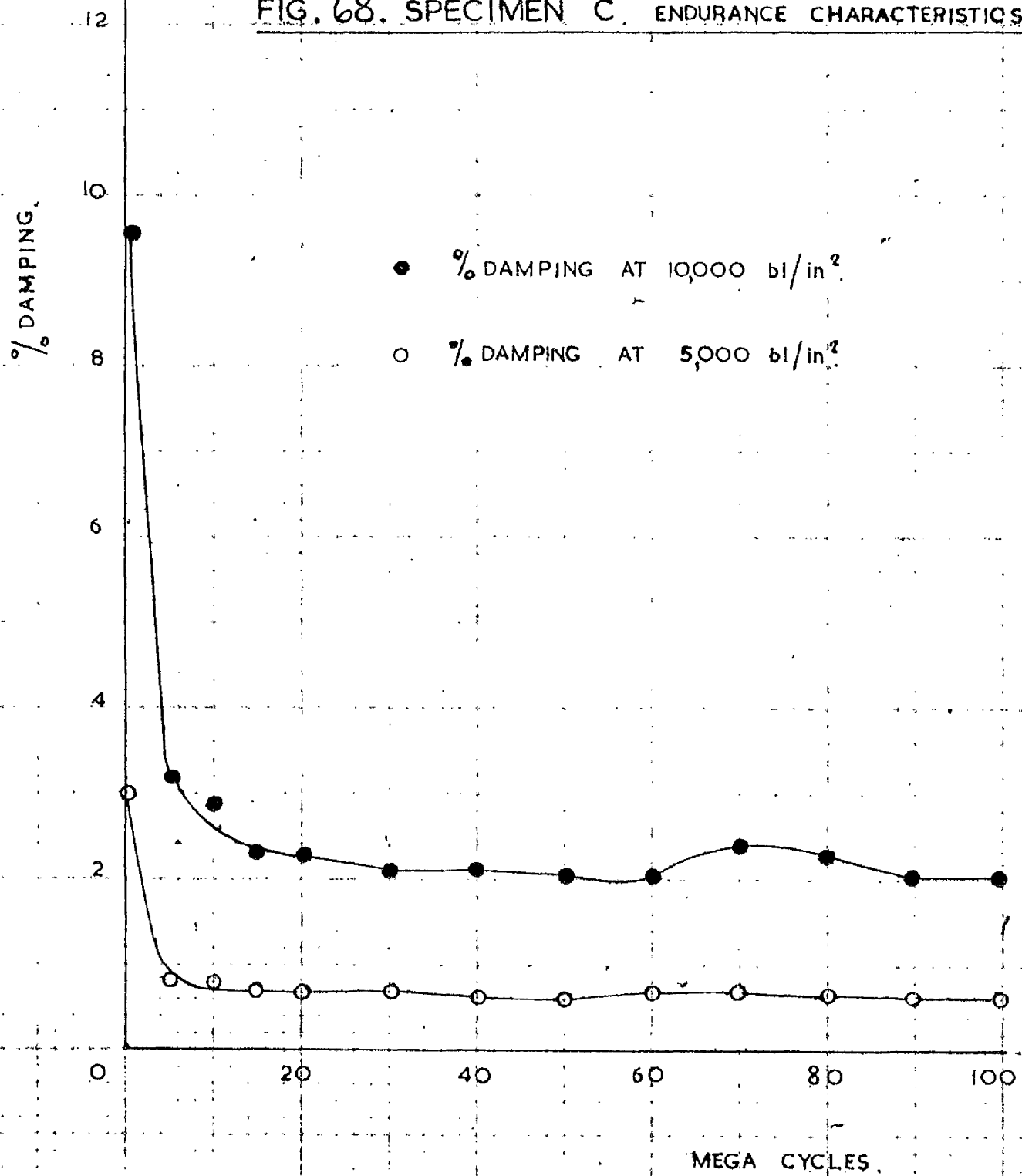


FIG. 69. SPECIMEN 'D' ENDURANCE CHARACTERISTICS.

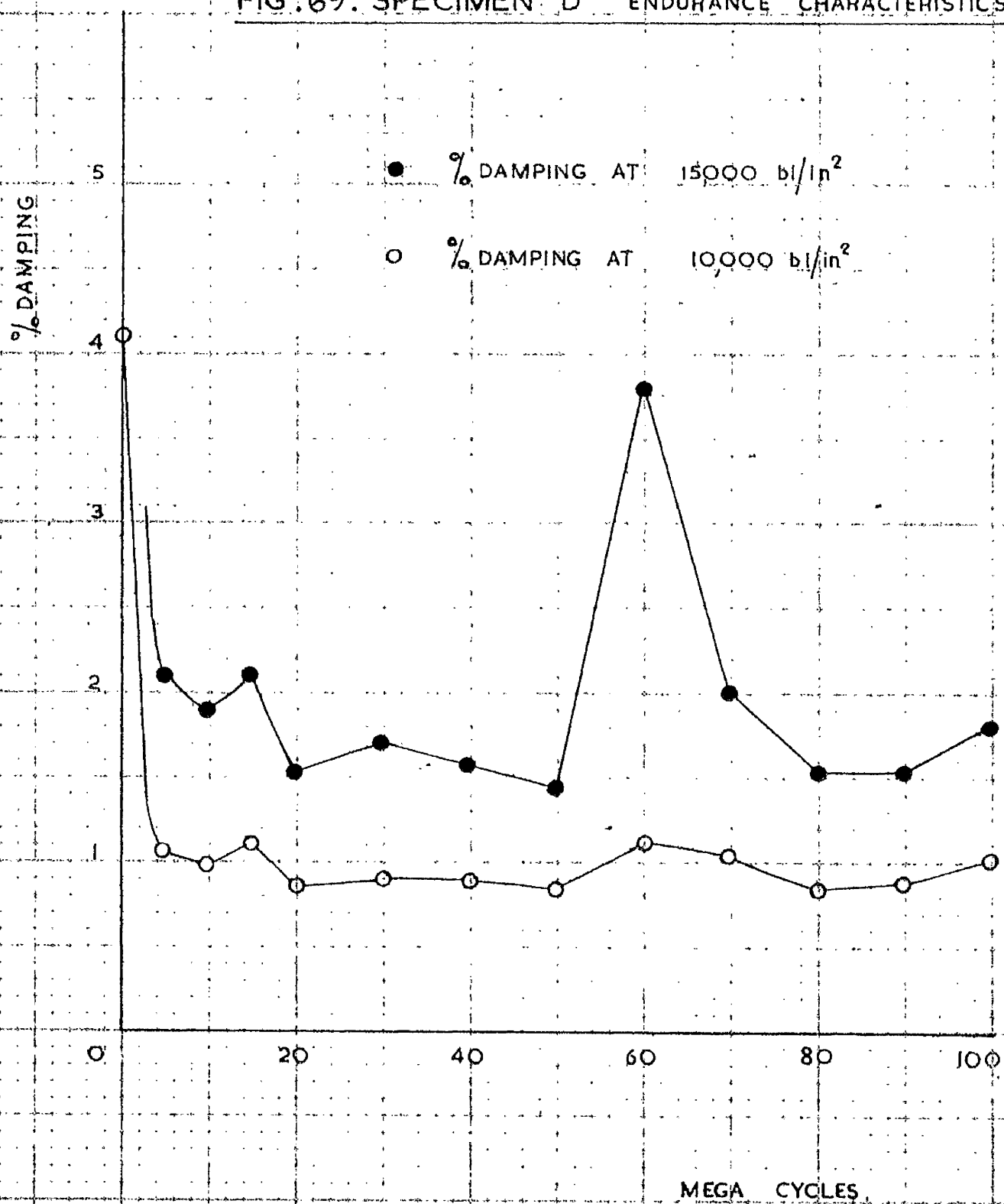


FIG. 70. SPECIMEN 'E' ENDURANCE CHARACTERISTICS.

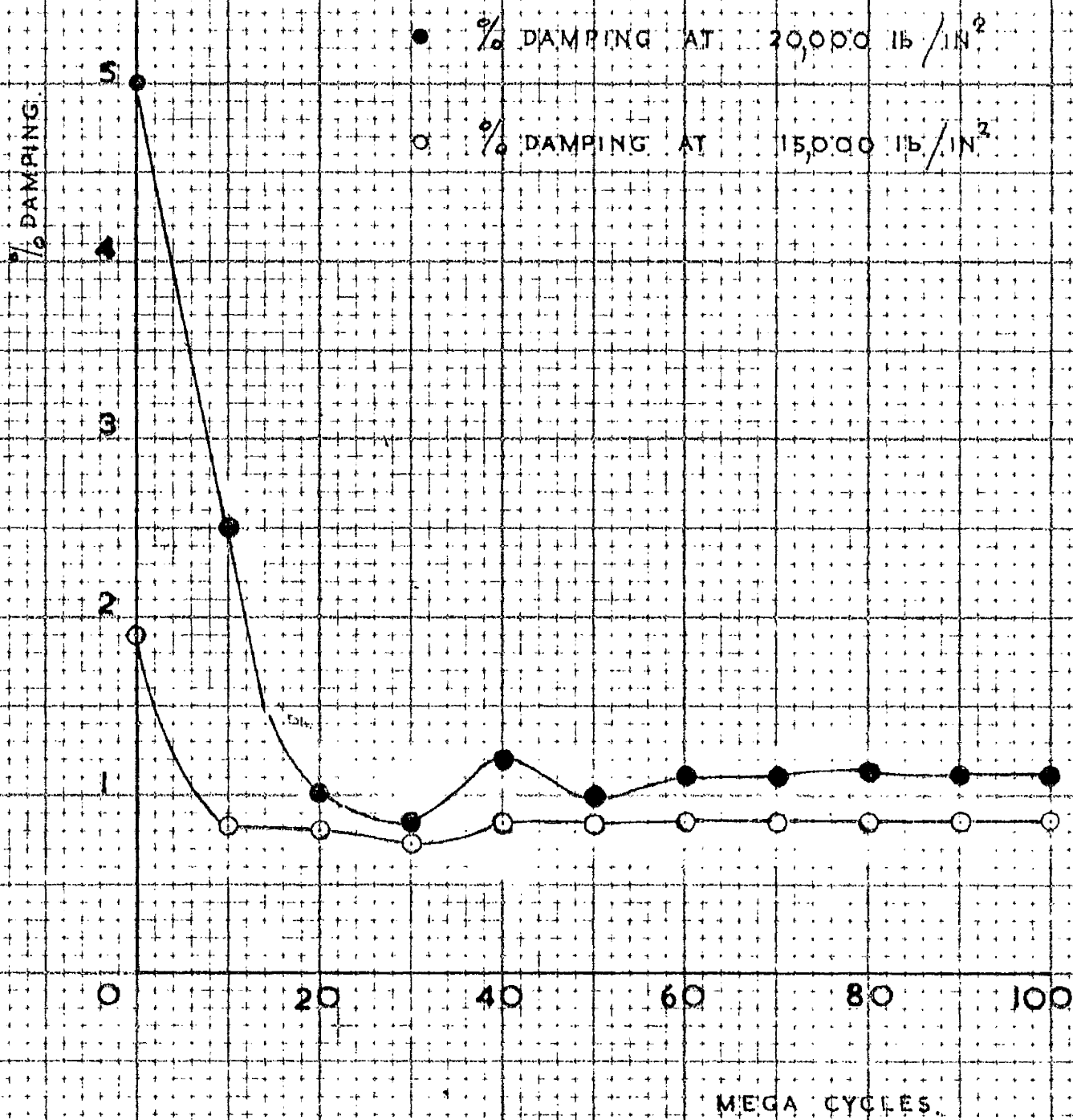


FIG. 71. % DAMPING / SHAFT STRESS SPECIMENS A, B, C, D, E.

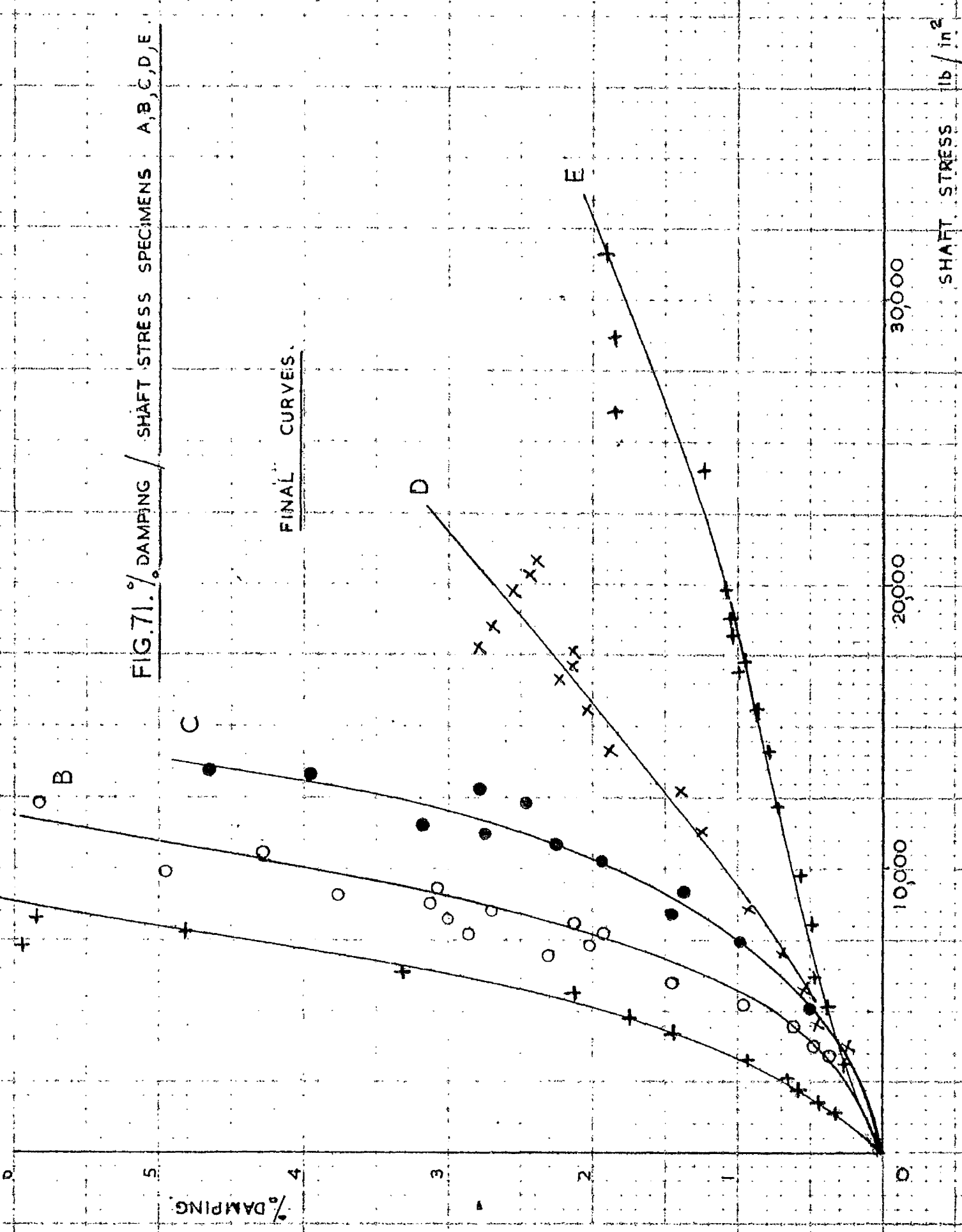
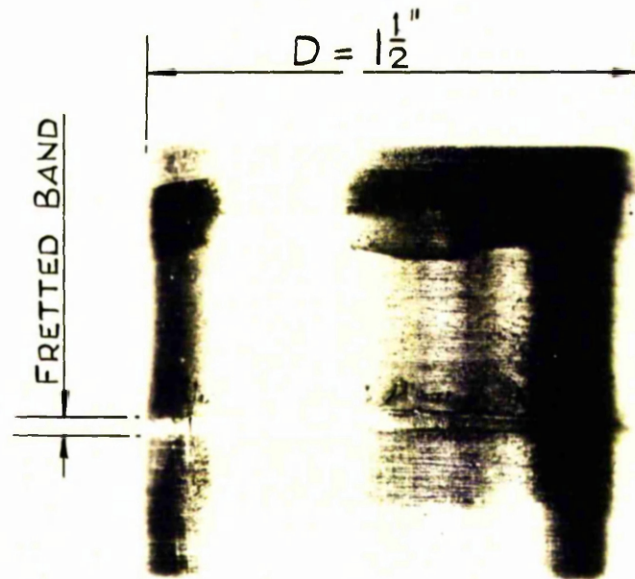
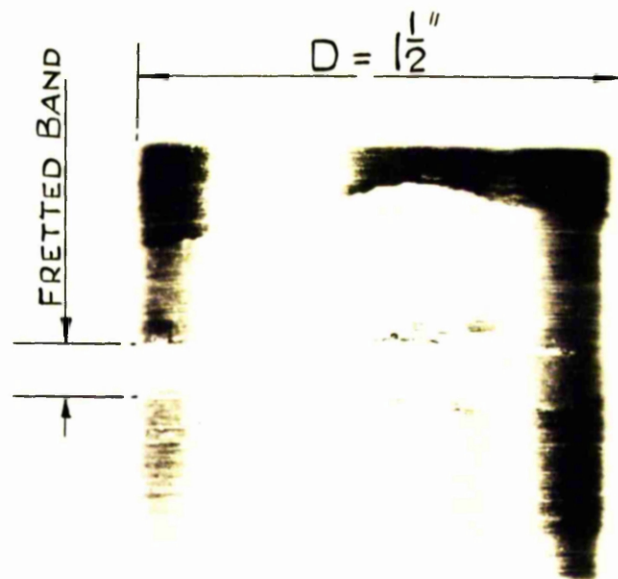


FIG. 72.



SPECIMEN E



SPECIMEN B

FIG. 73. / DAMPING — SHAFT STRESS SPECIMENS (1,2,3,4,5)

INITIAL CURVES

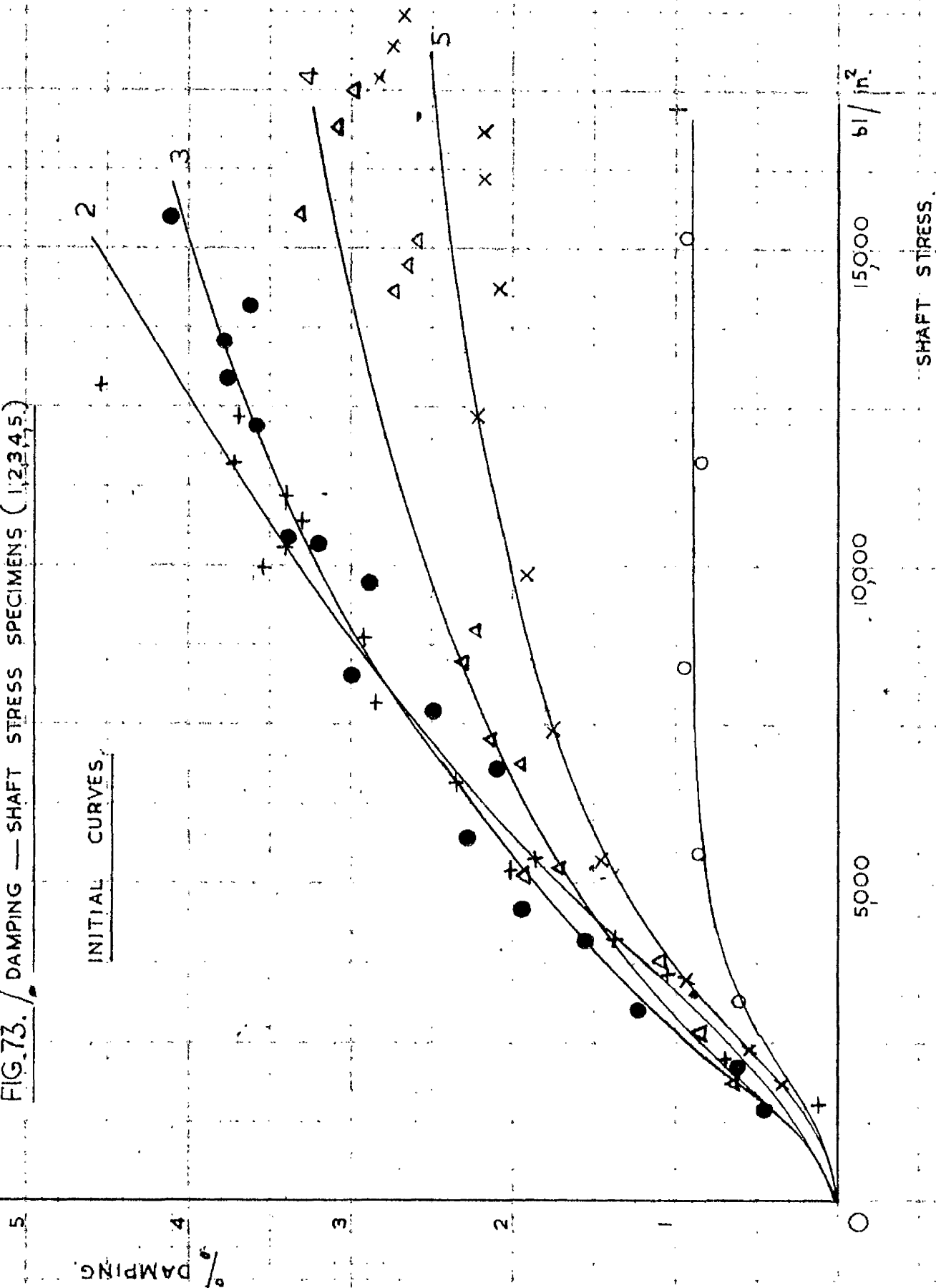
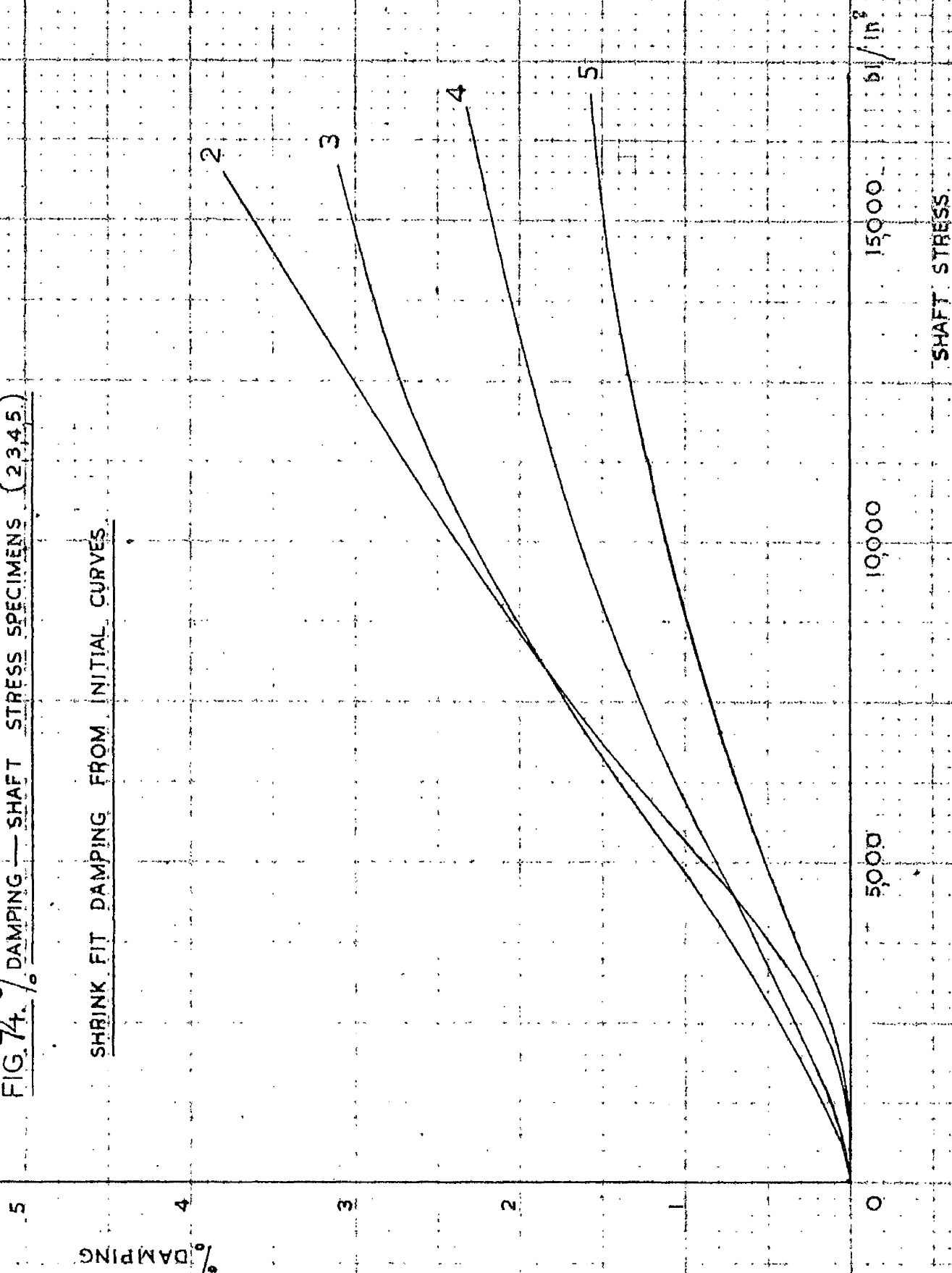


FIG. 74. $\%$ DAMPING — SHAFT STRESS SPECIMENS (2345.)

SHRINK FIT DAMPING FROM INITIAL CURVES



Appendix VII shows that the coefficient of friction varies with the shaft stress for any particular specimen, as well as from specimen to specimen.

To obtain some idea about the effect of interface pressure on coefficient of friction, the average values for each specimen have been calculated.

These average values of the coefficient of friction are plotted versus the surface pressure, as shown in Fig.75.

The centre parts of the curves of Fig.75 show values of the coefficient of friction which compare with those obtained by other investigators for similar conditions⁽¹⁾.

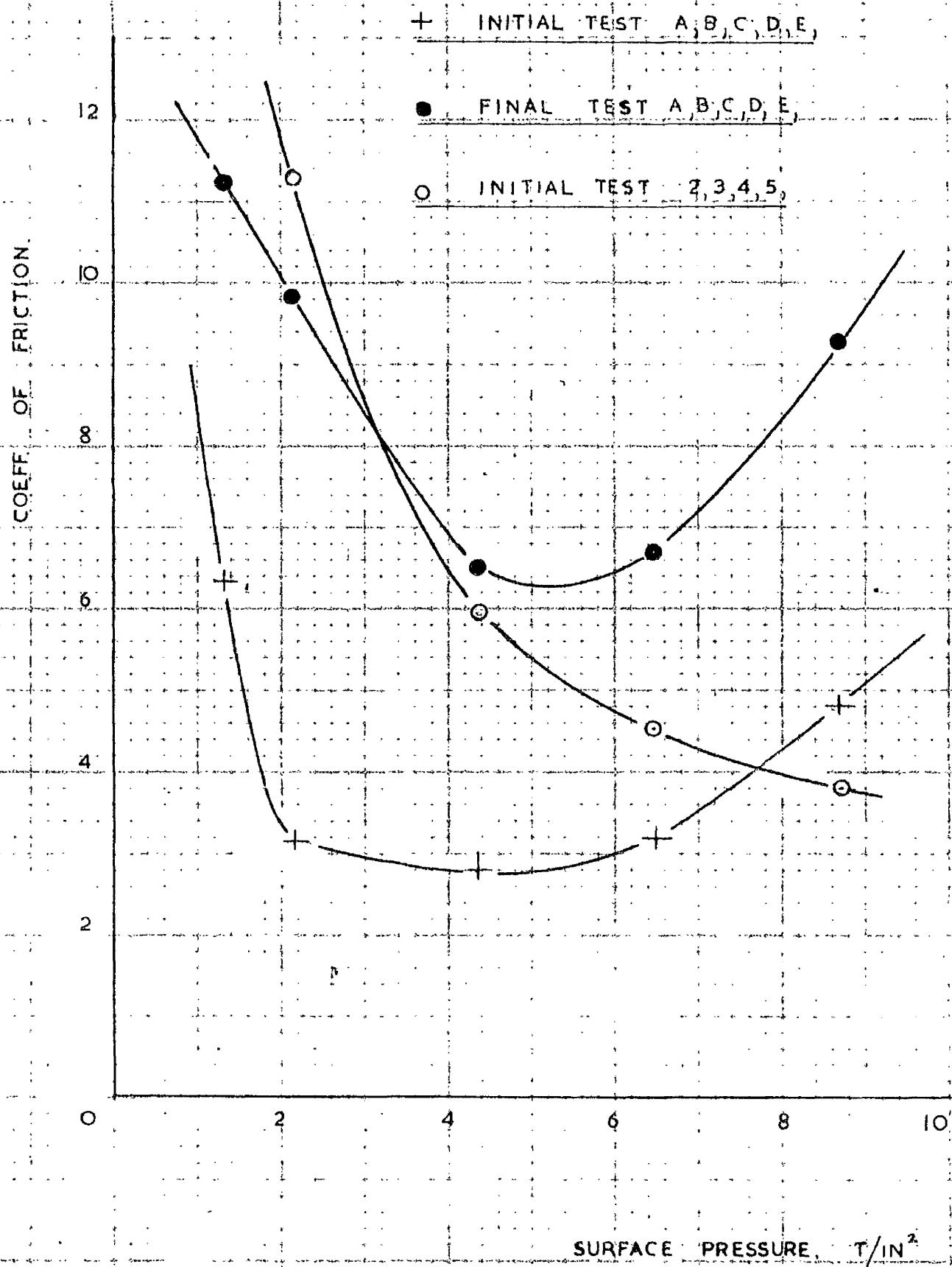
For the general trend of the curves, however, no previous papers which could form a comparison have been found.

It is the author's opinion that the results of Fig.75 are insufficient to form a basis for further discussion, and the graphs are therefore presented purely for the interest of further research.

Thus, the discussion of experimental results obtained for shrink-fitted assemblies loaded in torsion, is concluded.

(1) Davidson, W.R.S. - "Shrink-Fit Stress Systems in Built Crankshafts." - Ph.D. Thesis, Glasgow University, 1951.

FIG 75. COEFF. OF FRICTION / SURFACE PRESSURE



PRACTICAL IMPORTANCE OF SHRINK-FIT DAMPING.

From measurements taken on diesel engines in operation, Draminsky⁽¹⁾ shows that the crankshaft system of such engines possesses damping of the order of 2-4 per cent.

It is therefore clear that a source of damping which, for comparatively low shaft stresses can reach 10 per cent., will be of great practical importance.

Present design practice for built-up crankshafts, which advocates high interference fits and coefficients of friction, tends to reduce this importance, but it should be realised that a very valuable source of damping is thereby destroyed.

However, difficulties will obviously be encountered in designing crankshafts which possess high shrink-fit damping, and also retain their ability to carry large constant torques.

Finally, a danger attached to shrink-fit damping should be pointed out.

Since this damping decreased with running time, it is possible that shaft stresses, measured and accepted for new engines with built-up crankshafts, will later increase beyond the permissible value, and failures may consequently occur.

(1) Draminsky, P. - "Daempningen Ved Torsionsevingninger I Krumtapaksler", Copenhagen, 1947. Pages 99 and 100.

CONCLUSION.

Damping in shrink-fitted assemblies has been discovered, investigated and found to be of considerable practical importance.

It has been possible to give this damping a fundamental explanation related to elastic deflections and surface conditions of the assemblies.

Thus, the study of damping also yielded information about other characteristics, such as differential slip and stiffness.

APPENDIX I.

INERTIA FORCES CAUSED BY VIBRATIONAL MOTION OF THE OUT OF BALANCE MASSES OF A SINGLE CRANK.

Displacements, Velocities and Accelerations.

Let us consider a crank mechanism as shown in Fig.76. For the purpose of this analysis the masses of the actual piston, the connecting rod and the crank may be represented by one reciprocating mass moving along the piston centre line, and one rotating mass situated at the crank pin. These masses are connected through a weightless, infinitely stiff mechanism.

It will be required to find the accelerations of these two masses when the rotation of the crank consists of a vibrational motion superimposed on a constant angular velocity rotation.

(a) Rotating Out of Balance Mass.

Let us denote the angle between the piston centre line and the crank by θ , choosing anticlockwise rotation as positive. If A_n denotes the amplitude, and ϵ_n the phase angle of the n th. harmonic of torsional vibration of the crank, and ω the constant angular velocity, the angle θ will be given completely by the following expression:-

$$\theta = \omega t + \sum_{n=1}^{\infty} A_n \sin n(\omega t + \epsilon_n) \dots 1 A$$

Hence

$$\dot{\theta} = \omega + \sum_{n=1}^{\infty} n\omega A_n \cos n(\omega t + \epsilon_n) \quad \dots 2 A$$

and

$$\ddot{\theta} = - \sum_{n=1}^{\infty} n^2 \omega^2 A_n \sin n(\omega t + \epsilon_n) \quad \dots 3 A$$

The acceleration of the mass at the crank pin will be given by two components, the tangential acceleration and the radial acceleration. In terms of the angle _____ the tangential acceleration will be given by:-

$$\alpha_T = R\ddot{\theta} \quad \dots 4 A$$

where R. denotes the crank radius.

The radial acceleration, which is always pointing towards the centre of rotation, is given by:-

$$\alpha_R = R\dot{\theta}^2 \quad \dots 5 A$$

Making use of equations (2 A) and (3 A) the above two components of the acceleration of the rotating mass may now be expressed in terms of the vibrational motion of the crank, as follows (1):-

$$\alpha_T = -R\omega^2 \sum_{n=1}^{\infty} n^2 A_n \sin n(\omega t + \epsilon_n) \quad \dots 6 A$$

(1) Second order terms can be neglected since nA_n generally is small.

and

$$\underline{a_s = R\omega^2 \left(1 + 2 \sum_{n=1}^{\infty} n A_n \cos n(\omega t + \epsilon_n)\right)} \quad \dots 7 A$$

(b) Reciprocating Mass.

For a study of the accelerations of the reciprocating mass, it will be necessary to return to the crank mechanism which is shown in Fig. 76.

Let the displacement of the reciprocating mass from its position at T.D.C. be denoted by μ , taken positive towards the crank centre. From the geometry of the system this displacement may be expressed by the following equation, in which l denotes the length of the connecting rod, and R the crank radius as before:-

$$\underline{\mu = R + l - \left\{ R \cos \theta + l \left(1 - \left(\frac{R}{l} \sin \theta \right)^2 \right)^{\frac{1}{2}} \right\}} \quad \dots 8 A$$

For a further treatment equation (8 A) is now most conveniently expanded as a Fourier series:-

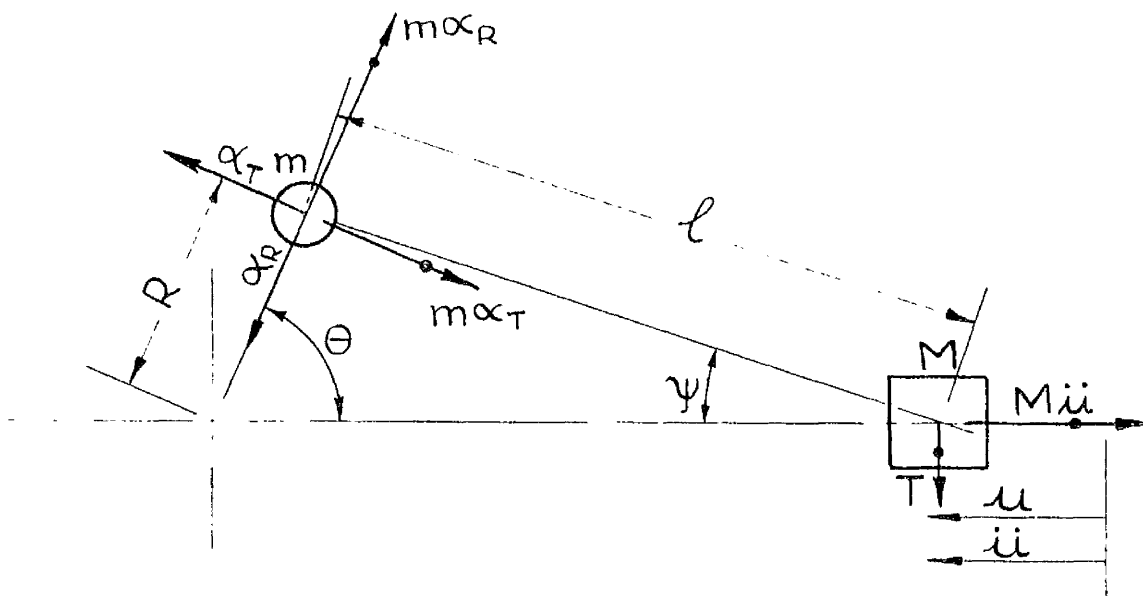
$$\underline{\mu = R + l - R \{ K_0 + \cos \theta + K_2 \cos 2\theta + K_4 \cos 4\theta \dots \}} \quad \dots 9 A$$

where the coefficients K_0 , K_2 , K_4 , etc. are given by the following equations:-

$$\underline{K_0 = \frac{l}{R} - \frac{1}{4} \frac{R}{l} - \frac{3}{64} \left(\frac{R}{l} \right)^3 - \frac{5}{256} \left(\frac{R}{l} \right)^5 \dots} \quad \dots 10 A$$

$$\underline{K_2 = \frac{1}{4} \frac{R}{l} + \frac{1}{16} \left(\frac{R}{l} \right)^3 + \frac{15}{512} \left(\frac{R}{l} \right)^5 \dots} \quad \dots 11 A$$

FIG. 76.



CRANK MECHANISM.

$$K_4 = -\frac{1}{64}\left(\frac{R}{l}\right)^3 - \frac{3}{256}\left(\frac{R}{l}\right)^5 \dots \dots \dots 12 \text{ A}$$

Hence:—

$$\ddot{u} = R(\sin \theta + 2K_2 \sin 2\theta + 4K_4 \sin 4\theta \dots) \dots \dots 13 \text{ A}$$

and

$$\begin{aligned} \ddot{u} = R(\sin \theta + 2K_2 \sin 2\theta + 4K_4 \sin 4\theta \dots) \ddot{\theta} \\ + R(\cos \theta + 4K_2 \cos 2\theta + 16K_4 \cos 4\theta \dots) \dot{\theta}^2 \end{aligned} \dots \dots 14 \text{ A}$$

Making use of the equations (2 A) and (3 A) we may now substitute for $\ddot{\theta}$ and $\dot{\theta}^2$ in equation (14 A) and thus we obtain⁽¹⁾:—

$$\begin{aligned} \ddot{u} = \omega^2 R \{ \cos \theta + 4K_2 \cos 2\theta \dots \} (1 + 2 \sum_{n=1}^{\infty} n A_n \cos n(\omega t + \epsilon_n)) \\ - (\sin \theta + 2K_2 \sin 2\theta \dots) \{ \sum_{n=1}^{\infty} n^2 A_n \sin n(\omega t + \epsilon_n) \} \end{aligned} \dots \dots 15 \text{ A}$$

Equation (15 A) may be approximated to⁽²⁾:—

$$\begin{aligned} \ddot{u} = \omega^2 R \{ \cos \theta + 4K_2 \cos 2\theta + 16K_4 \cos 4\theta \dots \\ + 2(\cos \theta + 4K_2 \cos 2\theta) \sum_{n=1}^{\infty} n A_n \cos n(\omega t + \epsilon_n) \\ - (\sin \theta + 2K_2 \sin 2\theta) \sum_{n=1}^{\infty} n^2 A_n \sin n(\omega t + \epsilon_n) \} \end{aligned} \dots \dots 16 \text{ A}$$

(1) Second order terms are again neglected.

(2) Since A_n is generally very small, nA_n and n^2A_n will be small. Also K_4 , K_6 , etc. are small, and consequently terms which contain products of the above components may be neglected.

Inertia Forces.(a) Rotating Out of Balance Mass.

The total out of balance of the rotating mass of the crank will be given by $\underline{m'r}$ where $\underline{m'}$ denotes the rotating mass, and \underline{r} the distance between the centre of gravity and the axis of rotation.

For our purpose it will be sufficiently accurate and more convenient to represent the actual out of balance by a mass \underline{m} situated at the crankpin, as seen in the previous section. The inertia forces set up are in this way represented correctly in magnitude and direction, but slightly offset in their point of application, if the mass \underline{m} is obtained through the following equation:-

$$\underline{mR = m'r} \quad . . . 17 A$$

Having obtained the best value for the mass situated at the crankpin, the inertia forces now follow readily. Making use of equations (6 A) and (7 A) respectively we obtain the complete value:-

$$\underline{m\alpha_r = -mR\omega^2 \sum_{n=1}^{\infty} n^2 A_n \sin n(\omega t + \epsilon_n)} \quad . . . 18 A$$

$$\underline{m\alpha_r = mR\omega^2 (1 + 2 \sum_{n=1}^{\infty} n A_n \cos n(\omega t + \epsilon_n))} \quad . . . 19 A$$

(b) Reciprocating Mass.

Let the symbol M denote the reciprocating mass, situated at the small end of the connecting rod. Making use of equation (16 A) gives the following complete expression for the inertia force acting on this mass along the cylinder centre line:-

$$\begin{aligned} M\ddot{u} = & M\omega^2 R \{ \cos \theta + 4K_2 \cos 2\theta + 16K_4 \cos 4\theta \dots \dots 20 A \\ & + 2(\cos \theta + 4K_2 \cos 2\theta) \sum_{n=1}^{\infty} n A_n \cos n(\omega t + \epsilon_n) \\ & - (\sin \theta + 2K_2 \sin 2\theta) \sum_{n=1}^{\infty} n^2 A_n \sin n(\omega t + \epsilon_n) \} \end{aligned}$$

It follows from simple force analysis that the inertia force given by equation (20 A) will be accompanied by a sidethrust T perpendicular to the cylinder wall (see Fig. 76).

This sidethrust will be given by:-

$$T = M\ddot{u} \tan \psi \dots \dots 21 A$$

From the geometry of the crank mechanism we have:-

$$\tan \psi = \frac{\frac{R}{l} \sin \theta}{(1 - (\frac{R}{l})^2 \sin^2 \theta)^{\frac{1}{2}}}$$

but since generally $\frac{R}{l} < \frac{1}{3}$ we may for our purpose use:-

$$\tan \psi = \frac{R}{l} \sin \theta$$

Hence the side thrust is given by:-

$$\underline{T = M\ddot{u} \frac{R}{l} \sin\theta} \quad . . . 22 A$$

The two forces given by equations (20 A) and (22 A) will be transmitted through the connecting rod and appear as loads on the crankshaft.

For calculations on the crankshaft it will be most convenient if all the applied forces are represented by their radial and tangential components on the crankpin and also the forces due to the reciprocating mass will therefore be presented in this way.

From Fig.76, it then follows that the total tangential inertia force on the crankpin will be given by:-

$$\underline{F_t = m\dot{a}_t + M\ddot{u} \sin\theta + T \cos\theta} \quad . . . 23 A$$

Similarly, the radial force will be given by:-

$$\underline{F_r = m\dot{a}_r + M\ddot{u} \cos\theta - T \sin\theta} \quad . . . 24 A$$

We may now introduce $(\omega t + \phi)$ instead of the angle θ , where ω is the constant angular velocity of the crankshaft and ϕ is the angle between crank 1. and the crank under consideration.

Making use of equations (18 A), (20 A) and (22 A) gives the following complete expression for the tangential force:-

$$\begin{aligned}
 \underline{\underline{F_r = R\omega^2 \left\{ -m \sum_{n=1}^{\infty} n^2 A_n \sin n(\omega t + \epsilon_n) \right.}} \quad \dots 25 A \\
 + M \left[\cos(\omega t + \theta) + 4K_2 \cos 2(\omega t + \theta) + 16K_4 \cos 4(\omega t + \theta) \dots \right. \\
 \left. + 2(\cos(\omega t + \theta) + 4K_2 \cos 2(\omega t + \theta)) \sum_{n=1}^{\infty} n A_n \cos n(\omega t + \epsilon_n) \right. \\
 \left. - (\sin(\omega t + \theta) + 2K_2 \sin 2(\omega t + \theta)) \sum_{n=1}^{\infty} n^2 A_n \sin n(\omega t + \epsilon_n) \right] \\
 \left. \times \left[\sin(\omega t + \theta) + \frac{R}{2l} \sin 2(\omega t + \theta) \right] \right\}
 \end{aligned}$$

Similarly, from equations (19 A), (20 A) and (22 A) we get an expression for the radial force:-

$$\begin{aligned}
 \underline{\underline{F_r = R\omega^2 \left\{ m \left(1 + 2 \sum_{n=1}^{\infty} n A_n \cos n(\omega t + \theta) \right) \right.}} \quad \dots 26 A \\
 + M \left[\cos(\omega t + \theta) + 4K_2 \cos 2(\omega t + \theta) + 16K_4 \cos 4(\omega t + \theta) \dots \right. \\
 \left. + 2(\cos(\omega t + \theta) + 4K_2 \cos 2(\omega t + \theta)) \sum_{n=1}^{\infty} n A_n \cos n(\omega t + \epsilon_n) \right. \\
 \left. - (\sin(\omega t + \theta) + 2K_2 \sin 2(\omega t + \theta)) \sum_{n=1}^{\infty} n^2 A_n \sin n(\omega t + \epsilon_n) \right] \\
 \left. \times \left[\cos(\omega t + \theta) - \frac{R}{2l} (1 - \cos(2\omega t + \theta)) \right] \right\}
 \end{aligned}$$

For further progress in the analysis we are only interested in the Nth. harmonics of the above two forces.

Further, it will be assumed that the Nth. harmonics of the torsional vibrations of the crank are at resonance, when its amplitude is large compared to that of any other

harmonic.

Making use of this, and after a considerable amount of algebra, it will be found that the tangential and radial components of the Nth. harmonic of the forces on the crank-pin are given to a good degree of approximation by the following two equations:-

$$\underline{(\bar{F}_T)_N = -R\omega^2 N^2 A_N \left(m + \frac{1}{2} \left(1 + \frac{1}{4} \left(\frac{R}{l}\right)^2\right)\right) \sin N(\omega t + \epsilon_N)} \quad . . . 27 A$$

$$\underline{(\bar{F}_R)_N = 2NR\omega^2 A_N \left(m + \frac{1}{2} \left(1 + \frac{1}{4} \left(\frac{R}{l}\right)^2\right)\right) \cos N(\omega t + \epsilon_N)} \quad . . . 28 A$$

It is noticed from equations (27 A) and (28 A) that the Nth. harmonics of the tangential and radial forces on the crankpin have phase angles which are independent of the crank angle, and solely dependent on the phase angle of the Nth. harmonic of the crank vibrations.

At resonance conditions when all cranks are either in phase or anti-phase, this angle as given by $N\epsilon_N$, will either be the same or 180° different for all cranks.

The success of the force calculations on the crankshaft is, to a great extent, based on this last observation, which is therefore of great importance.

Addendum:- From equation (26 A) it will be seen that the

constant value of the centrifugal force will be given by the following equation:-

$$\underline{C.F. = R\omega^2\left(m + \frac{M}{2}\left(1 + \frac{1}{2}\left(\frac{R}{r}\right)^2\right)\right). \quad \dots 29 \text{ A}}$$

=====

APPENDIX II.

OPTICAL SYSTEM.

A diagram of an optical system designed for measurements of torsional vibrations, is shown in Fig.77.

Light from a point source is reflected by a mirror and thereafter focussed by a lens on the screen of a camera.

The principle of the point light source is illustrated by Fig.78. Light from the filament of a point source bulb is focussed on a screen in which there is a small hole. The light coming through this hole will then behave as though it came from a point source positioned at the hole.

To obtain the calibration factor for the optical system the following nomenclature will be used:-

h = movement of virtual point object.

δ = movement of point image on screen.

a = distance of light source from lens.

b = distance of screen from lens.

s = distance of light source from mirror

θ = angular deflection of mirror.

From Fig.77 the following two equations are obtained:-

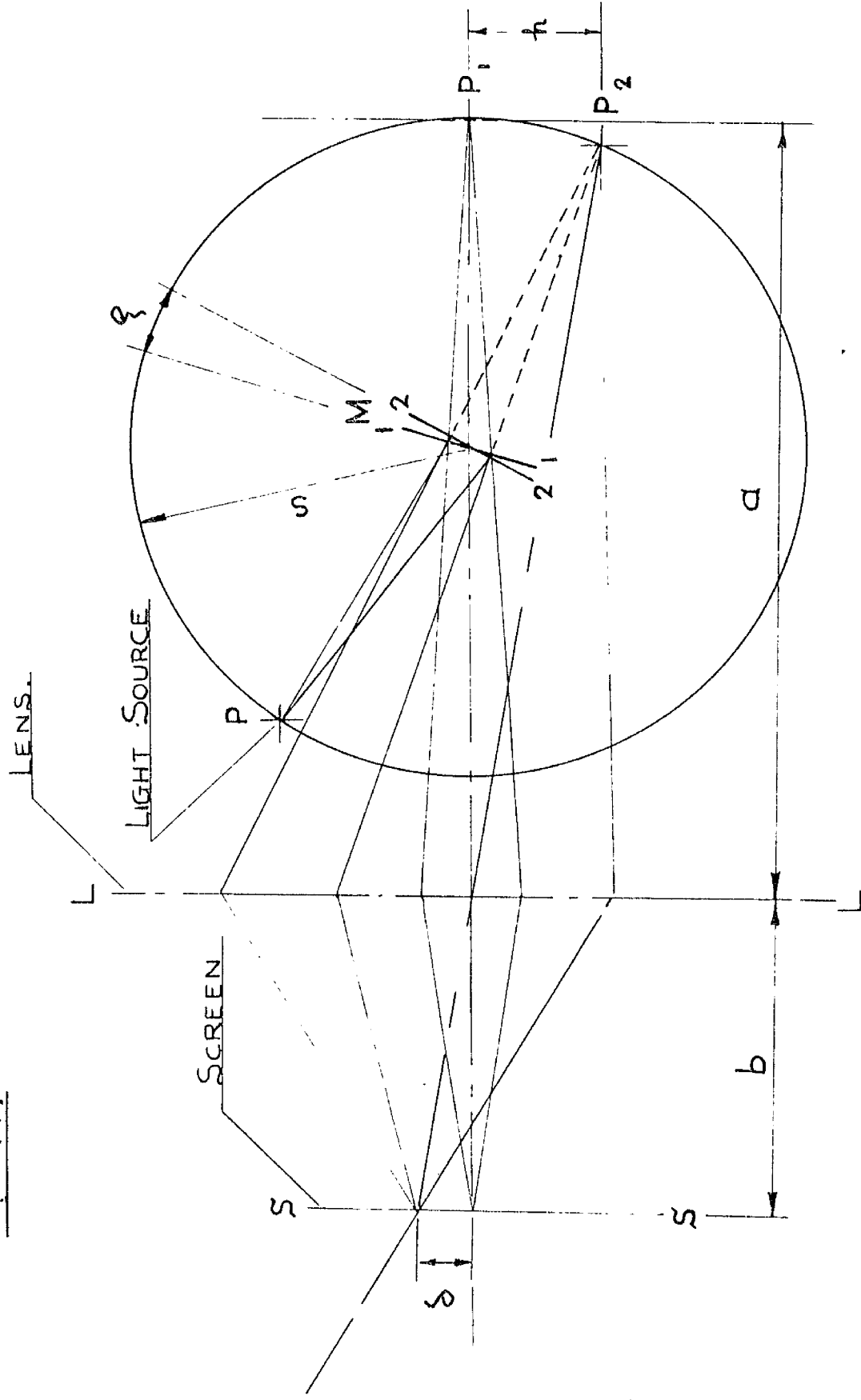
$$\frac{\delta}{b} = \frac{h}{a}$$

$$h = 2\theta s$$

Hence the calibration factor of the system will be given by:-

$$\frac{\delta}{\theta} = \frac{b}{a} 2s \quad . . . 91$$

FIG 77.



OPTICAL SYSTEM.

SKETCH OF POINT LIGHT SOURCE

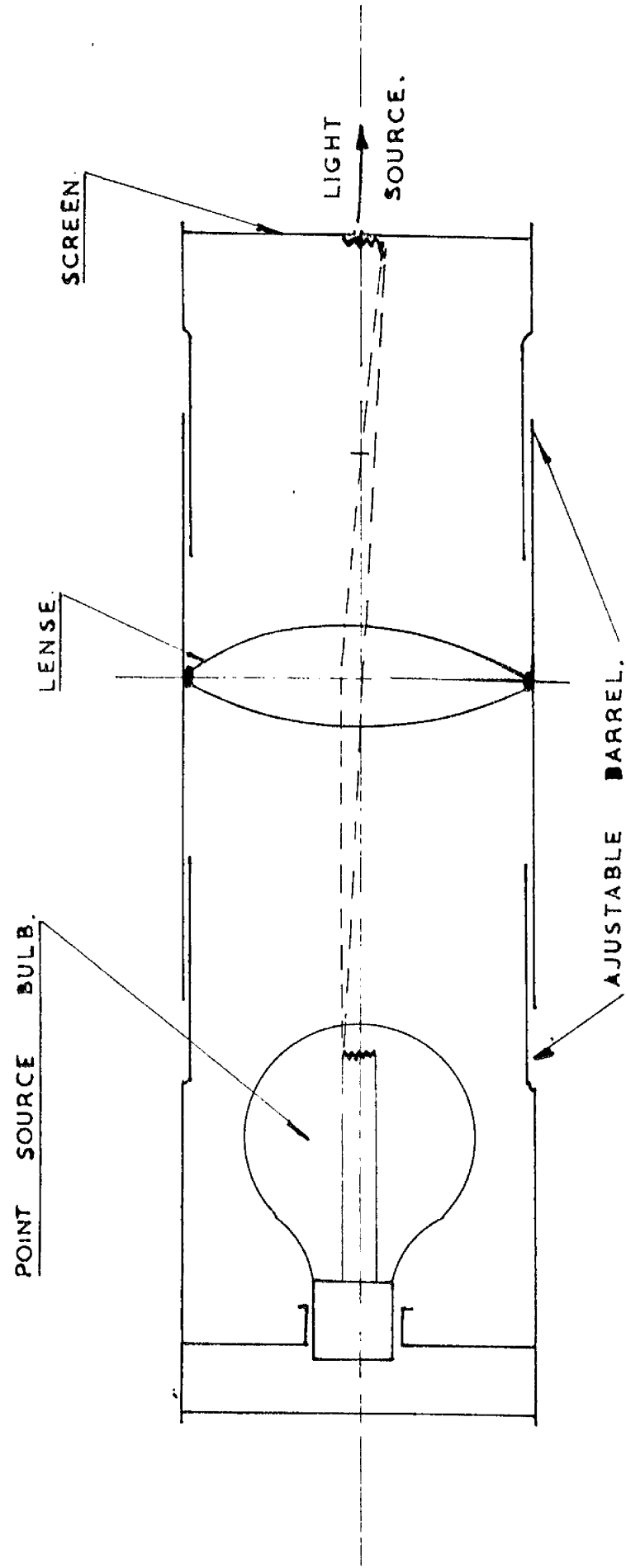


FIGURE 78.

APPENDIX III.

OSCILLATOR-DISCRIMINATOR UNIT

The circuit diagram of the Oscillator-Discriminator unit is shown in Fig.79.

The main details are as follows:-

V_1 E.F.50. (Oscillator)

V_2 6.J.5. (Cathode Follower)

V_3 S.P.61. (Amplifier)

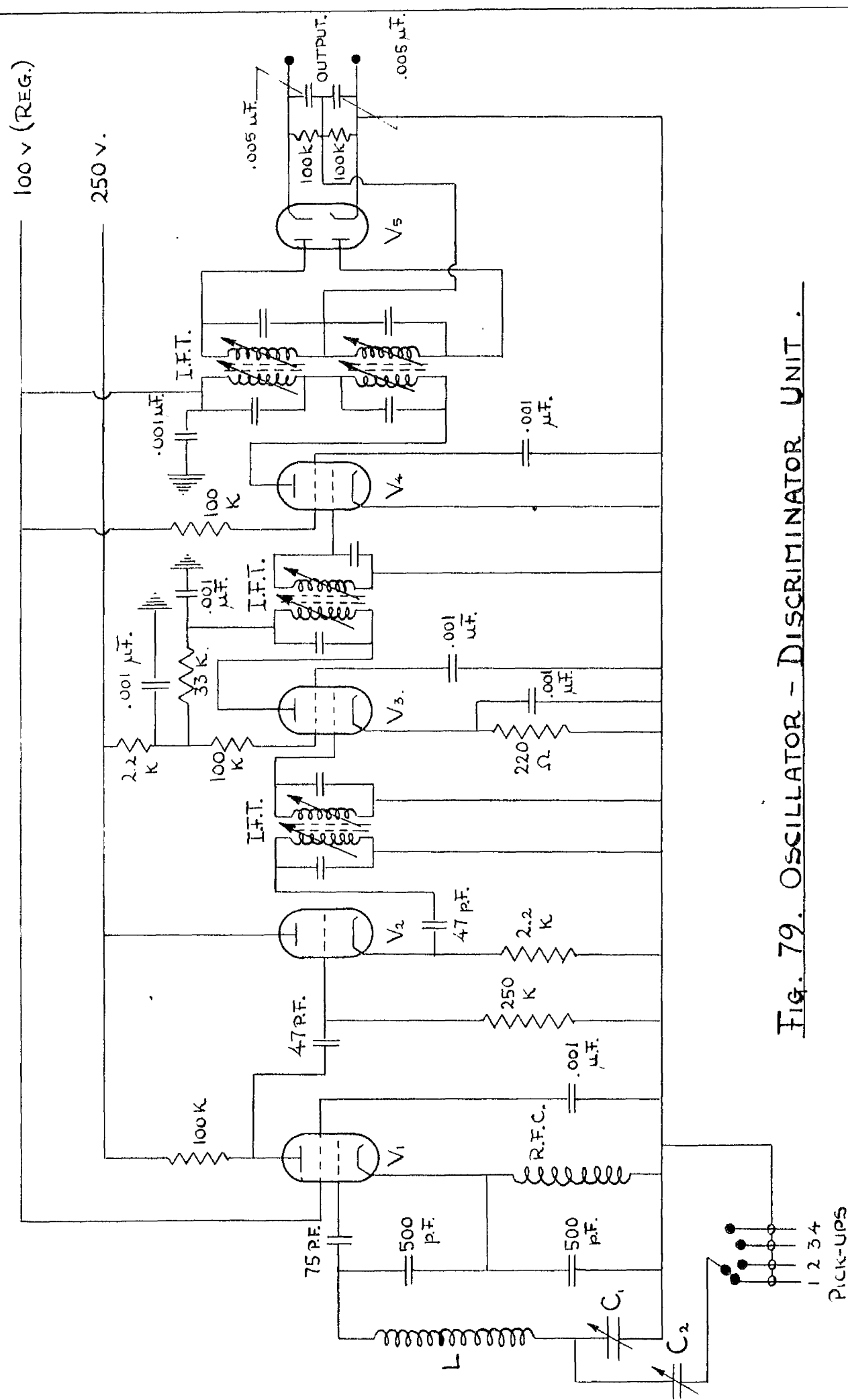
V_4 S.P.61. (Limiter)

V_5 6.H.6. (Discriminator)

C_1 . . . 0 - 75 p.F. I.F.T. - 1.7 M.C.

C_2 . . . 0 - 50 p.F. L_1/C_1 - to oscillator at 1.7 M.C.

Bandwidth . . .20 K.c. at 1.7 M.C.



APPENDIX IV.

DISPLACEMENT GRAPHS FOR CRANKSHAFT MAIN JOURNAL

Graphs are given for the lateral displacement of the crankshaft journal in Bearing 4 of the six cylinder diesel engine, R.R. C.60. Nr.51. for constant speeds ranging from 600 R.P.M. to 2000 R.P.M.

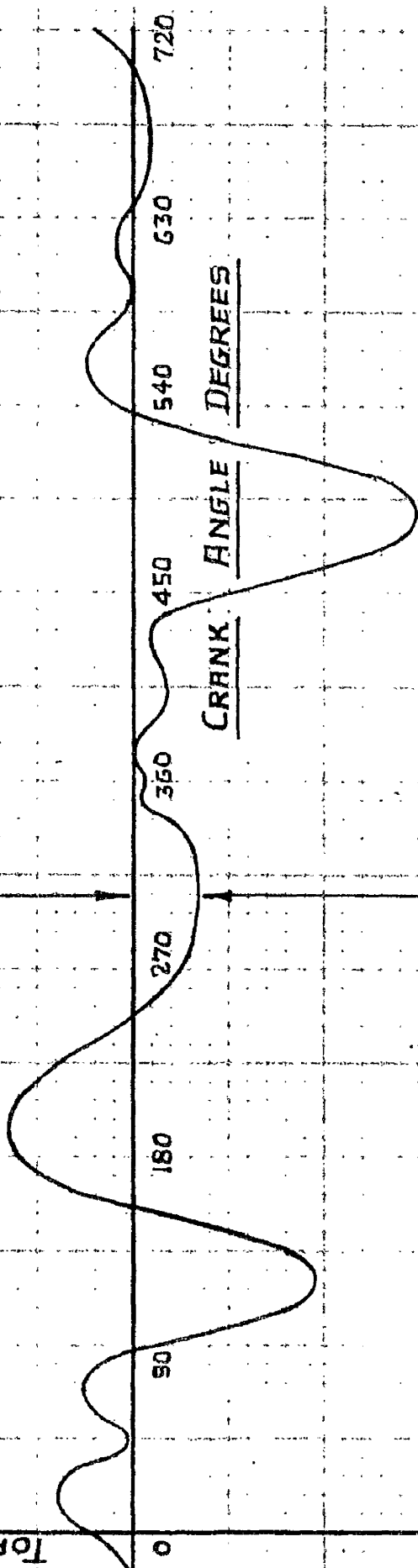
JOURNAL DISPLACEMENT

FIG. 80.

ENGINE SPEED 600 R.P.M.

OIL TEMP 60°C

JOURNAL DISPLACEMENT THOU
Top Dead Centre (CRANK 0°)



ECCENTRICITY RATIO $\epsilon = .129$

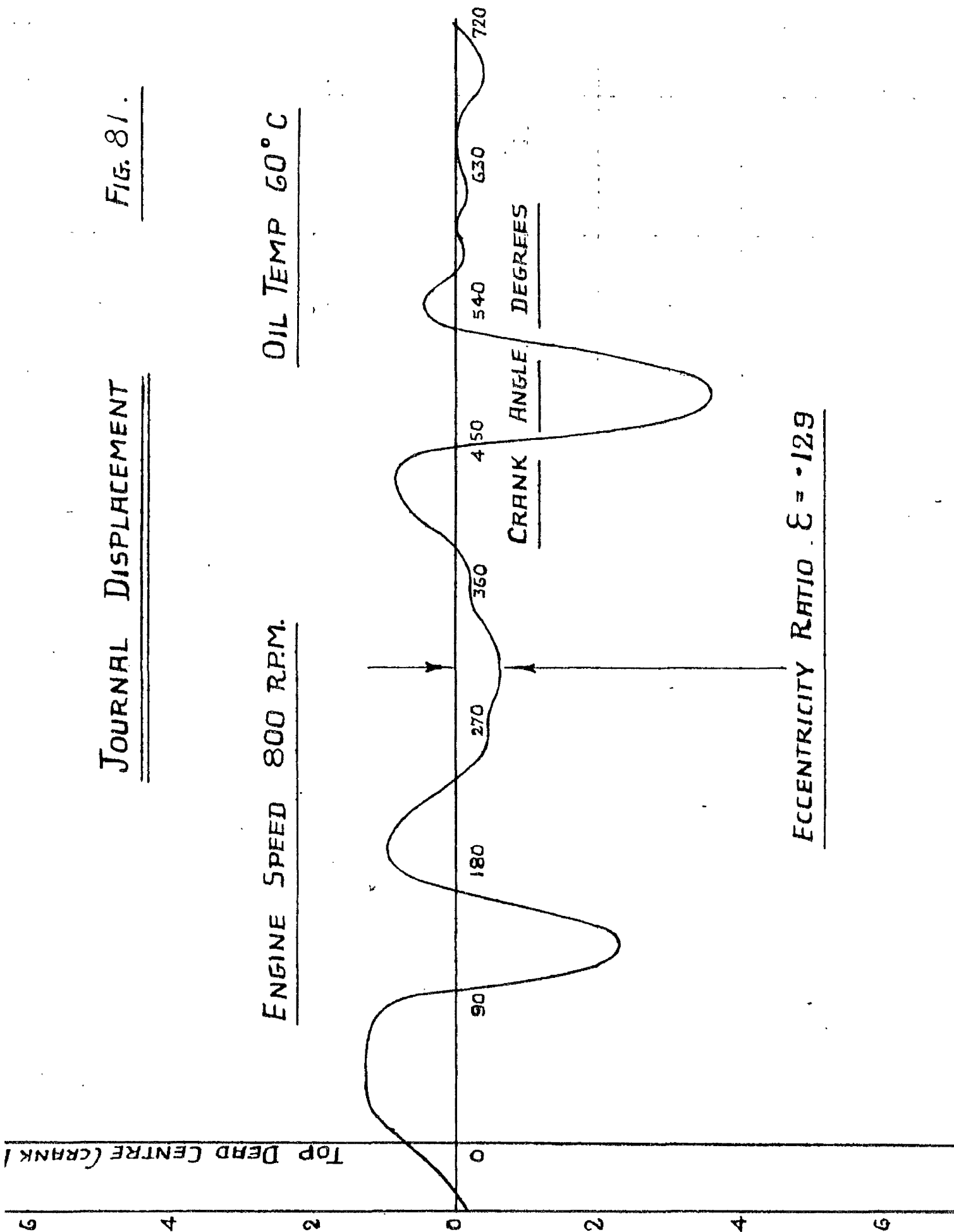
JOURNAL DISPLACEMENT

FIG. 81.

JOURNAL DISPLACEMENT THOU.

ENGINE SPEED 800 R.P.M.

OIL TEMP 60°C



ECCENTRICITY RATIO $\epsilon = .129$

JOURNAL DISPLACEMENT

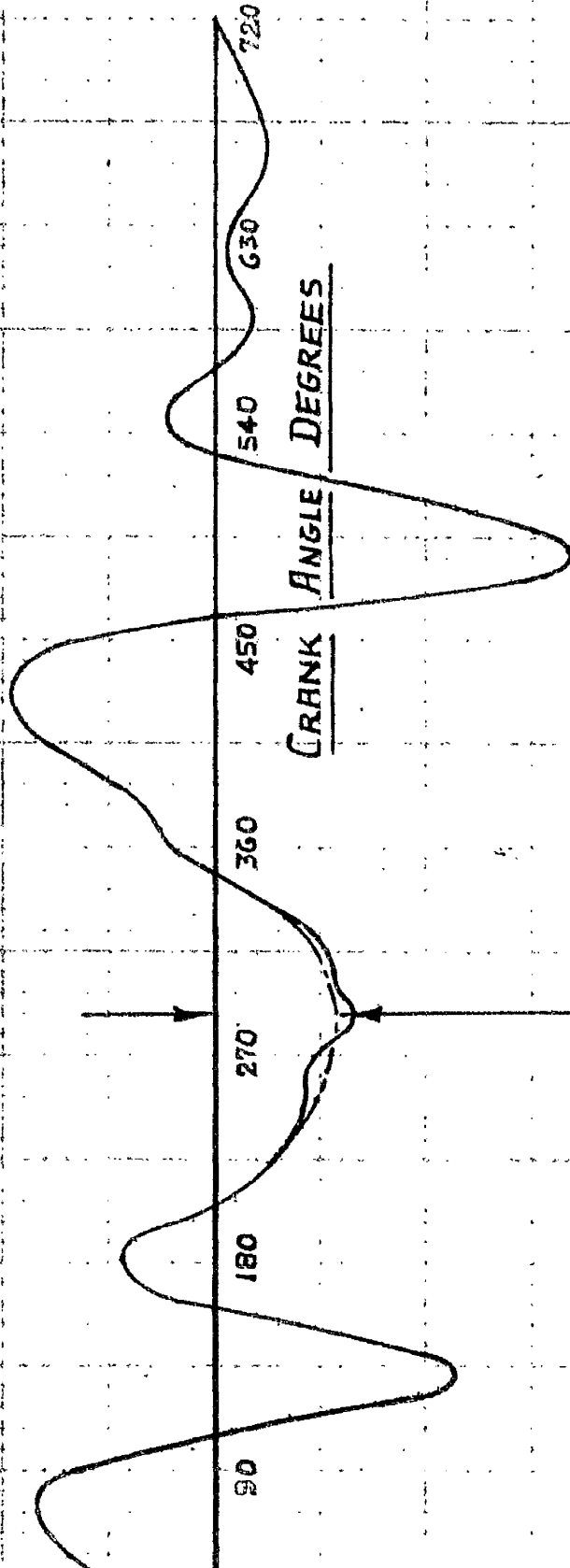
FIG. 82.

ENGINE SPEED 1000 R.P.M.

OIL TEMP 60°C

TOP DEAD CENTRE (CRANK)

JOURNAL DISPLACEMENT THOU



ECCENTRICITY RATIO $\epsilon = .236$

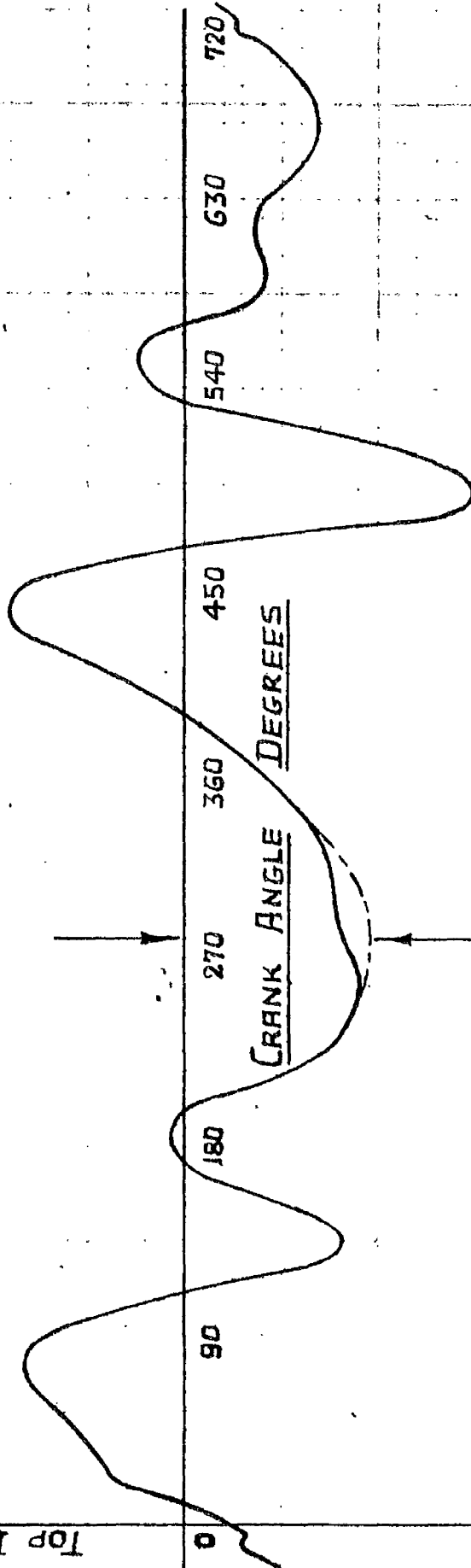
JOURNAL DISPLACEMENT

FIG. 83.

ENGINE SPEED 1200 R.P.M.

OIL TEMP. 60°C

ECCENTRICITY RATIO $\epsilon = .408$

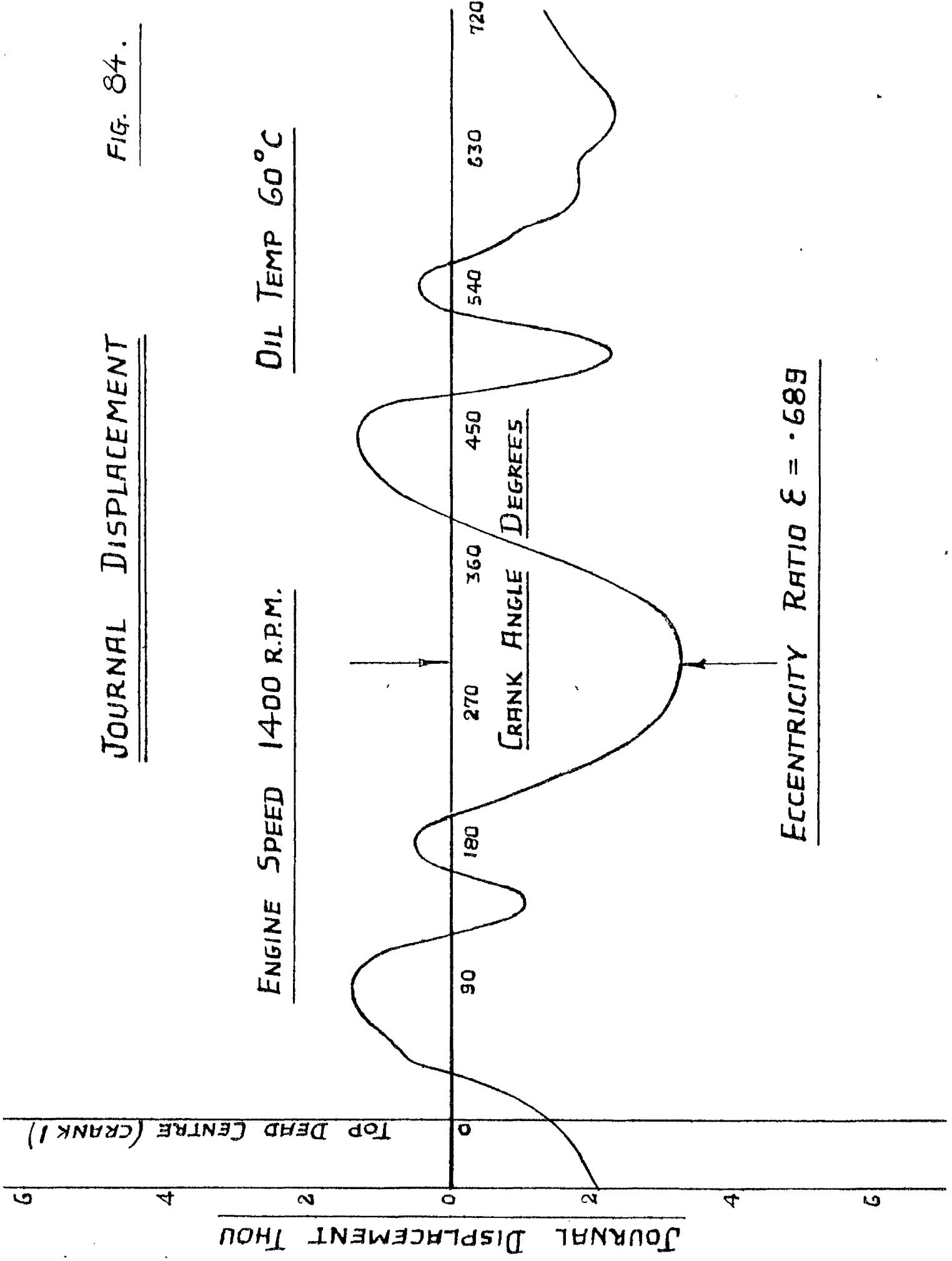


JOURNAL DISPLACEMENT

FIG. 84.

ENGINE SPEED 1400 R.P.M.

OIL TEMP 60°C

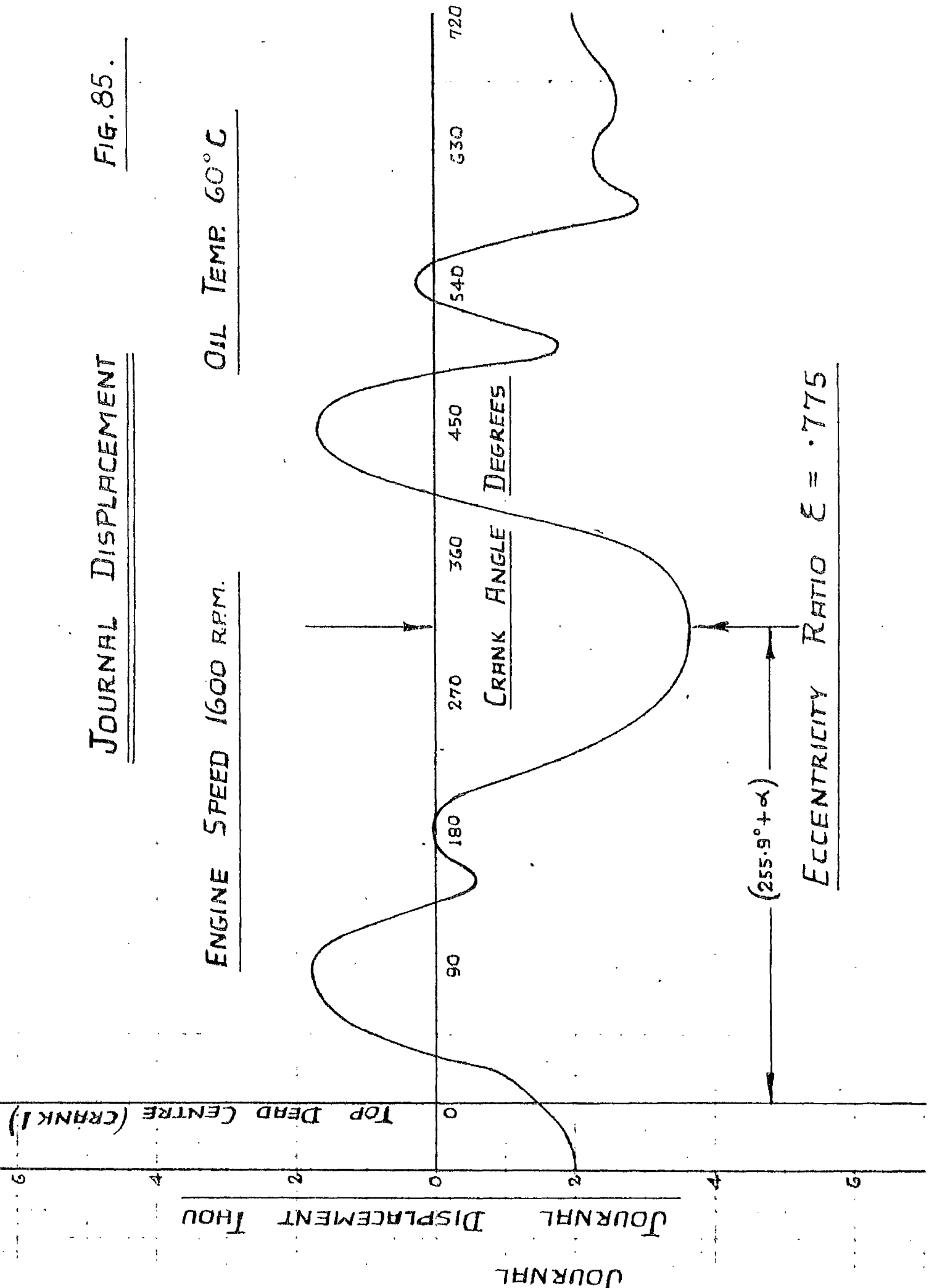


JOURNAL DISPLACEMENT

FIG. 85.

ENGINE SPEED 1600 R.P.M.

OIL TEMP. 60° C



$(255.9^\circ + \alpha)$

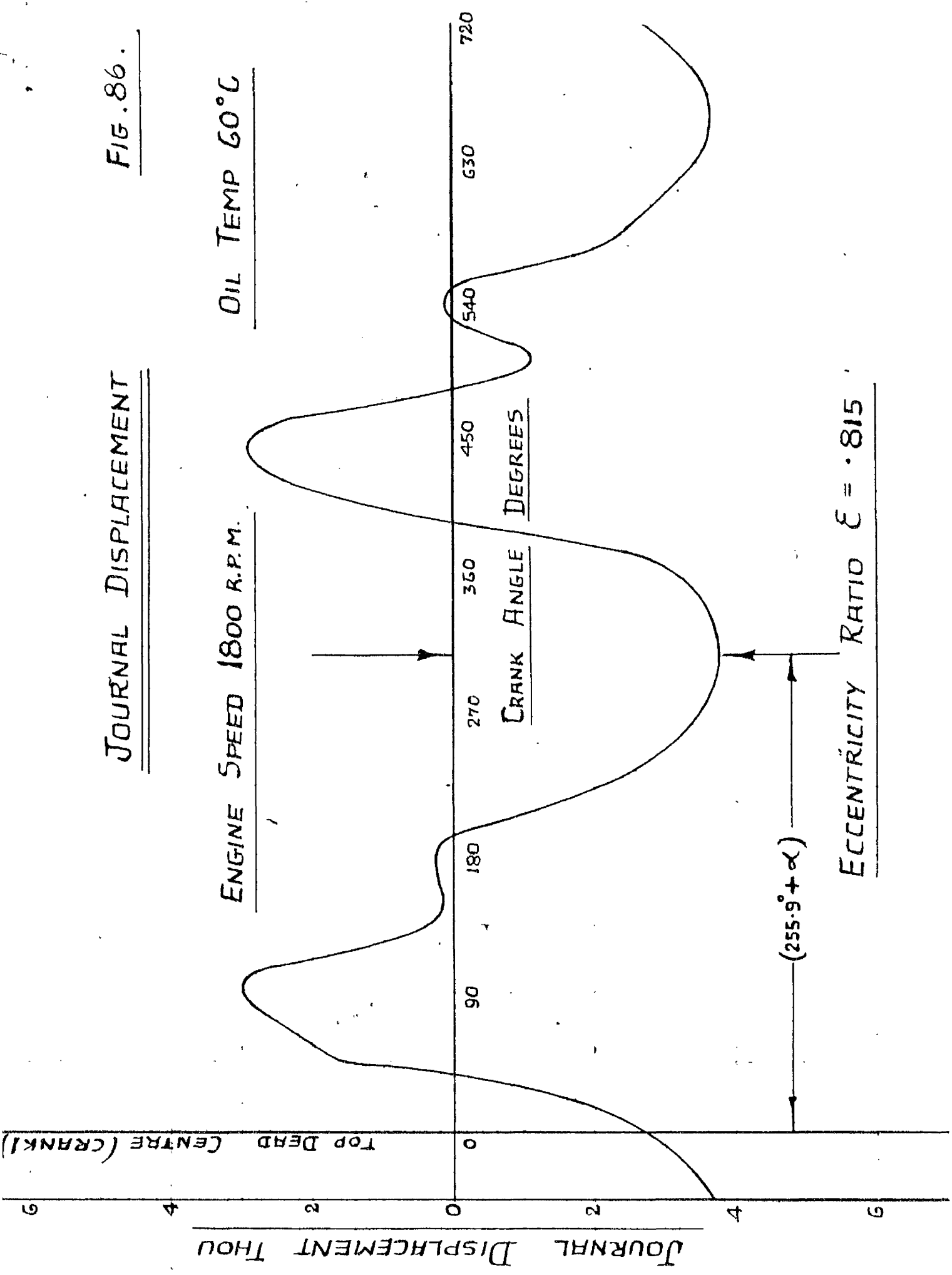
ECCENTRICITY RATIO $\epsilon = .775$

JOURNAL DISPLACEMENT

FILE 86.

ENGINE SPEED 1800 R.P.M.

OIL TEMP 60°C

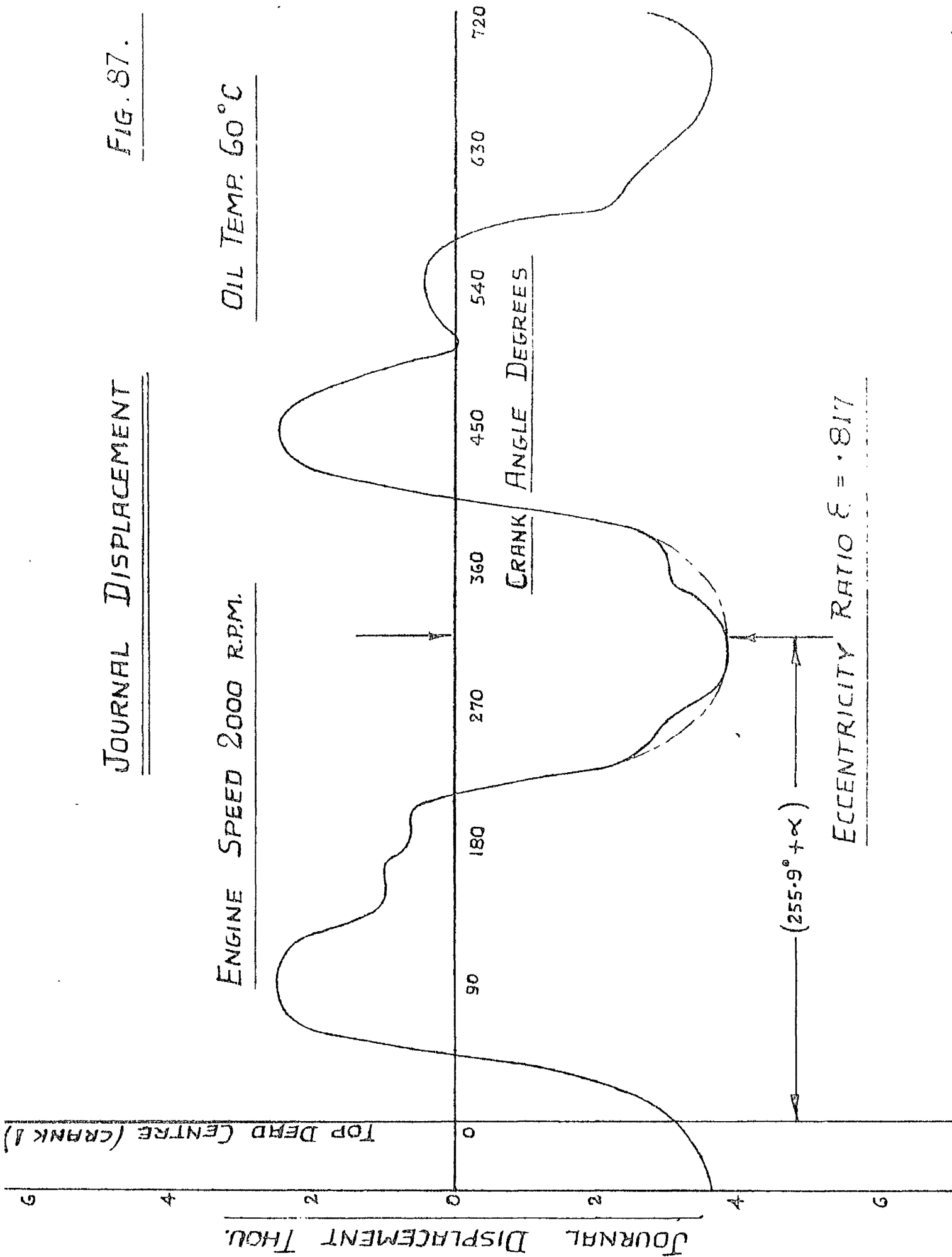


JOURNAL DISPLACEMENT

FIG. 87.

ENGINE SPEED 2000 R.P.M.

OIL TEMP. 60°C



APPENDIX V.

NUMERICAL CALCULATIONS RELATED TO SHRINK-FITTED
ASSEMBLIES.

Relaxation Nets:

This appendix contains a presentation of the numerical work which has been carried out in connection with the theoretical analysis of shrink-fitted assemblies.

To gain a fair picture of the important features of the problem, it was decided to find solutions in terms of the stress function for five different ratios of the friction grip to the nominal shear stress. (See Fig.89-92).

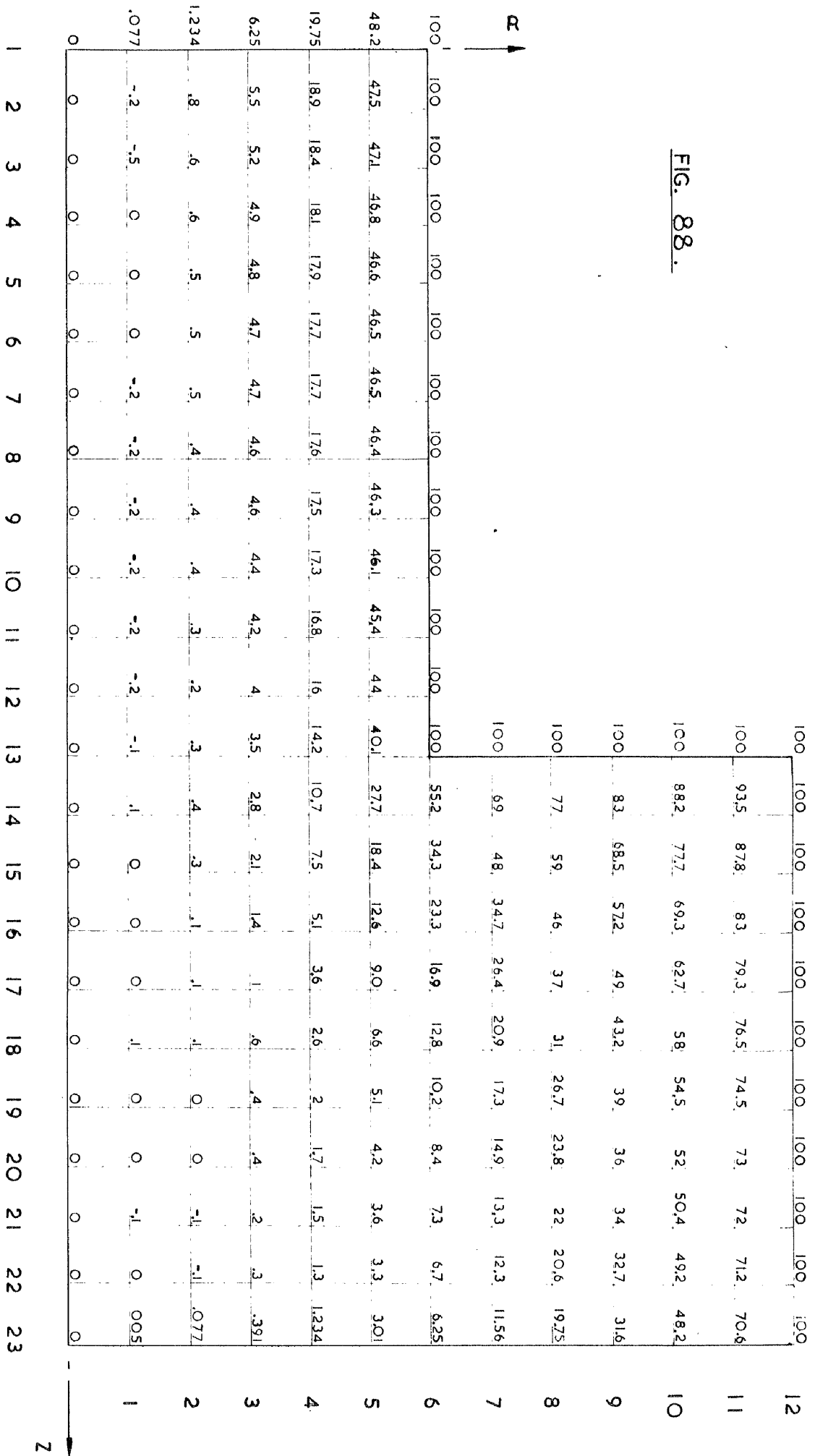
In addition to these, and for the purpose of comparison, a solution was also carried out for a solid shaft of the same geometrical configuration as the shrink-fitted assemblies. (See Fig.88).

For the solid shaft, and for the four shrink-fitted assemblies for which the ratio of the frictional grip to the nominal shear stress ranged from .525 to .225 inclusive, a relaxation net of six divisions over the shaft radius was found to be sufficiently accurate.

However, for the last solution, which was carried out for a higher friction grip ratio of .750, it was found necessary to use a finer mesh. (See Fig.92).

Solutions for still higher values of the friction grip

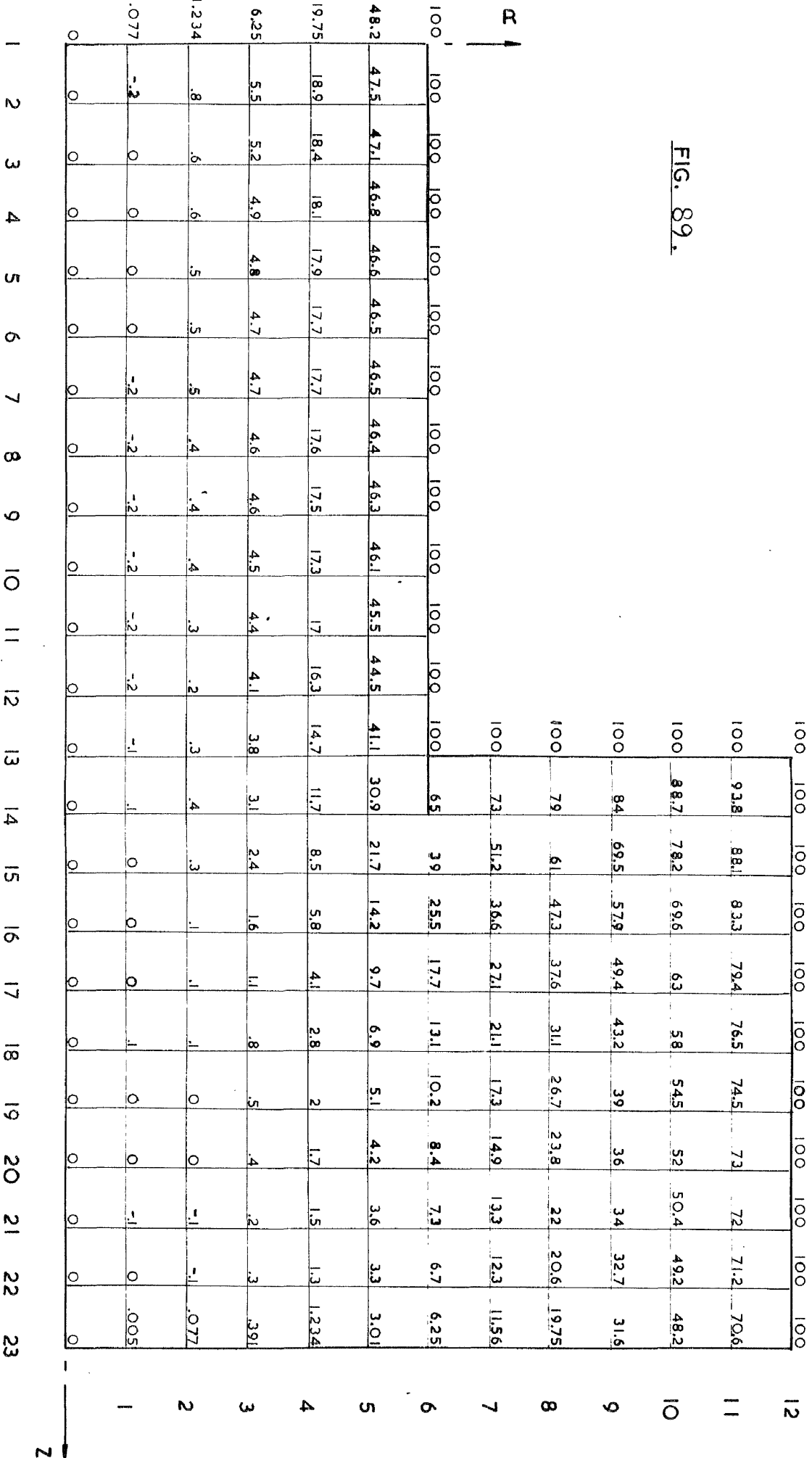
FIG. 88.



RELAXATION NET I.

SCALE: 4 X FULL SIZE.

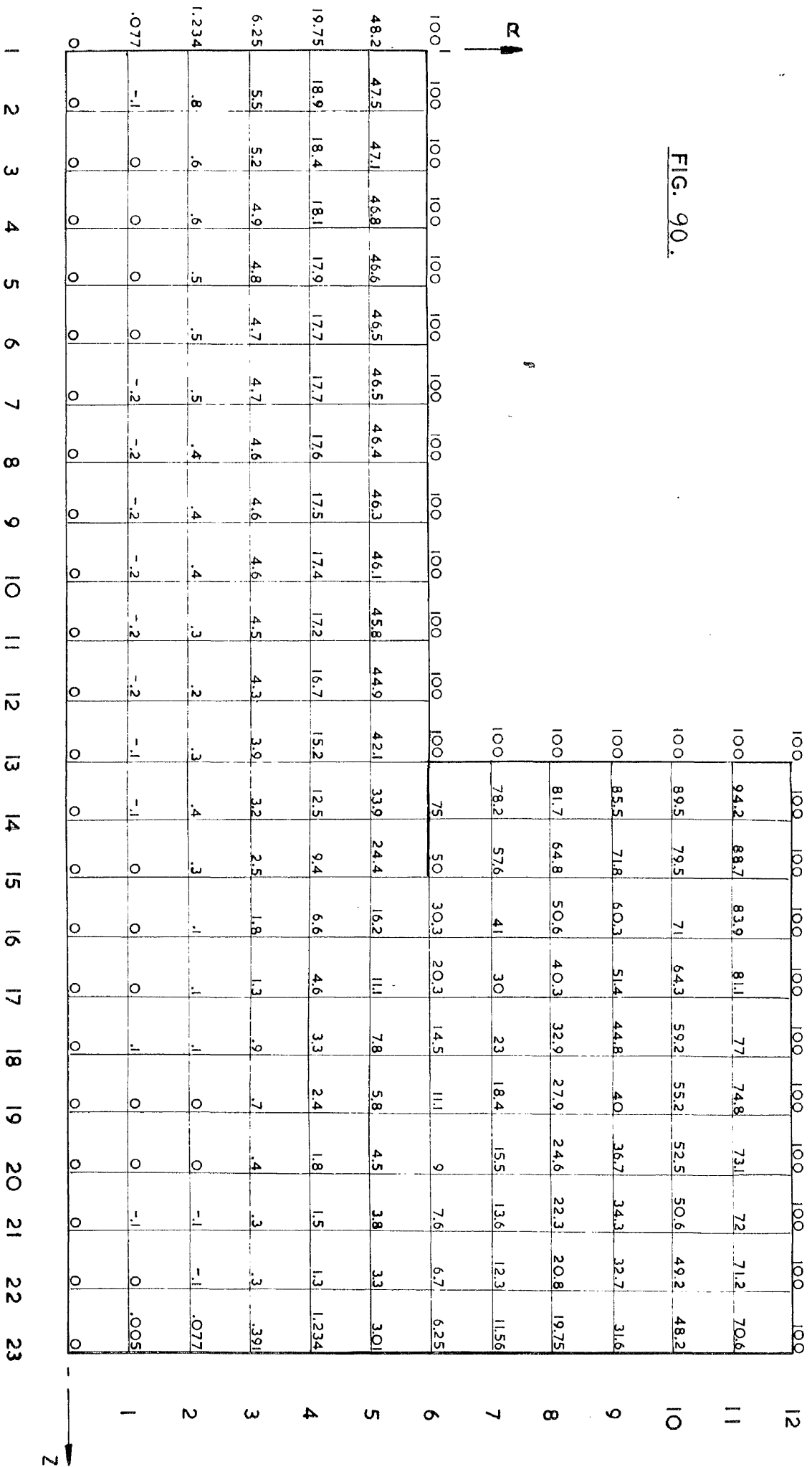
FIG. 89.



RELAXATION NET 2.

SCALE: 4X FULL SIZE.

FIG. 90.



RELAXATION NET 3.

SCALE: 4X FULL SIZE.

FIG. 91.

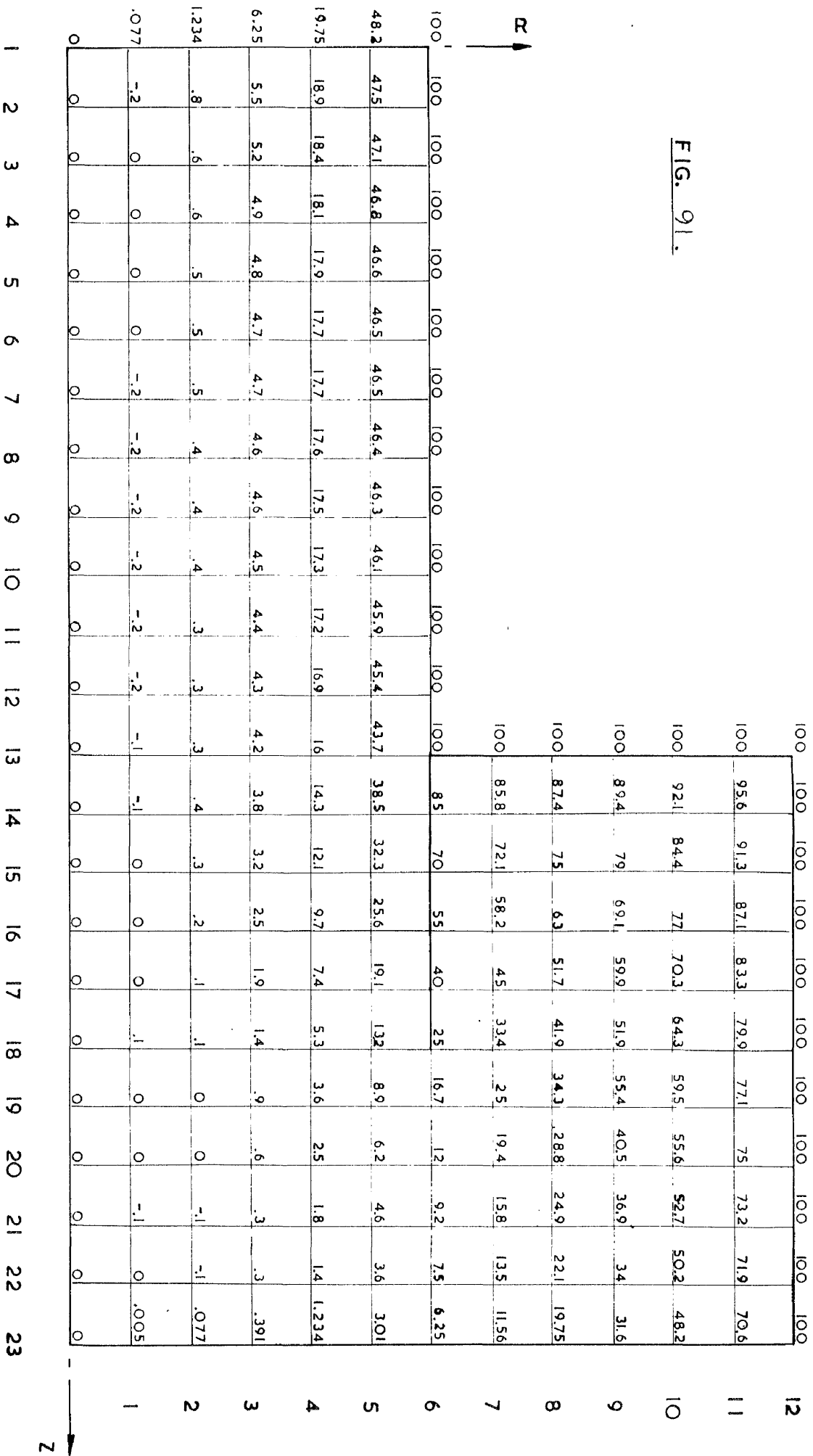
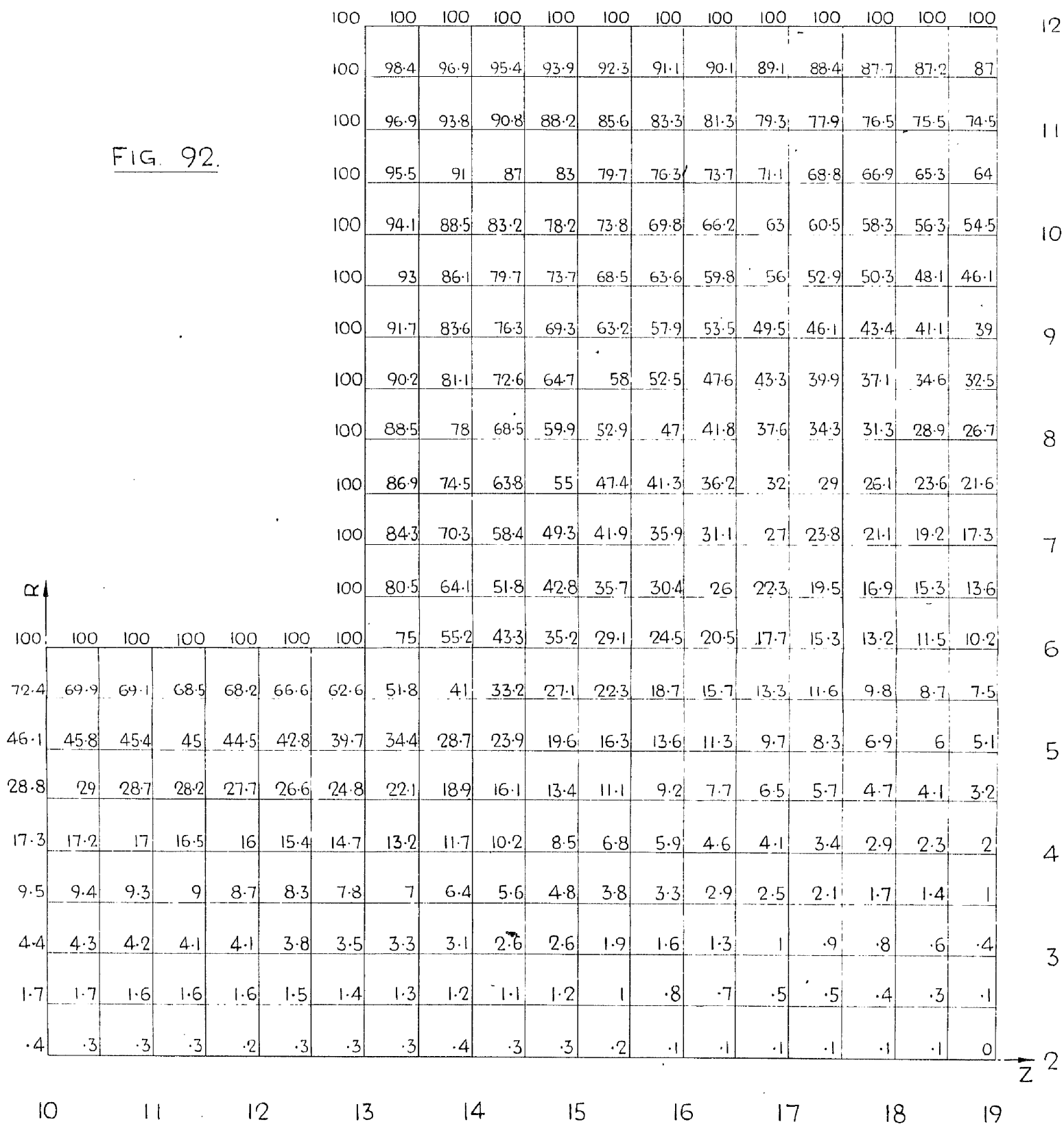


FIG. 92.



RELAXATION NET 6.

SCALE:- 7x FULL SIZE.

ratio were abandoned as being too labour consuming.

The relaxation nets for the shrink-fitted assemblies show a heavy line which indicates the range over which slip takes place, drawn from the corner where the shaft enters the hub.

A more exact measure of the depth of slip, however, has been obtained from later calculations based on the relaxation nets.

Specimen Calculation:

A specimen calculation will now be given to illustrate further developments from the relaxation nets.

First of all, it will be necessary to convert the values given for the stress function into strain ratios. It was found most convenient to do this in the following way.

Fig.93 shows graphs of the stress function plotted against r for various values of λ .

A sudden change in the gradient of some of these graphs, when they cross the mating surface between the hub and the shaft, indicates slip.

The gradients at the mating surface of the graphs of stress function plotted against radius are now measured and

FIG. 93.

GRAPHS OF ψ AGAINST r , NET No 4

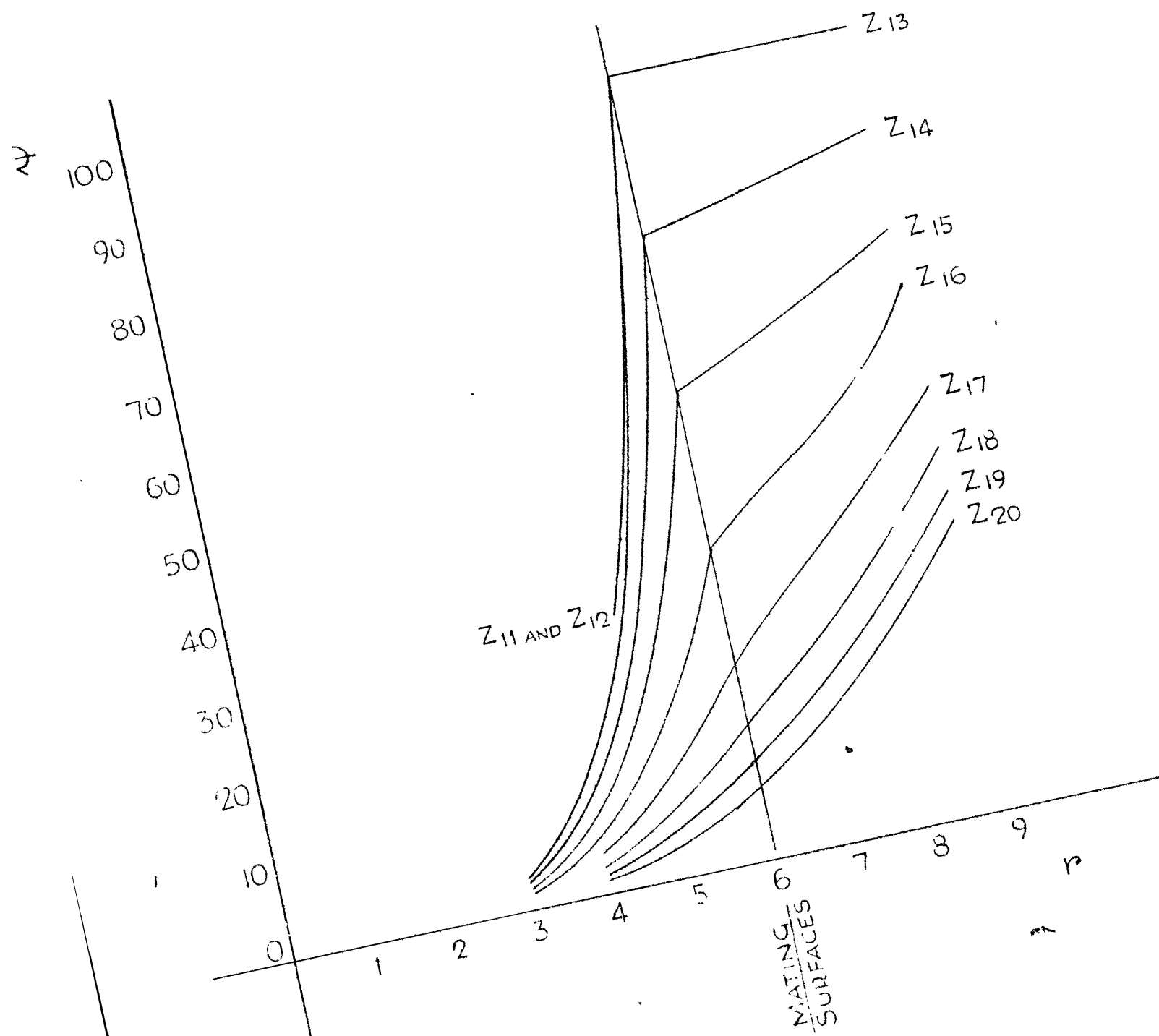


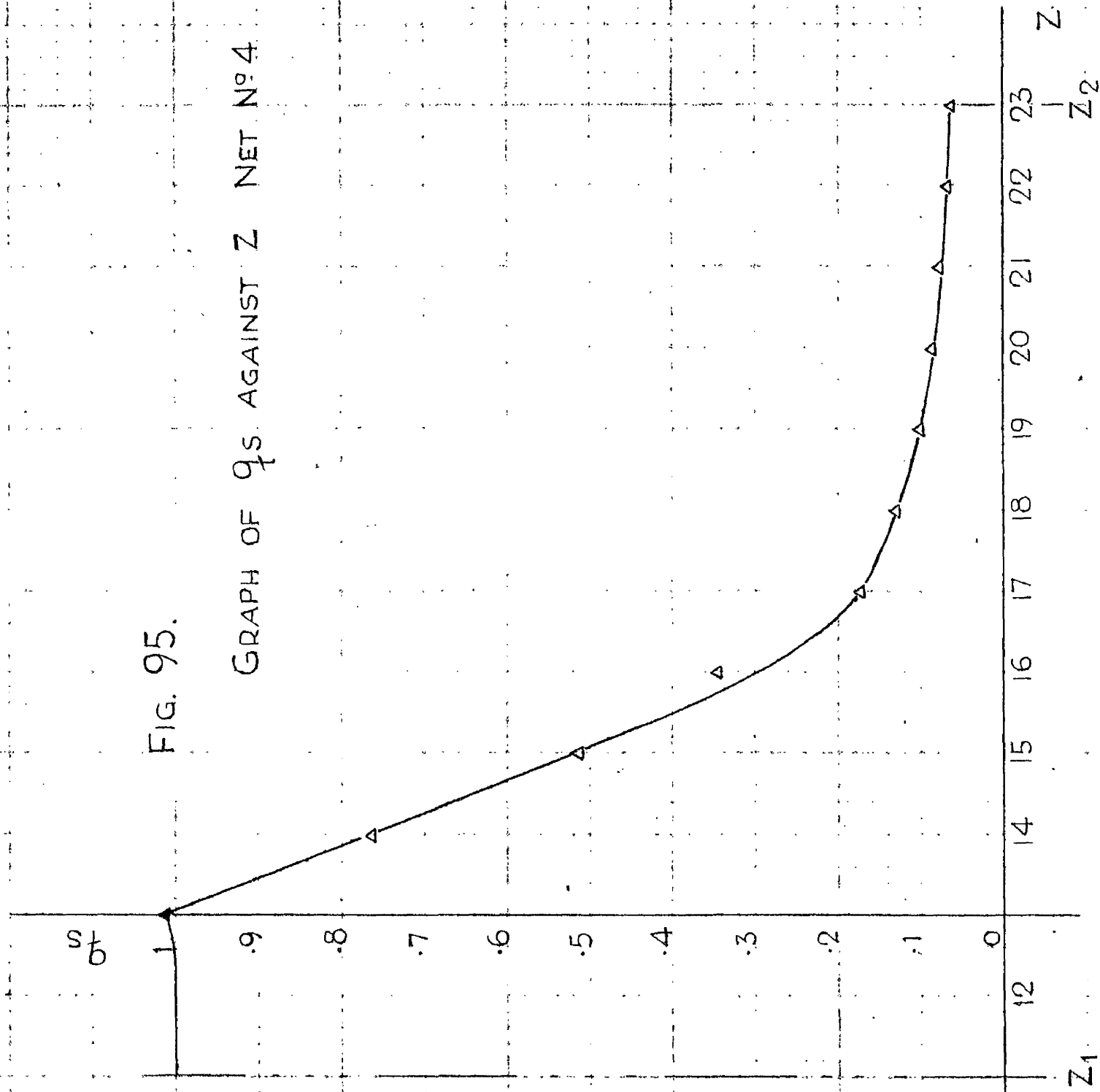
FIG. 94.

| Z | 11 | 12 | 13 | 14 | 15 | 16 | 17 | 18 | 19 | 20 | 21 | 22 | 23 |
|---|---|-----|------|------|------|------|------|------|------|------|------|------|------|
| $(\frac{\partial y}{\partial r})_s (\text{in}^2)$ | 533 | 533 | 543 | 408 | 275 | 185 | 91.2 | 69.2 | 54 | 47.6 | 42 | 36.8 | 33.3 |
| q_s | 1 | 1 | 1.02 | .764 | .515 | .347 | .171 | .130 | .101 | .089 | .079 | .069 | .063 |
| $(\frac{\partial y}{\partial r})_H (\text{in}^2)$ | <div style="display: flex; align-items: center; justify-content: center;"> <div style="border: 1px solid black; width: 100%; height: 100%; position: relative;"> <div style="position: absolute; top: 0; left: 0; right: 0; bottom: 0; border: 1px solid black;"></div> </div> </div> | | | | | | | | | | | | |
| q_H | | | | | | | | | | | | | |
| $q_s - q_H$ | | | | | | | | | | | | | |
| | | | 1.02 | .748 | .465 | .235 | 0 | | | 0 | 0 | 0 | 0 |

$$\text{NET N}^\circ 4, \quad \sigma = .300, \quad = 1.0$$

FIG. 95.

GRAPH OF q_s AGAINST Z NET N° 4



entered into Fig.94, both for the hub and the shaft, and, by making use of equation (74), the corresponding values for the strain ratio can easily be obtained.

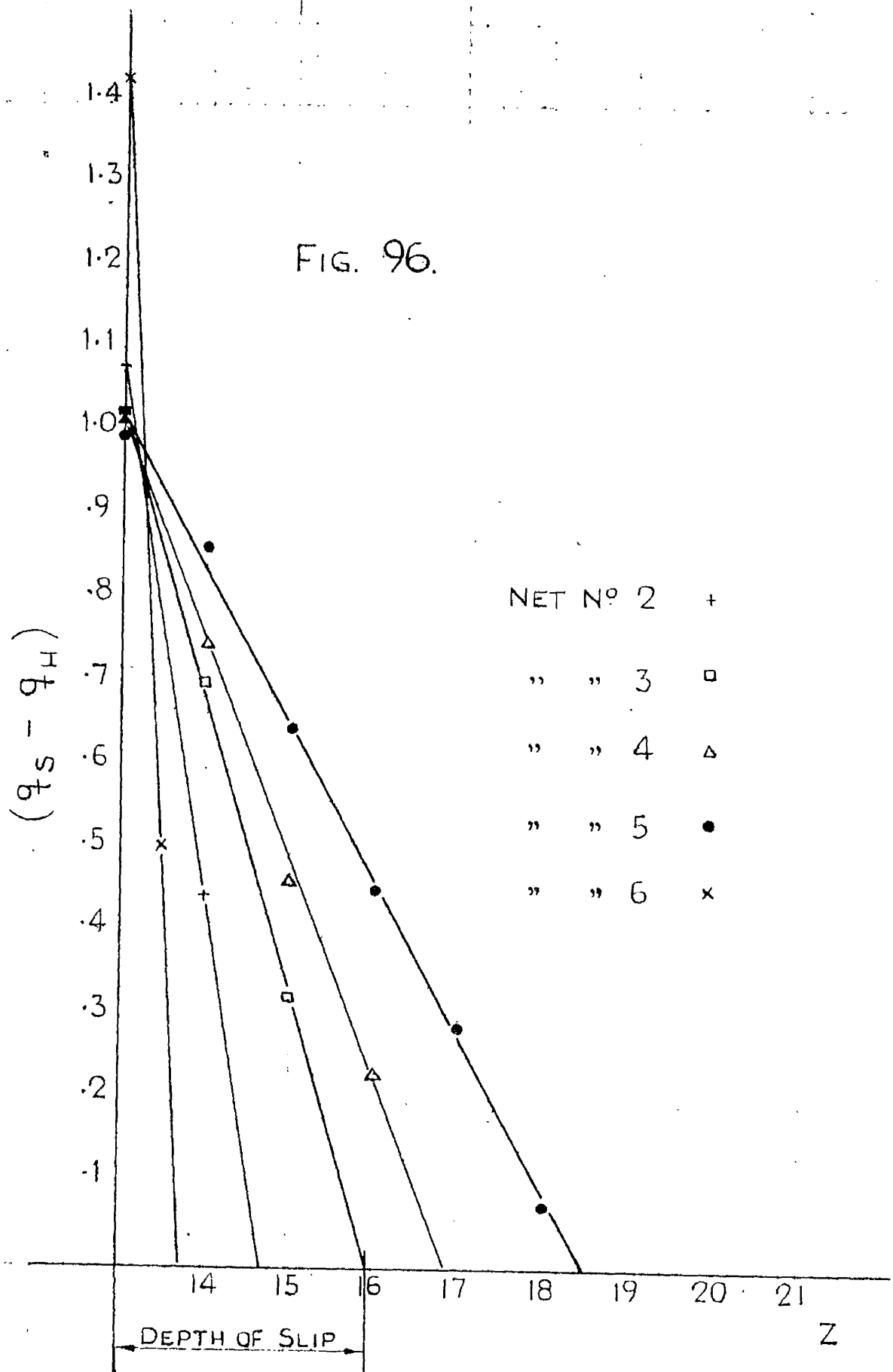
The integrals $\int_{z_1}^{z_2} q_z dz$ as required in equation (77) to obtain the torsional stiffness of the assemblies are evaluated graphically. The axial strain ratios in the shaft at a radius R_o are plotted against axial positions, and the area under this curve which is equal to the above integral is found by making use of a planimeter. (See Fig.95).

It is required to choose the limits such that the integral will contain all effects derived from the corner where the shaft enters the hub. Parts of the assemblies outside these limits can be treated as plain shafts.

Fig.96 shows the values of $(q_{zs} - q_{zh})$ plotted against z for all the five shrink-fitted assemblies under consideration. It will be noticed that to a fair approximation the variation of $(q_{zs} - q_{zh})$ with z is linear and, making use of this simplification, the integrals required for the evaluation of slip and damping capacity are easily obtained.

The integration will now be taken from the section of the shrink-fitted assembly at which slip begins to the

FIG. 96.



GRAPH OF $(q_s - q_H)$ AGAINST Z

corner where the shaft enters the hub.

The complete results of the numerical calculations carried out in this Appendix are now presented in Fig.97. These are values for stiffness, slip, stress concentration and damping capacity, calculated for five different values of the ratio of friction grip to nominal shaft stress.

For the purpose of graphical representation, the inverse of the friction grip ratio is used as a more convenient basis than the friction grip ratio.

FIG. 97.

| NET NR. | σ | $\frac{1}{\sigma}$ | I in^2 | SLIP ¹⁾ $\text{in} \times 10^4$ | DEPTH OF SLIP in | STIFFNESS $\text{lb in/RAD} \times 10^{-6}$ | STRESS CONCENTRATION | DAMPING ²⁾ % |
|---------|----------|--------------------|----------------------|---|------------------------------|--|----------------------|----------------------------|
| 1 | ∞ | 0 | 0 | 0 | 0 | 12.9 | ∞ | 0 |
| 6 | .750 | 1.333 | .0023 | .6 | .098 | 11.8 | 1.61 | 1.29 |
| 2 | .525 | 1.905 | .0081 | .94 | .212 | 11.3 | 1.21 | 3.2 |
| 3 | .375 | 2.665 | .0243 | 1.67 | .375 | 10.5 | 1.1 | 7.0 |
| 4 | .300 | 3.333 | .0395 | 2.07 | .480 | 10.0 | 1.06 | 9.25 |
| 5 | .225 | 4.444 | .0770 | 2.92 | .680 | 8.8 | 1.02 | 13.5 |

1. VALUES USED FOR CALCULATIONS OF SLIP, DEPTH OF SLIP

AND STIFFNESS: $G_e = 10,000 \text{ lb/in}^2$, $R_o = .75''$, $G = 12 \times 10^6 \text{ lb/in}^2$

2. FOR THE CALCULATION OF DAMPING: $\ell = 2.875''$

APPENDIX VI.

CONSTRUCTIONAL DETAILS

This Appendix gives some constructional details for the apparatus used for measurements of shrink-fit damping. (See Fig.58).

The specimen clamping is given in Fig.98.

The exciter driving rods are shown in Fig.99.

The arrangement clamping the exciter driving rods to the test-specimen for endurance testing is shown in Fig.100.

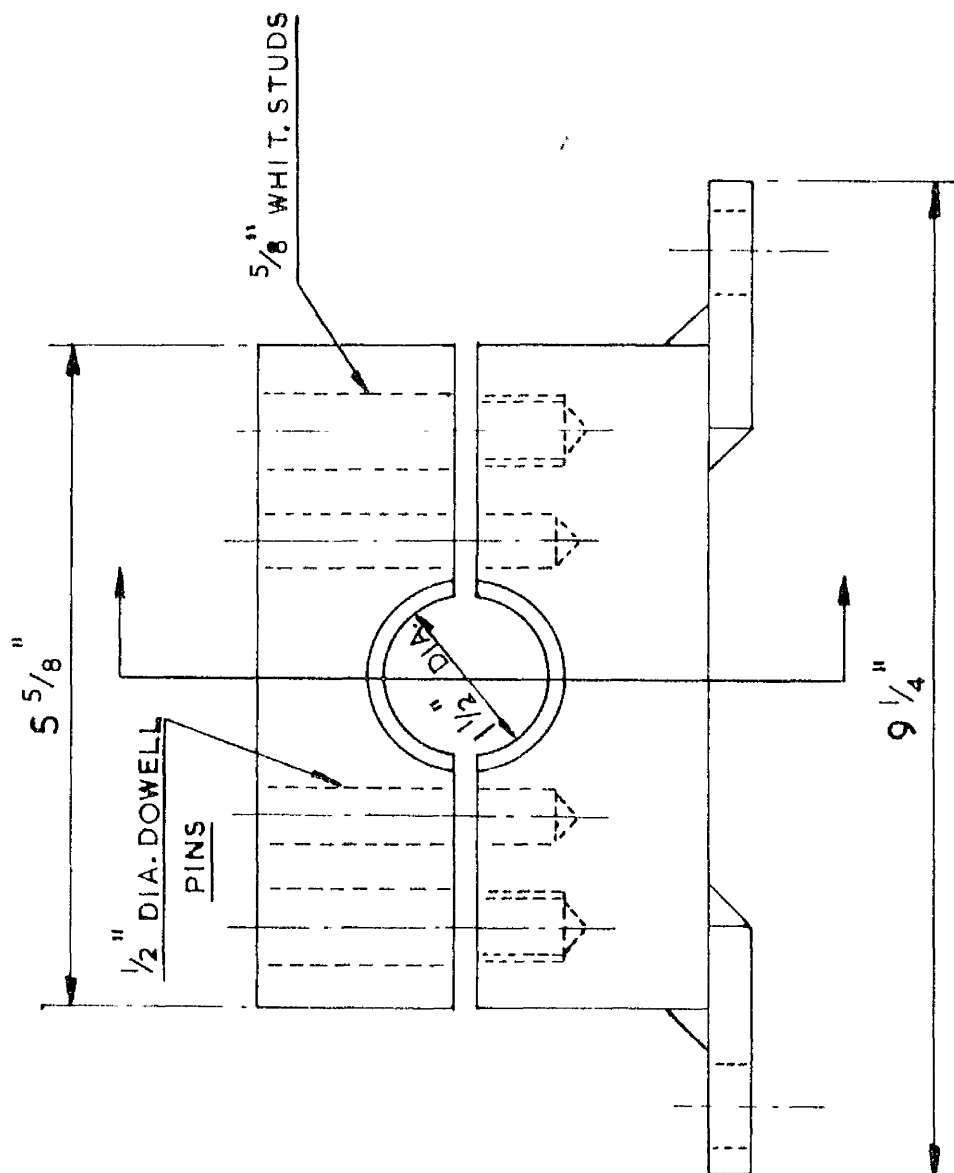
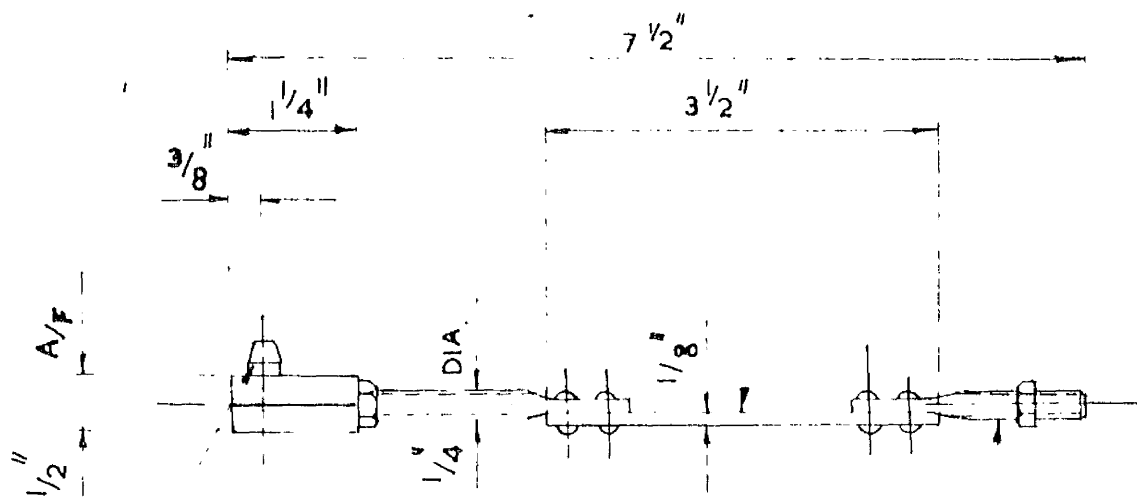
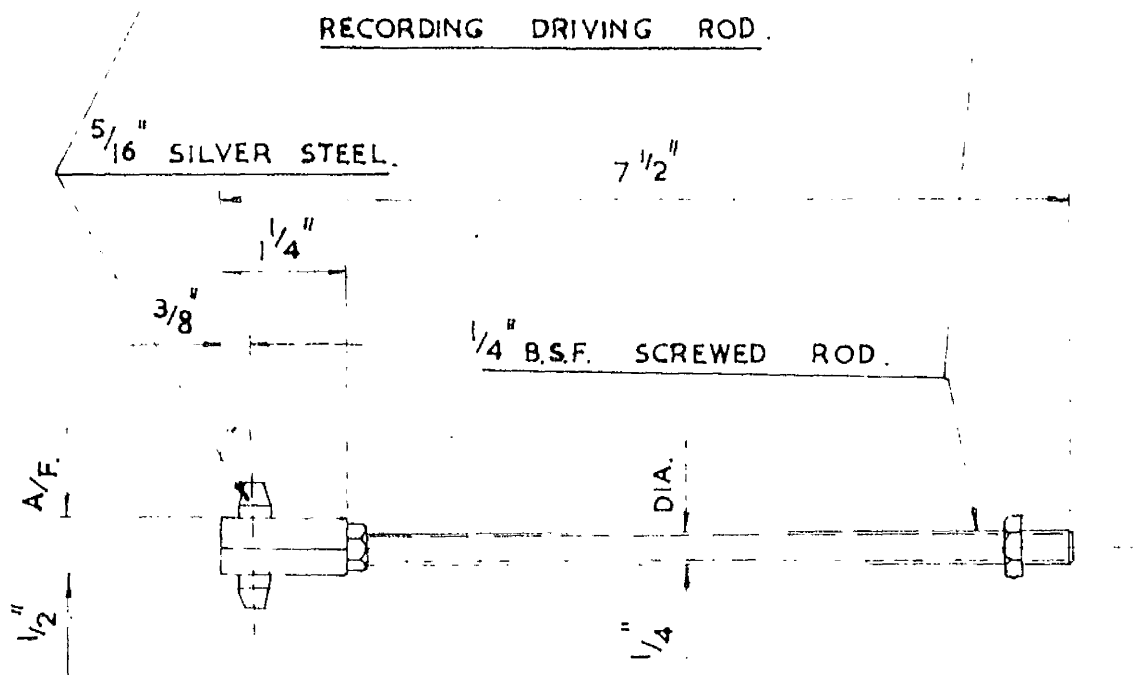


FIGURE 98.

FIBER BASE BAKELITE $1/2$ " WIDE.



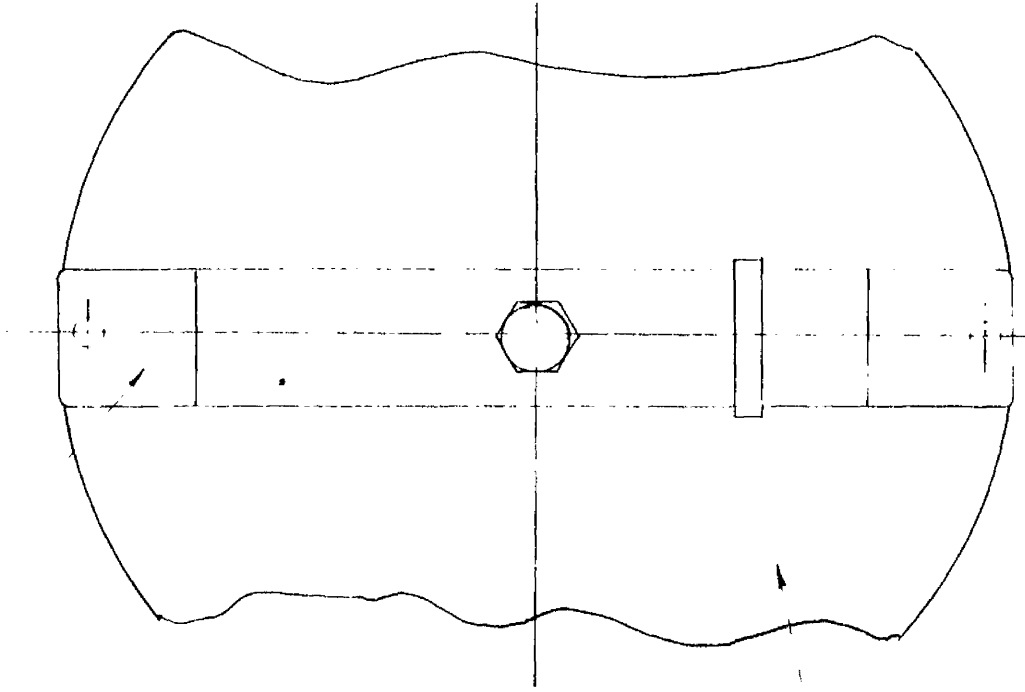
RECORDING DRIVING ROD.



ENDURANCE DRIVING ROD.

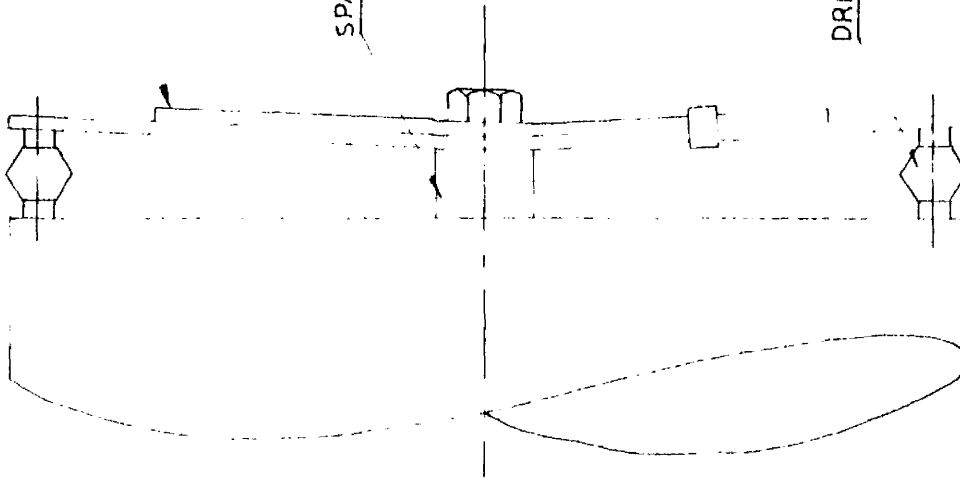
FIGURE 99.

SPRING STEEL $\frac{3}{32}$ " THICK BY $1\frac{1}{4}$ " WIDE.



TEST SPECIMEN

DRIVING RODS,



SPACER.

CLAMPING USED DURING ENDURANCE TESTS.

FIGURE 100.

APPENDIX VII.

COEFFICIENT OF FRICTION.

Calculations of the coefficient of friction were carried out by making use of experimental results in relation to the graph obtained by considering the elastic behaviour of shrink-fitted assemblies, of percentage damping versus the ratio of nominal stress⁽¹⁾ to friction grip. (See Fig.57).

Example Calculation:

Let us consider the initial curve for specimen C. at 6% damping. (See Fig.65).

The stress corresponding to 6% damping = 7,600 lb/in².
The interface pressure, p, is calculated using Lamé's equations, $p = 4.33 T./in.^2$.

From the theoretical graph (Fig.57), $\frac{1}{\sigma}$, corresponding to 6% damping, = 2.5

$$\frac{1}{\sigma} = \frac{G_e}{\mu p}$$

$$2.5 = \frac{7,600}{\mu \times 4.33 \times 2240}$$

Hence:-

$$\mu = .315$$

Results of the calculations are given by the Tables of Fig.101, 102, 103.

(1) All experimental readings of percentage damping are plotted versus nominal shaft stress.

FIG. 101

INITIAL TESTS

| SPECIMEN | | A | B | C | D | E |
|---------------------|----|------|------|------|------|------|
| P T/in ² | | 1.3 | 2.16 | 4.33 | 6.5 | 8.65 |
| % DAMPING | 1 | .486 | .258 | .219 | .304 | .555 |
| | 2 | .558 | .297 | .248 | .317 | .490 |
| | 3 | .625 | .310 | .271 | .322 | .467 |
| | 4 | .654 | .320 | .289 | .328 | .42 |
| | 5 | .672 | .336 | .304 | .330 | |
| | 6 | .687 | .339 | .315 | | |
| | 7 | .687 | .344 | .322 | | |
| | 8 | .677 | .333 | | | |
| | 9 | .665 | .330 | | | |
| | 10 | .640 | .312 | | | |
| AVERAGE μ . | | .635 | .318 | .281 | .320 | .483 |

COEFFICIENT OF FRICTION.

FIG. 102

| FINAL TESTS | | | | | | |
|---------------|--------------------|-------|------|------|------|-------|
| SPECIMEN | | A | B | C | D | E |
| P | T/in. ² | 1.3 | 2.16 | 4.33 | 6.5 | 8.65 |
| % DAMPING | 1 | .95 | .992 | .643 | .538 | .797 |
| | 2 | 1.12 | .995 | .664 | .678 | 1.064 |
| | 3 | 1.16 | .99 | .658 | .797 | |
| | 4 | 1.18 | .985 | .648 | | |
| | 5 | 1.19 | .99 | | | |
| | 6 | 1.21 | .97 | | | |
| AVERAGE μ | | 1.132 | .985 | .653 | .670 | .930 |

COEFFICIENT OF FRICTION

FIG. 103.

| INITIAL TESTS | | | | | |
|------------------|---|-------|------|------|------|
| SPECIMEN | | 2 | 3 | 4 | 5 |
| $P \quad T/in^2$ | | 2.16 | 4.33 | 6.5 | 8.65 |
| % DAMPING | 1 | .914 | .408 | .343 | .380 |
| | 2 | 1.11 | .560 | .567 | — |
| | 3 | 1.381 | .812 | — | — |
| AVERAGE μ . | | 1.135 | .593 | .455 | .380 |

COEFFICIENT OF FRICTION

REFERENCES

REFERENCES

VIBRATION - GENERAL

- Draminsky, B., Daempningen Ved Torsionsvingninger I Krumbtapakaler, Copenhagen, 1947.
- Hansen and Chenea, Mechanics of Vibrations, p.96.
- Morris, J., Cap., Coupled Engine Torsional and Propeller Flexural Vibrations; Inst. of Mech. Eng. (Proc.) Vol.153, 1946.
- Morris, J., Dynamic Forces in Aircraft Engines, Journal of Royal Aeronautical Society, Vol.XXI, April 1927.
- Morris, J., The Escalator Method in Engineering Vibration Problems.
- Shannon, J.F., Damping Influence in Torsional Oscillation, Inst. of Mech. Eng., Dec. 1955.
- Tuplin, W.A., Torsional Vibration, London, 1934.
- Wilson, W. Ker., Practical Solution of Torsional Vibration Problems, Chapman and Hall, London, 1941, Vol.2, p.265.

CRANKSHAFT

- B.I.C.E.R.A., The Stiffness of Crankshaft of Commerical Oil Engines, Engineering, Sept.1, 1950.
- Carter, B.G., An Empirical Formula for Crankshaft Stiffness in Torsion, Engineering, Vol.126, 1928, p.36.
- Davidson, W.R.S., Shrink-Fit Stress Systems in Built Crankshafts, Ph.D. Thesis, University of Glasgow, 1951.
- Dorey, S.F., Elastic Hystereses of Crankshaft Steels, Proc. Inst. Mech. Eng., 1932, Vol.123, p.479.
- Dorey, S.F., Strength of Marine Engine Shafting, North-East Institution of Engineers and Shipbuilders, Trans. Vol.IV 1938-9, p.203.
- Russell, R., Experimental Studies on Crankshaft Stiffness, Journal of Royal Technical College Glasgow, Vol.IV, 1937-40, p.467.

- Seelmann, Die Reduktion der Kurbelkröpfung, Z.VDI.s.601, 1925.
- Southwell, R.V., The Effective Torsional Rigidity of a Crank, Aeronautical Research Committee Reports and Memoranda, No.1211 (E.30), July 1927.
- Timoshenko, S., Torsion of Crankshafts, Trans.A.S.M.E., 1922, Vol.44, p.653.
- Timoshenko and Lessells, Applied Elasticity, Chap.VIII.
- Taplin, W.A., The Torsional Rigidity of Crankshafts, Engineering, Vol.144, s.275, 1937.

BEARINGS

- Burwell, J.T., The Calculated Performance of Dynamically Loaded Sleeve Bearings, Journal of Applied Mechanics, Sept. 1947, A-231.
- Cameron, A., Oil Whirl in Bearings - Theoretical Deduction of a Further Criterion, Engineering, Feb.1955, p.237.
- Cameron, A. and (Mrs.) Wood, W.L., The Full Journal Bearing, Inst. of Mech.Eng. (Proceedings), Vol.161, 1949.
- DuBois, G.B. and Ocvirk, F.W., The Short Bearing Approximation for Plain Journal Bearings, Ithaca, New York, Trans. A.S.M.E., Nov. 1955.
- Hagg, A.C., The Influence of Oil Film Journal Bearings on the Stability of Rotating Machines.
- Harrison, W.J., The Hydrodynamical Theory of the Lubrication of a Cylindrical Bearing under Variable Load, and a Pivot Bearing, Trans. Cambridge Philosophical Society, Vol.22, 1920, pp.373-388.
- Kollmann, K. and Hockel, H.L., Ermittlung der Dicke des Schmierfilms in den Grundlagern eines stationären Dieselmotors, M.T.Z. Jahrgang 14, Nr.5, Mai 1953.
- Hummel, C., V.D.I.Forschungsheft No.287, 1926.
- Jacobsen, Charnes and Saibel, Studies in Lubrication, Trans. A.S.M.E., Nov. 1955.
- Michell, A.G.M., Progress in Fluid Film Lubrication, Trans. A.S.M.E., Vol.51, 1929, pp.153-163.

Newkirk, B.L. and Taylor, H.D., General Electric Review, 28, (1925), p.559.

Nücker, Über den Schmiervorgang im Gleitlager, Forschungsheft 352.

Oevirk, F.W., Short Bearing Approximation for Full Journal Bearings, N.A.C.A.Tn. 2808, 1952.

Pattie, D., Operating Conditions of Journal Bearings under Fluctuating Loads, Ph.D. Thesis, University of Glasgow, 1950.

Pestel, E., Beitrag zur Ermittlung der Hydrodynamischen Dämpfungs und Federeigenschaften von Gleitlagern, Ing. Arch. Band XII Drittes Heft, 1954, p.151 (c).

Sommerfeld, A., The Hydrodynamic Theory of Lubrication Friction, Zeit. Math. und Phys., Vol.50, Nr.1 and 2, 1904, pp.97-155.

Stodola, A., Schweiz. Bauztg. 85, (1925), p.265.

Swift, H.W., Fluctuating Loads on Sleeve Bearings, Journal of the Institution of Civil Engineers Vol.5, 1937, pp.161-165.

MEASUREMENT

Brodshaw, E., A Change of Capacity Method, Journal of Scientific Instruments, Vol.22, p.112, 1945.

Carter, B.C., Shannon, J.F. and Forshaw, J.R., Measurement of Displacement and Strain by Capacity Methods, Mech.E. Proceedings Jan-Dec. 1945, p.152.

Clapp, J.K., An Inductance-Capacitance Oscillator of Unusual Frequency Stability, Proc.I.R.E., 36, No.3, p.356, March 1948.

Mansfield, W.P., The Equipment and Experimental Methods used in the Study of Internal Combustion Engines, Engineering, Vol.169, p.672.

Mills, C.H.G., A Capacitance Type Torquemeter, Journal of Scientific Instruments, 1948, 25, p.151.

Shakaf, H.M., Non-contacting Gauge for Microdisplacements, Electronics, 27, June 1954, pp.172-4.

Stansfield, R., The Measurement of Torsional Vibrations, Inst. of Mech. Eng., Feb. 1942.

Whiddington, R.W., The Ultra-Micrometer, Philosophical Magazine (V) 1920, 40, p.634.

Yates, H.G., Prediction and Measurement of Vibration in Marine Geared-Shaft Systems, Inst. of Mech. Eng., 1955.

SHRINK-FITS

Baughner, J.W., Transmission of Torques by Means of Press and Shrink-fits, Trans. A.S.M.E., 1931, Vol. 53, M.S.P. 53-10, p. 85.

Green, W.G., Effect of Axial Restraint on the Stress in Rotating Disc, Philosophical Magazine, 1929, Vol. 8, p. 993.

Horger, O.J., and Nelson, C.W., Design of Press- and Shrink-fitted Assemblies, Journal of App. Mech., 1937, Vol. 4, p. 183.

Love, The Mathematical Theory of Elasticity, 4th. ed.

Migny, P., Emmanchements à Force et Calcul des Serrages, Revue de l'Aluminium, v. 28, No. 174, Feb. 1951, pp. 73-9.

Peterson, R.E. and Wahl, A.M., Fatigue of Shafts at Fitted Members, with a Related Photoelastic Analysis, Trans. A.S.M.E., 1935, Vol. 57, p. 559.

Sonntag, R., Zum Torsionsproblem der abgesetzten Welle und anderer Wellenformen des Maschinenbaues, Z.A.M.M., Band 34, Jan/Feb. 1954, p. 19.

Steele, M.C., On the Overstraining of Thick-walled Cylinders under Internal Fluid Pressure and under Interference Fit Pressure, Ph.D. Thesis, University of Glasgow, 1950.

Thom, A. and Orr, J., The Solution of the Torsion Problem for Circular Shafts of Varying Diameter, Proc. Royal Society of London, Ser. A., Vol. 131, 1931, p. 30.

Thomson, A.S.T., Scott, A.W., Moir, C.M., Shrink-Fit Investigations on Simple Rings and on Full-Scale Crankshaft Webs, Proceedings of the Institute of Mechanical Engineers, 1954, Vol. 168, No. 32.

Timoshenko and MacCulloch, Elements of Strengths of Materials, p. 374.

Trock, B., Shrink-Fits: Holding Power can be Increased,
Iron Age, Vol.172, No.20, Nov.12, 1953, pp.175-7

Wenck, F., Erhoehung des Haftbeiwertes bei Schrumpfpassungen,
Werkstattstechnik u. Maschinenbau, v.41, n.9, 1951,
pp.359-361.

Willers, F.A., Zeitschr.f.Mathem.unPhys., Vol.55, p.225, 1907.

INTERNAL DAMPING

Cochardt, A.W., A Method for Determining the Internal Damping
of Machine Members, Paper 53-A-44, presented at the
annual meeting of the A.S.M.E. New York, N.Y., Dec.1953.

Cottel, Entwistle and Thomson, Measurement of Damping Capacity
of Metals in Torsional Vibration, Inst.of Metals, 1948,
Vol.74, p.373.

Foppl, The Practical Importance of Damping Capacity in Metals,
Especially Steels, Jnl.Iron and Steel Inst., 1936,
Vol.134, p.393.

Hanstock, R., Damping Capacity, Strain Hardening and Fatigue,
Proceedings of the Physical Society, 1947, Vol.59, p.275.

Hanstock, R. and Murray, A., Damping Capacity and the Fatigue
of Metals, The Journal of the Institute of Metals,
1946, Vol.72, p.97.

Hatfield, W.H., Stanfield, G. and Rotherham, L., The Damping
Capacity of Engineering Materials, North East Coast
Institution of Engineers and Shipbuilders, Trans.,
LVIII, part 7, June 1942.

Lazan, B.J., A Study with New Equipment of the Effects of
Fatigue Stress on the Damping Capacity and Elasticity of
Mild Steel, Trans.Amer.Soc. for Metals, Vol.92, 1950,
pp.499-548.

Lazan, B.J., Some Mechanical Properties of Plastics and Metals
under Sustained Vibrations, Trans.A.S.M.E., Vol.65,
1943, pp.87-102.

Lazan, B.J., Effect of Damping Constants and Stress Distribution
on the Resonance Response of Members, Jnl. of App.Mech.,
Trans.A.S.M.E., Vol.75, 1953, pp.201,209.

Pattison, J.R., An Apparatus for the Accurate Measurement of Internal Friction, The Review of Scientific Instruments, Vol.25, Nr.5, May 1954, p.490.

Pertz, B., Die Bestimmung der Baustoffdämpfung, Vieweg 1928.

Robertson, J.M. and Yorgiadis, A.J., Internal Friction in Engineering Materials, Trans.A.S.M.E., Jnl. of App.Mech., 1946, Vol.68, p.A.173.

Yorgiadis, A., Damping Capacity of Metals, Product Engineers, Nov.1954, pp.162-170.

MISCELLANEOUS

Aitken, A.C., Determinants and Matrices, Seventh Edition, 1951, p.3.

Allen, D.M. de G., Relaxation Methods, 1954.

Hete'nyi, M., Handbook of Experimental Stress Analyses, Chap.6. Electric-Inductance Gauges, by B.F.Langer.

Grinter, L.E., Numerical Methods of Analyses in Engineering, p.53.

Rabinowicz, Righmire, Tedholm and Williams, The Statistical Nature of Friction, Trans.A.S.M.E., 1955, Vol.77, pp.981-984.

\$

